Seismotectonics of Western Canada From Regional Moment Tensor Analysis

Johannes Peter Ristau

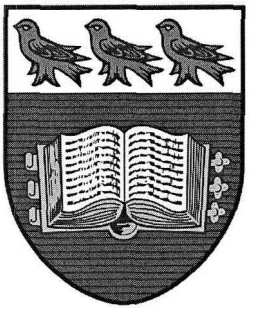

University of Victoria
2004

Seismotectonics of Western Canada From Regional Moment Tensor Analysis

by

Johannes Peter Ristau
B.Sc., University of Manitoba, 1995
M.Sc., University of Manitoba, 1999

A Dissertation Submitted in Partial Fulfillment of the
Requirements for the Degree of

DOCTOR OF PHILOSOPHY

in the School of Earth and Ocean Sciences

Supervisor: Dr. Garry C. Rogers

Abstract

Moment tensor analysis of regional earthquakes (distances $\sim<$ 1000 km) in western Canada is now possible due to the installation of more than 40 three-component broadband seismometers in western Canada and adjacent regions. In this study, regional moment tensor (RMT) analysis using robust waveform fitting techniques are employed to routinely calculate source mechanisms, moments, and depths of earthquakes with M $\geq\sim$ 4.0 in and near western Canada. This has resulted in about 10 times as many solutions per year for this region than have been calculated with teleseismic methods which are limited to earthquakes about M > 5.0.

To date, more than 380 RMT solutions have been calculated in this study for western Canada and adjacent regions for the years 1995–2004. These solutions provide new insights into a number of tectonic problems in western Canada. Local magnitudes (M_L) have been calibrated with moment magnitudes (M_w) providing a more consistent estimate of the magnitude of an earthquake. This is particularly important in the offshore region of British Columbia where RMT analysis shows that M_L is underestimated by 0.3–0.7 magnitude units compared with M_w, depending on the amount of oceanic crust present in the source-receiver travel path. This has important consequences for seismic hazard analysis and tectonic studies. Focal mechanisms from RMT solutions are also used to constrain the motions of the Explorer plate, a small oceanic plate off the coast of British Columbia. Rotation poles are calculated by leaving Pacific/Explorer motion unconstrained, and by constraining Pacific/Explorer motion using moment release rates along the Pacific/Explorer boundary. The Pacific/Explorer rotation rate decreases by a factor of 2 if Pacific/Explorer motion is constrained. This changes the convergence direction of the Explorer plate relative to the North America plate from NE-SW in the unconstrained case to N-S in the constrained case. This suggests that Explorer plate motion cannot be modeled with a single rotation pole and cannot be treated as a rigid plate. The Explorer plate is likely undergoing intense internal deformation. The strain tensor for the Explorer plate, calculated from RMT solutions, gives a strain rate of 7.8×10^{-8} yr^{-1} in a N-S direction.

Comparing moment (M_o) with M_L values for the northern and southern Canadian Cordillera demonstrates there is a 1:1 relationship between M_w, which is derived from M_o, and M_L. Stress tensors for the Canadian Cordillera give a NE-SW compressive stress direction ($\sigma 1$) for most of western Canada. The northern Canadian Cordillera shows a change

in $\sigma 1$ from E-W to N-S to NE-SW from south to north. Principal compressive strain and stress directions for the northern Canadian Cordillera have similar orientations suggesting that the earthquakes occur on faults which are favourably oriented for failure. In southern British Columbia the compressive stress regime is N-S and RMT data suggests that the N-S stress regime may extend through to the eastern Canadian Cordillera. RMT analysis will provide valuable data in the future to map the stress field in southern British Columbia. Stress tensor analysis of moment tensor and first motion solutions in the Queen Charlotte Islands region results in a local $\sigma 1$ azimuth of 20° which gives an angle of $\sim$ 45° to the northern segment of the Queen Charlotte fault. This may suggest that the northern Queen Charlotte fault has a higher frictional strength than the San Andreas fault where angles of up to 80° are observed between $\sigma 1$ and the fault strike. Moment tensor solutions in the Glacier Bay region show a change in P axis orientation from N-S to E-W which could indicate that the stress field is influenced by post-glacial rebound.

Contents

List of Figures

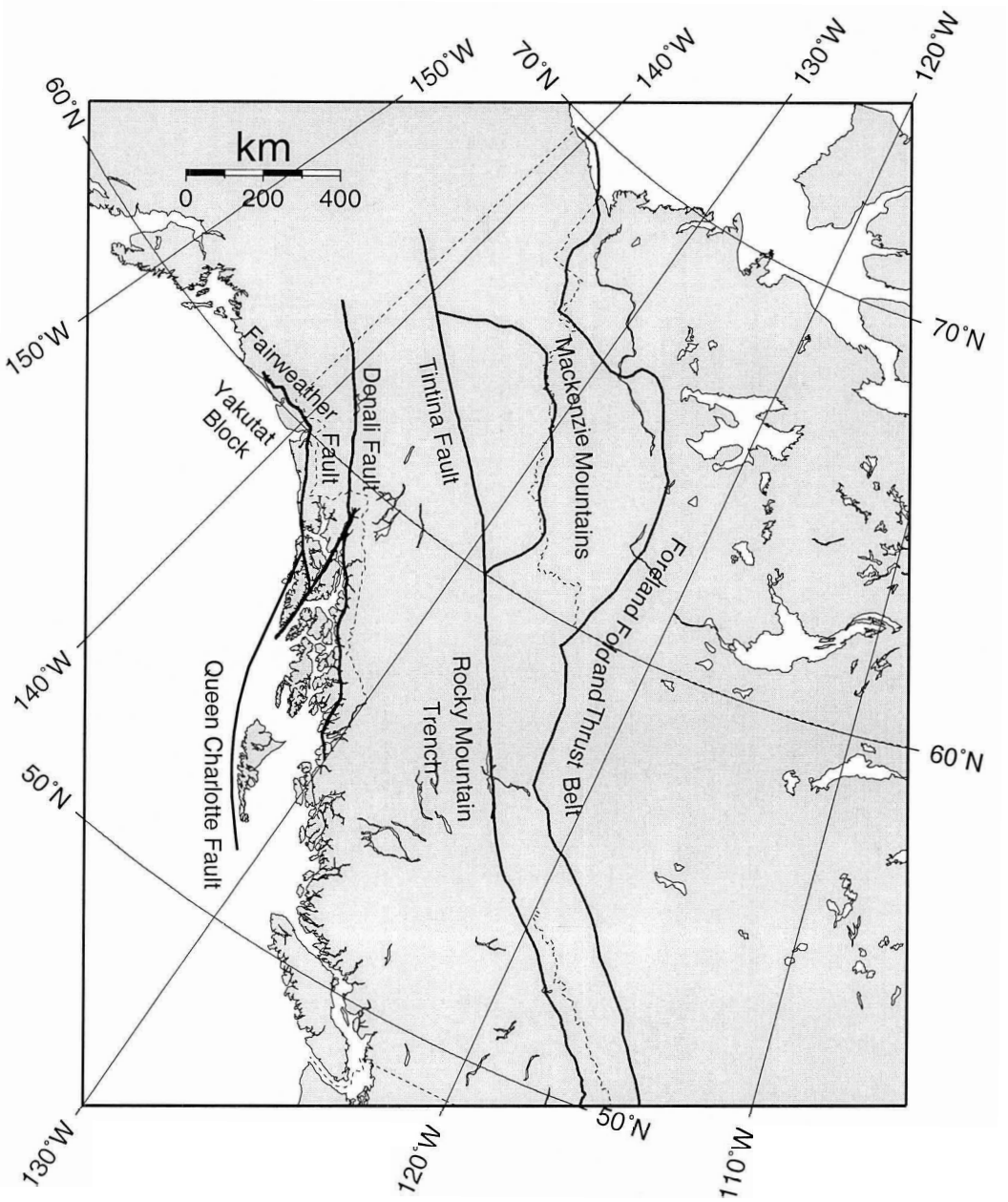

Figure 2.2 Major tectonic features of the Central and Southern Canadian Cordillera.

List of Tables

List of Symbols

d_n	observed waveforms for inversion
G_n	$n \times 6$ matrix containing the Green's functions for inversion
M	magnitude
m_b	body-wave magnitude
M_c	coda magnitude
M_D	duration magnitude
M_L	local magnitude
M_o	moment
M_s	surface-wave magnitude
M_w	moment magnitude
M_{ij}	individual moment tensor elements
$\bar{m}_i$	six moment tensor elements to be calculated
N axis	null axis
P axis	pressure axis
T axis	tension axis
$\bar{u}$	fault displacement
u_i, u_j	unit vector in the slip direction
$\varepsilon 1, \varepsilon 2, \varepsilon 3$	principal strain directions
ε_{ij}	individual strain tensor elements
μ	shear modulus
ν_i, ν_j	unit vector normal to the fault plane
$\sigma 1, \sigma 2, \sigma 3$	principal stress directions
τ	total shear stress on a surface

List of Acronyms

CCSB	Canadian Crustal Stress Database
CNSN	Canadian National Seismograph Network
PGC	Pacific Geoscience Centre
PNSN	Pacific Northwest Seismograph Network
OSU	Oregon State University
SAC	Seismic Analysis Code
USGS	United States Geological Survey

Acknowledgements

I would like to thank my supervisor, Garry Rogers, for proposing this research topic and for all of his advice, support, and encouragement during the completion of this dissertation. I would also like to thank the rest of my supervisory committee for taking the time to read this dissertation and for all of their helpful and valuable discussions and comments. They have encouraged me to expand this study into many different areas and have made it a much improved dissertation. Thanks to Roger Hansen for taking the time to travel from Alaska to be on the committee. A special thanks must be extended to Chuck Ammon for providing the moment tensor code and for a great deal of valuable advice on calculating regional moment tensor solutions. Honn Kao also provided helpful advice on calculating regional moment tensor solutions. Stephane Mazzotti supplied the code for calculating rotation poles and for calculating moment release rates. All of the staff at the Pacific Geoscience Centre have been extremely kind and ready to help me out at a moments notice over the years and they are all very much appreciated. This includes the seismology staff who answered, and still answer, all of my questions about everything seismic (Alison Bird, Wanda Bentkowski, Tim Claydon, Rick Hall, Taimi Mulder); the computer support people who have made sure that I always had a working computer and everything I needed to run on it (Richard Baldwin, Richard Franklin, Bruce Johnson, Robert Kung, Andreas Rosenberger, Steve Taylor); and other PGC staff for many valuable discussions over the years (Earl Davis, Herb Dragert, Tom James, Tony Lambert, Kelin Wang). And finally, a special thanks to the administrative staff who always made sure that I had the right forms filled out at the right time, made sure that I was getting paid even when I didn't know I was supposed to be, and generally made life a whole lot easier (Eléna Jenner, Rosemary MacKenzie, Darlene Upton).

I would like to thank all of the friends I have met during my time here in Victoria. Unfortunately there are too many to mention all of them by name. They include all of the other grad students, past and present, at PGC and UVic. Also, all of the people I have met through paddling on the Wild Things, the B.C. Buds, and HP & Special Sauce. I have had endless fun with them over the last four years and they are all very much appreciated. I would like to thank Lesley MacLaughlin and Dave Jackson for all of the dinners at their place since literally day one that I have been in Victoria, and Taimi Mulder and Judith Baker for letting me stay at their place when I first arrived and had no where else to stay. And I'll mention Shelley Parkhouse because she didn't fit into any of the other categories, and my friend Christine Clark for the bread recipe that made me very popular around here.

Finally, I thank my family — my parents, my aunt, my sister Helga, my brother's Ed and Dave, my brother-in-law John, and sister-in-law Wendi — for all of their support and encouragement over the last four years. They have made it possible for me to complete my doctorate and I love them all. And last, to my darling niece and nephew, Katie and Zak. They accepted the fact that I had to leave Winnipeg even though they didn't like it. I love them very much and miss them every day.

For Kaitlyn and Zachary

Sometimes, if you stand on the bottom rail of a bridge and lean over to watch the river slipping slowly away beneath you, you will suddenly know everything there is to be known.
Winnie-the-Pooh

The great tragedy of Science — the slaying of a beautiful hypothesis by an ugly fact.
Thomas H. Huxley

Chapter 1

Introduction

Western Canada covers a large area geographically and encompasses a number of varied tectonic regimes (Figure 1.1). These range from a subduction zone, to mountain building regions, to stable continental interiors. The main influence on the tectonics of western Canada is the relative motions of the Pacific and North America plates along the west coast of North America, which causes significant seismic activity through much of western Canada. Another major influence on the tectonics of western Canada is the subduction of the Juan de Fuca plate beneath North America and results in some of the world's largest earthquakes ($M > 9$). An area of high seismicity associated with the Explorer plate is also located offshore Vancouver Island.

The west coast of British Columbia is a tectonically complex region which includes the northern end of the Cascadia subduction zone and the Queen Charlotte Islands margin. The tectonic setting consists of the Pacific, North America, Juan de Fuca, and Explorer plates. A large number of minor to strong earthquakes occur in this region every year along with occasional major and great earthquakes (e.g. 26 January 1700 $M \sim 9.0$ Cascadia subduction zone megathrust event; 22 August 1949 $M = 8.1$ along the Queen Charlotte Fault; 23 June 1946 $M = 7.3$ Vancouver Island) (Figure 1.2). The majority of the offshore seismic activity occurs in the crust (depths < 10 km) although deeper events within the subducting Juan de Fuca plate are not uncommon.

The interior of British Columbia, and extending north through the Yukon and Northwest Territories to the Beaufort Sea, is a region of low to moderate seismic activity. The largest events have occurred in the Mackenzie Mountains region in the SW Northwest Territories (5 October 1985 $M = 6.6$; 23 December 1985 $M = 6.7$; 25 March 1988 $M = 6.2$)

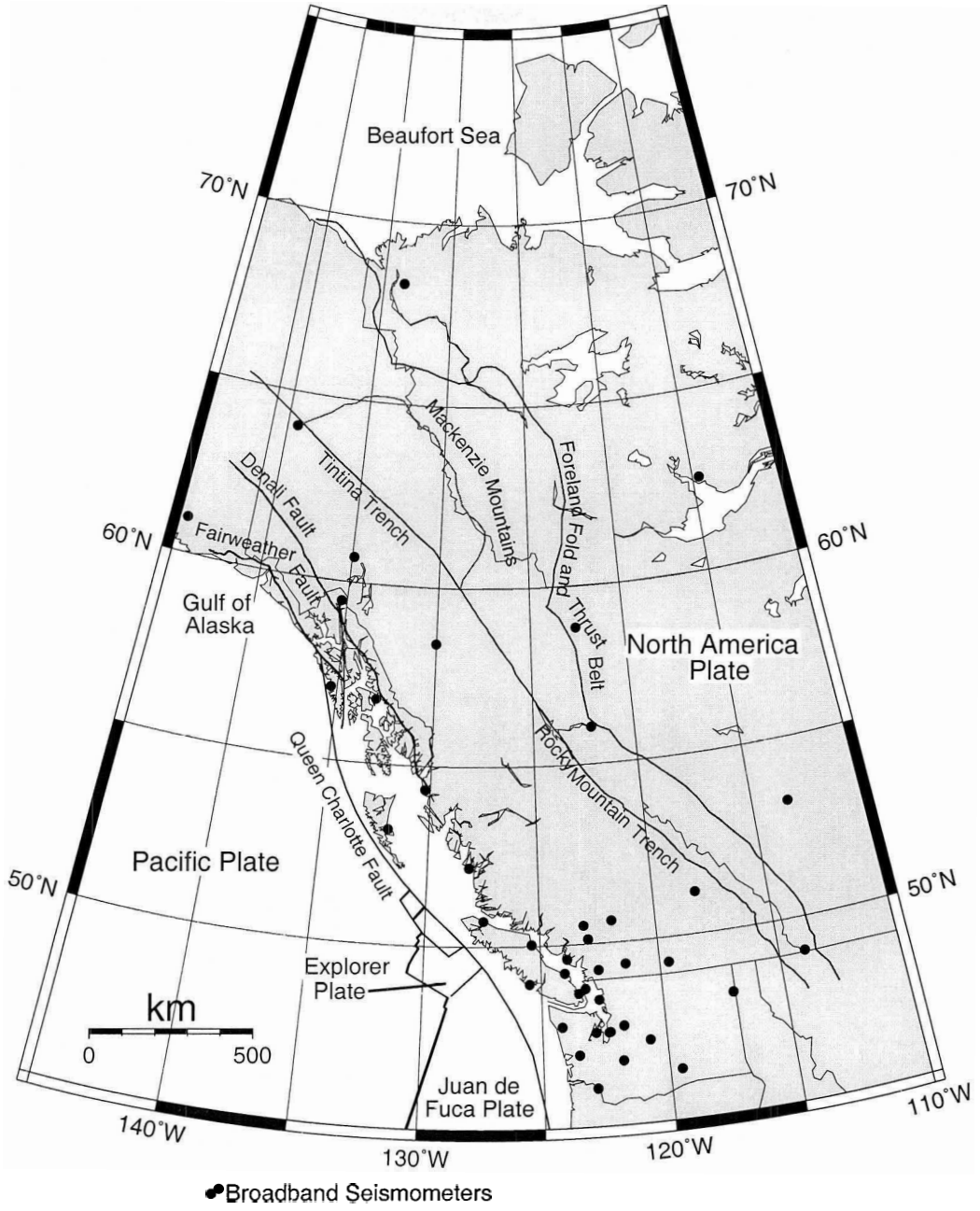

Figure 1.1 Overview of the tectonic setting of western Canada showing plate boundaries and major faults. Black dots are the locations of three-component broadband seismometers in western Canada, Washington, and southeast Alaska. This figure and many others in this dissertation were created using Generic Mapping Tools (GMT) (Wessel and Smith, 1991).

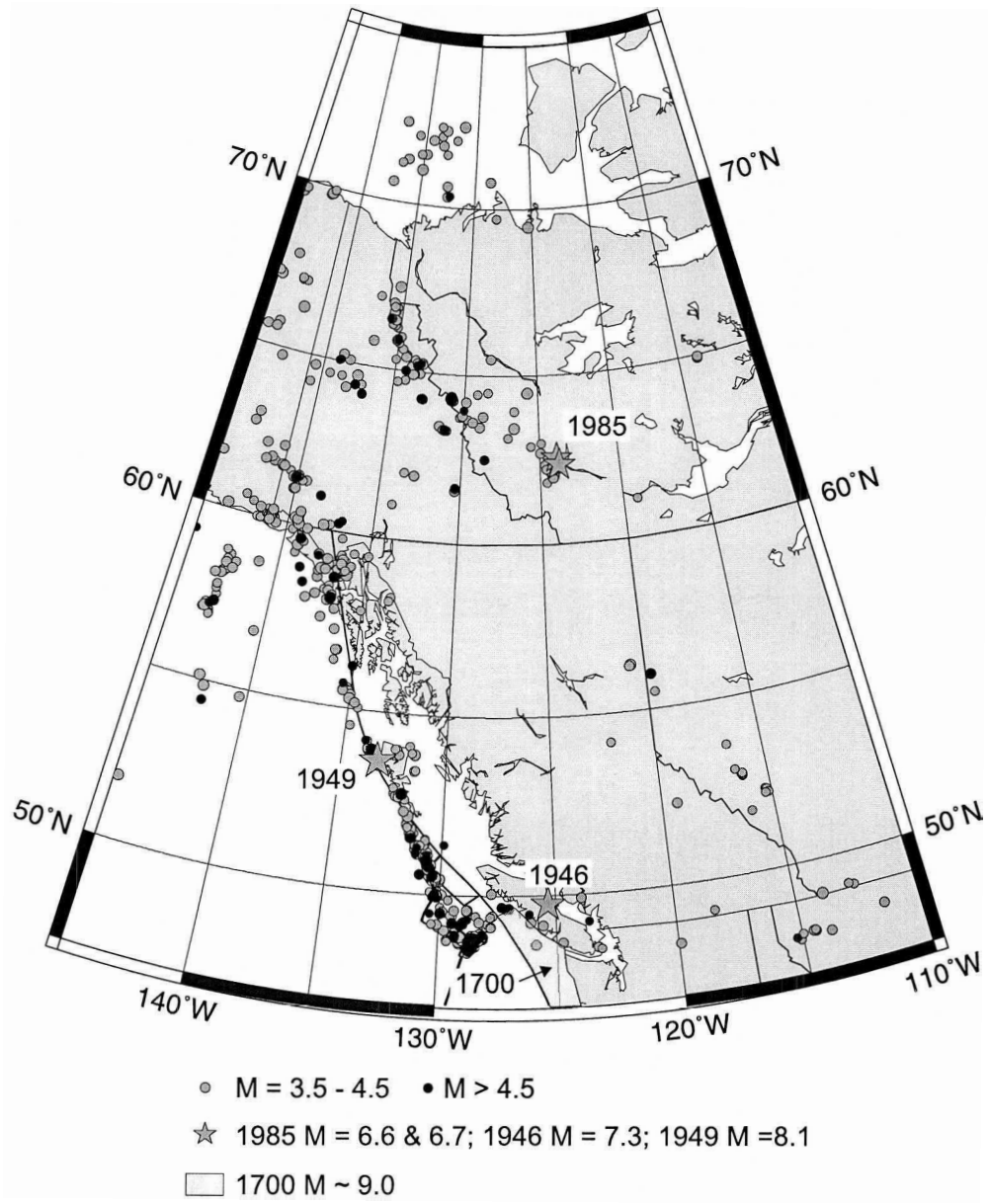

Figure 1.2 Locations of earthquakes with M $\geq$ 3.5 in western Canada and southeast Alaska between 1995 and 2001. Also shown are the locations of the 1700 M $\sim$ 9.0 (Cascadia subduction zone), 1946 M = 7.3 (Vancouver Island), 1949 M = 8.1 (Queen Charlotte Islands), and 1985 M = 6.6 and M = 6.7 (Nahanni region, Northwest Territories) events.

although a number of events with M > 4.0 have occurred throughout the interior of British Columbia, the Yukon, and Northwest Territories. Where the depths are determined, these events are primarily shallow crustal events (< 10 km depth). There is a high rate of seismicity in the Gulf of Alaska and southeast Alaska region where several major earthquakes have occurred in the last century, most recently the 3 November 2002, M = 7.9 in southern Alaska.

Beginning in the late 1980's and continuing through to the present, a regional seismograph network of three-component broadband digital seismographs has been established in western Canada, the U.S. Pacific northwest, and southeast Alaska. The network currently consists of more than 40 three-component broadband stations. In this study, source parameters (strike, dip, rake, moment, and centroid depth) of earthquakes with M $\geq\sim$ 4.0 are calculated by using moment tensor analysis of regional three-component broadband data. Theoretical Green's functions, calculated using region specific 1-D Earth models, are inverted with observed waveforms to give the source parameters. Since the mid- to late-1970's Harvard University (from here on referred to as Harvard) and the United States Geological Survey (USGS) have calculated moment tensor solutions for all earthquakes with M $>\sim$ 5.0 using teleseismic waveform data and generic whole Earth models to calculate the Green's functions (e.g. Dziewonski et al., 1981; Sipkin, 1986). At lower magnitudes there is little low frequency energy generated compared with large earthquakes and the Earth model used to calculate the Green's functions becomes more important. By using regional waveform data (source-receiver distances less than $\sim$ 1000 km) and region specific Earth models it is possible to calculate moment tensor solutions for earthquakes as small as M $\sim$ 4.0. This will result in approximately 10 times as many moment tensor solutions calculated per year as compared with teleseismic methods.

To date, more than 290 moment tensor solutions have been calculated for the coastal and offshore region of British Columbia in this research (1995–2003) and by Oregon State University (OSU) from 1994–1995 and Harvard from 1976–1993 (Figure 1.3 and Figure 1.4). These solutions provide a large data base of moment tensor solutions which will continue to grow with future earthquakes now that the method is semi-routine. In addition to the coastal and offshore events, more than 100 moment tensor solutions have been calculated for the interior of British Columbia and the Yukon and western Northwest Territories (Figure 1.3 and Figure 1.5). Focal mechanisms in these regions provide a better understanding of stress and strain within the western part of the North America plate.

Chapter 2 gives an overview of the current tectonic setting of the coastal and offshore re-

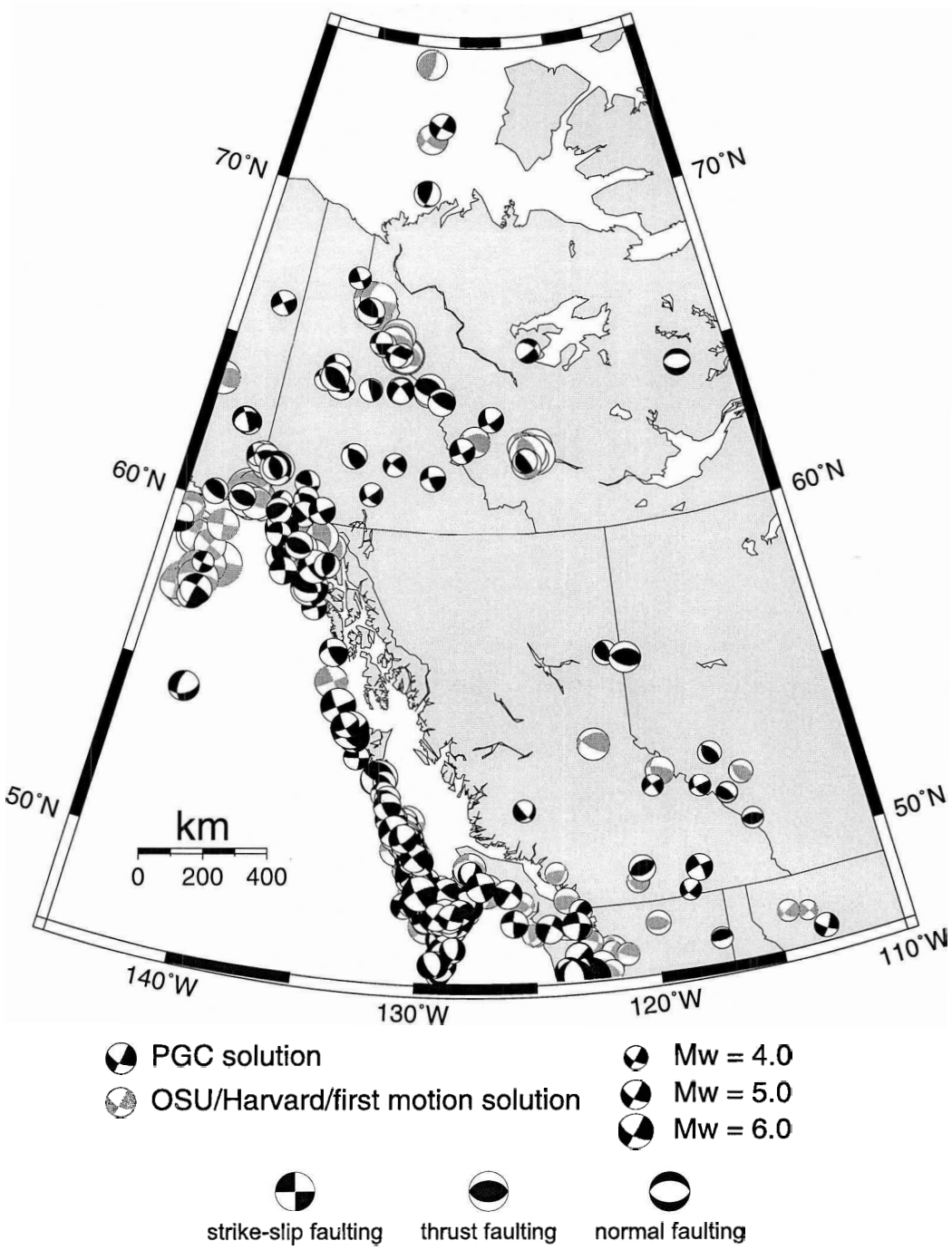

Figure 1.3 Moment tensor solutions calculated for western Canada and southeast Alaska from 1976–2003. Regional moment tensor solutions calculated in this research are in black; OSU regional moment tensor solutions calculated from 1994–1995, Harvard solutions calculated from 1976–1993, and first motion solutions from the Canadian Cordillera and Beaufort Sea, are shown in grey. At the bottom is a legend for the symbol types used for focal mechanisms.

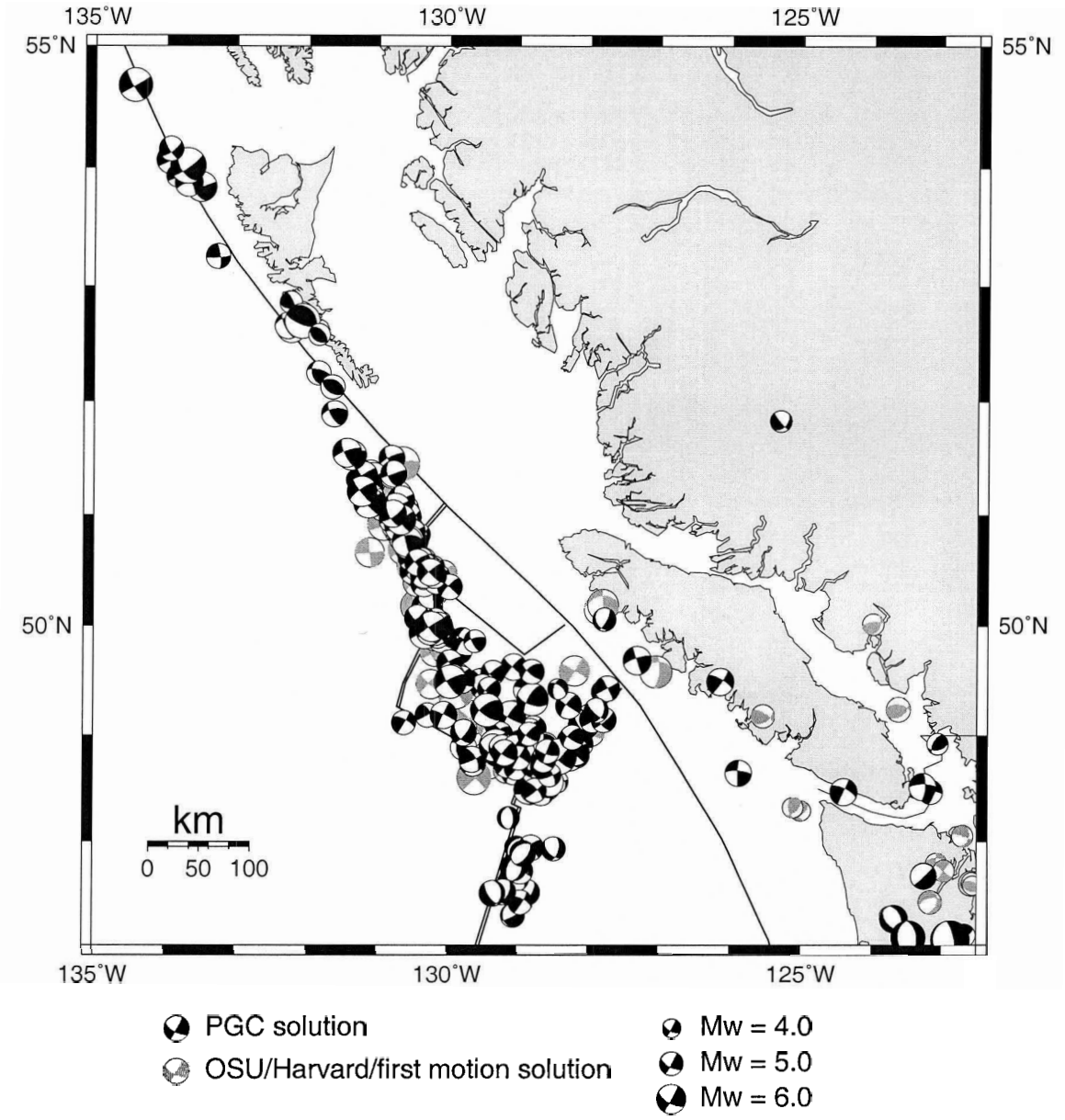

Figure 1.4 Moment tensor solutions calculated for the offshore and coastal regional of British Columbia and northwest Washington. Regional moment tensor solutions calculated in this research are in black; OSU regional moment tensor solutions calculated from 1994–1995 and Harvard solutions calculated from 1976–1993 are shown in grey.

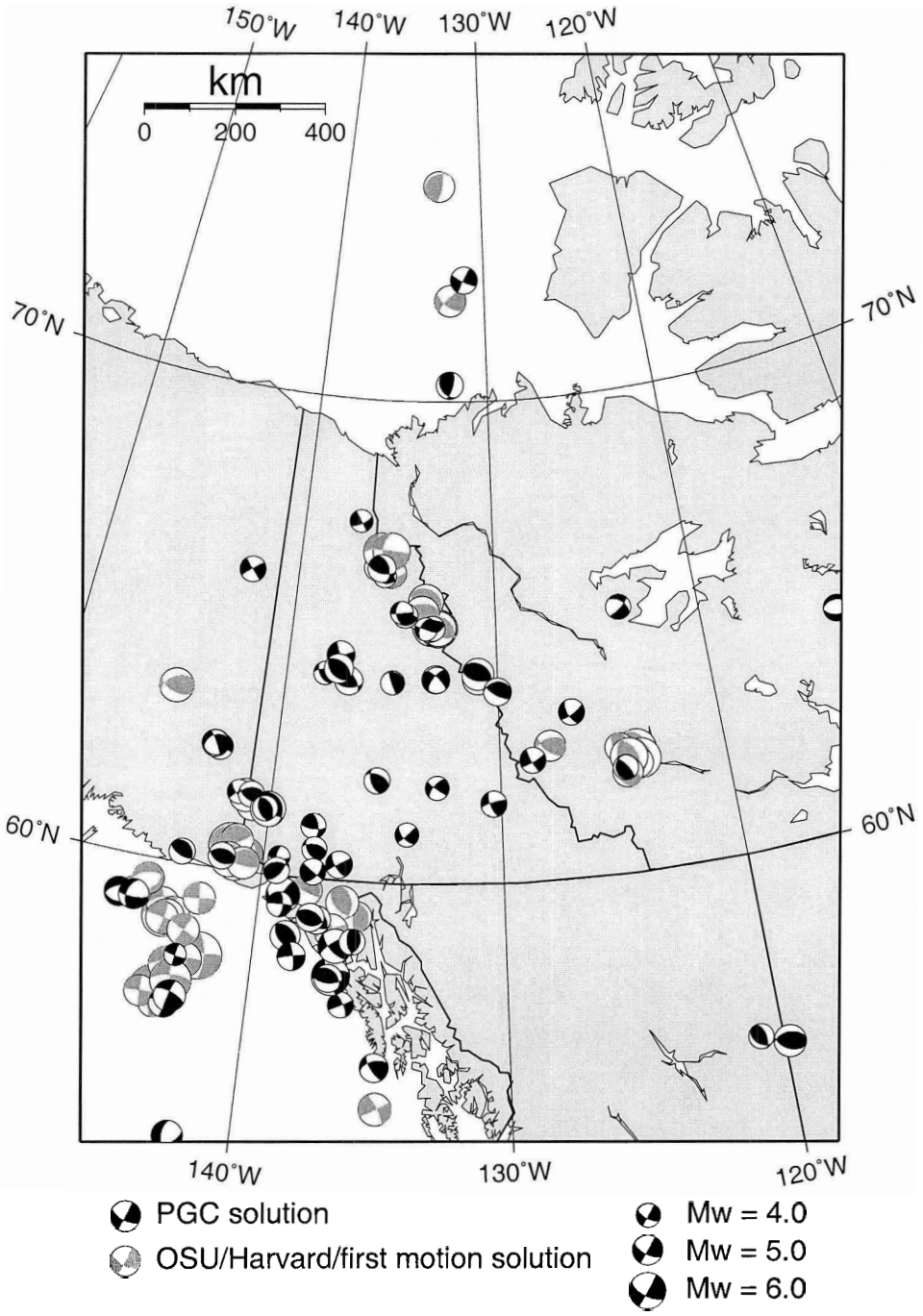

Figure 1.5 Moment tensor solutions calculated for the northern Canadian Cordillera and southeast Alaska/Gulf of Alaska region. Regional moment tensor solutions calculated in this research are in black; OSU regional moment tensor solutions calculated from 1994–1995, Harvard solutions calculated from 1976–1993, and first motion solutions from the northern Canadian Cordillera and Beaufort Sea are shown in grey.

gion of British Columbia, as well as the tectonic setting of the interior of British Columbia, the Yukon, and western Northwest Territories. In Chapter 3 the theory and procedure for calculating regional moment tensor solutions are discussed. Chapter 4 compares moment magnitude (M_w) with local magnitude (M_L) for earthquakes off the west coast of Vancouver Island and in the Queen Charlotte Islands region. It has been thought for sometime that M_L values calculated off the coast of British Columbia have been underestimated by at least 0.5 magnitude units compared with continental earthquakes. Therefore, there is a significant error in estimated seismic moments and regional moment release rates. M_w provides a more robust estimate of the magnitude of offshore earthquakes and with more than 290 M_w values available for the offshore region, M_L can be calibrated with M_w.

Chapter 5 uses regional moment tensor solutions to look at the motions of the Explorer plate. The Explorer plate is a microplate off the west coast of Vancouver Island, recently separated from the Juan de Fuca plate, and trapped between the Pacific, North America, and Juan de Fuca plates. Most of the seismic activity offshore Vancouver Island occurs within the Explorer plate and along its oceanic plate boundaries. Explorer plate rotation poles and rates along with strain rates and directions are calculated from regional moment tensor solutions. Chapter 6 uses moment tensor solutions to examine the current tectonic regime of the Yukon and western Northwest Territories along with the southeastern-most part of Alaska. The Yukon and Northwest Territories region are examples of a highly active interplate seismic zone. The high rate of seismicity is related to the active terrane collision tectonic setting in southern Alaska. Moment tensor solutions are used to calculate stress and strain directions, which are directly related to the seismic activity, and these directions are compared with GPS results.

Chapter 7 looks at the tectonics of the southern Canadian Cordillera by using regional moment tensor solutions to map the crustal stress pattern. The southern Canadian Cordillera is a region of relatively low seismicity. However, large ($M > 5.0$) earthquakes have occurred and the seismic hazard is still significant. Prior to the capability to calculate regional moment tensor solutions almost no focal mechanisms were available in the southern Canadian Cordillera. More than 20 moment tensor solutions have now been calculated for this region which provides valuable information about the contemporary tectonics of the southern Canadian Cordillera. Chapter 7 also uses regional moment tensor solutions to compare M_w with M_L and coda magnitude (M_c) in the Vancouver Island/Puget Sound region. The Vancouver Island/Puget Sound region is a densely populated region and is at risk from large ($M > 7.0$) earthquakes. More than 40 regional moment tensor solutions are available for events occurring in the overlying crust and subducting slab. These solutions

can be used to calibrate M_L and M_c with M_w in order to provide more accurate magnitude estimates for the Vancouver Island/Puget Sound region. In Chapter 8 the Queen Charlotte Islands and Glacier Bay, Alaska regions are discussed. The Queen Charlotte Islands is a region of moderate to high seismicity dominated by the Queen Charlotte fault where the Pacific plate is sliding north past the North America plate. This was the site of the M = 8.1 Queen Charlotte Islands earthquake and earthquakes with M > 6.0 are not uncommon. Regional moment tensor solutions are used to examine the Pacific/North America interaction along with previously calculated first motion focal mechanisms. The Glacier Bay region along the Alaska panhandle is a region experiencing rapid uplift due to post-glacial rebound. How much of the seismicity is related to post-glacial rebound and how much is to Pacific/North America interaction is unknown. Regional moment tensor solutions can provide previously unavailable data about the Glacier Bay region to help make the distinction between post-glacial rebound and tectonic seismicity.

Several appendices are included with information about the regional moment tensor solutions and the regional moment tensor method. Appendix A contains a list of all regional moment tensor solutions calculated in this research along with OSU regional moment tensor solutions and Harvard moment tensor solutions available for the study area. Appendix B shows examples of waveform fits from regional moment tensor solutions for a number of different regions in western Canada and various magnitudes. Appendix C contains a number of moment tensor solution comparisons. These include using different methods to calculate Green's functions, limiting the number of broadband stations used to calculate the solution, using synthetic seismograms to investigate the accuracy of the calculated depths, and comparing the regional moment tensor solutions calculated in this research with the equivalent OSU, Harvard, and the USGS solutions. Appendix D describes the different coordinate systems used in this research and by OSU and Harvard to calculate moment tensor solutions, and a method to convert first motion solutions to moment tensor solutions. Appendix E lists the Earth models used to the calculate the regional moment tensor solutions in this research.

Chapter 2

Tectonic Setting

2.1 Introduction

This chapter will discuss the current tectonic setting of western Canada which consists of a number of varied tectonic regimes. This regime includes the coastal and offshore region of British Columbia — a tectonically complex region comprised of the northern end of the Cascadia subduction zone, the Explorer plate region, and the Queen Charlotte Islands transform margin (Figure 2.1), and the interior of British Columbia and the Yukon and western Northwest Territories (Figure 2.2).

2.2 Juan de Fuca Plate

The Cascadia subduction zone is a region of active plate convergence where the Juan de Fuca plate, a small oceanic plate between the North America plate and Pacific plate, is subducting underneath the North America plate. The Cascadia subduction zone also includes the Explorer plate to the north of the Juan de Fuca plate and the Gorda plate to the south. These two plates are acting independently of the Juan de Fuca plate and are deforming internally. The Explorer plate region is discussed in section 2.3. The Gorda plate region is not part of this study. The Juan de Fuca plate is a remnant of the larger Farallon plate which began to fragment at about 55 Ma (Atwater, 1989) creating the Vancouver plate (Menard, 1978). The Pacific-Farallon ridge crest moved eastward and at about 30 Ma reached the continental margin so contact was made between the Pacific and North America plates. At this point the San Andreas transform fault system was initiated and, as the fault grew, it separated what have become known as the Juan de Fuca and Cocos

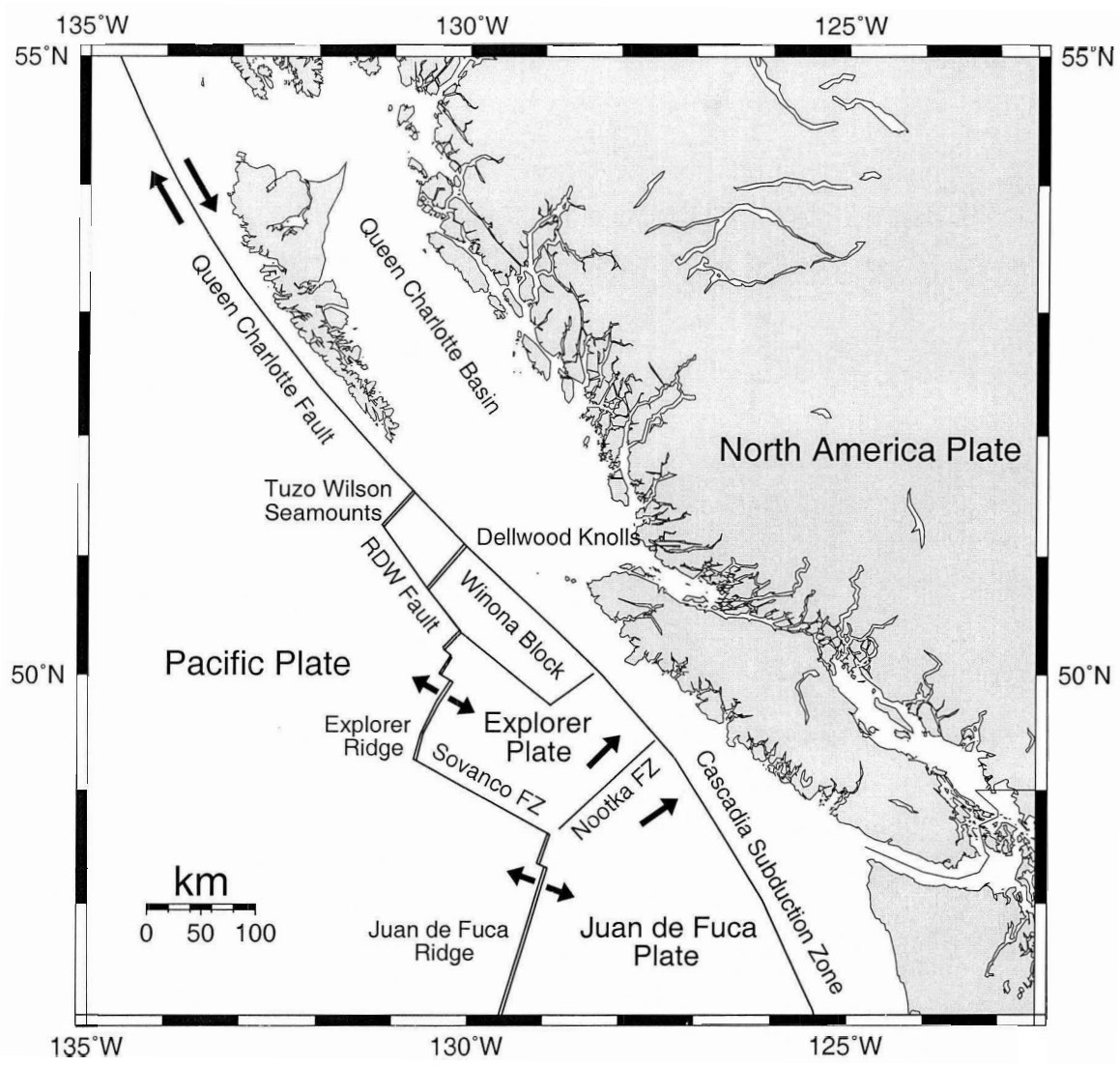

Figure 2.1 Tectonic setting of the coastal and offshore region of British Columbia. Arrows indicate the relative motions of the plates across the boundaries. RDW - Revere-Dellwood-Wilson.

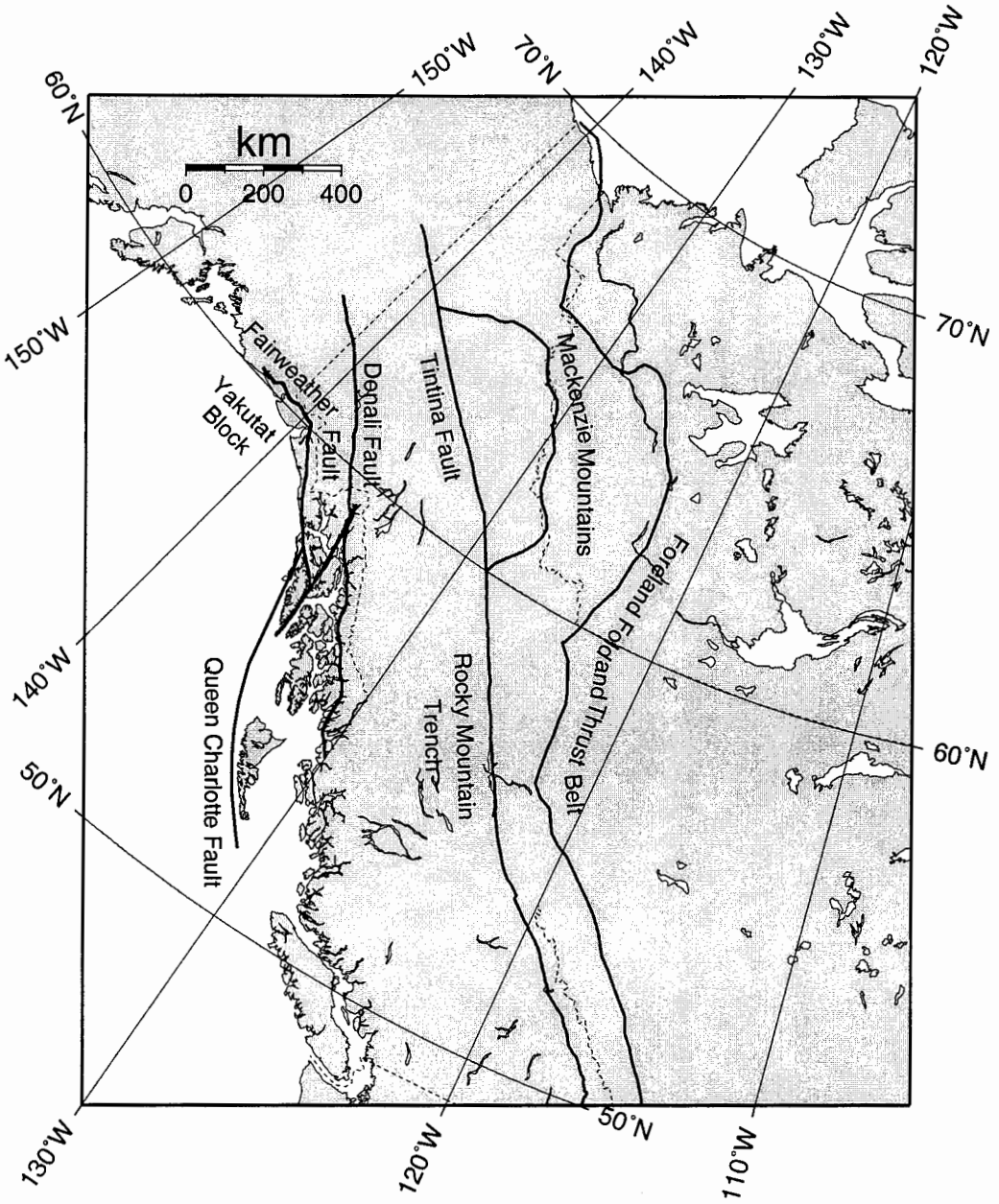

Figure 2.2 Major tectonic features of the Central and Southern Canadian Cordillera.

plates (Atwater, 1989). From about 30 Ma to the present the Juan de Fuca plate has continued to fragment with a complex history of clockwise and counterclockwise rotations and propagating rift events (Riddihough, 1977) resulting in the current plate configuration (Wilson, 1988).

Presently the northern end of the Juan de Fuca plate is bounded by the Cascadia subduction zone, Nootka fault zone, and the Juan de Fuca ridge (Figure 2.1). The rate of convergence between the Juan de Fuca and North America plates has steadily declined over the last 4 Ma and currently is approximately 40 mm/yr in a northeast direction (Riddihough, 1984). Between the latitudes of 47°N and 49°N the orientation of the margin changes from N-S to NW-SE. The maximum age of material being subducted is about 9 Ma at the southern end of the plate off central Oregon, and about 6 Ma at the northern end adjacent to the Nootka fault zone. Lithosphere this young is very thin, less than 30 km, very flexible, and extremely buoyant (Oldenburg, 1975; Molnar and Atwater, 1978).

The Cascadia subduction zone is unusual in that no large thrust earthquakes have been detected on the Juan de Fuca subduction interface in historical times ($\sim$ last 200 years), and no thrust earthquakes of any size in the instrumental record, although a few very small thrust events in the Gorda plate region have been detected. This could indicate that the subduction interface is either sliding smoothly with no buildup of strain, or that the interface is fully locked and building up strain. Paleoseismicity data from sites along the coast from southern Vancouver Island to northern California provide evidence that megathrust earthquakes have occurred along the Cascadia subduction zone at irregular intervals averaging about 600 years (Atwater, 1987; Adams, 1990; Hyndman, 1995; Leonard et al., 2004) with the most recent event occurring on 26 January 1700 (e.g. Satake et al., 1996). Geodetic data (e.g. Hyndman and Wang, 1995; Dragert et al., 1994; Mazzotti et al., 2003b) give evidence that the Cascadia subduction zone is currently locked and accumulating strain towards a future megathrust earthquake.

2.3 Pacific—North America—Juan de Fuca Triple Junction

The ridge-transform-trench triple junction between the Pacific, North America, and Juan de Fuca (Explorer-Winona-Dellwood) plates has been located off southern British Columbia for at least 10 Ma (Riddihough, 1977) and possibly as long as 40 Ma (Wilson, 1988). The triple junction remained stable at a point off Brooks Peninsula for the period 10 to 5 Ma then moved northwest at a rate of approximately 1.8 cm/yr (Riddihough, 1977). The triple junction is a morphologically complex region since the Juan de Fuca ridge does not intersect

the margin in a simple manner but breaks into the Explorer ridge, Revere-Dellwood-Wilson transform fault, and the Tuzo Wilson Seamounts and Dellwood Knolls. Carbotte et al., (1989) suggest that the triple junction, rather than occupying a discrete point, may be diffusely spread throughout the region between the northern end of the Explorer ridge and the Tuzo Wilson Seamounts.

North of the triple junction is the Queen Charlotte Islands margin with the dominant tectonic feature being the Queen Charlotte fault zone. The Queen Charlotte fault forms the boundary between the Pacific and North America plate and was the location of the largest instrumentally recorded earthquake in Canada (22 August 1949 M = 8.1). Plate tectonic models suggest right-lateral motion of about 55 mm/yr between the Pacific and North America plates (Minster and Jordan, 1978). The motion along the Queen Charlotte fault is primarily strike-slip. However, plate motion vectors show a component of convergence off the southern Queen Charlotte Islands suggesting that the deeper section of the fault, bounded on both sides by oceanic lithosphere, may be thrusting under the margin (Riddihough and Hyndman, 1989; Bérubé et al., 1989). The presence of earthquakes with thrust faulting mechanisms also suggest some convergence between the Pacific and North America plates.

In addition to the great 1949 earthquake, a M = 7 earthquake occurred on 24 June 1970 off the southern end of the Queen Charlotte Islands (Rogers, 1986). A number of earthquakes with M > 5.0 have also occurred in the vicinity of the 1949 and 1970 events, but there is a distinct seismic gap between the locations of the 1949 and 1970 rupture zones (Rogers, 1986). Earthquake locations and the presence of thrust faulting instead of the expected right-lateral strike-slip faulting for events in the southern Queen Charlotte Islands indicate the presence of subsidiary faults east of the Queen Charlotte fault (Bérubé et al., 1989). Earthquakes in the Queen Charlotte fault region have depths down to around 20 km (e.g. Hyndman and Ellis, 1981). Closer to shore the depths become shallower. Bird (1997) calculated an average depth of around 10 km for events in the Graham Island/Hecate Strait region.

Explorer Region

The Explorer region consists of three small oceanic plates or blocks — the Explorer plate (formed $\sim$ 4 Ma), and the Winona and Dellwood blocks (formed $\sim$ 2 Ma). The Explorer plate is currently being overridden by the North America plate at a rate of about 22 mm/yr (Riddihough, 1977; Mazzotti et al., 2003b). The Winona block formed when a pre-existing structural weakness moved away from the continental margin at $\sim$ 2 Ma (Davis

and Riddihough, 1982). The motions of the Winona and Dellwood blocks are poorly constrained. However, young compressional structures in the Winona Basin sediments indicate convergence with North America (Davis and Currie, 1993).

Several fault zones and spreading centres with high rates of seismic activity are present in the Explorer region. The Nootka fault zone is a NE-SW trending fault zone which separates the Juan de Fuca and Explorer plates. The Nootka fault zone was initiated $\sim$ 4 Ma and resulted in the creation of the independent Explorer plate which moves separately from the Juan de Fuca plate (Riddihough, 1984; Hyndman et al., 1979). Prior to $\sim$ 7.4 Ma the Explorer ridge and Juan de Fuca ridge were one continuous spreading centre. The Explorer ridge is characterized by a linear volcanic ridge which evolved as a result of the fragmentation of the northern Juan de Fuca plate (Davis and Currie, 1993). At $\sim$ 7.4 Ma the Sovanco transform fault began to form as an offset between the Explorer ridge and Juan de Fuca ridge (Wilson et al., 1984). The Sovanco transform fault has migrated southward due to southward propagation of the Explorer ridge and has been lengthened by asymmetric spreading to the east on the Explorer ridge (Botros and Johnson, 1988).

North of the Explorer ridge lies the Revere-Dellwood-Wilson transform fault which links the Explorer ridge and the spreading centres of the Dellwood Knolls and Tuzo Wilson Seamounts. The Tuzo Wilson Seamounts are comprised of two major and numerous minor submarine volcanic edifices. The Tuzo Wilson Seamounts have been proposed to be the site of the most recently initiated spreading between the Pacific and Explorer plates (e.g. Keen and Hyndman, 1979; Riddihough et al., 1980; Carbotte et al., 1989). The Dellwood Knolls are two small volcanic peaks located southeast of the Tuzo Wilson Seamounts between the Winona and Dellwood blocks where spreading is occurring in tandem with the Tuzo Wilson Seamounts (Carbotte et al., 1989; Davis and Currie, 1993).

The Explorer region is one of the most seismically active regions in Canada with most of the offshore earthquake activity occurring along the boundaries of the Explorer plate and Winona and Dellwood blocks, and within the Explorer plate. More than 100 earthquakes of $M > 5.0$ have occurred in the Explorer region in the last 70 years (Ellis and Rogers, 1986) and each year 20–25 earthquakes with $M > 3.5$ occur in this region. Magnitudes in the Explorer region range from microearthquakes to the 6 April 1992 $M_w = 6.7$ event along the Revere-Dellwood-Wilson fault.

2.4 British Columbia Interior

The interior of British Columbia is defined here as the Cordillera region seaward of the Rocky Mountain Trench extending from the Canada/United States border in the south to the British Columbia/Yukon border in the north (Figure 2.2). The interior of British Columbia has relatively low seismic activity compared with the regions to the north and south (Figure 2.3). The rate of seismic activity quickly drops inland from the coast and increases on the eastern side of the Cordillera, in the region of the Rocky Mountain Trench and the Foreland Fold and Thrust Belt. The largest events to occur in this region were M = 5.5 on 21 March 1986 and M = 5.4 on 14 April 2001. Focal mechanisms in the British Columbia interior show predominantly thrust faulting in a northeast-southwest direction corresponding to compressional tectonics. This contrasts markedly with the extensional regime just south of the Canada/United States border in the northern American Cordillera. In addition to the natural seismicity there are regions where earthquake activity appears to be associated with oil and gas extraction, notably the Fort St. John area of NE British Columbia (Horner et al., 1994) and near Rocky Mountain House, Alberta (Wetmiller, 1986).

2.5 Yukon and Northwest Territories

The Yakutat block is a composite oceanic-continental allochthonous terrane that has migrated northwestward with the Pacific plate and is colliding obliquely with North America in the Gulf of Alaska (Figure 2.2). Along its eastern margin, most or all of the motion is accommodated by the right-lateral strike-slip Fairweather fault (Fletcher and Freymueller, 1999). Along its western and northern boundaries, the Yakutat block is being thrust underneath North America (Plafker et. al., 1994). A consequence of this collision is strong seismicity in the Mackenzie and Richardson Mountains of the northern Canadian Cordillera $\sim$ 800 km northeast of the collision zone. In between the collision zone and the Mackenzie and Richardson Mountains, $\sim$ 800 km to the northeast, the seismic activity is quite low. Mazzotti and Hyndman (2002) propose that deformation in the Richardson and Mackenzie Mountains results from a transfer of strain from the Yakutat collision across the northern Cordillera.

The main structural feature in the northern Cordillera is the Mackenzie Fold Belt which is the northern end of the larger Foreland Fold and Thrust Belt. The tectonic evolution of this region covers much of Earth history. The Slave craton to the east dates to 4.0–3.5 Ga (Isachsen and Bowring, 1994). West of the Slave craton most of the orogenic activity occurred around 2.1–1.85 Ga (Hildebrand et al., 1987; Hoffman and Bowring, 1984). Crustal stresses in this region are similar to the Cordillera in British Columbia with horizontal

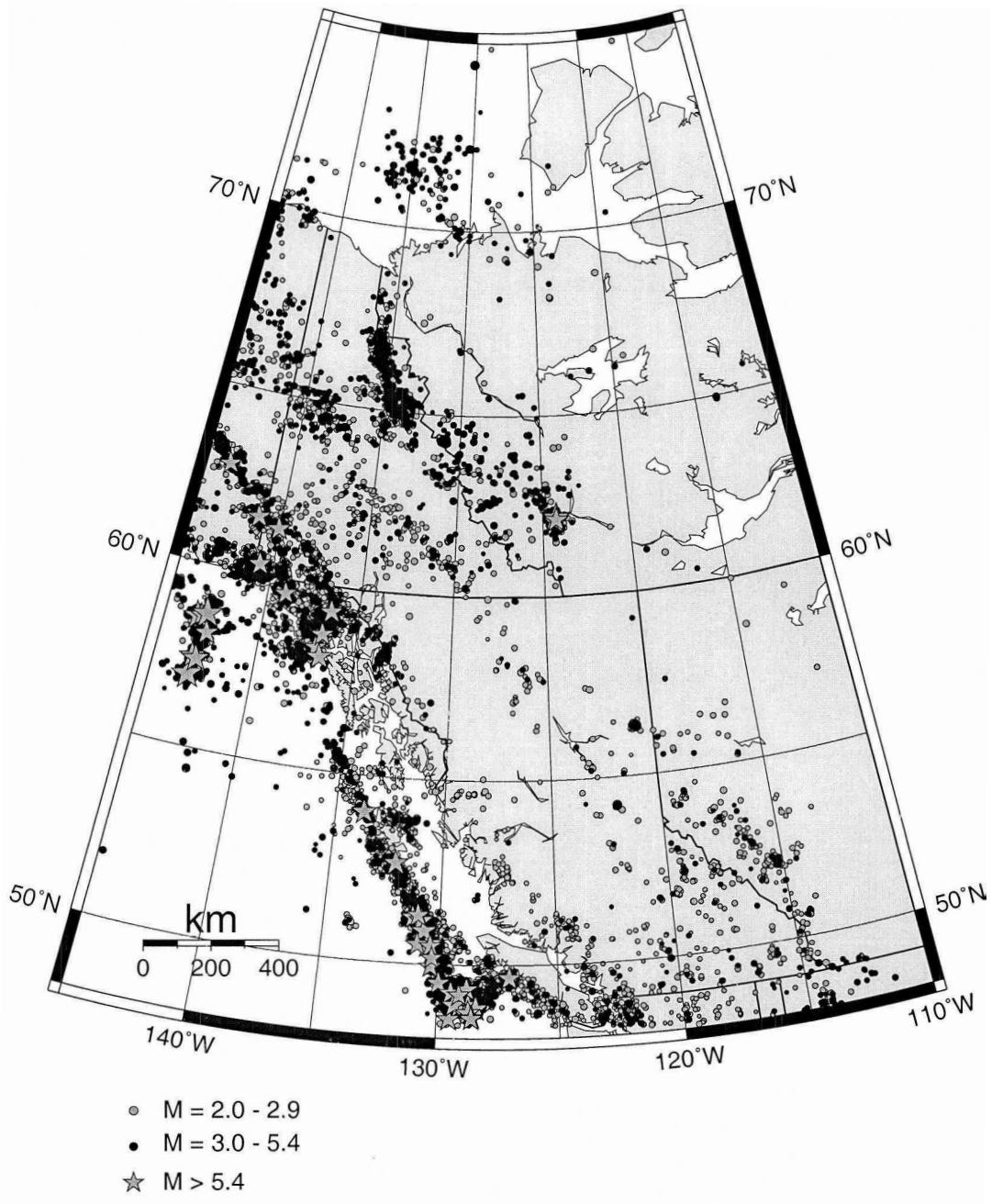

Figure 2.3 Seismicity (1982–2002) of the Cordillera and adjacent regions. The interior of British Columbia shows a much lower rate of seismic activity compared with the surrounding regions.

compressive stresses oriented in a NE-SW direction, although many north trending thrust faults and folds are prevalent throughout the region (Wetmiller et al., 1988).

Focal mechanisms in the southern Mackenzie Mountains (this study; Harvard catalogue) are shallow thrust faults striking N-S similar to the 5 October 1985 M = 6.6 and the 23 December 1985 M = 6.7 events. The 23 December 1985 event is the largest earthquake recorded in the eastern part of the Canadian Cordillera (Wetmiller et al., 1988). The seismicity pattern extends NW up to around 65°N latitude (Figure 2.3) and the focal mechanism orientations change to NE-SW compression and become a mixture of shallow thrust and right-lateral strike-slip faulting. The seismicity pattern then reverts to a N-S direction through to the Beaufort Sea. Few focal mechanisms are available for the Beaufort Sea region. However, the available mechanisms (this study; Harvard catalogue; Hasegawa et al. (1979)) show both E-W and N-S compression and a mixture of thrust and strike-slip faulting.

Chapter 3

Seismic Moment Tensor Theory and Method

3.1 Introduction

Routine calculation of moment tensor solutions at regional distances in western Canada and the United States Pacific Northwest has become possible in recent years due to the installation of more than 40 three-component broadband seismographs throughout western Canada, Washington, Oregon, and southeast Alaska (Figure 3.1) and increased computing power. This network has lowered the magnitude threshold for moment tensor analysis from about M = 5.0 to M = 4.0. In this study, robust waveform fitting techniques are employed to determine source mechanisms and depths of earthquakes with M $>\sim$ 3.5–4.0 in western Canada using code available from Chuck Ammon at Pennsylvania State University (Ammon, 2001). Some source parameters can also be estimated based on *P*-wave first motions, although sparse network coverage and inaccuracies in velocity models can result in unreliable solutions.

Earthquake source parameters are calculated by minimizing the least-squares misfit between observed and synthetic seismograms. The depth of the event is determined by calculating solutions over a range of depths, usually 3 km increments, and choosing the depth with the lowest rms misfit (e.g. Sipkin, 2000; Braunmiller et al., 1995). The inversion is carried out at regional distances ($<\sim$ 1000 km) and at low frequencies ($\sim$ 0.02–0.05 Hz) using data from all available stations simultaneously. At low frequencies the regional seis-

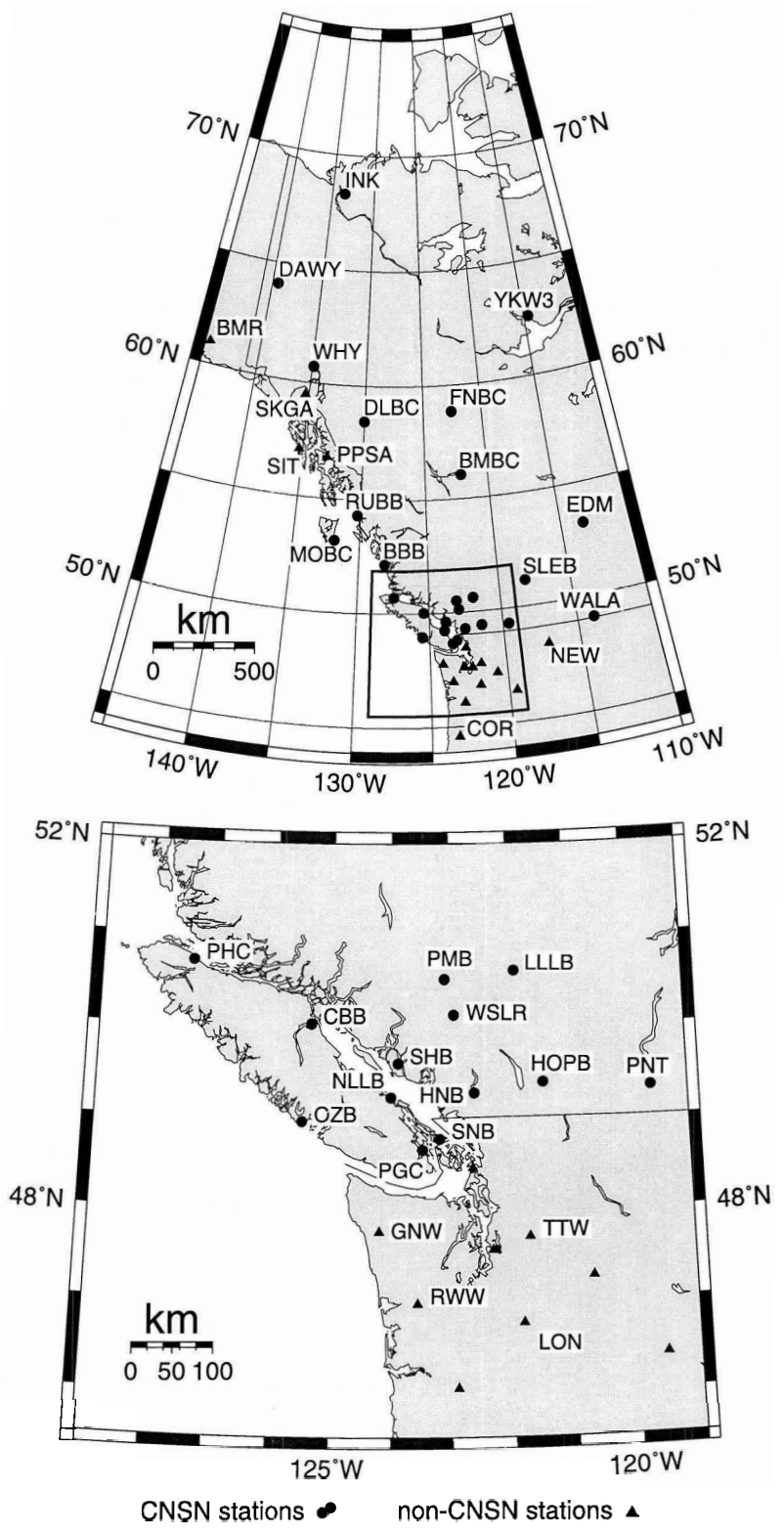

Figure 3.1 Three-component broadband stations in western Canada, the U.S. Pacific Northwest, and southeast Alaska.

mograms are dominated by surface waves which can be modeled using a simple 1-D velocity depth model (Randall, et al., 1995). The waveforms are then inverted using a time-domain moment tensor inversion scheme described by Langston (1981).

3.2 Seismic Moment Tensor Theory

The description of the physics of seismic sources is an important research area in seismology. A moment tensor completely describes in a first-order approximation the equivalent forces of a seismic point source (Jost and Herrmann, 1989). The strike, dip, slip, and seismic moment of an earthquake can be determined from the moment tensor and source depth can also be estimated from the inversion.

Tensors are a generalization of scalars and vectors. A tensor of order (or rank) zero is a scalar and a tensor of order one is a vector. Stress and strain tensors are represented by a tensor of order two, which can be written in matrix form as follows

$$\begin{bmatrix} M_{xx} & M_{xy} & M_{xz} \\ M_{yx} & M_{yy} & M_{yz} \\ M_{zx} & M_{zy} & M_{zz} \end{bmatrix}. \tag{3.1}$$

The main diagonal elements are pressure or tension forces (per unit area) and the others are shear forces (per unit area) (Figure 3.2).

In this study the strike of the fault plane, Φ, is measured clockwise from north with the fault plane dipping to the right when looking along the strike direction. The dip, δ, is measured down from the horizontal. The slip (rake), λ, is the angle between the strike direction and the direction the hanging wall moved relative to the foot wall (positive when measured counterclockwise as viewed from the hanging wall side) (Figure 3.3). With the strike, dip, and slip defined the Cartesian components of the moment tensor are

$$\begin{aligned} M_{xx} &= -M_o(\sin\delta\cos\lambda\sin 2\Phi + \sin 2\delta\sin\lambda\sin^2\Phi) \\ M_{yy} &= M_o(\sin\delta\cos\lambda\sin 2\Phi - \sin 2\delta\sin\lambda\cos^2\Phi) \\ M_{zz} &= M_o(\sin 2\delta\sin\lambda) \\ M_{xy} &= M_o(\sin\delta\cos\lambda\cos 2\Phi + 0.5\sin 2\delta\sin\lambda\sin 2\Phi) \\ M_{xz} &= -M_o(\cos\delta\cos\lambda\cos\Phi + \cos 2\delta\sin\lambda\sin\Phi) \\ M_{yz} &= -M_o(\cos\delta\cos\lambda\sin\Phi - \cos 2\delta\sin\lambda\cos\Phi) \end{aligned} \tag{3.2}$$

(Aki and Richards, 1980). The seismic moment, M_o, is defined as

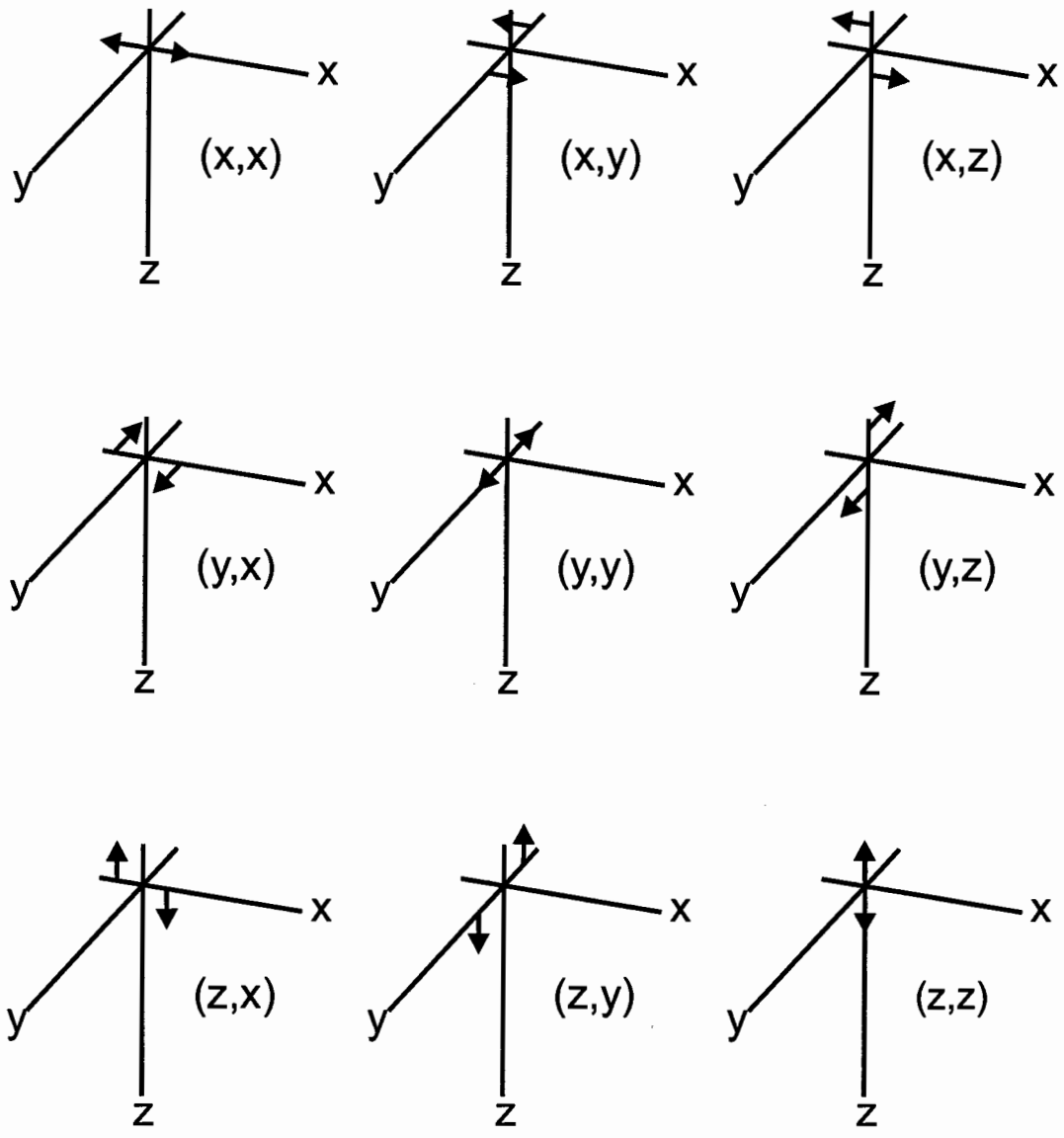

Figure 3.2 The nine generalized moment tensor elements (after Aki and Richards, 1980).

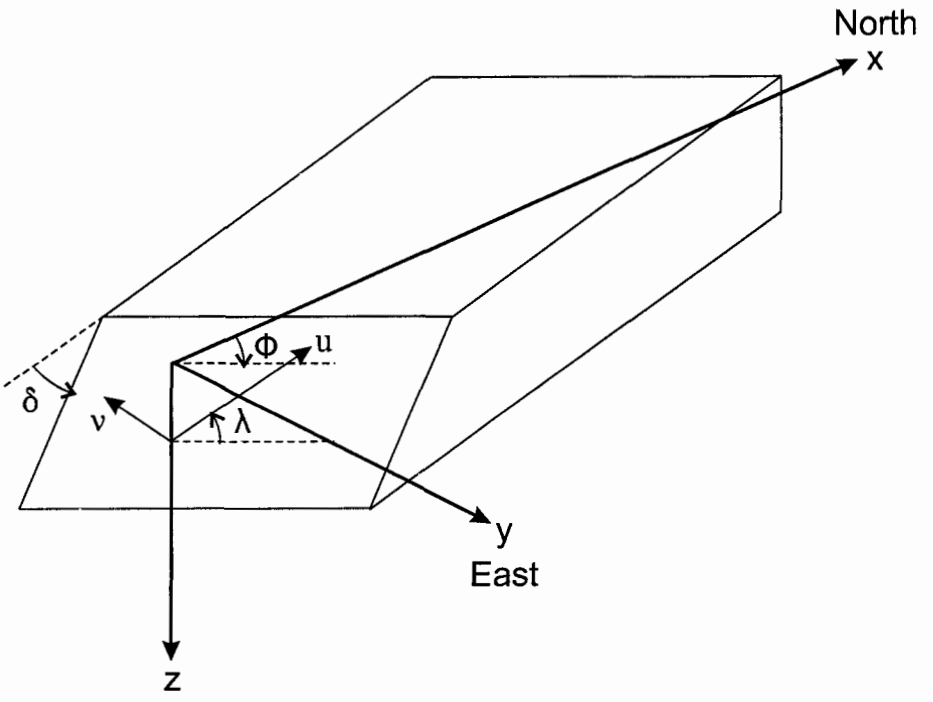

Figure 3.3 Definition of the cartesian coordinates used in this research. The origin is at the epicentre. Strike, ϕ, is measured clockwise from north, dip, δ, from horizontal down, and slip, λ, clockwise from horizontal. **u** and ν are the slip vector and fault normal, respectively (after Aki and Richards, 1980).

$$M_o = \mu A \bar{u} \tag{3.3}$$

where μ is the shear modulus, A is the area of the fault, and $\bar{u}$ is the average displacement on the fault.

An explosion will have no shear displacement, only main diagonal elements, and can be represented in tensor form as

$$\begin{bmatrix} M_o & 0 & 0 \\ 0 & M_o & 0 \\ 0 & 0 & M_o \end{bmatrix}. \tag{3.4}$$

A double couple will be represented by orthogonal tensor elements such as

$$\begin{bmatrix} 0 & M_o & 0 \\ M_o & 0 & 0 \\ 0 & 0 & 0 \end{bmatrix}. \tag{3.5}$$

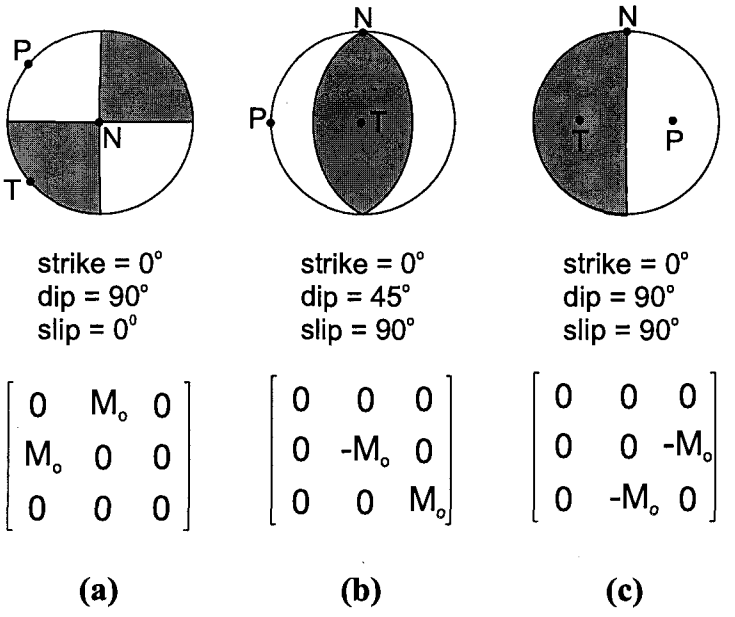

Figure 3.4 Focal mechanisms and moment tensor elements for the three general cases of a vertical strike-slip fault (a), a 45° dip-slip fault (b), and a vertical dip-slip fault (c).

Figure 3.4 shows the moment tensor elements for the three general cases of a vertical strike-slip, 45° dip-slip, and vertical dip-slip fault. Substituting the values for strike, dip, and slip for each of the cases in Figure 3.4 into equation 3.2 gives the moment tensor elements shown at the bottom of Figure 3.4. Any arbitrarily oriented fault plane can be expressed as a linear combination of these three cases.

A seismic moment tensor is always symmetric, i.e. $M_{xy} = M_{yx}, M_{xz} = M_{zx}$, etc., and can be rotated into any coordinate system. To rotate a tensor S, through an angle ϕ about a vertical axis the rotation is

$$B = A^T S A \tag{3.6}$$

where

$$A = \begin{bmatrix} \cos\phi & \sin\phi & 0 \\ -\sin\phi & \cos\phi & 0 \\ 0 & 0 & 1 \end{bmatrix} \tag{3.7}$$

and B is the rotated tensor.

One convenient rotation is to have the coordinate axes correspond to the P (pressure), T (tension), and N (null) axes (Figure 3.5). As an example, in Figure 3.4a the strike will become 45° and the dip and slip will remain the same. Using equation 3.6 and equation 3.7, equation 3.5 becomes

$$\begin{bmatrix} Mo & 0 & 0 \\ 0 & -Mo & 0 \\ 0 & 0 & 0 \end{bmatrix}. \tag{3.8}$$

When the moment tensor is diagonalized the main diagonal elements are the eigenvalues, m_i, of the tensor. The largest positive eigenvalue corresponds to the T axis, the largest negative eigenvalue to the P axis, and the intermediate eigenvalue to the N axis. In equation 3.8 it is assumed that M_{xx} is the largest eigenvalue, M_{yy} is the largest negative eigenvalue, and M_{zz} is the intermediate eigenvalue. The corresponding eigenvectors give the directions of the P, T, and N axes. The moment is then be calculated by

$$M_o = \frac{1}{2}(|m_1| + |m_2|) \tag{3.9}$$

where m_1 and m_2 are the largest eigenvalues in the absolute sense. The moment can also be calculated by

$$M_o = \sqrt{\frac{{m_1}^2 + {m_2}^2 + {m_3}^2}{2}} \tag{3.10}$$

where m_1, m_2, and m_3 are the three eigenvalues of the tensor. The moment magnitude (M_w) can be calculated from M_o by

$$M_w = \frac{\log M_o}{1.5} - 10.7 \tag{3.11}$$

where M_o is in dyne·cm, or

$$M_w = \frac{\log M_o - 9.0}{1.5} \tag{3.12}$$

where M_o is in Nm. This scale was derived by Kanamori (1977) to be consistent with surface-wave magnitude (M_s) but will not saturate since M_o does not saturate.

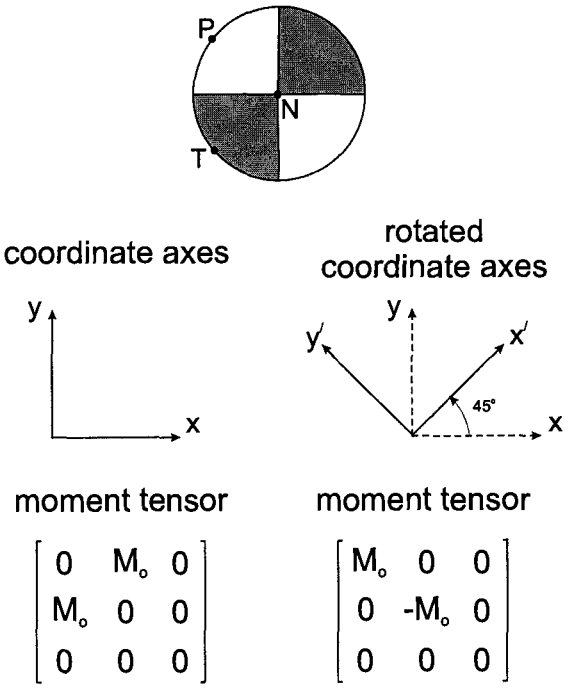

Figure 3.5 Moment tensors in different coordinate systems. By rotating the coordinate axes by 45° they can be made to correspond to the P and T axes.

3.3 Preparing the Observed Waveforms

Preparation of the observed waveforms is a relatively straightforward process which requires several steps including bandpass filtering of the waveforms for the appropriate frequency range, rotation of the horizontal components into radial and transverse components, removal of the instrument response, and sampling the data (Figure 3.6). Preparation of the observed waveforms is carried out using SAC (Seismic Analysis Code) software (Goldstein, 2000). For the vast majority of events the passband is 0.02–0.05 Hz. For earthquakes with M $\sim$ 4.0–5.5 this frequency range contains most of the low frequency energy and has a high signal-to-noise ratio. For larger events which radiate more energy at lower frequencies the passband is shifted to lower frequencies, while for smaller events the passband is shifted to higher frequencies to filter out long period noise. Depending on the size of the event and the data noise level, 5–10 stations are used. Three-component data are used. The data can be weighted but since closer stations are more consistent with the Earth model and have a larger amplitude, they contribute more to the solution. Therefore, further weighting is generally not necessary (Randall et al., 1995; Ammon, 2001).

For earthquakes occurring off the west coast of British Columbia, a number of broad-

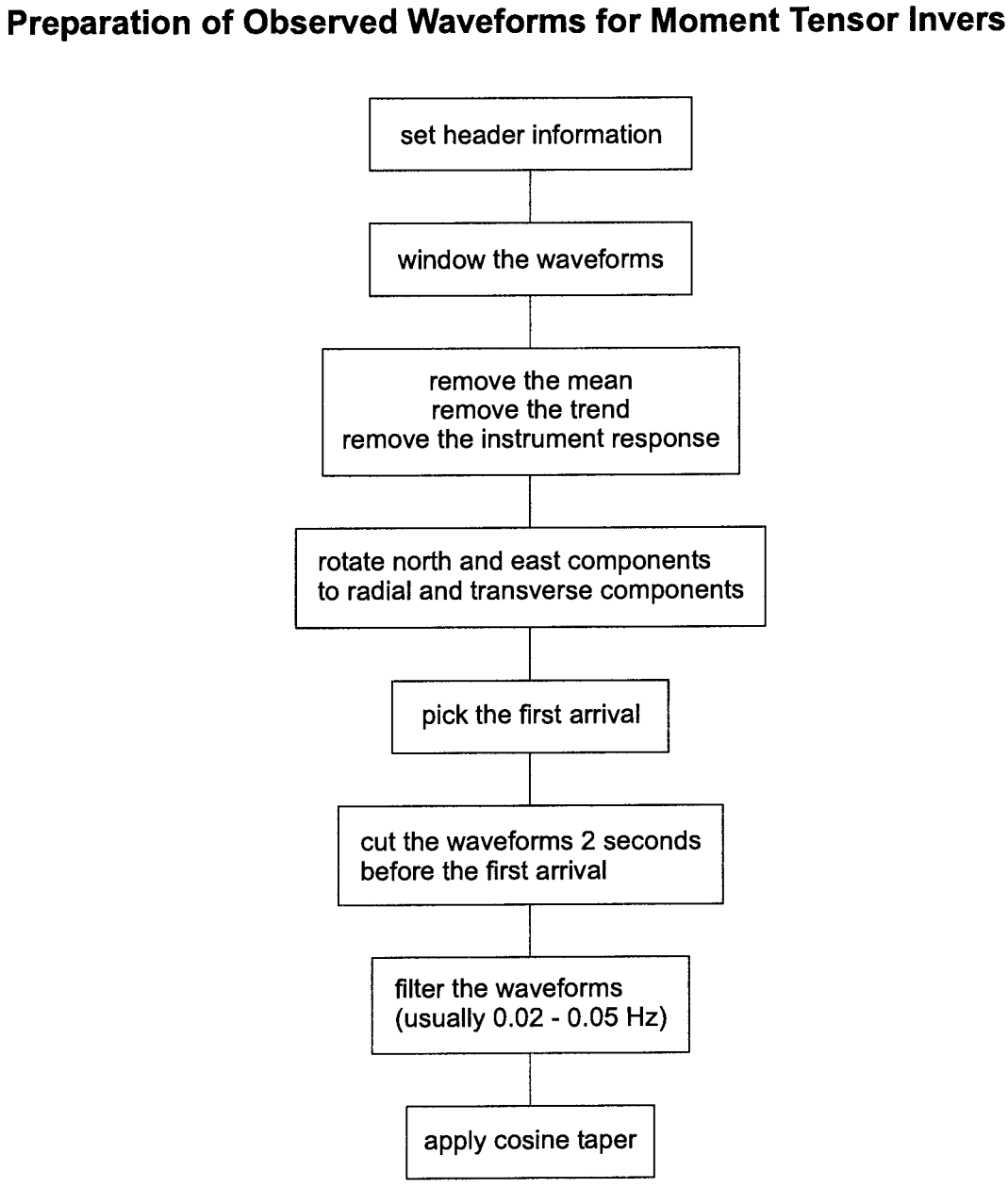

Figure 3.6 Flowchart outlining the steps required for preparing the observed seismograms for a moment tensor inversion.

band stations are available but they are all to the north and east of the events giving less than 180° azimuthal coverage. Although having a number of stations with good azimuthal coverage is desirable for calculating moment tensor solutions it is not required. Previous studies have obtained reliable moment tensor solutions with as few as one or two three-component broadband stations (e.g. Delouis and Legrand, 1999; Ratchkovski, 2001; Dreger and Helmberger, 1993). Therefore, having limited azimuthal coverage for offshore events is not a major concern. In Appendix C an example of a regional moment tensor solution calculated using one station, and an example using two stations is discussed. The regional moment tensor method could potentially be used to calculate moment tensor solutions for older events, prior to pre-digital data, when station coverage was limited. The events would have to be large enough to provide a good signal-to-noise ratio at distances greater than 1000 km but not too large as to go off scale on paper records. Earthquakes with $M_w \sim 4.5$–5.5 fit this criteria. Unfortunately there was no available digitized data from older events to directly test how well the method would work. Instead Appendix C shows several examples of regional moment tensor solutions calculated using only stations which were operational prior to the early 1990's compared with the solutions calculated using all of the presently available stations.

3.4 Green's Functions

3.4.1 Calculating Green's Functions

Several steps are required for calculating a regional moment tensor solution (Figure 3.7). The first step is to calculate the theoretical Green's functions. Green's functions are defined as the response of a system to an impulse. In the case of seismic moment tensors the system is the Earth and the impulse represents an earthquake. The response (seismogram) is the response of the Earth to the earthquake. The displacements are calculated by

$$d_n(\mathbf{x}, t) = \sum_{i=1}^{5} m_i * G_{in} \tag{3.13}$$

where d_n is the vertical, radial, or transverse displacement, $m_1 = M_{11}$, $m_2 = M_{22}$, $m_3 = M_{12}$, $m_4 = M_{13}$, and $m_5 = M_{23}$ (note $M_{33} = -(M_{11} + M_{22})$). G_{in} are the Green's functions corresponding to each of the respective moment tensor elements. Each Green's function i will give n components of displacements (in this case $n = 3$).

Synthetic Green's functions are calculated using an Earth model for the three general types of earthquake mechanisms: vertical strike-slip, vertical dip-slip, and 45° dip-slip faults. Vertical, radial, and transverse components are calculated for each orientation ex-

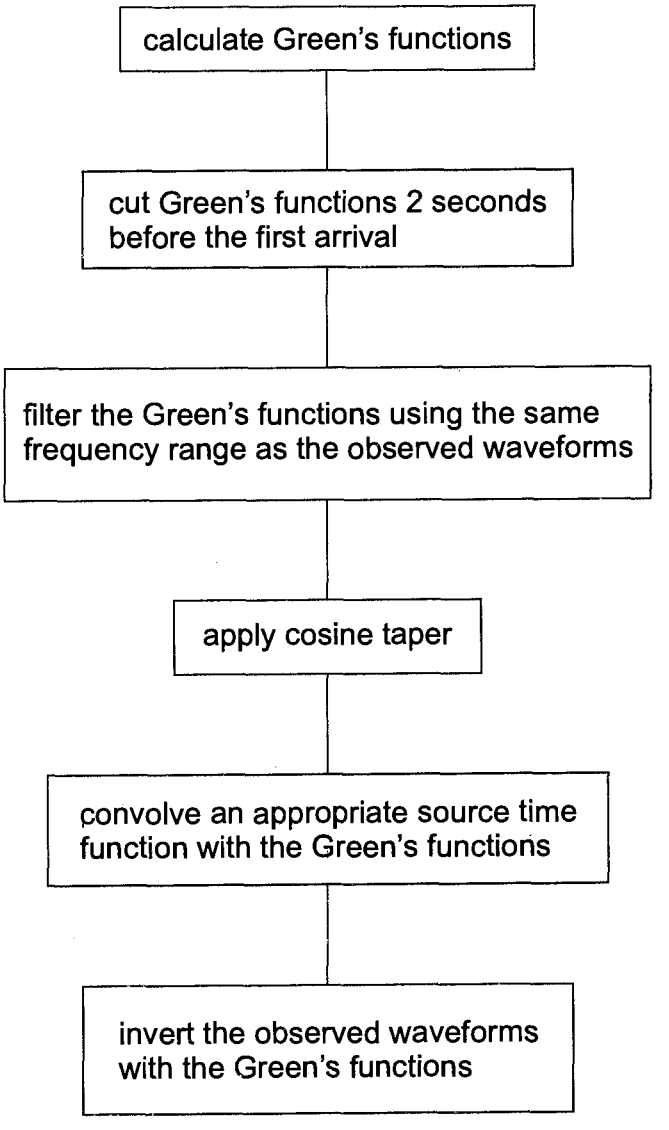

Figure 3.7 Flowchart outlining the steps required for calculating a regional moment tensor solution.

cept for the 45° dip-slip fault which does not have a transverse component (see Herrmann and Wang, 1985; Wang and Herrmann, 1980). Since a moment tensor is symmetric only six of the nine elements need to be calculated; $M_{xx}, M_{yy}, M_{zz}, M_{xy}, M_{xz}, M_{yz}$. There will be one set of Green's functions, consisting of six elements, for each station.

The Green's functions depend on the source-receiver distance and source depth, but not on the azimuth between the source and the receiver since the Earth model used to calculate the Green's functions is 1-D. Therefore, once the Green's functions are calculated at a given distance and depth for a particular Earth model, they can be saved and do not need to be calculated again. By calculating Green's functions over a range of distances and depths for a given Earth model, a library of Green's functions can be built up and the appropriate Green's functions for a particular station can simply be read in from the library instead of calculated. This greatly reduces the amount of computer time required for calculating a moment tensor solution since calculating the Green's functions takes most of the time. In this study Green's functions were calculated every 10 km and at a depth interval of 3 km. A 10 km distance interval means that a given Green's function will be off by no more than 5 km from the correct Green's function which is less than, or roughly equal to, the error in determining the location of an earthquake in most areas in western Canada (T. Mulder, per. comm.). Appendix C gives an example comparing a regional moment tensor solution calculated using Green's functions calculated to the nearest kilometre with a solution calculated using Green's functions calculated every 10 km.

3.4.2 Earth Models

Earthquakes in western Canada occur in a variety of tectonic settings and therefore a single 1-D Earth model is not sufficient to calculate regional moment tensor solutions. In this study several crustal models were used to calculate Green's functions depending on the source location and the source-receiver travel path. A list of the Earth models used can be found in Appendix E.

Calculating Green's functions for earthquakes occurring in the offshore region of Vancouver Island is particularly challenging. The source-receiver travel path is through oceanic crust, across the subduction zone, and into continental crust. A single 1-D Earth model cannot adequately represent the entire travel path. Stations located in the Queen Charlotte Islands region (e.g. MOBC, BBB, RUBB) have a source-receiver travel path which is mostly through oceanic crust and then through a transition from oceanic to continental crust. Stations on Vancouver Island (e.g. PHC, CBB, OZB, PGC) have a source-receiver travel path which includes the subducting slab as well as oceanic and continental crust

which makes the travel path more complex. Stations located in the interior of British Columbia (e.g. LLLB, PNT, BMBC, SLEB) have the majority of the travel path through continental crust and therefore a continental crust type Earth model works well. Western Canada is divided into six different regions for calculating regional moment tensor solutions (Figure 3.8). The appropriate Earth models are used for each station in each region. No earthquakes large enough to calculate an regional moment tensor solution have occurred in the hatchered region in Figure 3.8 during the study period. Therefore, no Earth models have been developed for this region.

To develop the Earth models, several moment tensor solutions calculated by OSU and Harvard were chosen as reference events. The Earth models were then developed empirically by attempting to reproduce a moment tensor solution using only one or two stations. The displacement field from a given double-couple mechanism is unique. Therefore, if the entire displacement field at a given point can be modeled, it should be possible to determine the source mechanism, i.e. three-component data from a single station should be sufficient to determine the source parameters of an earthquake. Appendix C compares examples of regional moment tensor solutions calculated using only one or two stations with solutions calculated using many stations.

Stations in the Queen Charlotte Islands region will be used as an example to illustrate the procedure that was followed to develop the crustal models. The Earth models used to begin with were the models employed to locate offshore earthquakes. BBB was chosen to start and the thickness and number of layers, velocities, Poisson's ratios, and densities in the Earth model were adjusted in order to produce theoretical waveforms which minimized the misfit between the observed waveforms and reproduced the moment tensor solution. Since the goal is to use a simple 1-D model to represent a complex source-receiver travel path, the crustal models are not entirely realistic. Instead it was decided it was more important that the models produce Green's functions which lead to theoretical waveforms that provide a good fit to the observed waveforms and give reasonable solutions. Once an Earth model was found that produced the desired solution for BBB, the same model was tested for MOBC. The assumption is that the source-receiver travel path for an offshore event should be similar for both BBB and MOBC. If the Earth model did not produce the desired solution for MOBC it was adjusted until the desired result was obtained. The new Earth model was then tested with BBB to check for consistent results. The procedure was repeated until an Earth model was found that gave consistent results for BBB and MOBC when used individually and together. A similar procedure was used for the other regions.

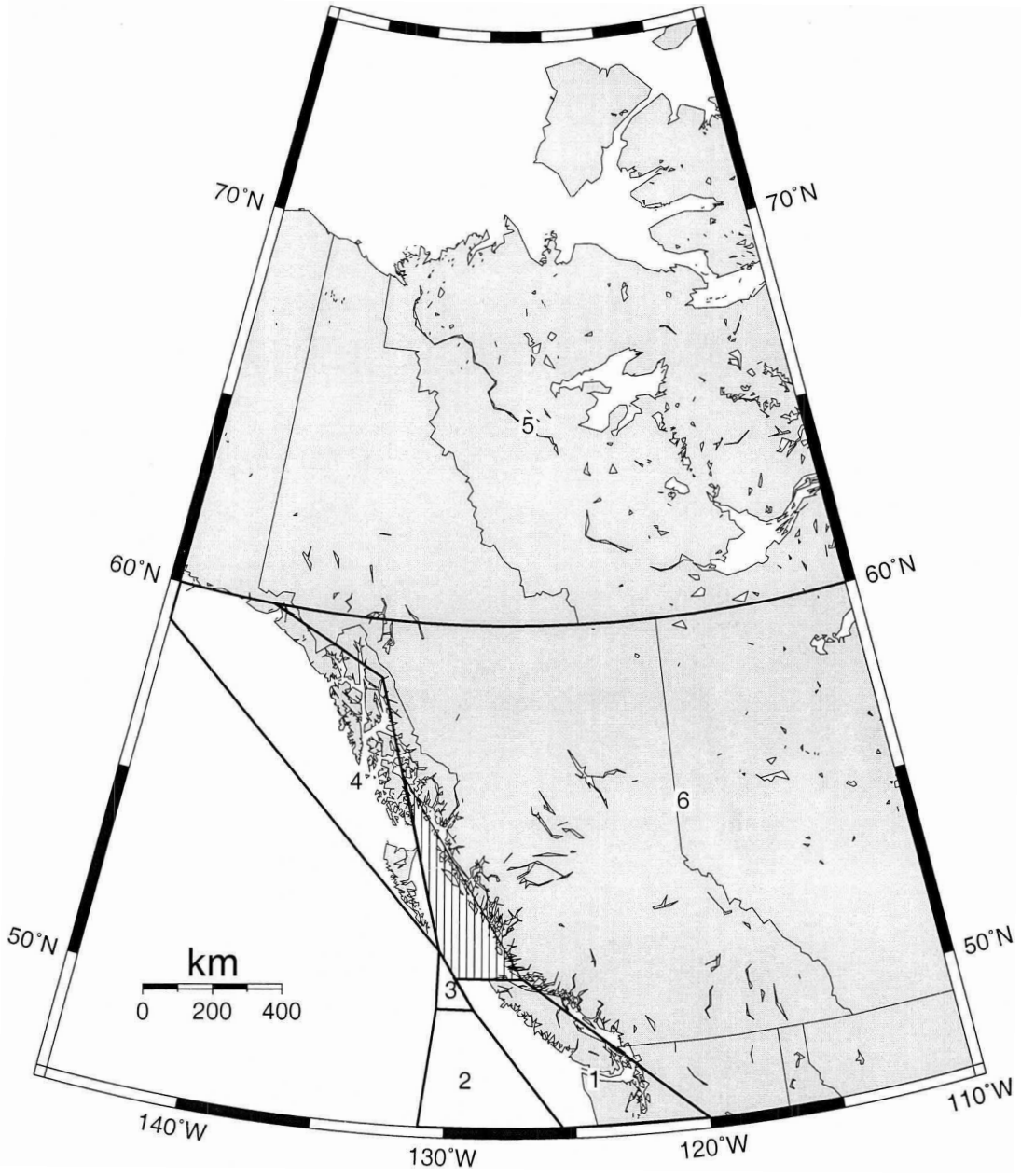

Figure 3.8 Six regions where Earth models have been developed for calculating regional moment tensor solutions. The appropriate Earth models are used depending on the location of the earthquake. No regional moment tensor solutions have been calculated for the hatchered region. Therefore, no Earth models have been developed for this region.

In the northern Cordillera (Yukon and Northwest Territories) the tectonic setting is more straightforward. All of the stations used to calculated regional moment tensor solutions in the northern Cordillera, with the exception of YKW3, will have a similar source-receiver travel path. Lithoprobe surveys have been conducted in the southern Yukon and Northwest Territories and the crustal models from those surveys were used to begin with. Again the starting Earth model was adjusted to minimize the misfit between the theoretical and observed waveforms. For station YKW3 a model more appropriate to the Canadian Shield was used which gave a good fit to the data.

3.5 Intermediate Steps

After the Green's functions are calculated they are cut two seconds before the first arrival to match the observed waveforms. The Green's functions are then lowpass filtered using the same frequency range as the observed waveforms and a cosine taper is applied. These parameters are not inverted for, but are applied to the Green's functions prior to the inversion. The goal is to use the same signal processing parameters on both the observed waveforms and the Green's functions.

The final step before the inversion is to convolve an appropriate source time function with the Green's functions. Large earthquakes (e.g. $>\sim$ 7.0) can have complex source time functions and may require a large amount of effort to adequately model. Smaller earthquakes can be represented with a fairly simple source time function. For regional moment tensor solutions for earthquakes with M $<\sim$ 6.5 a simple triangle or trapezoidal source time function is sufficient to model the source (Ammon, 2001). The source time function will have a rise time, centre time, and fall time. The parameters of the source time function are not inverted for but are set prior to the inversion. After the inversion the source time function parameters are changed and the inversion is again carried out. This process is repeated to find the source time function parameters which results in the minimum misfit between the theoretical and observed seismograms. Normally very few iterations are required to find the best source time function parameters. It should be noted that mathematically, once a Green's function is convolved with a source time function, it is no longer a Green's function. However, for simplicity and to avoid extra terminology, in this discussion a Green's function convolved with a source time function will still be referred to as a Green's function.

3.6 Inversion

Using the observed displacements, d_n, and the Green's functions, G_n, we can invert for the moment tensor elements. The most common method is by a least squares inversion where equation 3.13 is formulated in matrix form as

$$\mathbf{d} = \mathbf{G}\bar{\mathbf{m}} \tag{3.14}$$

where $\mathbf{d}$ consists of n waveforms, $\mathbf{G}$ is a $n \times 6$ matrix consisting of the Green's functions, and $\bar{\mathbf{m}}$ is the vector containing the moment tensor elements to be determined. Written out in full equation 3.14 would be

$$\begin{bmatrix} d_1 \\ d_2 \\ \vdots \\ d_n \end{bmatrix} = \begin{bmatrix} G_{11} & G_{12} & \cdots & G_{16} \\ G_{21} & G_{22} & \cdots & G_{26} \\ \vdots & \vdots & & \vdots \\ G_{n1} & G_{n2} & \cdots & G_{n6} \end{bmatrix} \begin{bmatrix} m_1 \\ m_2 \\ \vdots \\ m_6 \end{bmatrix}. \tag{3.15}$$

When $n > 6$ the system is overdetermined. The moment tensor can then be thought of as an unknown multi-channel filter whose input is the set of Green's functions and whose output is a set of theoretical seismograms. The input Green's functions are taken as known, and the inversion procedure determines the filter (moment tensor) that makes the output agree as well as possible, in a least-squares sense, with the observed seismograms (Sipkin, 1986).

The moment tensor inversion results give the moment tensor for which the eigenvalues and eigenvectors (which correspond to the P, T, and N axes) of the moment tensor can be calculated. The moment, moment magnitude, percentage of the double couple component, rms error, and strike, dip, and slip of the focal mechanism can then be determined. The percentage of the double couple component is calculated by

$$(1 - 2\epsilon) \times 100. \tag{3.16}$$

ϵ is given by

$$\epsilon = \frac{m_{min}}{m_{max}} \tag{3.17}$$

where m_{min} and m_{max} are the smallest and largest eigenvalues respectively in the absolute sense (Dziewonski et al., 1981). The regional moment tensor solutions calculated in this study have an average double couple percentage of 70%, and more than half the solutions are more than 75% double couple. It takes less than one hour to calculate a regional

moment tensor solution if the Green's functions have already been calculated. There is an earthquake large enough to a regional moment tensor solution approximately every one to two weeks in western Canada.

3.7 Moment Tensor Solutions

Regional moment tensor solutions for more than 370 earthquakes in western Canada, the U.S. Pacific Northwest, and southeast Alaska have been calculated for 1995–2003 (Appendix A). Appendix A also contains a list of the regional moment tensor solutions calculated by OSU from 1994–1998 and Harvard centroid moment tensor solutions from 1976–2003. A more detailed list containing moment tensor elements for the PGC regional moment tensor solutions and selected Harvard centroid moment tensor solutions is available as an electronic supplement. All of the regional moment tensor solutions calculated by OSU, except 14, were re-calculated in order to have a consistent data set. The 14 solutions that were not re-calculated were due to the original waveform data not being available and those events are indicated by a "*" in Table A.2. Harvard solutions in Table A.3 for which a regional moment tensor solution was also calculated are indicated by a "*". All of the moment tensor solutions calculated for western Canada are listed in Appendix A regardless of whether a regional moment tensor solution was calculated in this study. Therefore, in many cases two or three moment tensor solutions will be available for a single event.

Examples of waveform fits for several regional moment tensor solutions of varying magnitude and location are presented in Appendix B. These examples show the varying quality of the regional moment tensor solutions depending on the magnitude and location of the event. Appendix C shows a comparison between regional moment tensor solutions calculated in this research and the equivalent Harvard and USGS moment tensor solutions for three larger events. Appendix C also compares several regional moment tensor solutions calculated in this research with OSU regional moment tensor solutions for the same events to demonstrate that the two methods give solutions that are consistent.

Chapter 4

Moment Magnitude - Local Magnitude Calibration

4.1 Introduction

There are four main magnitude scales used to estimate the size of an earthquake: local magnitude (M_L), body-wave magnitude (m_b), surface-wave magnitude (M_s), and moment magnitude (M_w). M_L is measured using the maximum peak-to-peak amplitude of the regional distance S wave. M_L is described in more detail in section 4.2. Beyond regional distances the direct P arrival is a distinct phase and m_b can be calculated based on the P-wave amplitude. The typical period range for the P-phase is 1–10 s (Lay and Wallace, 1995). At distances beyond about 600 km, long period seismograms of shallow earthquakes are dominated by surface waves with a period of approximately 20 s (Lay and Wallace, 1995). M_s is calculated using the amplitude of the 20 s Rayleigh wave. Deep earthquakes ($>\sim$ 50 km) do not generate much surface wave amplitude and there is no correction for source depth. Therefore, M_s is not accurate for deep earthquakes. M_w is not limited to a particular phase but instead uses the entire waveform to calculate the magnitude. M_w is described in detail in Chapter 3.

M_L was the first magnitude scale to be developed in an attempt to quantitatively describe the size of an earthquake. It was developed by Richter (1935) specifically for earthquakes in southern California. M_L is now widely used using standard techniques but in tectonic environments that can be completely different from southern California. There-

fore, it is necessary to calibrate M_L so that it gives magnitudes that are consistent with other magnitude scales such as m_b, M_s or especially M_w.

It has been known for some time that M_L values calculated by PGC for earthquakes off Canada's west coast are underestimated by at least 0.5 magnitude units compared with other magnitude scales (e.g. Milne et al., 1978; Hyndman and Weichert, 1983). Comparison of M_L with m_b has been previously examined for earthquakes off the west coast of Vancouver Island (e.g. Weichert and Horner, 1985) and for the Gulf Islands/southern Vancouver Island region (e.g. Rogers and Muraro, 1981). These studies have found M_L to be consistently lower than m_b by 0.4 to 0.9 magnitude units depending on the region.

With the ability to calculate regional moment tensor solutions for earthquakes with $M >\sim 3.5$–4.0 in western Canada, it has become possible to build up a large catalogue of M_w's for offshore events. More than 250 moment tensor solutions for earthquakes off Canada's west coast have been calculated in this study for 1995–2003. These solutions, along with 14 regional moment tensor solutions calculated by Oregon State University (OSU) from 1994–1995 and 26 Harvard centroid moment tensor solutions from 1976–1993, allow for the first M_w-M_L calibration for earthquakes off Canada's west coast.

4.2 The Local Magnitude Scale

The original Richter (1935) formula is written as

$$M_L = \log A - \log A_o \tag{4.1}$$

where A and A_o are the amplitude of the displacements of the earthquake and a reference event at a prescribed distance, respectively, as measured on a Wood-Anderson seismograph. Richter's original method used the largest peak-to-peak amplitude regardless of the phase (Richter, 1935). However, in practice M_L is normally standardized as using the maximum amplitude of the regional distance S-wave denoted L_g (Hutton and Boore, 1987; Lay and Wallace, 1995). The L_g phase is a multiply reflected SH-wave which travels along a wave guide near the surface of the continental crust. M_L values can vary considerably from station to station depending on the radiation pattern and travel path. Therefore, M_L is normally calculated at several stations at a range of azimuths and the values averaged to give the M_L for the earthquake (Lay and Wallace, 1995).

For earthquakes in western Canada, including the offshore region, the method used for the Canadian catalogue to calculate M_L is similar to Richter (1935). The main difference

is that the maximum amplitude is measured from the vertical component whereas Richter (1935) used the horizontal components. Up until the last decade most stations in western Canada were vertical single-component stations. Therefore, an M_L formula was derived using vertical component data even though the *SH*-wave is horizontal. There are also two corrections that are applied. One is a modification of the Richter (1935) distance correction which was originally calculated out to 600 km. The distance correction has been extended to 1000 km for earthquakes in western Canada. The second correction is a period correction to adjust for the different frequency responses of the seismometers currently used compared with a Wood-Anderson seismometer.

The main difficulty in calculating M_L off Canada's west coast is that a portion of the source-receiver travel path is through oceanic crust. The L_g phase does not propagate through oceanic crust when the length of the oceanic crustal path is greater than 100 to 200 km due to the structure of the crustal wave guide, in particular the crustal thickness (Press and Ewing, 1952; Zhang and Lay, 1995). For events occurring off Canada's west coast, M_L is calculated using the maximum amplitude of the S_n phase (head wave traveling along the Moho). The formula used for calculating M_L using the S_n phase is the same as for calculating M_L using the L_g phase. This includes using the same distance correction (W. Bentkowski, per. comm.).

4.3 Moment Magnitude - Local Magnitude Calibration

4.3.1 Previous Studies

No previous studies have been carried out to compare M_L with M_w off Canada's west coast. Hanks and Kanamori (1979) derived a M_o-M_L relation for continental earthquakes but it is not valid for earthquakes occurring in oceanic crust. Braunmiller and Nábělek (2002) compared M_w's from OSU regional moment tensor solutions and Harvard centroid moment tensor solutions with m_b and M_s values for the region off Canada's west coast from 1994–1998. They found that M_w is systematically larger than m_b by 0.46 magnitude units on average, and M_w and M_s are equivalent only for $M_s \geq 5.8$. These results are consistent with M_w also being systematically larger than M_L (see Appendix C for more details on PGC versus OSU regional moment tensor solutions).

4.3.2 Canadian Cordillera Earthquakes

Events occurring in the onshore region of western Canada provide an opportunity to verify that M_w and M_L are equivalent when the source-receiver travel path is entirely through

continental crust. The onshore region is defined here as the interior of British Columbia, Alberta, and the Yukon and Northwest Territories. Also included are a few events from NW Montana near the Alberta/Montana border. All of the events were examined as one region (Figure 4.1a) and divided into events occurring north of 60°N (Figure 4.1b) and south of 60°N (Figure 4.1c). The dashed line represents an ideal 1:1 relationship between M_w and M_L and the solid line is a best-fit line assuming a slope parallel to the 1:1 line (see section 4.3.3 for details). In all three cases M_w and M_L show very good agreement along the 1:1 line demonstrating that M_w and M_L are consistent in western Canada when the source-receiver travel path is entirely through continental crust.

4.3.3 Offshore Earthquakes

In the offshore region of Vancouver Island more than 290 moment tensor solutions have been calculated in this study and by OSU and Harvard with magnitudes ranging from M_w = 3.4–6.7. To determine a M_w-M_L relation the region off Canada's west coast is divided into three zones (Figure 4.2). The difference between the three zones is the amount of oceanic crust present in the source-receiver travel path. The majority of the stations used in calculating both M_w and M_L are located on Vancouver Island and southwest British Columbia near the coast. Figure 4.2 shows examples of the source-receiver travel path to station PGC which would represent a typical travel path for offshore events. For events in Zone 1 virtually the entire travel path is through the North America plate which, along the continental margin, is mostly continental crust (although some components of the continental crust may have originated as oceanic crust). For events occurring in Zone 2 and Zone 3 part of the travel path is through oceanic crust with Zone 3 having a greater amount of oceanic travel path.

Events along the Nootka Fault Zone provide an opportunity to examine the effects of increasing amounts of oceanic crust in the travel path. All of the earthquakes occur along the same fault zone but the amount of oceanic crust in the travel path varies from $\sim$ 0–150 km (Figure 4.3). Figure 4.4a shows the distance from the source to station BBB for all the events along the Nootka Fault Zone. BBB was chosen since the amount of continental crust present in the travel path is roughly the same for all of the events. There were four earthquakes (strike-slip, $\sim$ 20–30 km depth) that occurred just off the west coast of Vancouver Island in approximately the same location (Figure 4.3). Using the average distance between these four events and BBB as the amount of continental crust present in the source-receiver travel path, the amount of oceanic crust present can be calculated (Figure 4.4b).

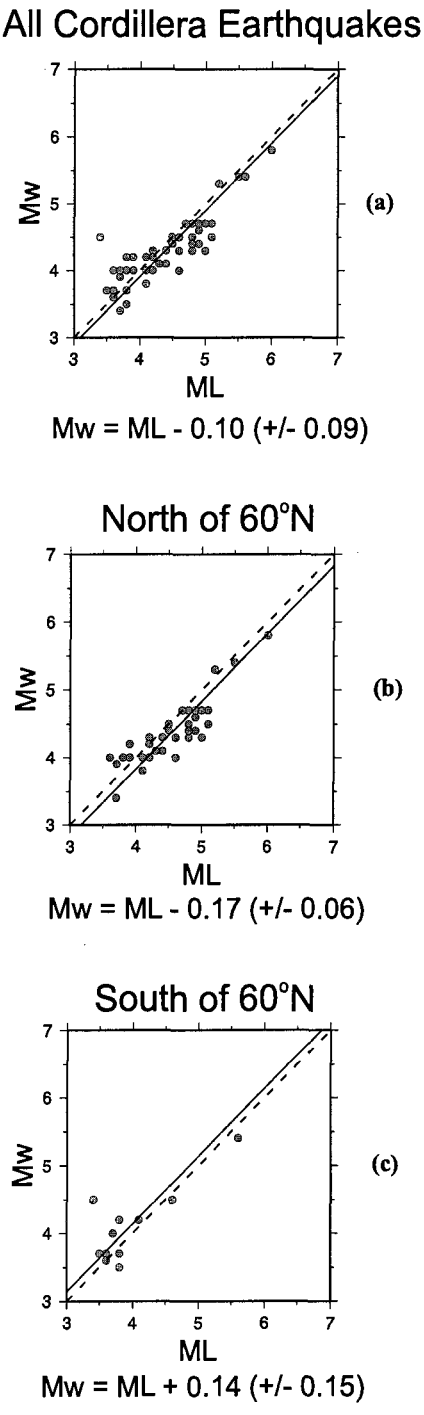

Figure 4.1 (**a**) M_w-M_L comparison for onshore events in western Canada. In each case the dashed line represents an ideal 1:1 relationship between M_w and M_L and the solid line is a best-fit line assuming a slope parallel to the 1:1 line. (**b**) M_w-M_L comparison for events north of 60°N. (**c**) M_w-M_L comparison for events south of 60°N.

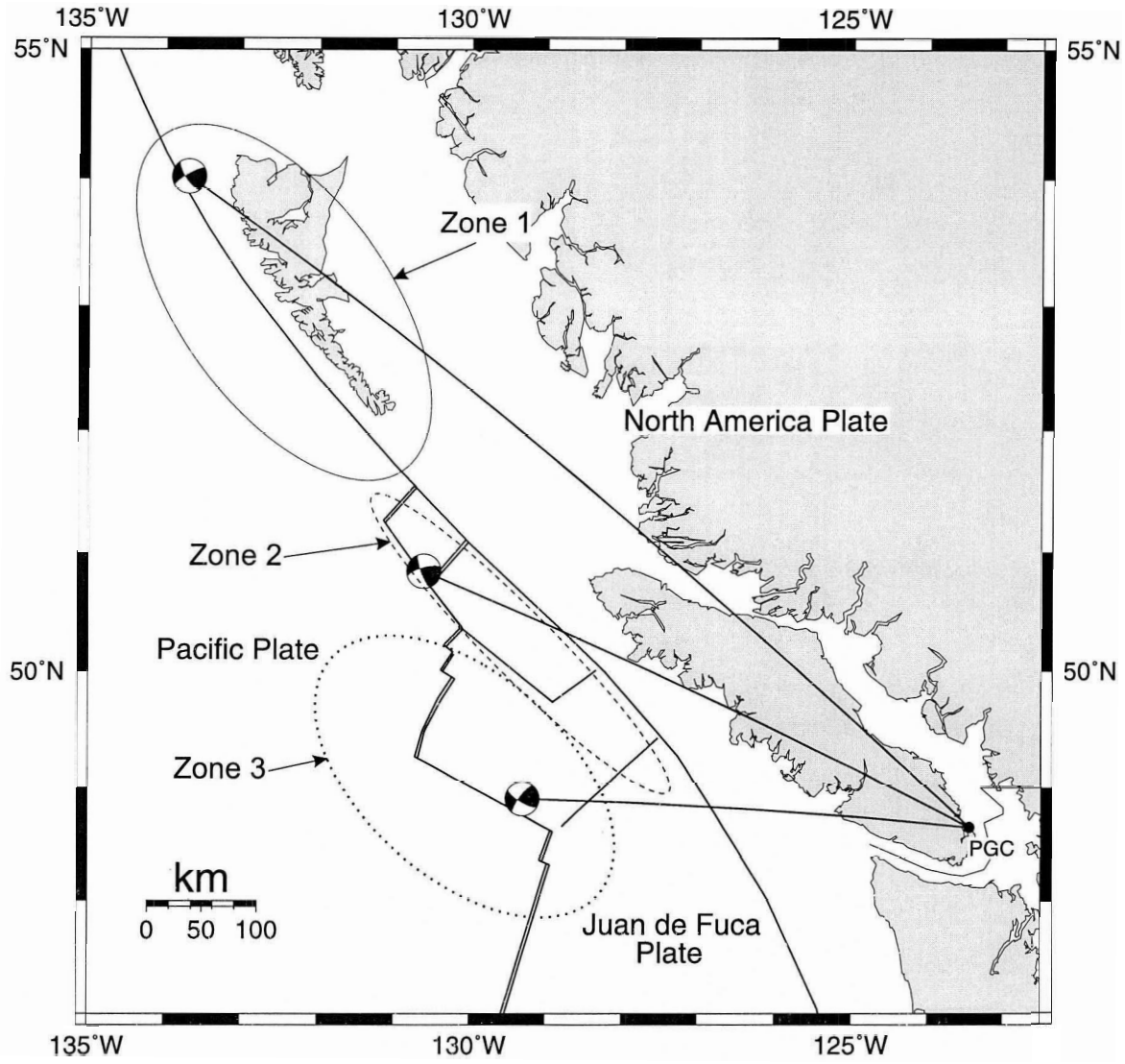

Figure 4.2 The three zones used in calculating the M_w-M_L relationship for the offshore region of western Canada. Also shown are representative travel paths for events occurring in each of the zones.

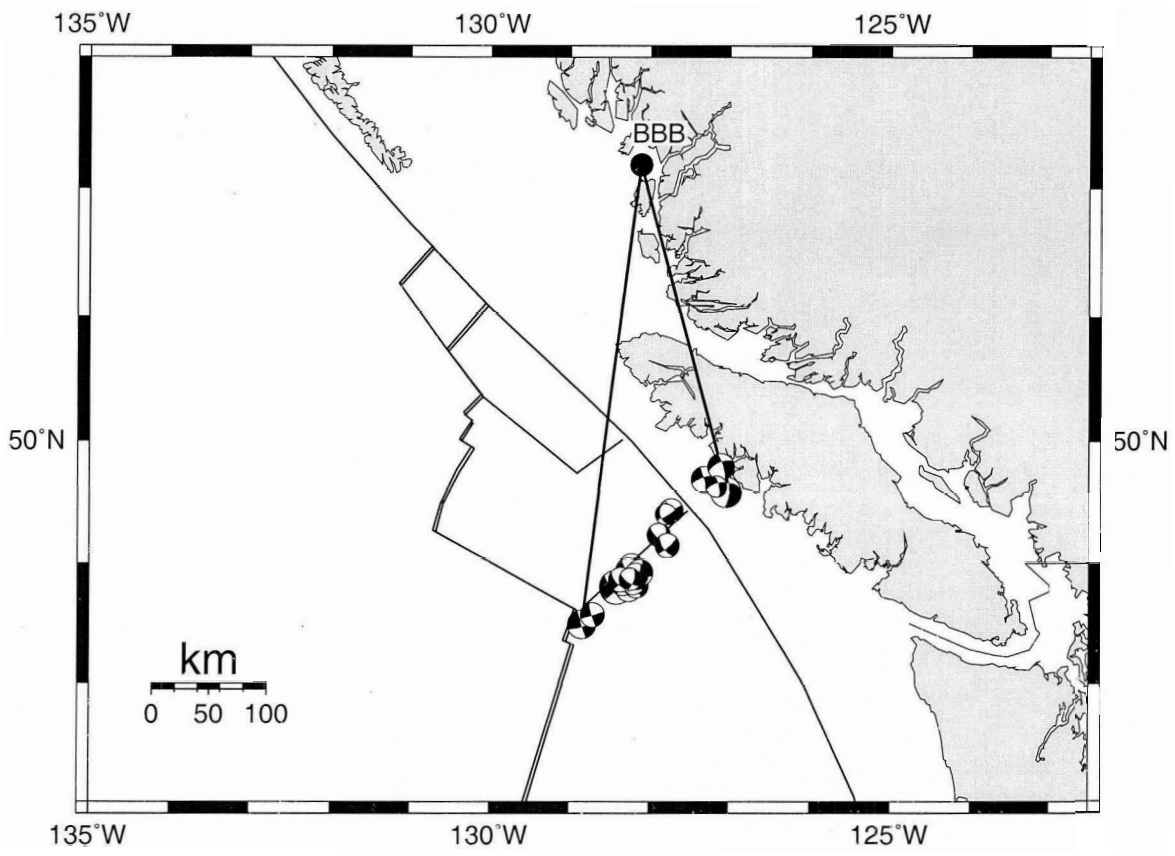

Figure 4.3 Location of events along the Nootka fault zone relative to stations BBB and the amount of oceanic crust present in the travel path.

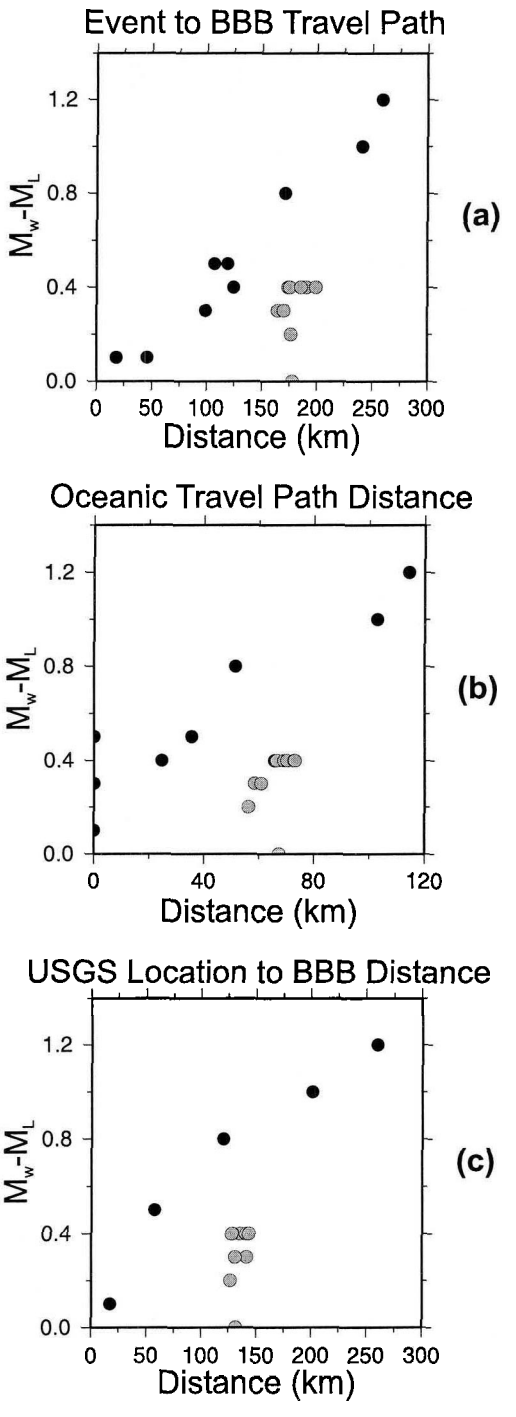

Figure 4.4 **(a)** Distance from events along the Nootka Fault Zone to station BBB and discrepancy between M_w and M_L. Grey events occurred in the period 1996/10/06–1996/10/14. **(b)** Amount of oceanic crust present in the travel path for events in **(a)**. **(c)** Source-receiver distance as in **(a)** except using locations from the USGS catalogue.

All of the events show an increasing discrepancy in M_w-M_L as the amount of oceanic crust present in the source-receiver travel path increases. The exception is the grey group of events which all occurred within a week of each other in early October, 1996 — a M_w = 6.3 mainshock on 6 October 1996 and several large aftershocks. To see if there might be any errors in the locations of the events, the source-receiver distances were calculated using locations from the USGS catalogue (Figure 4.4c). Note that the USGS did not calculate locations for all of the events in Figure 4.4b The same pattern is present when using the USGS locations which suggests that the locations are correct. Since all of the events are related to one another there may be something anomalous about them, but thus far there is no reason to exclude these events from the analysis.

Figure 4.5 shows the number of events and magnitude distribution for each of the three zones in Figure 4.2. Zone 2 and Zone 3 are examined as one region and as separate regions. The data set for Zone 1 is relatively small, less than 20 events; however, a total of 274 events are used in Zone 2 and Zone 3 with most having M_w's between 4.0 and 5.0. The number of events and the magnitude distribution for Zone 2 and Zone 3 are very similar.

Figure 4.6 shows all of the events plotted for each of the three zones. Zone 2 and Zone 3 are shown as one region and as separate regions. For each zone the dashed line represents an ideal 1:1 relationship between M_w and M_L, and the solid line is a best-fit line assuming a slope of one (i.e. parallel to the 1:1 line). The offset for the best-fit line is calculated by taking the average of the residuals between M_w and the 1:1 line. The variance of the residuals is used as the error.

In Zone 1 (top left, Figure 4.6) the data set is fairly small — less than 20 events — but they agree very well with the best-fit line. In Zone 1 M_L is, on average, 0.29 ± 0.07 magnitude units lower than M_w. When Zone 2 and Zone 3 are combined (top right, Figure 4.6) there is a fairly wide scatter in the data; however, M_w is consistently larger than M_L. In this case M_w is larger than M_L by 0.62 ± 0.08 magnitude units on average. When Zone 2 and Zone 3 are analyzed separately there is a distinct difference between them (Figure 4.6, bottom left and bottom right). When Zone 2 is analyzed on its own the discrepancy between M_w and M_L is not as large — 0.55 ± 0.06 magnitude units on average — and the scatter in the data is lower. In contrast, when Zone 3 is analyzed on its own the discrepancy between M_w and M_L is larger — 0.69 ± 0.10 magnitude units on average.

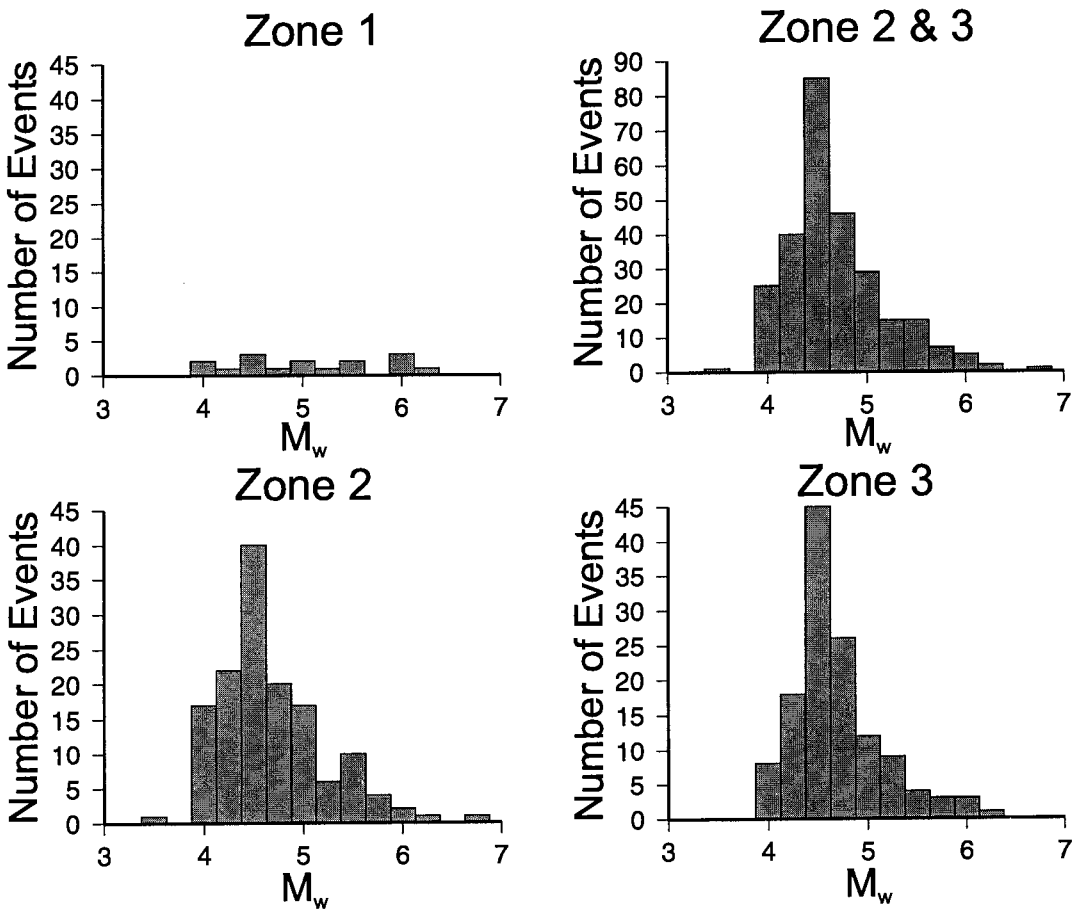

Figure 4.5 Histograms showing the number of events and magnitude distribution for each of the zones.

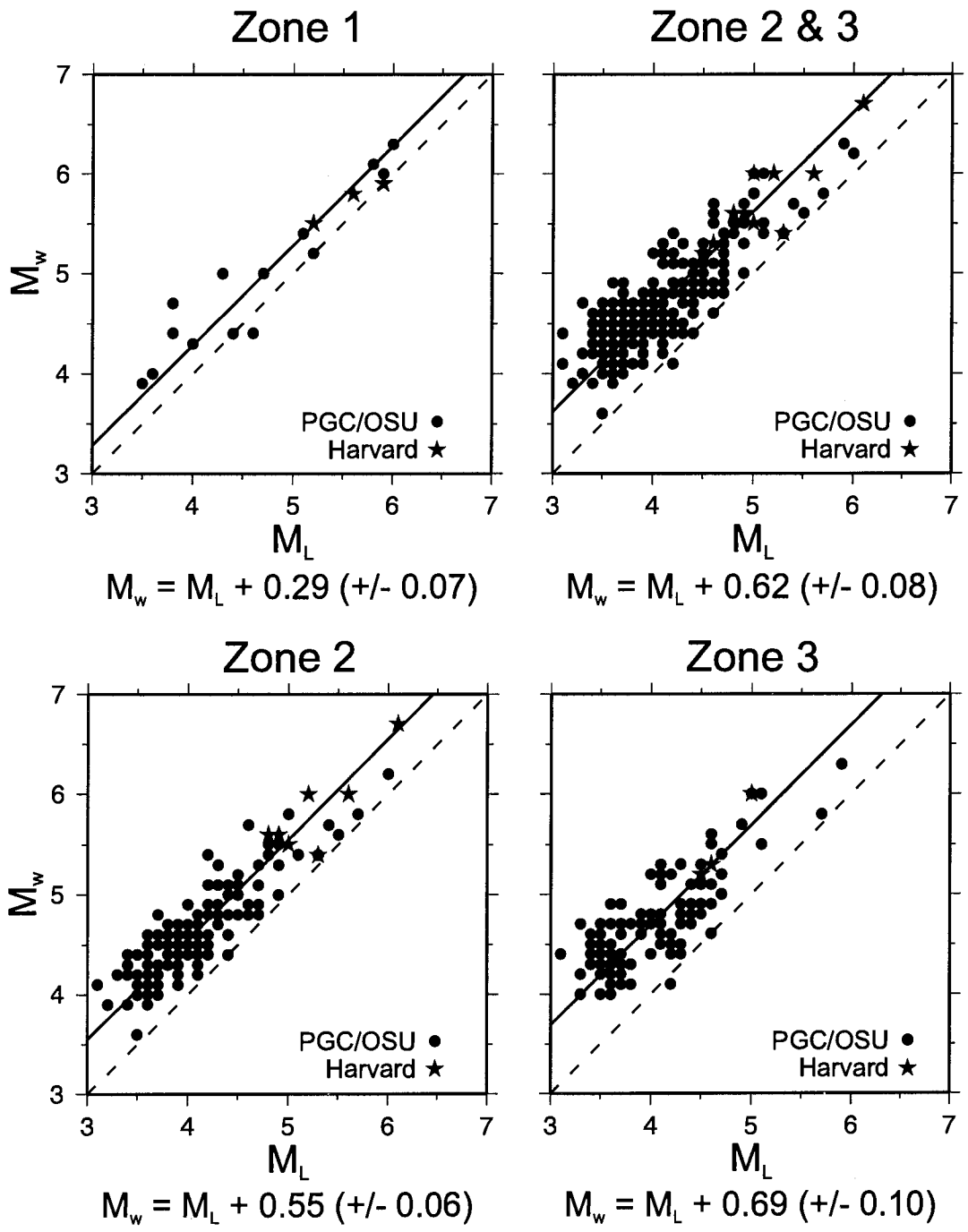

Figure 4.6 M_w-M_L comparison for all three regions. In each case the dashed line represents an ideal 1:1 relationship between M_w and M_L, and the solid line is a best-fit line assuming a slope parallel to the 1:1 line. The M_L correction is indicated for each zone.

4.4 Summary

For the purpose of correlating M_w with M_L in the region off Canada's west coast, three zones can be resolved with the amount of oceanic crust present in the source-receiver travel path being the main difference between them. In all three regions M_w correlates well with M_L but with an offset in magnitude, with M_L being consistently lower than M_w.

Zone 1 is clearly a distinct region from Zone 2 and Zone 3 with most of the source-receiver travel path being through continental crust. The discrepancy between M_w and M_L is also the lowest in Zone 1 (0.29 ± 0.07 magnitude units). Zone 2 and Zone 3 can be examined as one region or as separate regions. Both regions have a mixture of oceanic and continental crust in the source-receiver travel path but events in Zone 3 must travel through a greater amount of oceanic crust. Therefore, the discrepancy between M_w and M_L is larger in Zone 3 than in Zone 2 (0.69 ± 0.10 magnitude units versus 0.55 ± 0.06 magnitude units). However, treating Zone 2 and Zone 3 as one region also gives reasonable results with M_w being larger than M_L by 0.62 ± 0.08 magnitude units; the combined zone is also easier to deal with on a practical level. The different M_w-M_L discrepancies between Zone 2 and Zone 3 demonstrate that as the source moves closer to the continental margin M_L becomes closer to M_w.

Calibrating the M_L values that have been calculated for the past 27 years with M_w is important in that it allows the western Canadian earthquake database to be used more effectively for tectonic studies and seismic hazard analysis. One research area where this is important is in calculating earthquake moment release rates for faults around the Explorer plate and comparing those to predicted plate motions calculated by other methods such as GPS measurements. If the magnitudes used to calculate the moment release rates are seriously undervalued then it will not be possible to accurately compare them with plate motion results determined from other methods. Underestimating the magnitudes of offshore earthquake will also have important consequences for seismic hazard estimates. An increase in magnitude of 0.6 of an earthquake corresponds to an increase in moment release by a factor of 8. For a region such as Vancouver Island, which has the highest seismic hazard risk in Canada, this information is crucial. Vancouver Island is not at great risk from offshore earthquakes with $M_w = 6.0$–6.5 as these occur too far offshore to cause damage. However, there is the potential for major $M_w \sim 7.0$ earthquakes along the boundaries of the Explorer plate which could cause damage on Vancouver Island.

Chapter 5

Explorer Region Tectonics

5.1 Introduction

Moment tensor solutions are valuable for analyzing the tectonic environment of regions with high rates of seismicity. Slip directions derived from moment tensor solutions can be used to investigate plate motions by calculating rotation poles and rotation rates. A group of moment tensor solutions also has the property that the sum of their moment tensor elements is proportional to the average strain tensor produced by the seismic activity. Strain rates and directions can then be calculated from the strain tensor.

In this chapter, slip directions derived from moment tensor solutions are used to calculate instantaneous rotation poles for the Explorer plate relative to the Pacific and Juan de Fuca plates. From the calculated Pacific/Explorer rotation pole and a previously determined Pacific/North America rotation pole, a North America/Explorer rotation pole can be calculated. Also in this chapter, the strain rate and orientation of the principal strain axes for the Explorer plate are calculated from moment tensor solutions for events occurring within the Explorer plate. The results are compared with conclusions based on GPS measurements from Vancouver Island to determine how much of the Explorer plate deformation is being accommodated seismically. There is currently one GPS station available to calculate the convergence rate for the Explorer plate, and the rate is dependent on the locked zone model.

5.2 Calculating Rotation Poles

The slip direction of an earthquake can be determined from the focal mechanism of the earthquake assuming it is possible to distinguish the fault plane from the auxiliary plane. For earthquakes occurring along the boundary of the Explorer plate it is almost always obvious which of the two planes is the fault plane. The location of the rotation pole for a plate is calculated by extending a line normal to the slip direction for each earthquake and determining where the lines intersect (Figure 5.1). In actual practice the lines will not intersect at a single point but instead have a range of possible rotation pole locations.

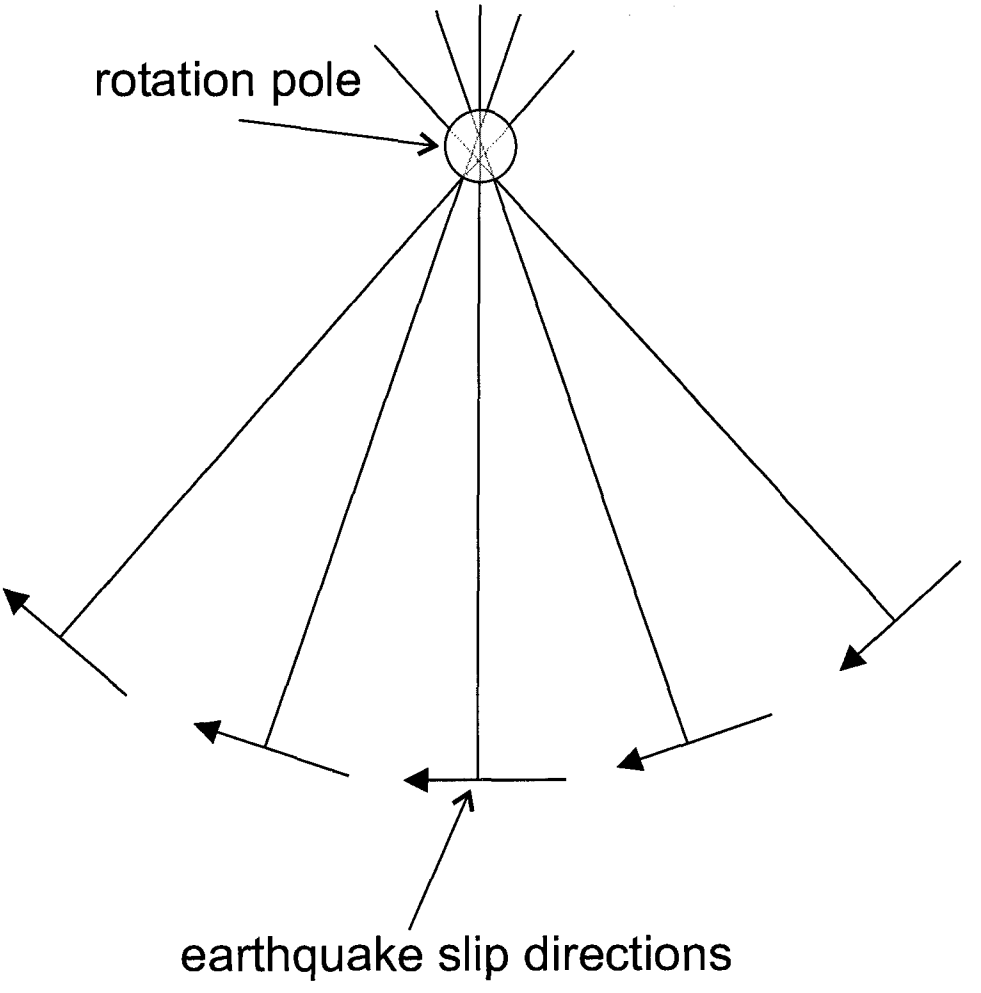

Figure 5.1 Determining the location of a rotation pole from earthquake slip directions.

Pacific/Explorer earthquake slip directions along the Revere-Dellwood-Wilson fault and south to the Sovanco Fracture Zone are similarly oriented, but change systematically from a NNW-SSE orientation along the Revere-Dellwood-Wilson fault to a NW-SE direction along the Sovanco Fracture Zone (Figure 5.2). The slip directions define the current Pacific/Explorer plate motion direction and the systematic change implies the rotation pole is located northeast of the Explorer plate. Braunmiller and Nábělek (2002) calculated Pacific/Explorer, Juan de Fuca/Explorer, and North America/Explorer rotation poles using slip directions derived from regional moment tensor solutions calculated at OSU from 1994–1998. This study builds on that work by using regional moment tensor solutions calculated through 2003 to give a larger database of focal mechanisms.

The instantaneous rotation poles are calculated two ways. The first method is to have no constraints on the rate of motion between the Explorer and Pacific plates. The second method uses moment release rates along the Pacific/Explorer boundary calculated from magnitude-recurrence relations to constrain the rate of motion between the Explorer and Pacific plates.

5.3 Unconstrained Pacific/Explorer Motion

For the unconstrained rate of motion between the Explorer and Pacific plates, the calculated Pacific/Explorer instantaneous rotation pole is located at 54.48°N, 120.78°W (Table 5.1). To estimate the rotation rate a 0.8 Ma Pacific/Juan de Fuca rotation pole (15.46°N, 156.45°W, 0.43 °/Ma) is used (Wilson, 1993)). In this chapter rotation rates follow the standard convention of having counterclockwise motion as positive. With slip directions from two transform boundaries (Pacific/Explorer and Juan de Fuca/Explorer), the pole location and rate of Pacific/Explorer rotation can be calculated by vector addition. A Juan de Fuca/Explorer rotation pole is also calculated. A Pacific/Explorer rotation rate of 3.72 °/Ma is determined (Table 5.1). To calculate the North America/Explorer rotation pole, a recent GPS derived Pacific/North America pole (51.5°N, 73.7°W, -0.765 °/Ma) is used (DeMets and Dixon, 1999). Vector addition with the Pacific/North America and Pacific/Explorer poles give a North America/Explorer rotation pole location and rate (Table 5.1).

The unconstrained rotation poles compare well with the Model A rotation poles calculated by Braunmiller and Nábělek (2002). Braunmiller and Nábělek (2002) Model A did not use slip directions from along the Nootka fault so an additional constraint was needed to estimate the rotation rate. They used North America/Explorer motion perpendicular

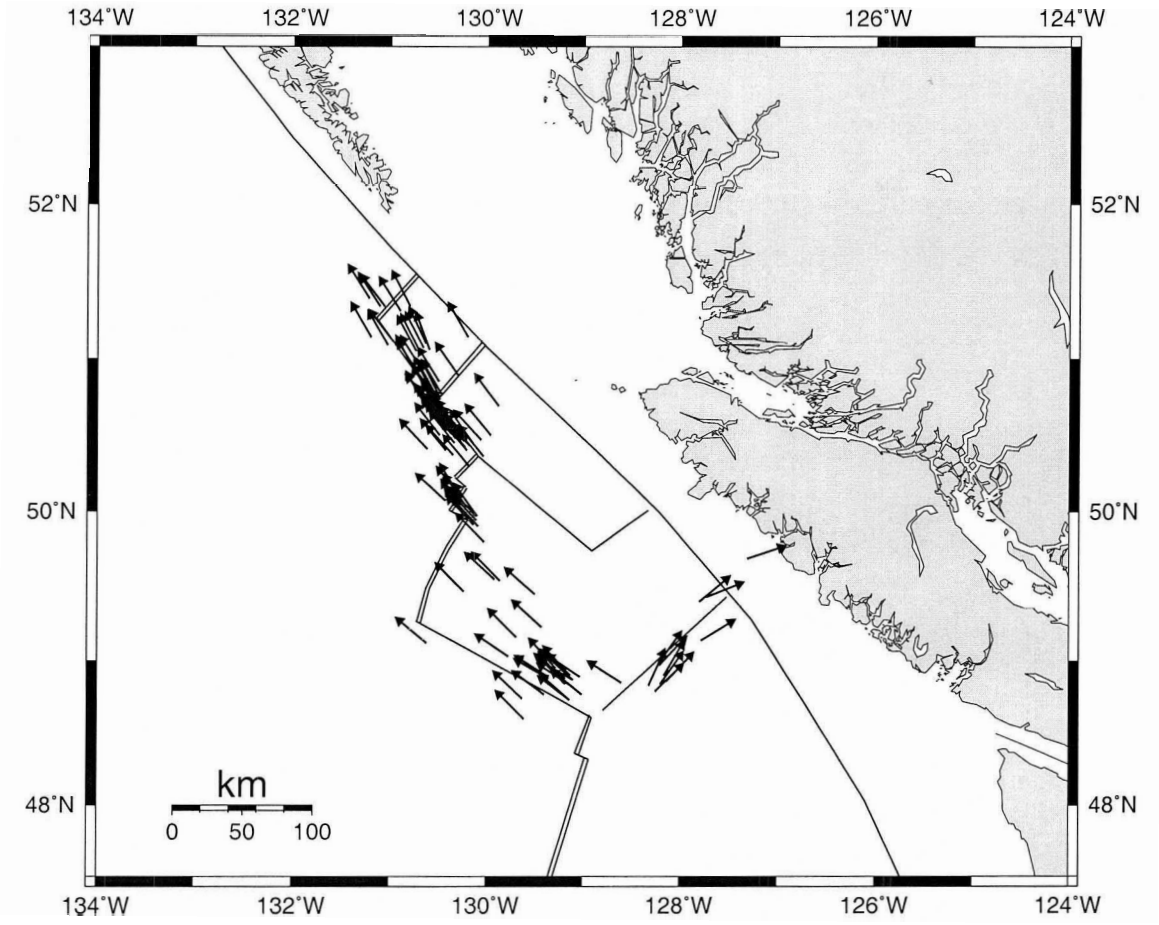

Figure 5.2 Pacific/Explorer slip directions along the Explorer plate boundary calculated from moment tensor solutions. The slip directions change systematically from a NW-SE direction along the Sovanco Fracture Zone to a NNW-SSE direction along the Revere-Dellwood-Wilson fault. The slip directions also change along the length of the Nootka Fault Zone.

Plate Pair	Lat (°N)	Long (°W)	ω (°/Ma)
Unconstrained PAC/EXP rate			
PAC/EXP			
PGC	54.48	120.78	3.72
OSU (Model A)	53.99	120.04	3.30
OSU (Model B)	54.80	116.62	3.10
JDF/EXP			
PGC	48.42	126.83	3.87
OSU (Model A)	45.92	125.76	3.37
OSU (Model B)	46.35	123.38	3.16
NAM/EXP			
PGC	52.42	131.52	3.07
OSU (Model A)	52.67	131.90	2.65
OSU (Model B)	53.97	129.00	2.44
Constrained PAC/EXP rate			
PAC/EXP	55.85	117.20	1.77
JDF/EXP	47.99	127.05	1.85
NAM/EXP	50.00	144.06	1.13

Table 5.1 Explorer plate instantaneous rotation poles calculated in this study. Second plate moves relative to the first plate, positive rotation rate ω indicates counter-clockwise rotation. Plate abbreviations: EXP, Explorer; PAC, Pacific; JDF, Juan de Fuca; NAM, North America.

to Pacific/Explorer which minimized North America/Explorer motion at the triple junction. Both the poles calculated here and those by Braunmiller and Nábělek (2002) differ significantly from the Pacific/Explorer pole calculated by Riddihough (1984) using magnetic anomalies. The Riddihough (1984) Pacific/Explorer pole is located southwest of the Explorer plate (44.2°N, 135.7°W). However, the rate (3.1°/Ma) is fairly consistent with the moment tensor derived poles.

Figure 5.3 (*top*) shows the locations and rates of the various rotation poles along with error ellipses for the Pacific/Explorer and Juan de Fuca/Explorer poles. Also shown is a vector indicating the convergence of the Explorer plate with North America calculated at 50°N, 120°W (near Brooks Peninsula, Vancouver Island). The convergence direction has an azimuth of N49°E and a rate of 19.5 mm/yr which agrees very well with the estimate from GPS results for central and southern Vancouver Island (e.g. Mazzotti et al., 2002).

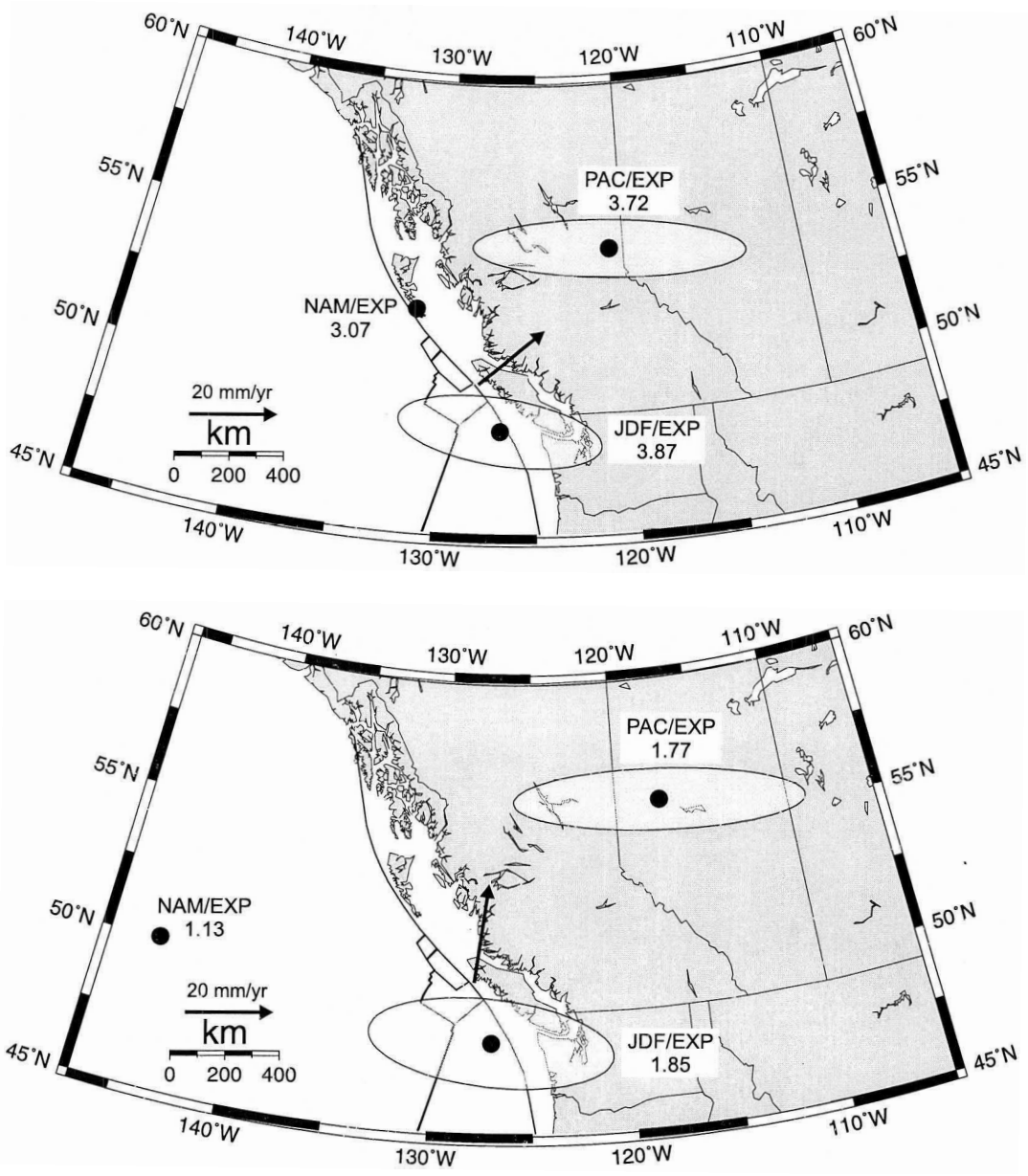

Figure 5.3 Explorer plate instantaneous rotation poles. EXP: Explorer, PAC: Pacific, NAM: North America, JDF: Juan de Fuca. Rates are given in °/Ma if the second plate moves counter-clockwise relative to the first plate. Arrows indicate the convergence rate and direction of the Explorer plate relative to North America at 50°N, 128°W calculated from the NAM/EXP rotation pole. (*Top*) Rotation poles calculated with no constraints on the rate of motion between the Explorer and Pacific plates. (*Bottom*) Rotation poles calculated with the Explorer-Pacific rate of motion constrained using moment release rates.

5.4 Constrained Pacific/Explorer Motion

5.4.1 Slip Rates From Recurrence Relations

For this method moment release rates along the Revere-Dellwood-Wilson Fault and Sovanco Fracture Zone are used to calculate a slip rate to constrain the rate of motion between the Pacific and Explorer plates. Moment release rates along the Nootka Fault Zone are also used to constrain the Juan de Fuca/Explorer rate of motion. Several methods have been developed to estimate the recurrence rate for earthquakes of a certain size over a specified time interval (e.g. Molnar, 1979; Weichert, 1980; Anderson and Luco, 1983) which allow an estimate of the slip rate that takes all earthquakes, observed and long term average, into account.

All of the methods for calculating recurrence rates use the Gutenberg and Richter (1954) frequency-magnitude relationship,

$$\log N = a - bM, \tag{5.1}$$

which describes the number of earthquakes N with magnitude greater than, or equal to, M that are expected to occur in a year. a and b are the well known constants which determine the expected number of earthquakes of a given size to occur per year. These values can be determined from earthquake statistics. Table 5.2 lists the completeness data used for each magnitude range. The minimum magnitude (M_{min}), maximum magnitude (M_{max}), and year to which they are complete are given.

M_{min}	M_{max}	Year
3.6	5.4	1965
5.5	6.9	1917
7.0	9.0	1899

Table 5.2 Completeness table for earthquakes off the coast of Vancouver Island.

Recurrence rate methods also use the moment-magnitude relation (e.g. Kanamori and Anderson, 1975) which relates moment (M_o) to magnitude (M)

$$\log M_o = c + dM \tag{5.2}$$

where c is of the order of 9.0 and d the order of 1.5 in SI units. From Molnar (1979) equations 5.1 and 5.2 can be combined to give the number of events $N(M_o)$ with seismic moment greater than or equal to M_o (in dyne·cm). It can be written as

$$N(M_o) = \alpha M_o^{-\beta} \tag{5.3}$$

where

$$\alpha = 10^{\left(a+\frac{bd}{c}\right)} \quad \text{and} \quad \beta = b/c.$$

If $N(M_o)$ is the number of events/year, then α has units of (dyne·cm)/year. The total seismic moment per unit time is obtained by integrating the moment contributions over magnitude M in the magnitude-recurrence relation up to some maximum magnitude M_x. Hyndman and Weichert (1983) derived a cumulative recurrence function for the total moment rate,

$$\sum M_o = \frac{d}{b}\left[\frac{\exp[2.303(d-b)M_x]10^{a+c}}{2.303(d-b)}\right], \tag{5.4}$$

where $\sum M_o$ is the total moment rate per year. The estimated slip rate, $\bar{u}$, can then be calculated using equation 3.3 ($M_o = \mu A \bar{u}$) and dividing by the time interval.

5.4.2 Constrained Rotation Poles

Events from 1954–2002 along the Sovanco Fracture Zone and Revere-Dellwood-Wilson Fault with $M_L \geq 2.3$ from the PGC earthquake catalogue (Figure 5.4) are converted to M_w using the relation from Chapter 4 by adding 0.62 to the M_L values. Earthquakes internal to the Explorer plate are not used in the recurrence rate calculations. From the regional moment tensor solutions, the average depth for events along the Revere-Dellwood-Wilson Fault and Sovanco Fracture Zone is 9.5 km with a standard deviation of 2.5 km. A width of 5 km is then used for the seismogenic zone for the recurrence rate calculations. Wells and Coppersmith (1994) derived an empirical relationship between magnitude and fault area,

$$M = 4.07 + 0.98\log(A). \tag{5.5}$$

Equation 5.5, with a fault length of 330 km and a fault width of 5 km, gives a maximum magnitude of $M_x = 7.2$. Code provided by S. Mazzotti (per. comm.) using the method

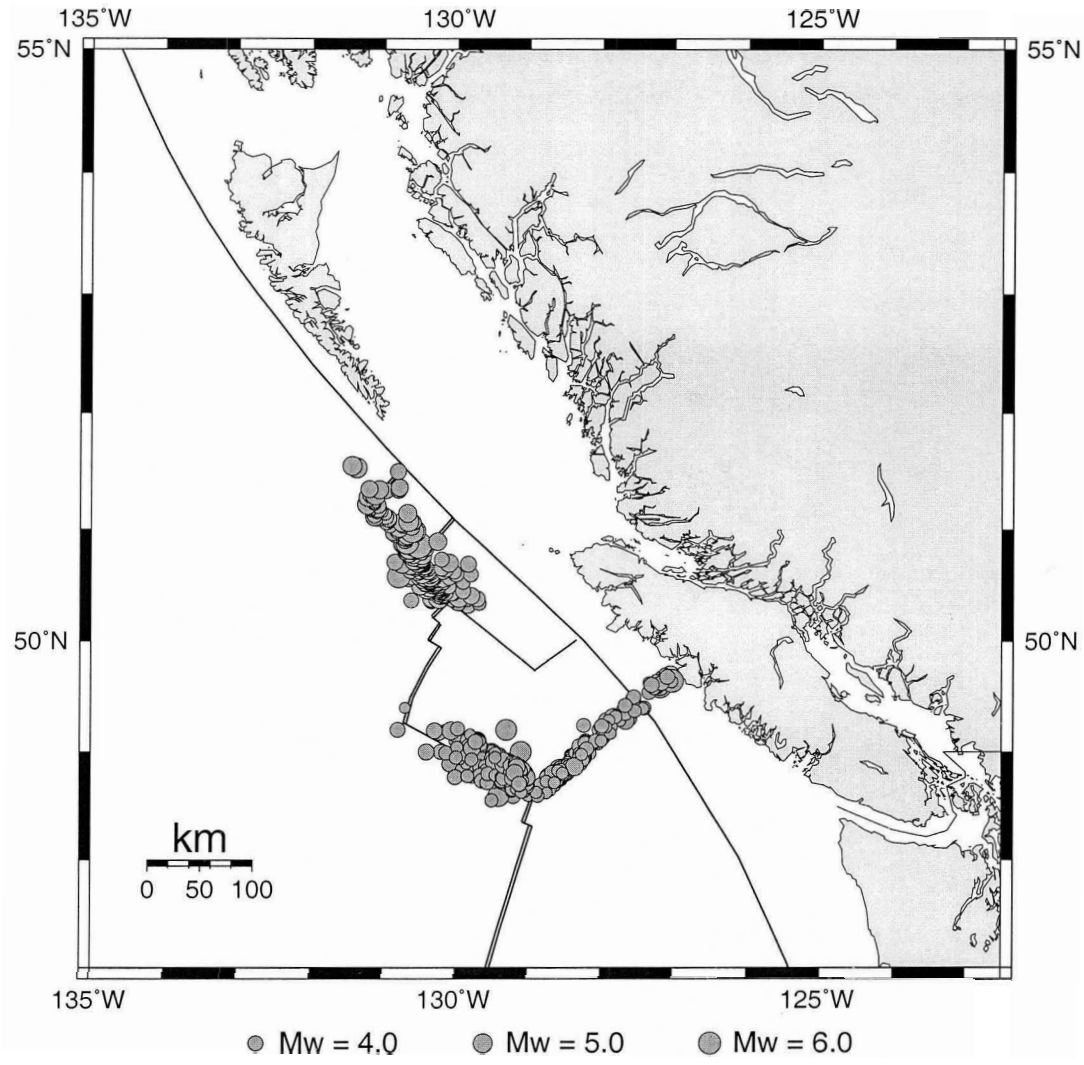

Figure 5.4 Events from along the Revere-Dellwood-Wilson Fault, Sovanco Fracture Zone, and Nootka Fault Zone used to calculate magnitude-frequency statistics to constrain Pacific/Explorer and Juan de Fuca/Explorer plate motion. 0.62 was added to the M_L values to convert them to M_w (see chapter 4 for details).

of Weichert (1980) is used to calculate magnitude-frequency recurrence statistics, a and b values, total moment rate, and slip rate for the data set (Figure 5.5). The a and b values are 4.19 and 0.87 respectively, the total moment rate is 1.0×10^{18} Nm/yr, and the slip rate is 19.2 ± 2.6 mm/yr.

The locations of the Pacific/Explorer and Juan de Fuca/Explorer poles are similar to the unconstrained case but the rotation rates are less than half that of the unconstrained case (Table 5.1). The locations of the poles are also consistent with the Braunmiller and Nábělek (2002) Model B poles but the rates are much lower. The resulting North America/Explorer pole is located west of the Explorer region and the rate is far lower (1.13 °/Ma) than for the unconstrained case (Table 5.1, Figure 5.3 (*bottom*)). The convergence for the Explorer plate with North America, calculated at the same location as the unconstrained case, is similar in magnitude (22.4 mm/yr) but has a much more northerly orientation (N6°E). This result is consistent with recent inference from GPS measurements from northern Vancouver Island (H. Dragert and S. Mazzotti, per. comm.).

Rotation poles are also calculated by constraining the Juan de Fuca/Explorer rate of motion using events along the Nootka Fault Zone. Here the Nootka Fault Zone is defined as extending from the Nootka Fault Zone/Juan de Fuca Ridge/Sovanco Fracture Zone triple junction to Vancouver Island. Defining the the Nootka Fault Zone as stopping at the North America plate boundary, near the foot of the continental slope, does not have a significant effect on the results. The earthquakes used in the recurrence rate calculations are constrained to a narrow range on either side of the Nootka Fault Zone (Figure 5.4). From the regional moment tensor solutions the average depth for events along the Nootka Fault Zone is 10 ± 4.5 km. The a and b values are 3.68 and 0.97 respectively, the total moment rate is 7.8×10^{16} Nm/yr, and the slip rate is 1.5 ± 0.5 mm/yr (Figure 5.6). Adding Juan de Fuca/Explorer motion as a constraint does not change the locations or rates of the rotation poles calculated using Pacific/Explorer motion as a constraint. E. Willoughby (per. comm.) calculated slip rates for the Nootka Fault Zone but did not constrain the events as tightly around the fault zone to account for errors in locations. This resulted in a higher slip rate of 18.2 mm/yr. Using this slip rate as a constraint does not affect the results.

The implication of these results, along with the GPS measurements, is that the Explorer plate cannot be treated as a rigid plate and its motion cannot be adequately described with a single rotation pole. The Explorer plate may either be undergoing intense internal deformation as a result of being trapped between the Pacific and North America plates, or possibly be being broken apart. The fairly high rate of seismicity within the Explorer

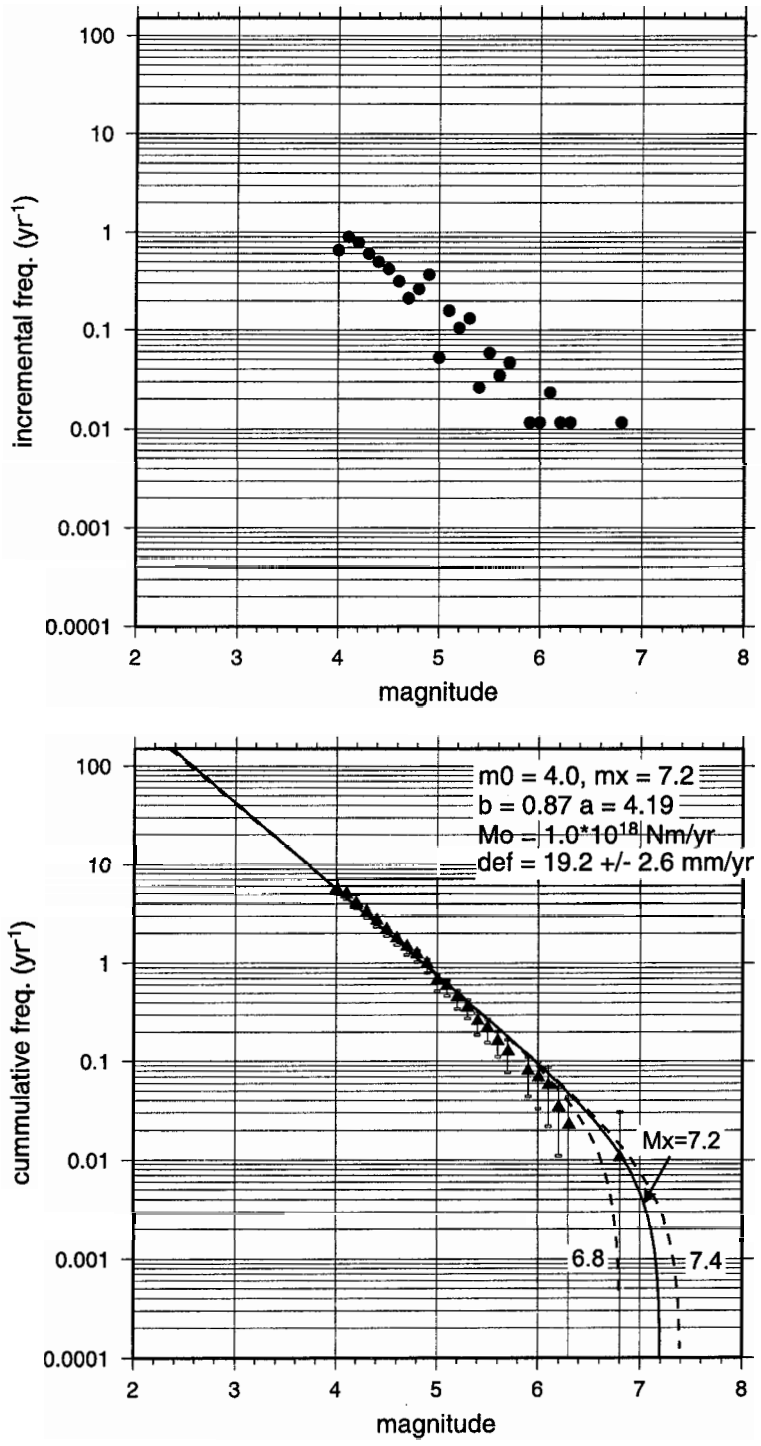

Figure 5.5 Earthquake magnitude versus incremental frequency (*top*) and versus cumulative frequency (*bottom*) for events along the Revere-Dellwood-Wilson Fault/Sovanco Fracture Zone calculated using seismicity from 1954–2002. 0.62 was added to the M_L values to convert them to M_w (see chapter 4 for details).

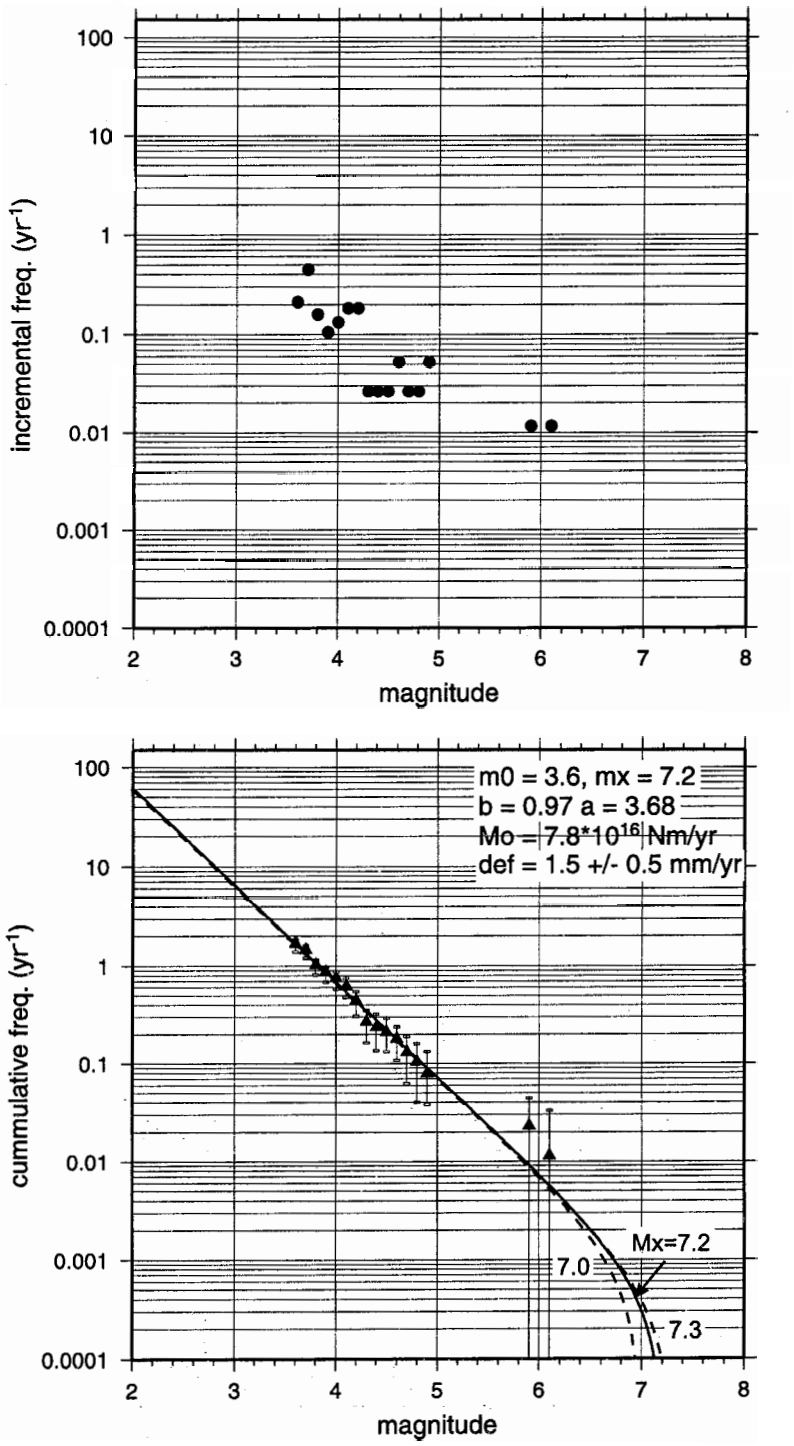

Figure 5.6 Earthquake magnitude versus incremental frequency (*top*) and versus cumulative frequency (*bottom*) for events along the Nootka Fault Zone calculated using seismicity from 1954–2002. 0.62 was added to the M_L values to convert them to M_w (see chapter 4 for details).

plate supports the idea that there is a large amount of deformation happening within the plate. The slip rates derived from the magnitude-frequency recurrence statistics are important in calculating the constrained pole locations and rotation rates. The recurrence rate method uses earthquake statistics to account for observed and unobserved events. Therefore earthquakes missing from the catalogue can be accounted for.

5.5 Explorer Plate Strain

5.5.1 The Strain Tensor

One of the most important properties of moment tensor solutions is that for any group of earthquakes, the sum of their moment tensors is proportional to the average strain tensor for deformation that is produced by the seismic activity. If all of the tectonic activity occurs seismically, the summed moment tensor is proportional to the total change in strain. If any of the deformation occurs aseismically then the moment tensor only provides information about the seismic portion of the deformation.

Kostrov (1974) showed that for an earthquake occurring within a volume V, the average strain tensor $\bar{\varepsilon}_{ij}$ of the region is related to the sum of the moment tensor elements of the earthquakes within it by

$$\bar{\varepsilon}_{ij} = \frac{1}{2\mu V} \sum_{n=1}^{N} M_{ij}^{n} \tag{5.6}$$

where M_{ij}^{n} is the ij^{th} component of the moment tensor of the n^{th} earthquake occurring in the volume, and μ is the shear modulus of the rock within the volume. Dividing M_{ij}^{n} by the time interval τ over which the observations are made gives the moment rate tensor, $\dot{M}_{ij}$. Dividing $\bar{\varepsilon}_{ij}$ by τ gives the strain rate tensor $\dot{\varepsilon}_{ij}$ (Ekström and England, 1989).

The strain tensor can be related to strain rates measured geodetically at the free surface as shown in Figure 5.7 where the arrows represent GPS measured motions. The strain rate components, ε_{ij}, are averages over the surface area A. The z-axis is vertical and the x- and y-axes lie on the free surface. Free surface stress conditions imply that $\varepsilon_{xz} = \varepsilon_{zx} = 0$ and $\varepsilon_{yz} = \varepsilon_{zy} = 0$, and if only strike-slip faults are involved in the moment release, $\varepsilon_{zz} = -(\varepsilon_{xx} + \varepsilon_{yy}) = -\Delta$ (Savage and Simpson, 1997). The complete moment rate tensor is then

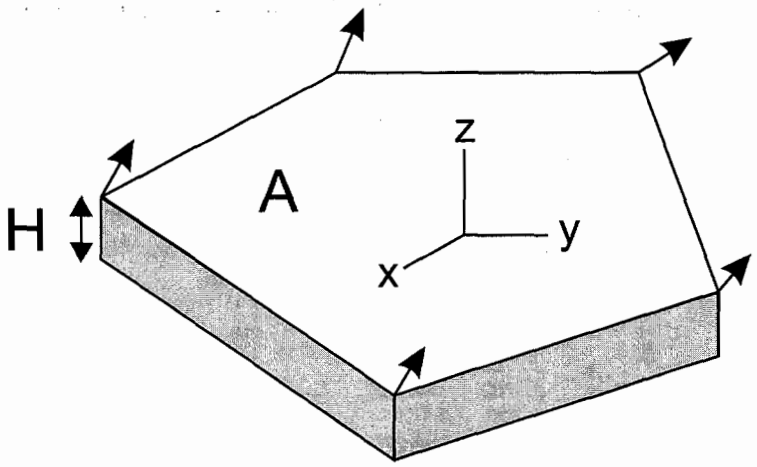

Figure 5.7 Crustal prism for which the moment rate is estimated. A represents the surficial area of the polygon at the Earth's surface and H is the thickness (after Savage and Simpson, 1997).

$$\dot{M} = 2\mu H A \begin{bmatrix} \varepsilon_{xx} & \varepsilon_{xy} & 0 \\ \varepsilon_{yx} & \varepsilon_{yy} & 0 \\ 0 & 0 & -\Delta \end{bmatrix}. \tag{5.7}$$

The moment rate tensor can be referred to its principal axes by a rotation of the coordinate system about a vertical axis using equation 3.6

$$\dot{M} = 2\mu H A \begin{bmatrix} \varepsilon_x & 0 & 0 \\ 0 & \varepsilon_y & 0 \\ 0 & 0 & -\Delta \end{bmatrix}. \tag{5.8}$$

The surface areal dilatation rate is

$$\Delta = \varepsilon_{xx} + \varepsilon_{yy} = \varepsilon_x + \varepsilon_y, \tag{5.9}$$

and the total surface shear strain is

$$\gamma = [(\varepsilon_{xx} - \varepsilon_{yy})^2 + 4\varepsilon_{xy}^2]^{1/2} = \varepsilon_x - \varepsilon_y, \tag{5.10}$$

where ε_x and ε_y are the principal extension and compression rates given by

$$\varepsilon_x = (\Delta + \gamma)/2 \text{ and } \varepsilon_y = (\Delta - \gamma)/2. \tag{5.11}$$

An important special case of equation 5.6 is slip along a fault. Suppose N similarly oriented strike-slip earthquakes occur along a plate boundary with a horizontal length L, width W, and vertical extent T (Figure 5.8). The total scalar moment is the sum of the scalar moments of the N individual earthquakes, and the average slip along the boundary is S. The average strain of the volume $V = LTW$ is $\varepsilon_{xy} = \varepsilon_{yx} = S/2W$ (Figure 5.8). Equation 5.6 then gives

$$\frac{S}{2W} = \frac{1}{2\mu V}\sum_{k=1}^{N} M_{o_k} = \frac{1}{2\mu LTW}\sum_{k=1}^{N} M_{o_k}. \tag{5.12}$$

Equation 5.12 can be simplified to

$$\sum_{k=1}^{N} M_{o_k} = \mu LTS \tag{5.13}$$

which is equivalent to equation 5.6 for similarly oriented earthquakes along a simple plate boundary. In addition, if there is only one earthquake $A = LT$ and equation 5.13 is identical to equation 3.3 (Frohlich and Apperson, 1992). It is important to note that, while equation 5.6 is always valid, equation 5.13 is only applicable when all the moment tensors are the same except for their scalar moments, such as when they all occur along the same fault or along parallel faults.

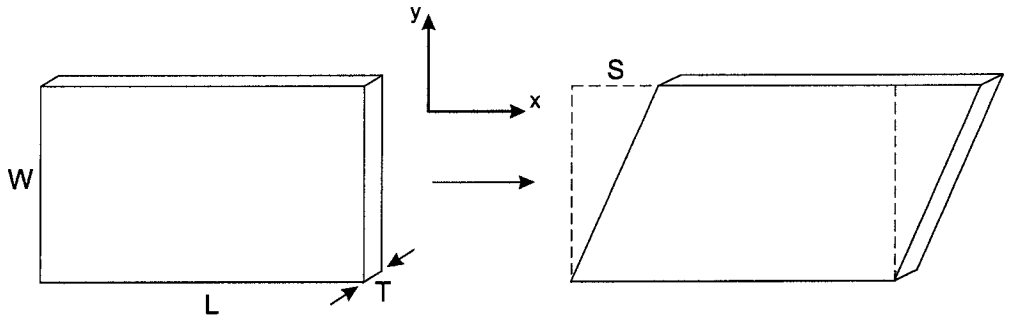

$$g = \begin{bmatrix} 0 & S/2W & 0 \\ S/2W & 0 & 0 \\ 0 & 0 & 0 \end{bmatrix}$$

Figure 5.8 Relationship between strain and seismic moment. If a zone with width W, length L, and thickness T undergoes a simple shear with displacement S, then the strain $\varepsilon_{12} = \varepsilon_{21}$ is S/2W and all the other components of the strain tensor are zero (after Frohlich and Apperson, 1992).

5.5.2 Explorer Plate Strain Rates

Moment tensor solutions for earthquakes occurring within the Explorer plate (Figure 5.9) are used to calculate the strain rate due to seismic activity. Events occurring within the Explorer plate will be related to the internal deformation of the Explorer plate and not due to plate motions on the edges of the plate. A total of 37 solutions are available (Table 5.3) and the total seismic moment and sums for each of the moment tensor elements are shown at the ends of the columns. Strain tensors are dominated by large earthquakes and a single major earthquake can significantly change the strain rates and directions. In this data set the 17 December 1980 $M_w = 6.7$ ($M_o = 1.4 \times 10^{19}$ Nm) accounts for 70% of the total moment release for the Explorer plate.

The resulting strain tensor is given by the sum of the individual moment tensor components of the earthquakes in Table 5.3,

$$\bar{\varepsilon}_{ij} = \begin{bmatrix} -19571.15 & -4132.15 & 49.92 \\ -4132.15 & 20752.51 & 1217.92 \\ 49.92 & 1217.92 & -2315.74 \end{bmatrix} \times 10^{15}\text{Nm}. \tag{5.14}$$

The moment rate tensor for the Explorer plate is given by equation 5.7 and dividing by a time interval of 24.24 years

$$\dot{M} = 2\mu HA \begin{bmatrix} -807.39 & -170.47 & 0 \\ -170.47 & 856.13 & 0 \\ 0 & 0 & -48.74 \end{bmatrix} \times 10^{15}\text{Nm}. \tag{5.15}$$

Rotating 5.15 into its principal axes gives a moment rate tensor of

$$\dot{M} = 2\mu HA \begin{bmatrix} -824.68 & 0 & 0 \\ 0 & 873.42 & 0 \\ 0 & 0 & -48.74 \end{bmatrix} \times 10^{15}\text{Nm}. \tag{5.16}$$

The $\dot{M}_{xx}$ component of equation 5.16 is the moment rate in the compressional direction and the $\dot{M}_{yy}$ component is the moment rate in the tensional direction. The strain rate can then be calculated using equation 5.6. The standard deviation for the depths of events in the Explorer plate region is 3.5 km. Therefore, 7 km is used as an estimate for the thickness of the seismogenic zone for the Explorer plate. Using a shear modulus, μ, of 3.5×10^{10} N/m^2, a surface area of approximately 21 500 km^2 for the Explorer plate and a seismogenic thickness of 7 km, the strain rate is 7.8×10^{-8} yr^{-1} in the compressional direction which is the direction of Explorer plate convergence with North America. Over

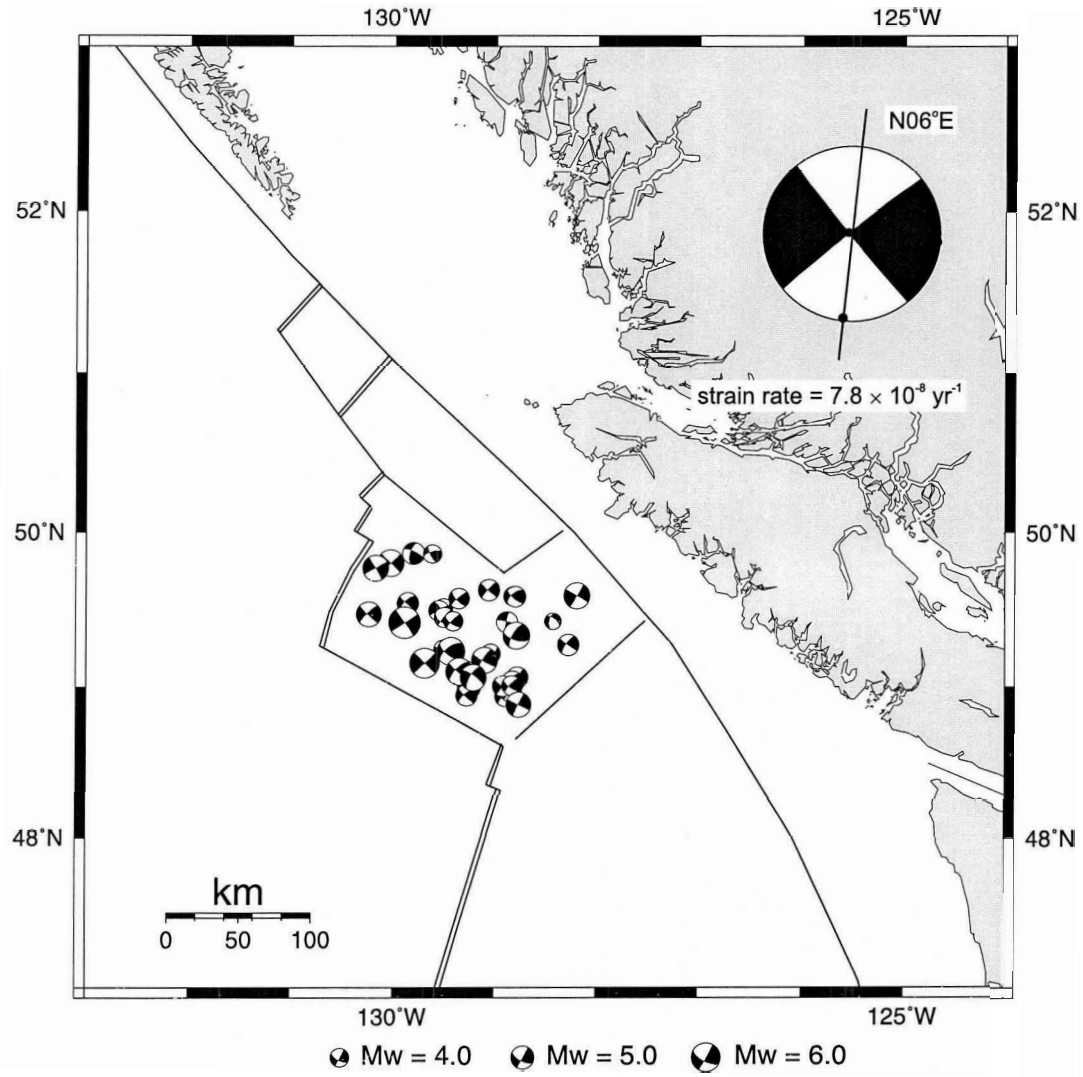

Figure 5.9 Moment tensor solutions for earthquakes occurring within the Explorer plate used to calculate the Explorer plate strain rate due to seismic activity. A representation of the summed moment tensor is shown in the upper right corner with the line indicating the maximum compressive strain direction ($\varepsilon 1$). The strain rate is 7.8×10^{-8} yr^{-1}.

Date yyyymmdd	Latitude	Longitude	Mw	Mo (Nm)	Mxx	Myy	Mzz	Mxy	Mxz	Myz
197806111455	49.156	-129.691	6.3	3.4E18	-3150.00	3590.00	-440.00	-30.00	0.00	0.00
197903130951	49.770	-130.177	5.4	1.6E17	-1380.00	145.00	-7.00	-81.00	0.00	0.00
197903131200	49.802	-130.027	5.7	3.9E17	-393.00	395.00	-2.00	-6.00	0.00	0.00
198005162234	49.593	-128.191	5.4	1.2E17	-104.00	112.00	-9.00	61.00	0.00	0.00
198012171622	49.417	-129.888	6.7	1.4E19	-12300.00	13800.00	-1400.00	-5000.00	0.00	0.00
198805261901	48.886	-128.765	5.2	7.6E16	-49.10	69.80	-20.70	47.00	1.40	3.90
199201130608	49.060	-129.212	5.4	1.3E17	-99.00	105.00	-6.00	45.00	67.00	-5.00
199402120704	49.102	-129.350	5.7	4.0E17	-597.10	798.80	-201.60	105.70	-30.70	364.00
199601031312	49.473	-130.242	5.2	7.9E16	-88.18	99.23	-11.05	2.92	-2.83	-4.70
199601281130	48.945	-129.276	4.6	7.7E15	-15.25	18.06	-2.81	-1.21	-0.94	4.20
199609092228	49.011	-128.833	4.2	1.9E15	1.92	1.54	0.38	0.38	-0.10	0.66
199611041738	49.510	-129.800	4.9	2.4E16	-21.40	16.20	5.20	9.25	2.10	10.70
199611210124	49.586	-128.795	4.4	5.2E15	-5.14	3.30	1.84	-0.08	0.85	2.50
199611210130	49.588	-128.816	4.2	2.0E15	-1.86	1.86	-0.01	0.48	0.53	0.38
199612022154	49.660	-129.970	4.6	9.9E15	-9.73	5.96	3.77	-4.50	2.07	1.12
199802181846	49.543	-129.858	4.6	7.7E15	-7.14	6.56	0.59	0.28	1.96	2.87
199907021145	49.230	-129.433	5.8	5.5E17	-454.00	295.00	160.00	6.85	22.50	379.00
199907050334	49.427	-129.410	4.1	1.4E15	-1.42	1.02	0.40	0.27	-0.28	0.44
200006221415	49.427	-128.427	3.6	3.1E14	-0.10	0.29	-0.19	0.17	0.08	0.01
200101131102	48.999	-129.253	4.9	2.1E16	-12.80	21.70	-8.90	-6.00	6.53	4.36
200101230939	49.334	-128.787	5.7	3.5E17	-683.00	1030.00	-343.00	577.00	-41.20	382.00
200101231443	49.174	-129.099	5.5	1.7E17	-136.00	146.00	-10.30	82.30	21.90	53.50
200101231454	49.420	-128.880	4.5	6.1E15	-18.40	30.80	-12.30	52.70	6.91	11.10
200101231515	49.101	-129.285	4.5	5.4E15	-4.88	4.28	0.60	0.00	2.47	-1.38
200101231703	49.215	-129.042	4.1	1.5E15	-11.90	15.90	-4.06	0.07	-1.92	-2.56
200105131409	49.450	-129.499	4.3	2.8E15	-2.24	1.65	0.59	0.79	-1.36	1.21
200105230215	49.861	-129.616	4.0	1.2E15	-0.72	0.60	0.11	-0.70	-0.28	0.73
200108011619	49.274	-128.274	4.6	8.0E15	-7.46	6.90	0.56	2.42	2.04	1.44
200112090121	49.575	-129.352	4.4	5.3E15	-5.34	4.32	1.02	-0.51	-0.99	1.57
200112310752	49.497	-129.554	4.3	2.8E15	-2.27	2.16	0.11	-1.32	1.09	-0.28

Table 5.3 Explorer plate moment tensor solutions.

Date yyyymmdd	Latitude	Longitude	Mw	Mo (Nm)	Mxx	Myy	Mzz	Mxy	Mxz	Myz
200204180051	49.513	-129.505	4.0	9.7E14	-0.55	0.96	-0.41	-0.19	-0.39	0.24
200204180119	49.629	-129.058	4.6	7.5E15	-7.42	7.28	0.14	1.04	0.21	1.25
200207101019	49.006	-128.918	4.3	3.1E15	-2.18	3.39	-1.21	0.69	-0.03	0.28
200207102131	49.030	-128.821	4.8	2.0E16	-4.42	5.74	-1.32	2.36	-1.48	4.40
200207110052	49.062	-128.775	4.6	8.1E15	-2.24	1.75	0.49	1.60	1.99	1.23
200207130722	49.241	-129.503	4.3	3.5E15	-10.30	8.94	1.37	4.43	-1.43	4.81
200207140019	48.976	-128.840	4.7	1.2E16	-17.90	22.20	-4.37	7.43	1.37	4.81
200207150531	48.941	-128.897	4.4	4.0E15	-3.44	3.91	-0.47	0.10	1.53	-0.41
200210162232	49.864	-129.803	4.7	1.3E16	5.67	-8.43	2.76	-8.14	-6.53	1.37
				2.0E+19	-19602.28	20774.67	-2306.77	-4127.40	54.09	1229.74

Date: year, month, day, hour, minute. M_w: moment magnitude. Mo: seismic moment.
Mxx, Myy, Mzz, Mxy, Mxz, Myz: moment tensor elements in units of 10^{15} Nm.

Table 5.3 Explorer plate moment tensor solutions (continued).

a distance of 100 km this gives a plate interior deformation rate of 7.8 mm/yr.

GPS strain rates from southern and central Vancouver Island indicate shortening between 4×10^{-8} and 8×10^{-8} yr^{-1} (Henton et al., 2000; Mazzotti et al., 2002). GPS strain rates have not been calculated for northern Vancouver Island, which would be the most comparable to the Explorer plate, but the strain rates are expected to be similar to southern and central Vancouver Island (H. Dragert, per. comm.). The moment tensor derived strain rate of 7.8×10^{-8} yr^{-1} for the Explorer plate is near the upper bound for the GPS derived strain rate, but still consistent with the GPS strain rate. The GPS strain rate is measured from Vancouver Island instead of on the Explorer plate. If GPS receivers could be placed on the Explorer plate the calculated strain rates would be expected to be higher (H. Dragert, per. comm.). The shortening direction progressively rotates from nearly E-W in central and northern Oregon to nearly NE-SW in southern coastal British Columbia (Mazzotti et al., 2002; Figure 5.10). While there is no strain direction calculated from GPS data for northern Vancouver Island, GPS velocity vectors show motion in a near N-S direction for northern Vancouver Island (Mazzotti et al., 2003b). The strain tensor has a compressional axis with an azimuth of N6°E which is consistent with the GPS velocity vectors from northern Vancouver Island.

5.6 Summary

Regional moment tensor solutions provide important constraints on the motions of the Explorer plate. Moment tensor solutions are used to calculate rotation poles and rates of the Explorer plate relative to the Pacific and Juan de Fuca plates and then, through vector addition, to determine the motion of the Explorer plate relative to the North America plate. The rotation poles are calculated by leaving Pacific/Explorer motion unconstrained and by constraining Pacific/Explorer motion using moment release rates along the Pacific/Explorer plate boundary.

The locations of the Pacific/Explorer and Juan de Fuca/Explorer rotation poles are similar in both methods but the rotation rate decreases by a factor of 2 if Pacific/Explorer motion is constrained. This affects the location and rate of the North America/Explorer rotation pole. The convergence rate of the Explorer plate relative to the North America plate is similar between the two methods but the convergence direction changes from NE-SW in the unconstrained case to almost N-S in the constrained case. The unconstrained convergence direction is consistent with GPS measurements from central and southern Vancouver Island while the constrained convergence direction is consistent with GPS measurements

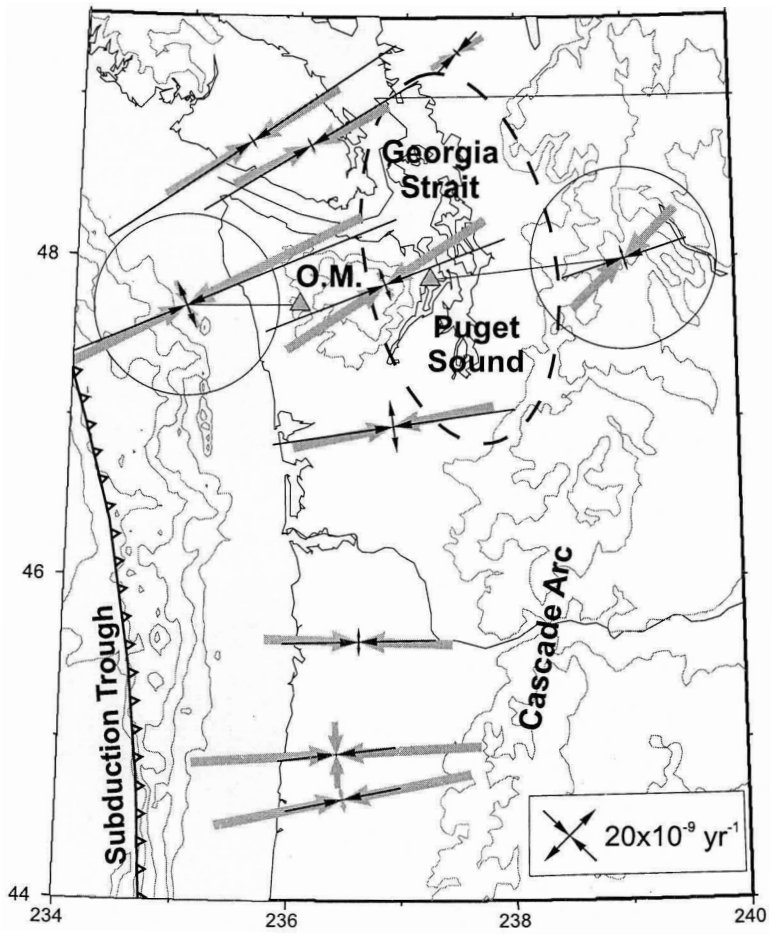

Figure 5.10 GPS versus model strain rates. Large shaded and thin solid arrows represent the principal axes of GPS and inter-seismic model strain rates averaged over $\sim 150 \times 150$ km. Strain arrows within circles represent strain rates estimated in the western and eastern sides of the northern Washington forearc (shaded triangles indicate the centre of those two regions). O.M.: Olympic Mountains. (Mazzotti et al., 2002)

from northern Vancouver Island. This implies that the Explorer plate cannot be treated as a rigid plate and its motion cannot be described by a single rotation pole. The Explorer plate is likely undergoing intense internal deformation as a result of being trapped between the much larger Pacific and North America plates.

Moment tensor solutions are also used to calculate a strain tensor for the Explorer plate. The strain tensor is used to determine the principal strain axes for the Explorer plate and calculate a strain rate. The moment tensor derived strain rates for the Explorer plate are consistent with GPS strain rates from central and southern Vancouver Island. GPS strain rates for northern Vancouver Island have not been calculated but would be expected to be similar to central and southern Vancouver Island. The moment tensor derived compressive strain direction is almost N-S which is consistent with GPS velocity vectors from northern Vancouver Island.

Chapter 6

Northern Canadian Cordillera Tectonics

6.1 Introduction

The Yukon and western Northwest Territories is a region of strong seismicity concentrated in the Richardson and Mackenzie Mountains, and along the Alaska panhandle where the Yakutat block is colliding with North America (Figure 6.1). Along the Alaska panhandle earthquake focal mechanisms mainly indicate seismic slip is parallel to the direction of relative motion between North America and the Pacific plate. As the margin bends west and encounters the southeastern edge of the Yakutat block, partitioning of seismic slip is evident both onshore and offshore (Doser and Lomas, 2000; Figure 6.2). Strike-slip faulting has occurred along the Fairweather and Denali faults, including the 3 November 2002 $M_w = 7.9$ event along the Denali fault in eastern Alaska. In the St. Elias Mountains region, thrust faulting is occurring along and above the plate interface (Doser and Lomas, 2000). The St. Elias Mountains region has also produced several major earthquakes in the last 100 years with the most recent being the 28 February 1979 $M_w = 7.5$ thrust event.

East of the Yakutat collision, between the Denali and Tintina faults, the seismicity decreases rapidly, indicating little deformation in this region. The seismicity increases again in the Richardson and Mackenzie Mountains region (Figure 6.1). This a region of numerous geologically mapped strike-slip and low-angle thrust faults (Figure 6.2) along which most of the seismicity likely occurs and there is a history of large magnitude (M >

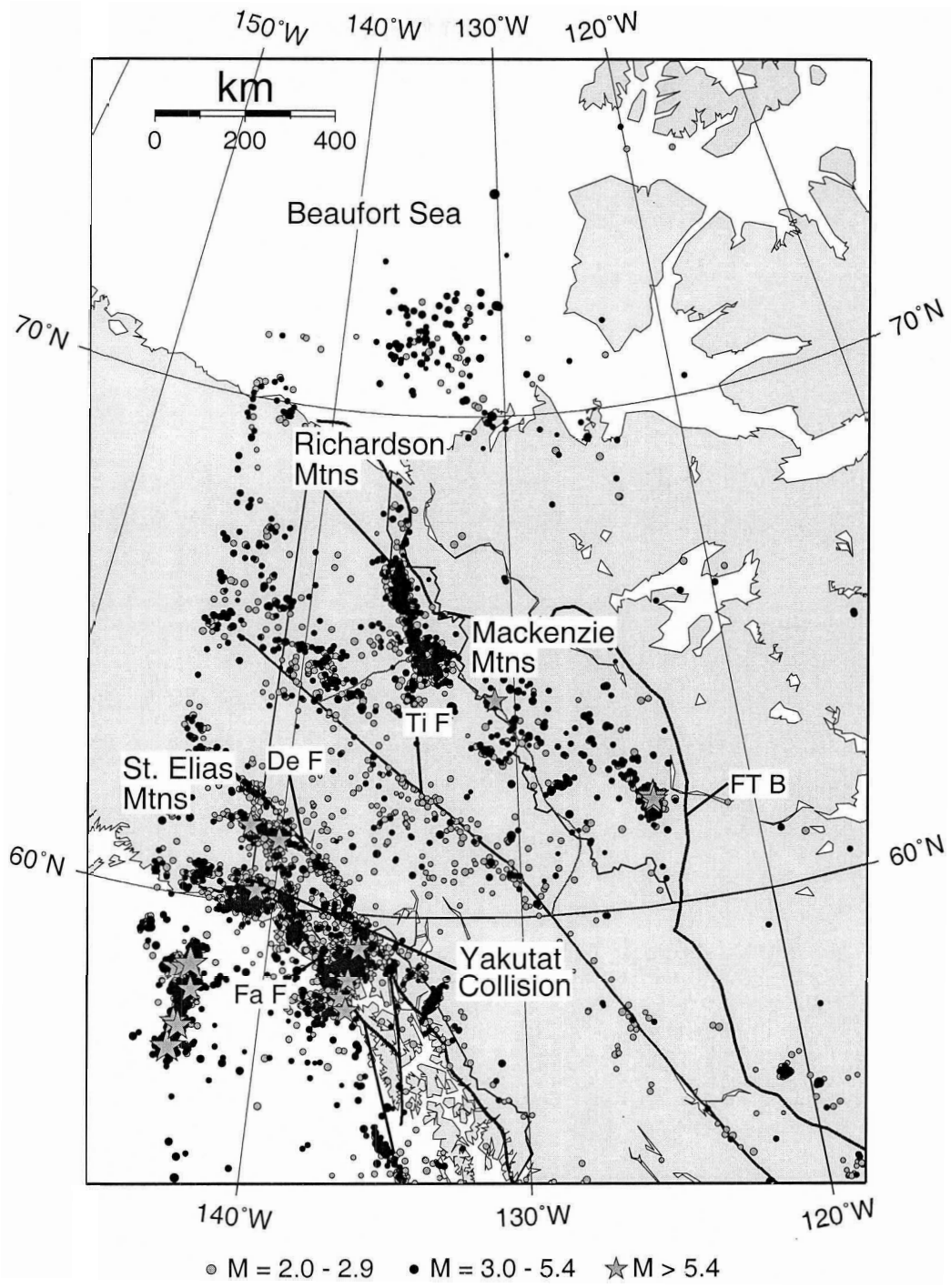

Figure 6.1 Seismicity of the northern Canadian Cordillera for 1983–2002 along with the main faults. Fa F - Fairweather Fault; De F - Denali Fault; Ti F - Tintina Fault; FT B - Fold and Thrust Belt.

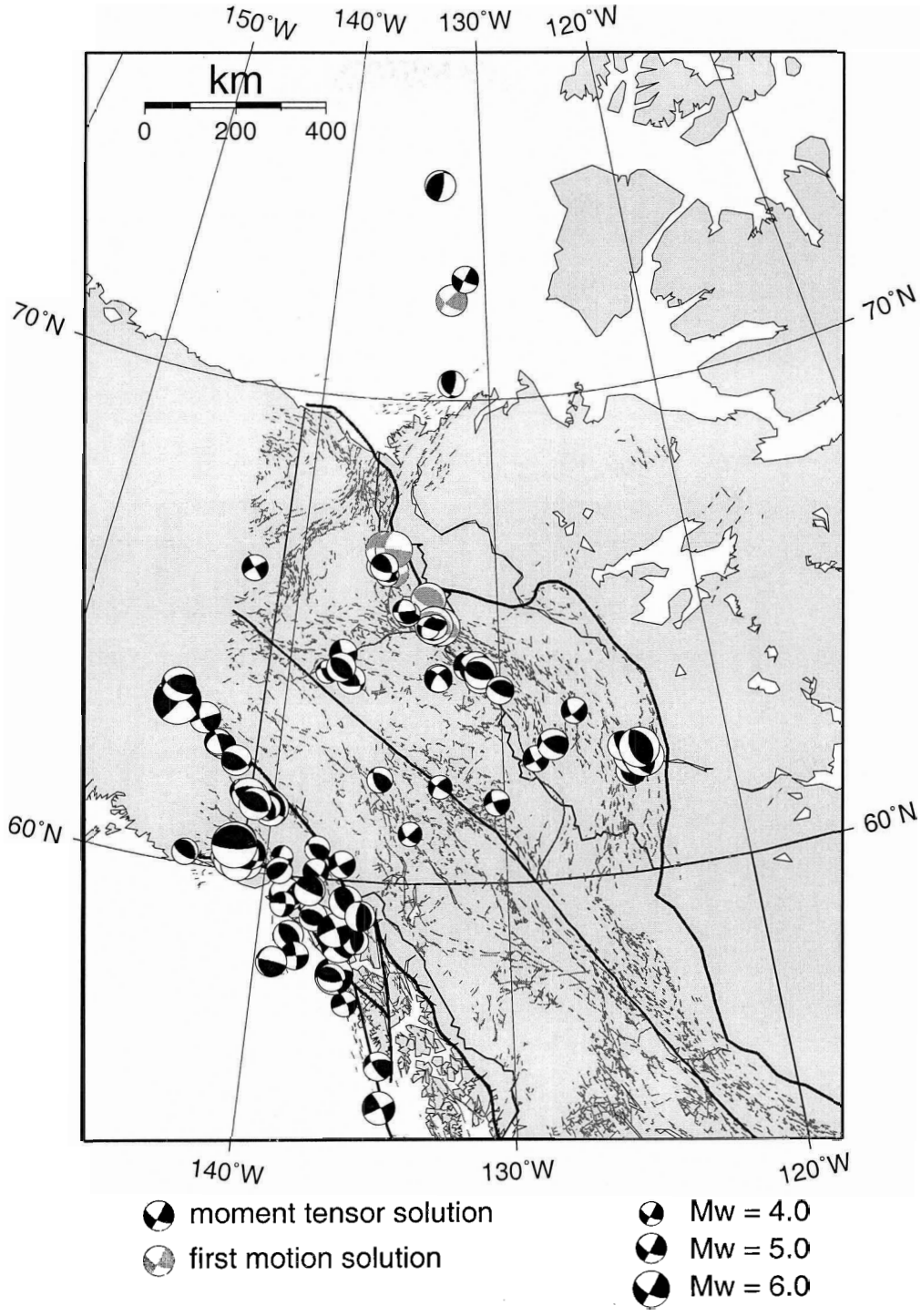

Figure 6.2 Focal mechanisms in the Yukon and Northwest Territories and southeast Alaska. Shown are PGC regional moment tensor solutions and Harvard centroid moment tensor solutions (black) and available first motion solutions (grey). Major faults shown as thick black lines and minor faults are light grey lines.

6) events. The seismicity occurs in a NW-SE pattern from around 60°N–65°N and then changes to a N-S pattern through to the Beaufort Sea where there is a small concentration of earthquakes. Earthquakes in this region are not confined to the major faults but also occur on numerous minor faults (light grey in Figure 6.2) or on unmapped faults. The largest earthquakes in the region were the 5 October and 23 December, 1985 Nahanni events (M_w = 6.6 and 6.7 respectively). The October event triggered the fourth largest landslide known in Canada in the 20th century, and the December event had the strongest near-field seismic accelerations (> 2 g) ever recorded for an earthquake (Wetmiller et al., 1989). Several M = 5.0–6.0 events have also occurred throughout the Yukon and SW Northwest Territories. Focal mechanisms vary between thrust and right-lateral strike-slip faulting (Figure 6.2). However, the pressure axes have a consistent NE-SW orientation except in the Nahanni region where it is almost E-W. Why the pressure axis orientation is different in the Nahanni region is uncertain. One possibility is that the regional stress regime is reactivating optimally aligned faults in the northern Canadian Cordillera.

There is a small concentration of seismicity in the Beaufort Sea, mainly offshore of the Mackenzie Delta along the continental margin. This region experiences an average of one $M \geq 4.0$ earthquake per year (Hasegawa et al., 1979) and four focal mechanisms (three moment tensor solutions, one first motion) exist for the region. Hasegawa et al. (1979) determined that the horizontal component of the stress field is tension normal to the axis of the continental margin and suggested that it is the result of the uncompensated load of Quaternary sediments and tectonic stresses. The available focal mechanisms consist of two strike-slip events with N-S compression, with thrust mechanisms to the north and south showing E-W compression (Figure 6.2). The two regional moment tensor solutions are of relatively poor quality and not too much should be inferred from them. The Beaufort Sea/Mackenzie Delta region is widely considered to be one of the next major sources of conventional gas (Lane, 2002) which adds to the importance of understanding the seismicity and tectonics of the region. At this time there have been relatively few studies of the seismicity in the Beaufort Sea/Mackenzie Delta region and the available information is limited.

6.2 The Stress Tensor

Several inversion schemes have been developed for calculating composite stress tensors from earthquake focal mechanisms including Michael (1984), Gephart and Forsyth (1984), and Angelier (1984). In this study stress tensors for the Yukon and Northwest Territories are calculated with ZMAP6 (Wiemer, 2001) using the Michael (1987) method, an extension of

the Michael (1984) method. The Michael (1987) method does not require the fault plane to be chosen a priori.

To define the stress field of a region from focal mechanisms, a number of mechanisms must be available. McKenzie (1969) showed that the maximum compressive stress may have an orientation anywhere within the dilatational quadrant of the focal mechanism, and that the P and T axes from a single fault plane solution may vary significantly from the principal stress directions depending on the orientation and strength of the faults. This means that principal stresses are poorly constrained by a single focal mechanism. However, if there are a variety of focal mechanisms on faults with different orientations within a region of uniform stress then the principal stress directions can be determined.

The stress tensor is calculated using standard linear least-squares inversion techniques to find the stress model which most closely matches the observed data. The assumptions are that slip on the fault plane occurs in the direction of the resolved shear stress and that the stress orientation is homogeneous in the selected volume. The inversion solves for the three principal stresses, $\sigma 1$, $\sigma 2$, $\sigma 3$ where $\sigma 1 \geq \sigma 2 \geq \sigma 3$. One other parameter, ϕ, can also be calculated. ϕ is a measure of the relative sizes of the principal stresses and is defined by Angelier (1979) as

$$\phi = \frac{\sigma 2 - \sigma 3}{\sigma 1 - \sigma 3}. \tag{6.1}$$

Once the stress tensor is calculated, ϕ and error limits can be computed at the same time as the principal stresses and axes (Michael, 1984). The misfit for each focal mechanism is defined as the smallest rotation angle about an axis of any orientation that would bring the direction of slip on either of the two nodal planes into agreement with the slip predicted by the stress model. Confidence limits are calculated using bootstrap resampling. If a data set consists of N focal mechanisms, bootstrap resampling randomly picks N focal mechanisms from the data set of N focal mechanisms. The new data set will have some mechanisms repeated 2 or more times and other mechanisms not chosen at all. However, the new data set will have the same distribution of errors as the original data set. The new data set is then inverted for the stress field. Repeating the process many times will find the true variation in the process.

6.3 Earthquake Focal Mechanisms, Stress, and Strain

6.3.1 Focal Mechanisms

More than 100 focal mechanisms have been calculated for earthquakes in the northern Canadian Cordillera and adjacent Yakutat collision zone (Figure 6.2). They include first motion solutions for a few larger earthquakes prior to the mid-1970's (e.g. Cassidy and Bent, 1993; Cassidy and Bent, 2003; Hasegawa et al., 1979) and moment tensor solutions for a large number of events since the mid-1970's. The moment tensor solutions consist of Harvard centroid moment tensor solutions and regional moment tensor solutions calculated in this study. The focal mechanisms vary between strike-slip and thrust faulting across the northern Canadian Cordillera and through to the Yakutat collision zone, with a few normal faulting mechanisms also present.

In the vicinity of the Yakutat collision zone a number of right lateral strike-slip and thrust faulting mechanisms are present (Figure 6.3). They are consistent with the relative motions of the Pacific and North America plates and with partitioning of the relative motion in the Yakutat collision zone. Along the Queen Charlotte and Fairweather faults the motion is primarily strike-slip with the slip vectors parallel with the predicted Pacific-North America plate motions (Figure 6.2; Doser and Lomas, 2000). The Fairweather fault is considered the eastern boundary of the Yakutat block and major earthquakes in 1927 (M = 7.1), 1958 (M = 7.9), and 1972 (M = 7.6) have occurred along the Fairweather fault. Further to the north and west along the Fairweather fault the Yakutat block begins to collide directly with North America and the focal mechanisms become mainly thrust. Numerous thrust faults are present and the region experiences high rates of seismicity and rapid uplift in the St. Elias and Chugach Mountains region. The most recent major earthquake was the 1979 M_w = 7.4 event which apparently ruptured the plate interface between the North America and Pacific plates (Lahr et al., 1979; Estabrook et al., 1992). Along the Denali fault the focal mechanisms are predominately right lateral strike-slip with some thrust faulting. The 3 November 2002 M_w = 7.9 earthquake along the Denali fault, one of the largest strike-slip earthquakes ever recorded in North America, began as a thrust event with $\sim$ 40 km of surface rupture and then ruptured $\sim$ 218 km as a right lateral strike-slip event. Focal mechanisms for the larger aftershocks are a mixture of strike-slip, normal, and thrust mechanisms (Ratchkovski et al, 2003)

Between the Denali fault and Tintina trench the seismicity decreases dramatically (Figure 6.1) and only a few focal mechanisms are available (Figure 6.2). These are a mixture of strike-slip and thrust mechanisms. Northeast of the Tintina trench, $\sim$ 600–800 km north-

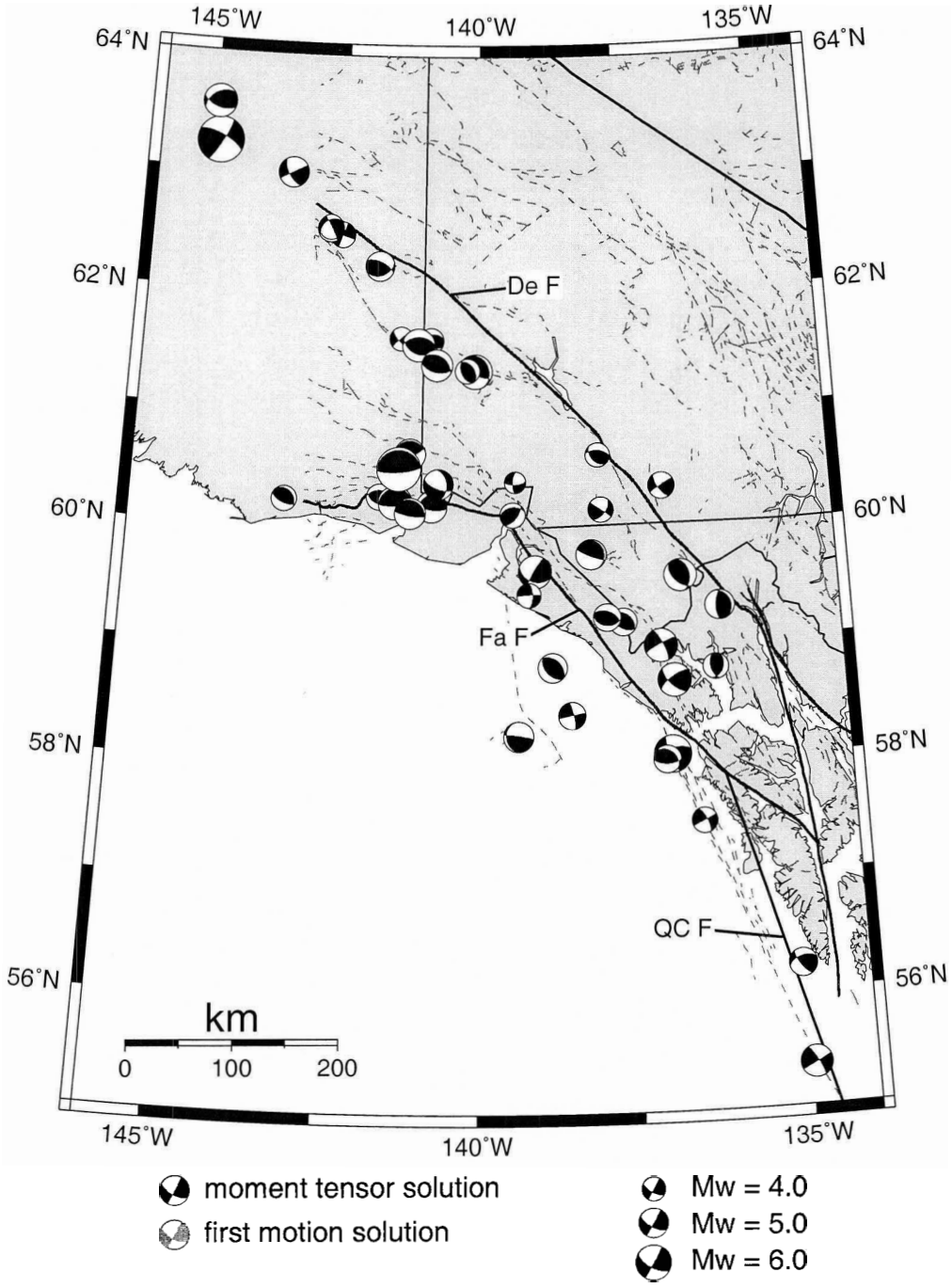

Figure 6.3 Focal mechanisms in the Yakutat collision zone region. De F - Denali Fault; Fa F - Fairweather Fault; QC F - Queen Charlotte Fault.

east of the Yakutat collision zone, the rate of seismicity increases and a number of moment tensor and first motion solutions have been calculated in the Mackenzie and Richardson Mountains region (Figure 6.4). Mazzotti and Hyndman (2002) propose that the increased rate of seismicity is due to a transfer of strain from the Yakutat collision zone across the northern Canadian Cordillera to the Mackenzie and Richardson Mountains with little intervening deformation.

Focal mechanisms in the Mackenzie and Richardson Mountains are a mixture of strike-slip and thrust mechanisms (Figure 6.4). At the southern end of the Mackenzie Mountains, in the Nahanni region of the southwest Northwest Territories, the available focal mechanisms all show thrust faulting. This is the region of the 5 October and 23 December 1985 Nahanni earthquakes (M_w = 6.6 and 6.7 respectively), the largest earthquakes recorded in the northern Canadian Cordillera. These earthquakes were nearly two magnitude units larger than any previously recorded events in the southern Mackenzie Mountains and generated a large number of aftershocks. The central and northern Mackenzie Mountains have a mixture of strike-slip and thrust faulting earthquakes. A sequence of strong earthquakes (M = 6.0–6.5) occurred in this region between 1953 and 1957 and first motion solutions show thrust faulting along a shallow dipping plane in a NNE-SSW direction (Cassidy and Bent, 2003). In the Richardson Mountains to the north, focal mechanisms become more dominantly strike-slip. A pair of large earthquakes (M = 6.2 and 6.5) occurred in May and June 1940. First motion solutions for these events show strike-slip faulting along either a N-S or E-W plane (Cassidy and Bent, 1993).

6.3.2 Stress Orientations

Directions of crustal stress can be estimated from moment tensor and first motion solutions using the method described in section 6.2. Composite stress tensors are calculated for four regions in the northern Canadian Cordillera and Yakutat collision zone — the Richardson Mountains, the northern and central Mackenzie Mountains, the Nahanni region, and the Yakutat collision zone (Figure 6.5). Figure 6.6 shows details of the stress tensors calculated using ZMAP6 (Wiemer, 2001) for each region. The 95% confidence limits in Figure 6.6 are represented by the distribution of small symbols around the large symbols. Unlike strain tensors, stress tensors do not depend on the size of the earthquake so large earthquakes do not dominate the results.

Along the eastern mountain front there is a change in the maximum compressive stress direction ($\sigma 1$) between the Nahanni region (southern Mackenzie Mountains), the central and northern Mackenzie Mountains, and the Richardson Mountains (Figure 6.5). In the

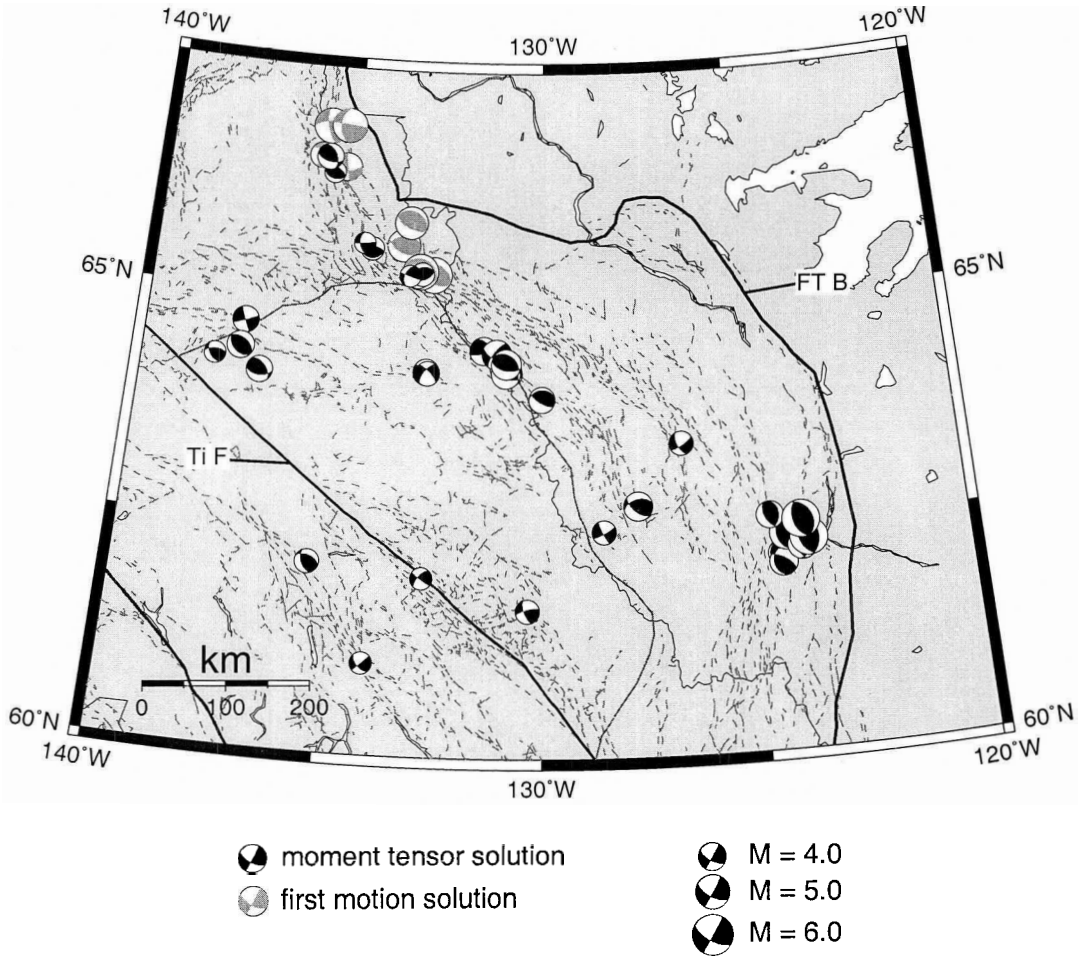

Figure 6.4 Focal mechanisms in the Mackenzie/Richardson Mountains. Ti F - Tintina Fault; FT B - Fold and Thrust belt.

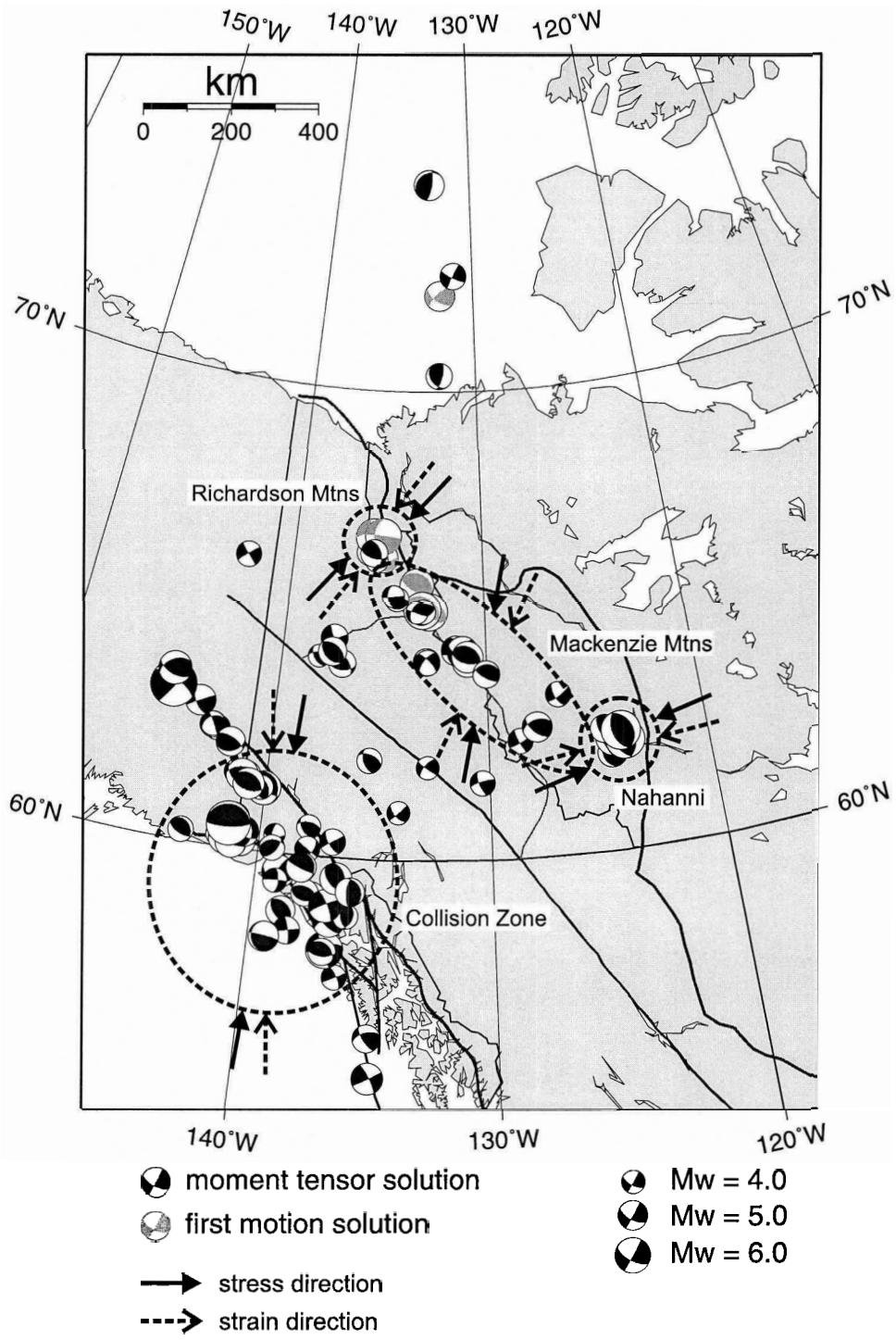

Figure 6.5 Composite stress and strain orientations for the northern Canadian Cordillera and Yakutat collision zone. Dashed lines indicate the groupings of earthquakes used to calculate the stress and strain directions, and arrows are the compressive stress orientation and strain orientation for each group.

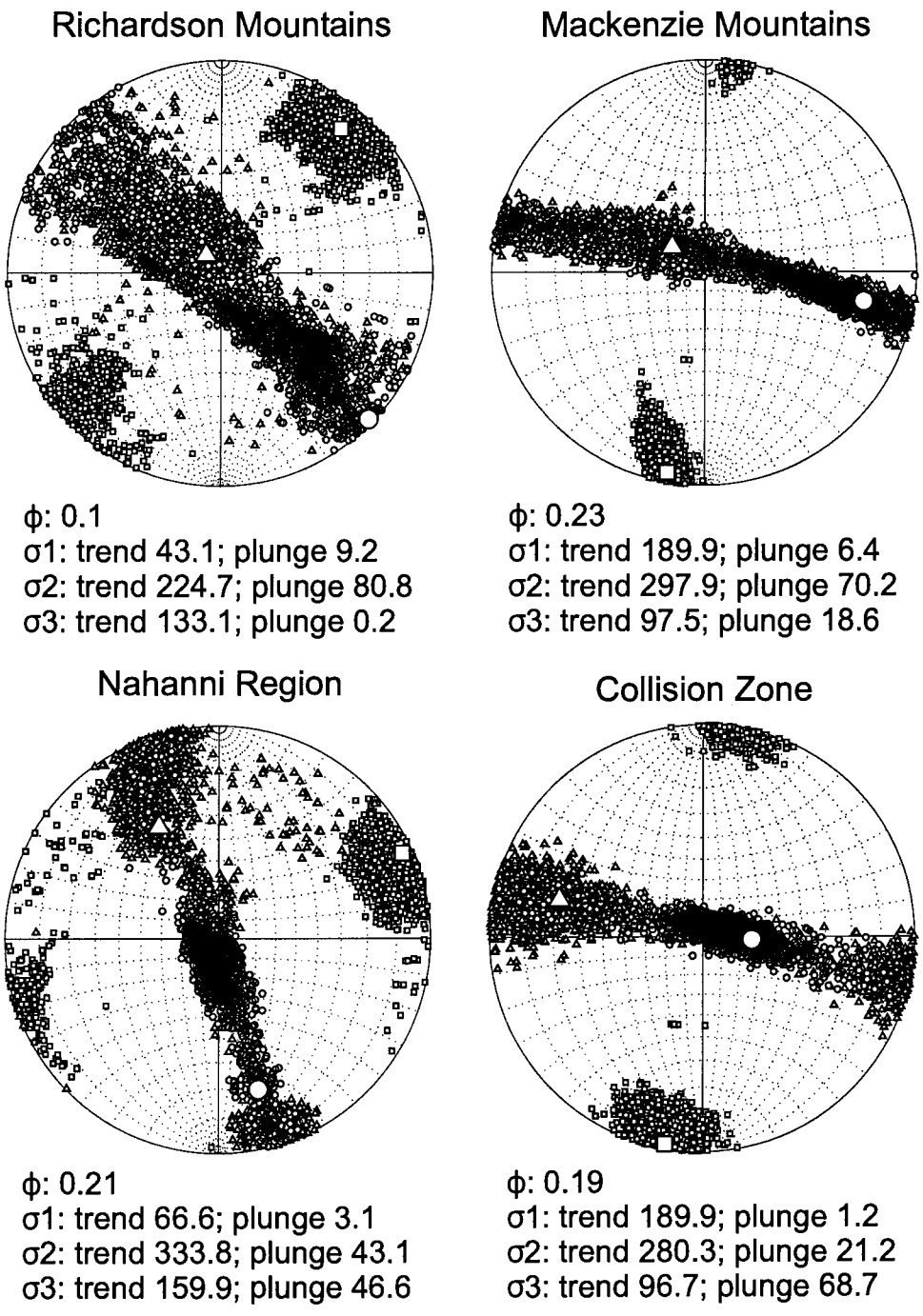

Figure 6.6 Stress tensors calculated for the four regions shown in Figure 6.5. $\sigma 1$, $\sigma 2$, and $\sigma 3$ are the principal stresses ordered from most compressional to most dilatational. ϕ is a measure of the relative sizes of the principal stresses (see section 6.2).

Nahanni region (mainly thrust) $\sigma 1$ is in a ENE-WSW direction. $\sigma 1$ then changes to nearly N-S in the central and northern Mackenzie Mountains (again, mainly thrust) and then to a NE-SW direction in the Richardson Mountains (mainly strike-slip). In the Yakutat collision zone $\sigma 1$ is also nearly N-S, identical to the central and northern Mackenzie Mountains.

The calculated stress tensors in Figure 6.6 vary in quality depending on the number of focal mechanisms present in each grouping and whether they are all similar mechanisms or vary between strike-slip and thrust mechanisms. If there are few focal mechanisms or many with a similar mechanism the computed confidence limits become large due to the inversion matrix becoming close to singular. This results in the data fitting the best model very well; however, the large confidence limits would indicate that many other models could also fit the data well (Michael, 1984).

In the Nahanni region the data set consists of eight mechanisms, all of which are thrust faulting with a similar slip direction. The resulting stress tensor (Figure 6.6 (*bottom left*)) has fairly large confidence limits for each of the principal stresses due to the similarity of the mechanisms. The Richardson Mountains data set is also small (six mechanisms) and dominated by strike-slip focal mechanisms and therefore the stress tensor also has large confidence limits (Figure 6.6 (*top left*)). In contrast the data set for the central and northern Mackenzie Mountains is considerably larger (25 mechanisms) and is a mixture of strike-slip and thrust mechanisms. The stress tensor has a very well defined $\sigma 1$ orientation with small confidence limits (Figure 6.6 (*top right*)). The Yakutat collision zone data set is also large (34 mechanisms) and has a mixture of strike-slip and thrust mechanisms; however, the majority are thrust faulting. The confidence limits are somewhat larger than for the central and northern Mackenzie Mountains but the maximum compressive stress is still well defined (Figure 6.6 (*bottom right*)). Table 6.1 summarizes the principal stress axes for the four regions.

The $\sigma 1$ confidence limits for the central and northern Mackenzie Mountains do not overlap with the confidence limits for the Richardson Mountains or the Nahanni region. This indicates that $\sigma 1$ for the central and northern Mackenzie Mountains is likely distinct from the other two regions. The $\sigma 1$ confidence limits for the Richardson Mountains and the Nahanni region overlap only for a small range which suggests that these two regions also have compressive stress directions which are distinct from one another. The ratio of the principal stresses, ϕ, is ~ 0.2 for all of the groupings with the exception of the Richardson Mountains ($\phi = 0.1$). When ϕ is close to zero, $\sigma 2$ and $\sigma 3$ are approximately equal. This may suggest that the state of stress is different in some way for the Richardson Mountains

than for the Mackenzie Mountains. However, the small and poorly constrained data set in the Richardson Mountains makes it difficult to draw any firm conclusions.

Region	$\sigma 1$		$\sigma 2$		$\sigma 3$	
	az	pl	az	pl	az	pl
YZ	190	1	280	21	97	69
Na	67	3	334	43	160	47
RM	43	10	225	81	133	0
MM	190	6	298	70	98	19

YZ - Yakutat Collision Zone; Na - Nahanni region; RM - Richardson Mtns; MM - Mackenzie Mtns.

Table 6.1 Principal axes orientations for the northern Canadian Cordillera stress tensors.

6.3.3 Strain Orientations

Relating First Motion Solutions to Moment Tensor Solutions

It is possible to estimate moment tensor elements from first motion solutions if a relationship between the seismic moment (M_o) and the magnitude calculated for the event exists (see Appendix D for more details on first motion solutions and moment tensors). The calculated magnitudes for first motion solutions available for the northern Canadian Cordillera are M_L. Using the method described in Chapter 4, a relationship between M_o and M_L can be established for the northern Canadian Cordillera and Yakutat collision zone. Figure 6.7 shows the relationship between M_o and M_L for the northern Canadian Cordillera and Yakutat collision zone determined from the available moment tensor solutions. The thick black line is the Hanks and Kanamori (1979) derived relationship between M_o and M_L ($\log(M_o) = 9.05 + 1.5M_L$). There is excellent agreement between these data and the Hanks and Kanamori (1979) relationship within the 95% confidence limits (dashed lines in Figure 6.7) which corresponds to a 1:1 relation between M_w and M_L for the northern Canadian Cordillera and Yakutat collision zone.

Strain Orientations for the Northern Canadian Cordillera

Strain tensors can be calculated for each of the earthquake groupings in Figure 6.5 using the method described in section 5.5.1, recognizing that the results are dominated by the largest earthquakes. Table 6.2 lists the summed moment tensor values which gives the

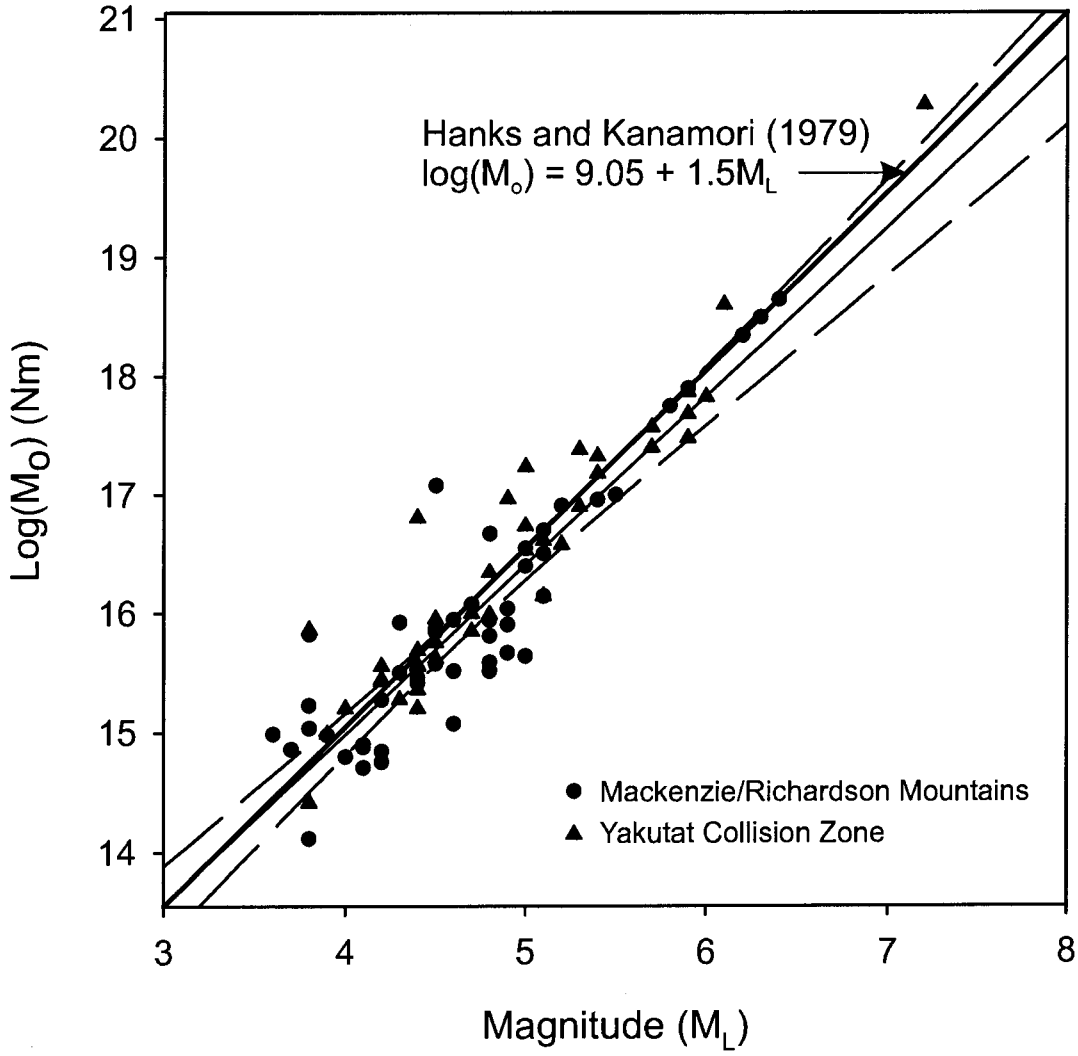

Figure 6.7 M_o/M_L relationship for events in the northern Canadian Cordillera and Yakutat collision zone. The thin solid line is a best-fit line between $\log(M_o)$ and M_L and the dashed lines are 95% confidence limits. The thick solid line is the Hanks and Kanamori (1979) relation between M_o and M_L

strain tensor for each of the groups. Also shown is the total scalar moment for the summed moment tensors and the scalar moment from the largest earthquake in each group. Table 6.3 lists the T, N, and P axes calculated from each of the strain tensors in Table 6.2.

Region	M_{xx}	M_{yy}	M_{zz}	M_{xy}	M_{xz}	M_{yz}	$M_{o_{tot}}$	$M_{o_{max}}$
YZ	-92.39	13.33	79.05	-9.71	171.05	-16.29	192.37	190.00
Na	-5.20	-22.38	27.59	-4.97	1.16	1.69	25.73	15.00
RM	-1.14	0.25	0.89	-4.39	-2.09	1.15	5.11	3.20
MM	-7.35	-1.52	8.87	-3.49	3.33	1.71	9.68	4.50

Region abbreviations are the same as in Table 6.1. Moment tensor elements are given in units of 10^{18} Nm. $M_{o_{tot}}$ is the total scalar moment for each region in 10^{18} Nm. $M_{o_{max}}$ is the maximum scalar moment (in 10^{18} Nm) for a single earthquake in each region.

Table 6.2 Summed moment tensor elements for the northern Canadian Cordillera.

Region	Axis	value	plunge	azimuth
YZ	T	186.73	58	348
	N	11.26	5	87
	P	-198.00	32	180
Na	T	27.68	88	45
	N	-3.88	1	165
	P	-23.79	2	255
RM	T	5.18	28	133
	N	-0.15	60	292
	P	-5.03	9	38
MM	T	9.62	79	29
	N	0.11	1	295
	P	-9.73	11	205

Region abbreviations are the same as in Table 6.1
Principal axes values are given in 10^{18} Nm.

Table 6.3 Principal axes orientations for the northern Canadian Cordillera strain tensors.

In the Yakutat collision zone the strain tensor is dominated by the 28 February 1979 M_w = 7.5 earthquake which contributes almost 99% of the total scalar moment. The resulting strain tensor for the region is a thrust faulting mechanism dipping shallowly to the

north (or steeply to the south), the same as the focal mechanism for the dominant earthquake. The orientation of the greatest principal strain is typical of an E-W striking thrust fault such as the Fairweather fault where the largest earthquake in the selected group occurred. The principal strain direction is also consistent with a NW-SE striking strike-slip fault such as the Denali fault. The observed strain field is able to explain motion on both the Fairweather and Denali faults.

In the Nahanni region all of the mechanisms are nearly E-W thrust faulting and the largest earthquake, the 23 December 1985 M_w = 6.7 event, contributes 58% of the total scalar moment. The strain tensor is a nearly E-W dipping thrust mechanism which is what would be expected. In the Nahanni region and Fold and Thrust belt all of the small faults to the west have an almost N-S strike which is consistent with the observed strain field.

In the Richardson Mountains the largest earthquake contributes 63% of the total scalar moment and the resulting strain tensor is a right lateral strike mechanism similar to the largest earthquake. Most of the observed focal mechanisms are right lateral strike-slip but a few thrust mechanisms with NE-SW dipping nodal planes are also present. As in the Yakutat collision zone, the observed strain field is able to explain both the strike-slip and the thrust mechanisms. In the central and northern Mackenzie the largest earthquake contributes 46% to the total scalar moment and the region is characterized by a thrust type strain tensor dipping in a NNE-SSW direction. The observed faults in the area have a general NW-SE trend. The observed strain field is typical for the thrust mechanisms but not for the strike-slip mechanisms.

6.3.4 Comparison of Stress and Strain Orientations

If the material in which an earthquake occurs is relatively uniform in strength, the principal stress (where $\sigma 1$, $\sigma 2$, and $\sigma 3$ are the maximum, intermediate, and minimum stresses, respectively) and principal strain axes (where $\varepsilon 1$, $\varepsilon 2$, and $\varepsilon 3$ are the maximum, intermediate, and minimum strains, respectively) should be the same, or relatively close (Figure 6.8 (*left*)). However, if the principal axes are the same it does not prove that the material is uniform in strength (Wyss et al., 1992). If there is a dominant plane of weakness in a volume, slip can occur on the plane even if the maximum compressive stress is at high angles to the fault. In this case the orientations of the principal stress and strain axes may be quite different (Figure 6.8 (*right*)) since the angle between $\varepsilon 1$ and the slip direction is always 45° while $\sigma 1$ can lie anywhere in the dilatational quadrant (McKenzie, 1969). In this section the principal stress and strain axes for the earthquake groupings in Figure 6.5 are compared to see if there are any significant differences between them.

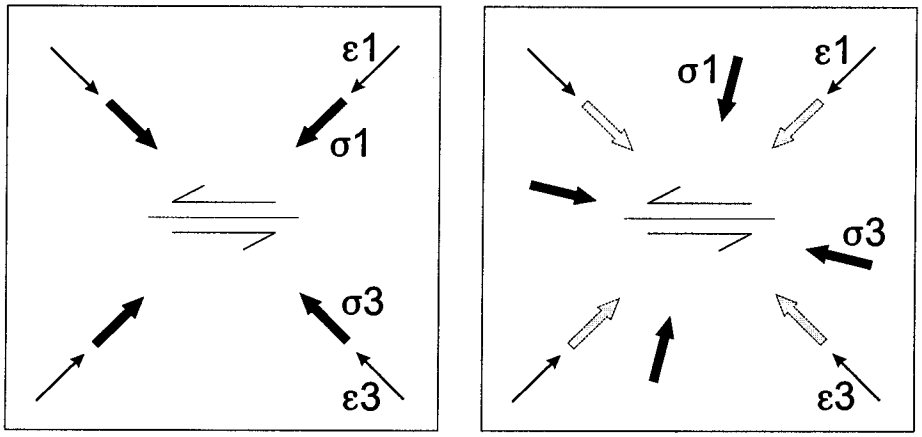

Figure 6.8 (*Left*) Schematic sketch of a medium with a fault that is not a pronounced zone of weakness such that the material can be considered uniform in strength. In this case the principal stress and strain axes will be approximately the same. (*Right*) A medium with a major zone of weakness where slip will occur even if the resolved shear stress is at high angles to the fault. In this case the orientations of the principal stress and strain axes may differ considerably (after Wyss et al., 1992)

The strain directions for each of the earthquake groupings are shown in Figure 6.5. In the Richardson Mountains and Nahanni region, the strain directions are very similar to the stress directions. In the Yakutat collision zone region the strain direction is rotated 10° counterclockwise to the stress direction. In this case the strain direction is dominated by the 28 February 1979 $M_w = 7.5$ earthquake which was a thrust event with slip in a N-S direction. In the central and northern Mackenzie Mountains the strain direction is rotated 15° clockwise relative to the stress direction. The dominant earthquakes in this group are the 11 January 1953 ($M_L = 6.3$) and the 1 March 1955 ($M_L = 6.4$) events in the northern Mackenzie Mountains. Both were thrust events with a NE-SW P axis orientation. In the central Mackenzie Mountains there are a number of focal mechanisms with more of a N-S P axis orientation which accounts for the change in direction between the stress and strain axes.

The northern and central Mackenzie Mountains are examined more closely by dividing the focal mechanisms into two groups (Figure 6.9), and Figure 6.10 shows the stress calculations for the two groups in Figure 6.9. In the central Mackenzie Mountains the focal mechanisms are a mixture of thrust and strike-slip mechanisms (Figure 6.9) and the maximum compressive stress direction is very well defined (Figure 6.10). The strain direction is rotated 16° clockwise relative to the stress direction. In the northern Mackenzie

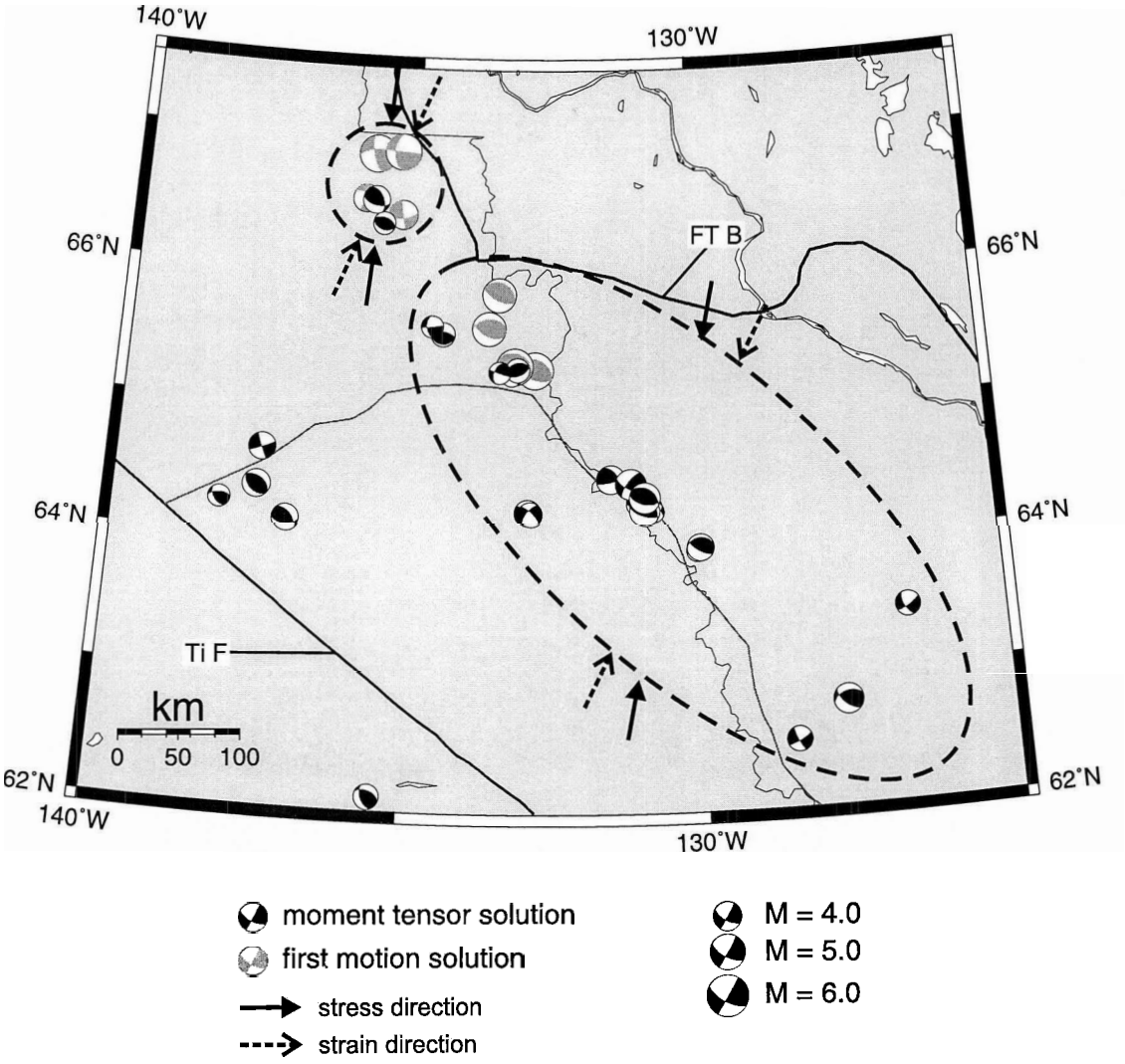

Figure 6.9 Composite strain and stress directions for the northern and central Mackenzie Mountains. Dashed lines indicate the groupings of earthquakes used to calculate the stress and strain directions, and arrows are the compressive stress orientation and strain orientation for each group. Ti F - Tintina Fault; FT B - Fold and Thrust Belt.

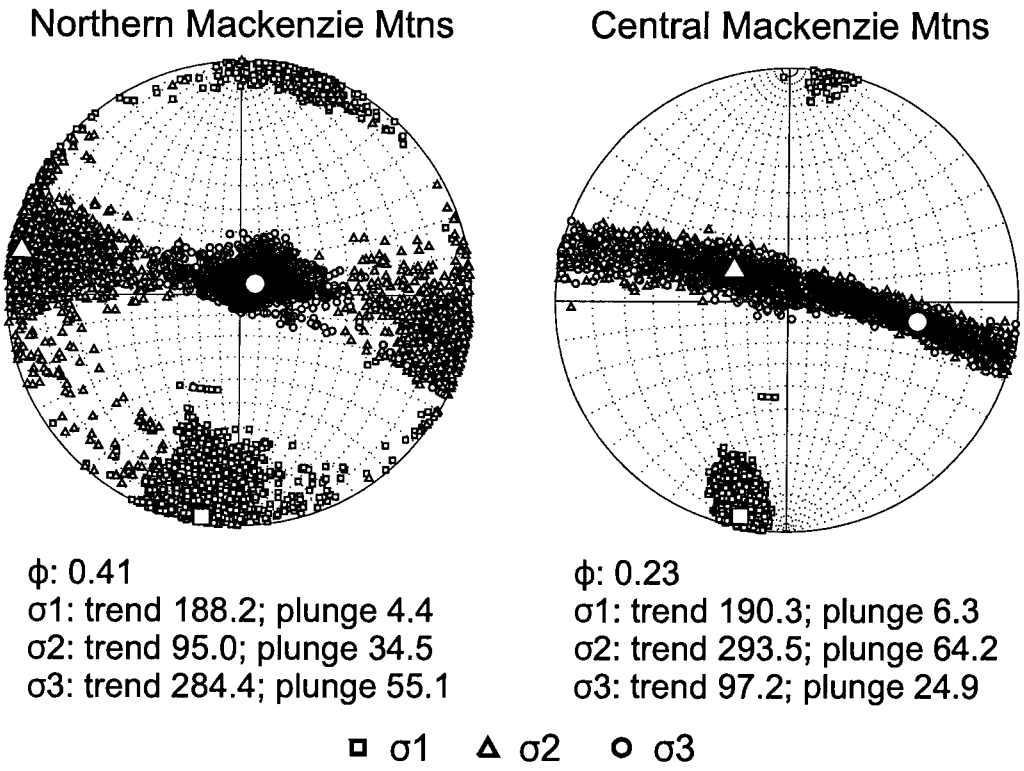

Figure 6.10 Stress tensors calculated for the two regions shown in Figure 6.9. $\sigma 1$, $\sigma 2$, and $\sigma 3$ are the principal stresses ordered from most compressional to most dilatational. ϕ is a measure of the relative sizes of the principal stresses (see section 6.2).

Mountains the focal mechanisms are predominately strike-slip and the resulting maximum compressive stress direction is not very well defined (Figure 6.10). The compressive strain direction is rotated 17° clockwise relative to the compressive stress direction (Figure 6.9). The stress and strain fields for the northern Mackenzie Mountains are essentially the same as for the central Mackenzie Mountains.

It is difficult to say for certain whether a 15° difference in principal compressive strain and compressive stress directions is significant. The principal compressive strain direction does fall within the 95% $\sigma 1$ confidence limits for the northern Mackenzie Mountains region, and is close for the central Mackenzie Mountains. Estimating errors in strain tensors is difficult. However, since the principal strain direction will depend largely on the orientation of the principal axes of the focal mechanisms, in particular that of the largest earthquake, the error in the focal mechanism principal axes can be used as a crude error estimate. Frohlich and Davis (1999) studied how well constrained the P, T, and N axes are in Harvard and USGS moment tensor solutions. Frohlich and Davis (1999) concluded that the majority of the moment tensor solutions have uncertainties of less than 15° in the principal axes orientations, and the uncertainty is $\sim 5 - 10°$ for well constrained, shallow solutions. Therefore, the error in the principal strain axes orientations presented here is likely $\sim 10°$. Thus, the principal compressive strain and compressive stress directions are within their respective uncertainties. If the difference is significant then the smaller earthquakes may occur on faults favourably aligned for failure in the prevailing stress field, while larger events rupture weaker faults not optimally aligned for failure but with low shear strength. If the difference is not significant then the larger earthquakes also occur on faults which are favourably aligned for failure in the prevailing stress field.

6.4 Summary

Nearly 100 regional moment tensor solutions have been calculated for the northern Canadian Cordillera and Yakutat collision zone which adds a great deal of information to that already available for these regions. Comparing M_o calculated from regional moment tensor solutions with M_L values shows that M_o and M_L are consistent in the northern Canadian Cordillera and southeast Alaska. This is an important result for calculating moment release rates in the northern Canadian Cordillera.

Regional moment tensor solutions are used to investigate the crustal stress and strain regime for northern Canada and southeast Alaska. Focal mechanisms are divided into four groups for the analysis: the Nahanni region in the southern Mackenzie Mountains, the

central and northern Mackenzie Mountains, the Richardson Mountains, and the Yakutat collision zone. $\sigma 1$ changes from nearly E-W in the Nahanni region to nearly N-S in the Mackenzie Mountains to NE-SW in the Richardson Mountains. In the Yakutat collision zone $\sigma 1$ is the same as the Mackenzie Mountains region. The principal strain directions in each of the four groups are similar to the principal stress directions except in the central and northern Mackenzie Mountains where the compressive strain direction is rotated 15° clockwise relative to the compressive stress direction. Dividing the central and northern Mackenzie Mountains into two groups yields the same results. It is uncertain whether a 17° difference in principal compressive strain and stress directions is significant. However, the compressive strain and stress directions are within their respective uncertainties. If the difference is significant then these results suggest that the largest earthquakes in the central and northern Mackenzie Mountains occur on faults not favourably oriented for failure and may be weak. If the difference is not significant then the larger earthquakes occur on faults which are favourably aligned for failure in the prevailing stress field.

Chapter 7

Southern Canadian Cordillera and Vancouver Island/Puget Sound Tectonics

7.1 Introduction

The southern Canadian Cordillera (defined here as the Canadian Cordillera south of 60°N and including northwestern Montana and northern Idaho and Washington, but excluding the Vancouver Island/Puget Sound region) has a much lower rate of seismicity than the Explorer plate or northern Canadian Cordillera regions. Prior to having the capability to calculate regional moment tensor solutions there have been very few focal mechanisms available for the southern Canadian Cordillera (two Harvard centroid moment tensor solutions and one first motion solution (Rogers et al., 1980)). More than 20 regional moment tensor solutions have since been calculated for the southern Canadian Cordillera. These solutions greatly increase the number of focal mechanisms available for the southern Canadian Cordillera and provide valuable tectonic information about a region where relatively little information has previously been available.

Nearly 40 regional moment tensor solutions are also available for the Vancouver Island/Puget Sound region of the Cascadia subduction zone. The regional moment tensor solutions are for both crustal events in the North America plate and events occurring within the subducting Juan de Fuca plate. These solutions provide valuable information about

the stress field and the relationship between different magnitude scales in the Vancouver Island/Puget Sound region.

7.2 Southern Canadian Cordillera Seismic Activity

The southern Canadian Cordillera is a region of relatively low seismic activity compared with the northern Canadian Cordillera. The seismicity in the interior of central British Columbia is very low and increases to the east in the region of the Rocky Mountain Trench and western Alberta, and to the south around the Canada/United States border (Figure 7.1). The largest events to occur in the southern Canadian Cordillera are $m_b \sim 5.6$–6.1 on 4 February 1918 near McNaughton Lake, about 150 km north of Revelstoke, British Columbia (Rogers and Ellis, 1979), and more recently $M_w = 5.5$ on 21 March 1986 near Prince George, British Columbia (Rogers et al., 1990) and $M_w = 5.4$ on 14 April 2001 near Dawson Creek, British Columbia. Most of the seismic activity is due to natural seismicity. However, there are regions where earthquake activity appears to be associated with hydrocarbon extraction, in particular the Fort St. John area of British Columbia and the Rocky Mountain House region of Alberta (e.g. Wetmiller, 1986; Horner et al., 1994).

Prior to having the capability to calculate regional moment tensor solutions, focal mechanisms in the southern Canadian Cordillera were scarce. The first focal mechanism calculated in the southeastern Canadian Cordillera was for the 14 May 1978 $M_L = 4.8$ earthquake near McNaughton Lake (Rogers, et al., 1980). With the ability to calculate regional moment tensor solutions more than 20 moment tensor solutions have been calculated for the southern Canadian Cordillera. Focal mechanisms in the southern Canadian Cordillera show mostly thrust faulting north of about 50°N indicating a compressional tectonic regime (Figure 7.2) consistent with the major geological features in the area. This style of faulting is also similar to the northern Canadian Cordillera. This contrasts markedly with focal mechanisms from the western United States, just south of the Canada/United States border, which show normal faulting corresponding to an extensional tectonic regime. Braunmiller (1998) calculated a number of regional moment tensor solutions for the continental western United States and virtually all are normal faulting mechanisms. Around the Canada/United States border is a transition zone from a compressional tectonic regime in western Canada to a extensional tectonic regime in the western United States (e.g. Sbar et al., 1972; Zoback and Zoback, 1980). In the Canada/United States border region the regional moment tensor solutions are predominantly strike-slip mechanisms (Figure 7.2).

An analysis similar to section 6.3.3 can be performed on moment tensor solutions from

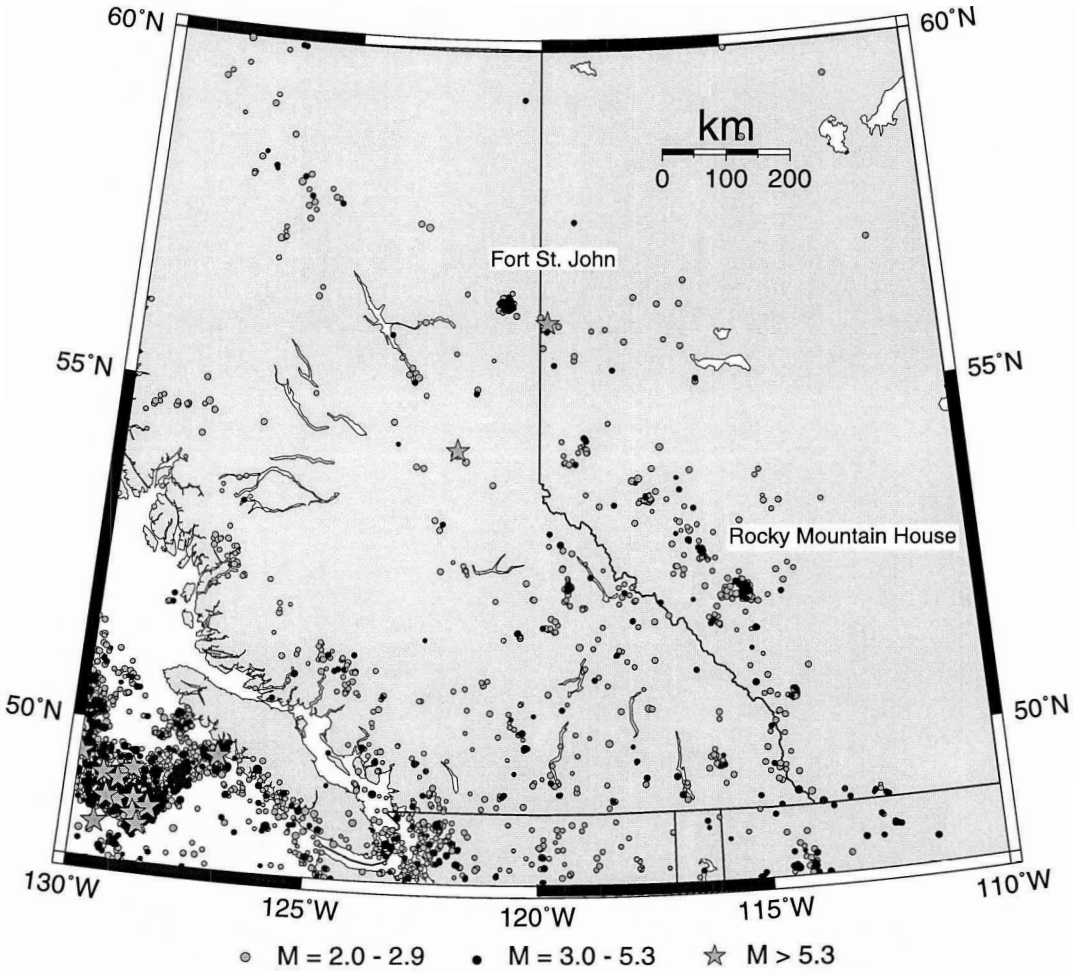

Figure 7.1 Seismicity (1982–2002) for the southern Canadian Cordillera. The southern Canadian Cordillera has a much lower rate of seismicity than the northern Canadian Cordillera.

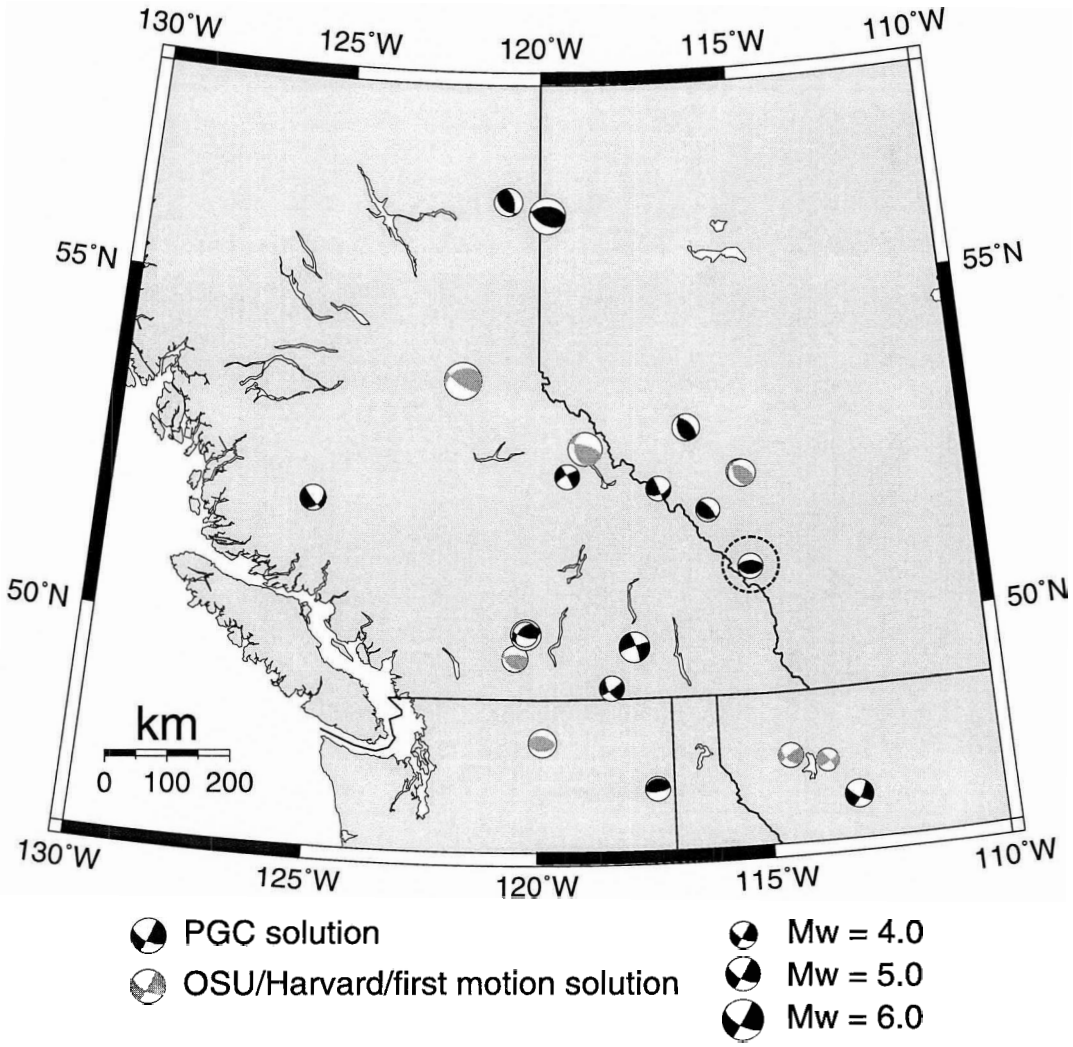

Figure 7.2 Moment tensor solutions calculated for the southern Canadian Cordillera. North of around 50°N the mechanisms are mainly thrust faulting mechanisms consistent with compressional tectonics. The solutions then change to strike-slip faulting around the Canada-United States border. The circled mechanism is singled out for analysis in section 7.3.2.

the southern Canadian Cordillera to establish a relationship between seismic moment, M_o and M_L. Figure 7.3 (*top*) shows the comparison between M_o and M_L for the southern Canadian Cordillera determined from the available moment tensor solutions. The thick black line is the Hanks and Kanamori (1979) derived relationship between M_o and M_L ($\log(M_o) = 9.05 + 1.5M_L$). The agreement between M_o and M_L is not as good as for the northern Canadian Cordillera (Figure 6.7); however, the data set is much smaller and some of the solutions are not as well constrained. Above $M_L \sim 3.8$ the observed data and the Hanks and Kanamori (1979) relation agree within the 95% confidence limits (dashed lines in Figure 7.3), and below $M_L \sim 3.8$ the Hanks and Kanamori (1979) relation is still close to the 95% confidence limits.

The events indicated by triangle symbols in Figure 7.3 (*top*) all have M_L's less than 3.5 and have a large discrepancy between M_w and M_L. These events have poor quality regional moment tensor solutions and the moments may not be reliable. Removing these events gives the M_o/M_L relation shown in Figure 7.3 (*bottom*). In this case there is good agreement between the data and the Hanks and Kanamori (1979) relationship within the 95% confidence limits. With the small data set it is difficult to reach any firm conclusions but it appears that M_o and M_L have a similar relationship for the southern Canadian Cordillera as they have in the northern Canadian Cordillera. More regional moment tensor solutions in the future will give better constraints on the M_o/M_L relation for the southern Canadian Cordillera.

Figure 7.4 shows a spatial comparison of M_w to M_L for events in the southern Canadian Cordillera. The events are divided into three groups depending on the difference between M_w and M_L: $M_w - M_L \geq 0.5$; $M_w - M_L = 0.0 - 0.4$; and $M_w - M_L < 0.0$. While the three southernmost events all have $M_w - M_L = 0.0 - 0.4$, the discrepancy between M_w and M_L does not show any obvious correlation with the location of the event within the southern Canadian Cordillera.

7.3 Crustal Stresses

Information on crustal stresses in Canada has increased substantially in the last 25 years. Adams (1987) began compiling information from a variety of sources including focal mechanisms, oil well breakouts, hydraulic fracturing, and overcoring (Adams and Bell, 1991). This data is compiled in the Canadian Crustal Stress Database (CCSB). Very few focal mechanisms exist in the CCSB for the northern and southern Canadian Cordillera. Stress information for the continental region of western Canada in the CCSB is mainly limited to

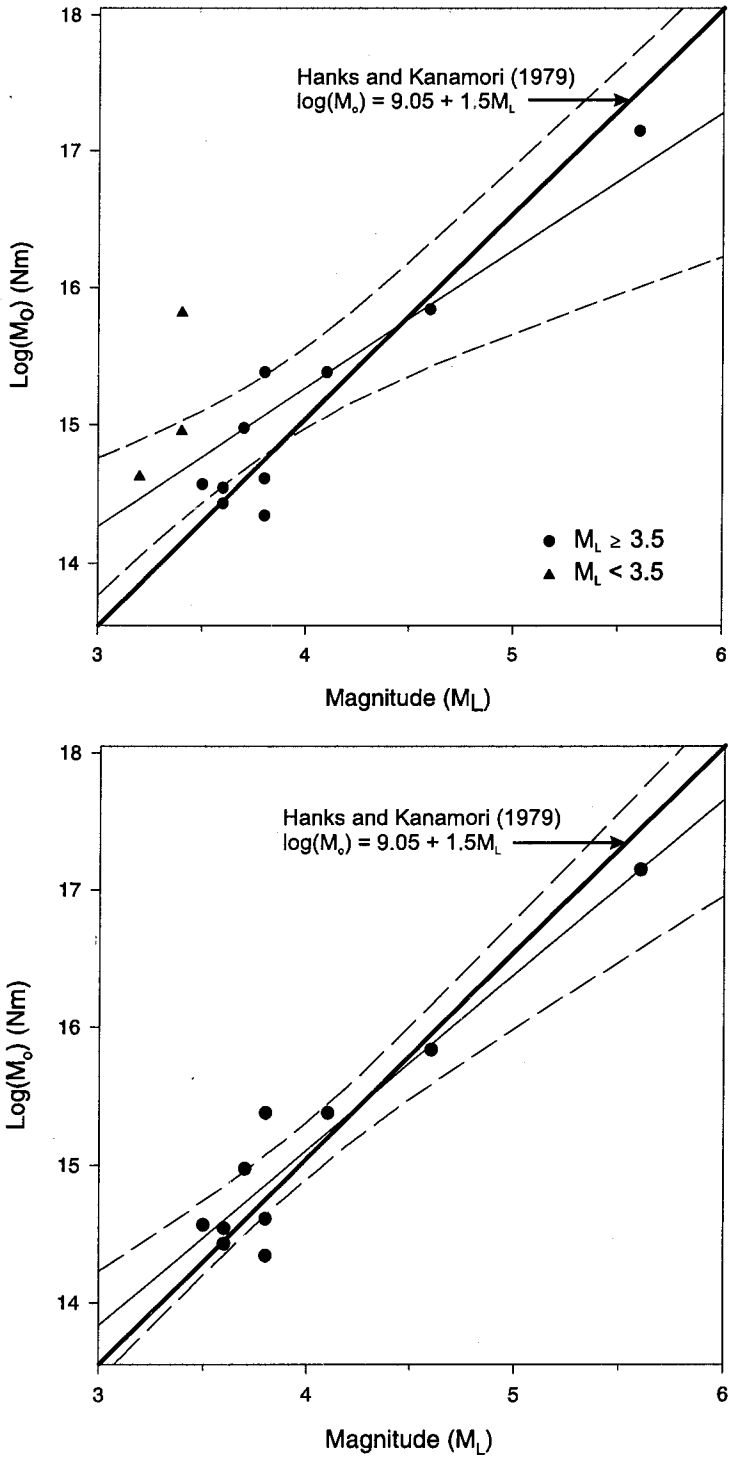

Figure 7.3 (*Top*) Relationship between M_o and M_L for events in the southern Canadian Cordillera. The thin solid line is a best-fit line between $\log(M_o)$ and M_L and the dashed lines are 95% confidence limits. The thick solid line is the Hanks and Kanamori (1979) relation between M_o and M_L. (*Bottom*) Same as above except events with $M_L < 3.5$ have been removed from the data set.

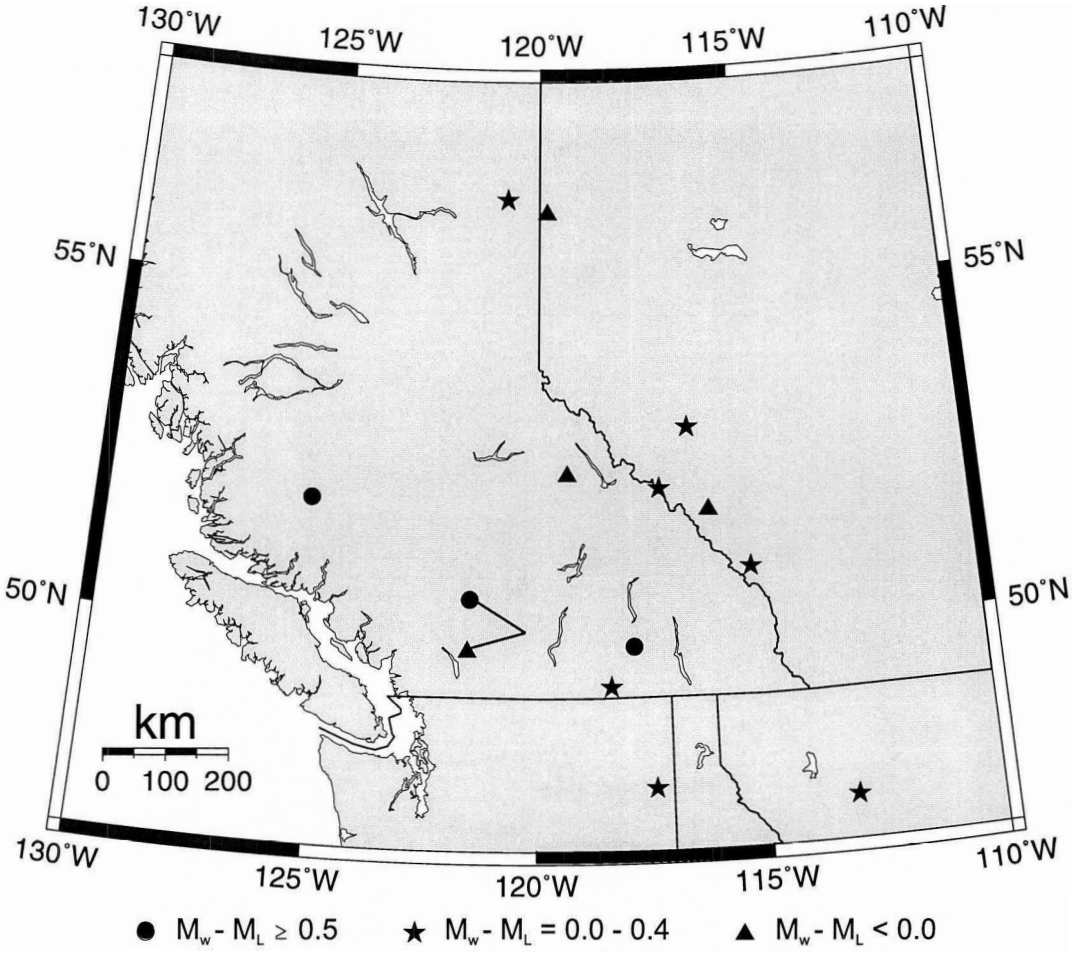

Figure 7.4 Spatial comparison of M_w/M_L for events in the southern Canadian Cordillera. The discrepancy between M_w and M_L does not show any correlation with the location of the event within the southern Canadian Cordillera.

oil well breakouts in western Alberta and in the Mackenzie delta region in the Northwest Territories (Adams, 1987; Adams and Bell, 1991).

With the ability to calculate regional moment tensor solutions there are now nearly 100 moment tensor solutions available for the northern and southern Canadian Cordillera. Many of these solutions are located where previous stress information is not available from oil well breakouts or any previously determined focal mechanisms. As a result this will be the first analysis of crustal stresses from focal mechanisms for much of western Canada. It is important to note that larger earthquakes are influenced by the local fault pattern and not just the stress direction. It is only by averaging a number of focal mechanisms with varying faulting types that it is possible to determine the stress regime.

7.3.1 Orientation of Principal Horizontal Stresses

The regional stress pattern for western Canada from earthquake focal mechanisms can be mapped by plotting the principal stress directions. This is most effective when the principal axes are horizontal or near-horizontal. Virtually all focal mechanisms in western Canada are strike-slip or thrust and therefore the maximum compressive stress axes will be near-horizontal and the compressive stress direction can be represented by plotting the azimuth of the P axis. Figure 7.5 shows the azimuths of P axes plotted from focal mechanisms for western Canada. To reflect the varying plunge of the P axis, the arrows are scaled according to the plunge with a 0° plunge being the largest and 90° plunge having zero length. Figure 7.6 plots the T axis azimuth for the same focal mechanisms as in Figure 7.5. A plunge close to 0° in the T axis plot corresponds to strike-slip or normal faulting and a plunge close to 90° corresponds to thrust faulting.

The pattern for the compressive stress is relatively straightforward for most of western Canada. In the northern Canadian Cordillera the compressive stress is mainly oriented in a NE-SW direction from the Gulf of Alaska through to the Mackenzie Mountains. The exception is the Nahanni region in the southwestern Northwest Territories where the compressive stress is nearly E-W. These results have been discussed in detail in chapter 6.

The southern Canadian Cordillera shows some variation in the compressive stress direction. In the eastern Canadian Cordillera, around the British Columbia/Alberta border region, the compressive stress direction is NE-SW, similar to Adams (1987) results from oil well breakouts in western Alberta. This is also consistent with the compressive stress direction in the northern Canadian Cordillera and supports the idea that the whole of

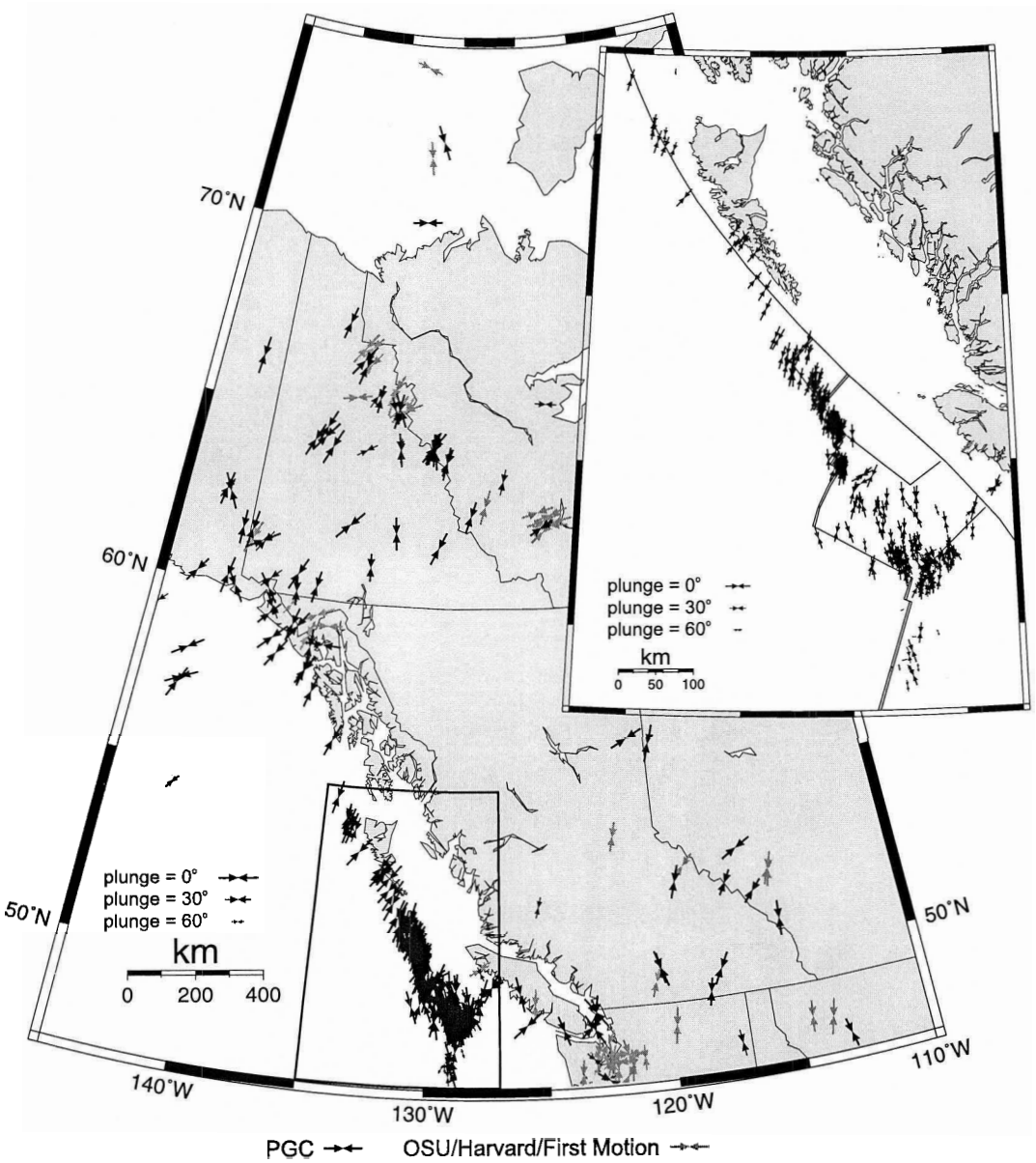

Figure 7.5 P axis azimuths from focal mechanisms in western Canada. The arrow lengths are scaled according the the plunge of the axis with 0° plunge being the largest and 90° having zero length.

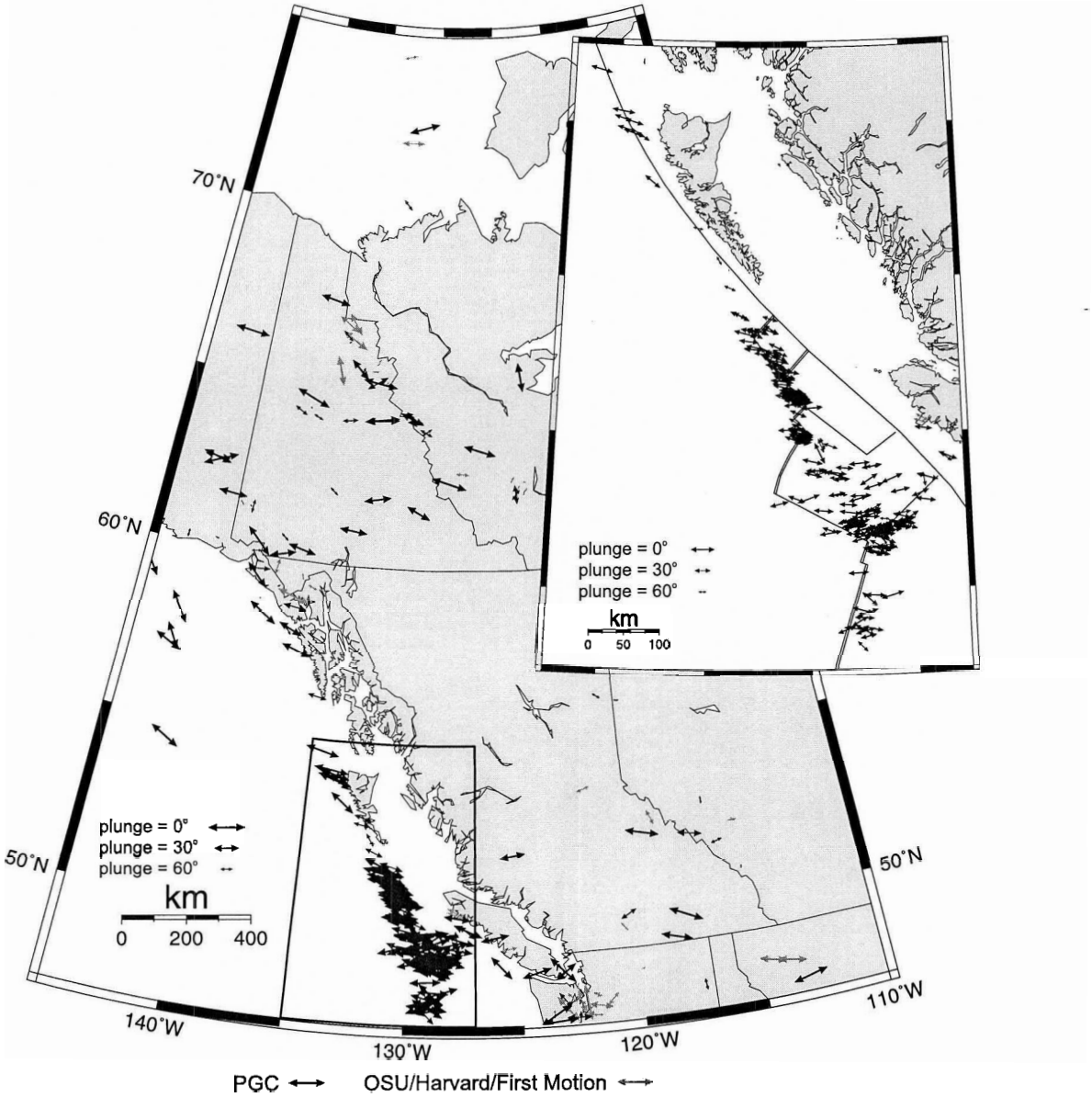

Figure 7.6 T axis azimuths from focal mechanisms in western Canada. The arrow lengths are scaled according the the plunge of the axis with 0° plunge being the largest and 90° having zero length.

the Canadian Cordillera is being compressed in a NE-SW direction. In southwest British Columbia and northwest Washington the compressive stress direction is N-S, consistent with Mulder (1995) results from first motion focal mechanisms. This stress regime is attributed to oblique subduction of the Juan de Fuca plate and right-lateral shear motion of the Pacific and North America plates causing N-S compression (Wang et al., 1997). In southwest British Columbia and northwest Washington the Juan de Fuca plate is coupled with the North America plate and results in margin parallel compression in the continental crust. In the eastern Cordillera the Juan de Fuca plate no longer influences the North America plate and compressive crustal stresses are similar with the rest of western Canada. In the intervening area, central British Columbia, relatively little data has previously been available to map how the compressive stress field changes from N-S to NE-SW. At what point the compressive stress field changes direction is of interest as this will mark the transition zone where the coupling effect of the Juan de Fuca plate is no longer observed within the North America plate.

The moment tensor solutions from the Canada/United States border region all have P axes oriented approximately N-S through to the eastern Cordillera. Regional moment tensor solutions calculated by Braunmiller (1998) in the western United States are largely normal faulting mechanisms but there are a few strike-slip and thrust solutions. The strike-slip and thrust mechanisms have N-S oriented P axes through to around 115°W where the P axes change to a mixture of N-S and NE-SW orientations. The moment tensor data suggests that the influence of the coupling of the Juan de Fuca plate is significant through most of southern British Columbia and Washington. However, another interpretation could be that the N-S compression in southeastern British Columbia is related to the E-W extensional stress regime observed in the western United States. This will be discussed further in section 7.3.2.

7.3.2 Stress Tensor Analysis

The crustal stress field can be analyzed further by calculating stress tensors from the focal mechanisms using the method discussed in section 6.2. The focal mechanisms are a mixture of strike-slip and thrust mechanisms which means the stress tensor should be fairly well constrained. The stress tensor calculated using all of the focal mechanisms in Figure 7.2 is shown in Figure 7.7 (*top*). The calculated stress tensor has a well constrained compressive stress direction ($\sigma 1$) oriented in a NNE-SSW direction. $\sigma 2$ and $\sigma 3$ overlap considerably which is expected with a mixture of strike-slip and thrust mechanisms.

By a visual inspection of the focal mechanisms in Figure 7.2 and the P axis azimuths in

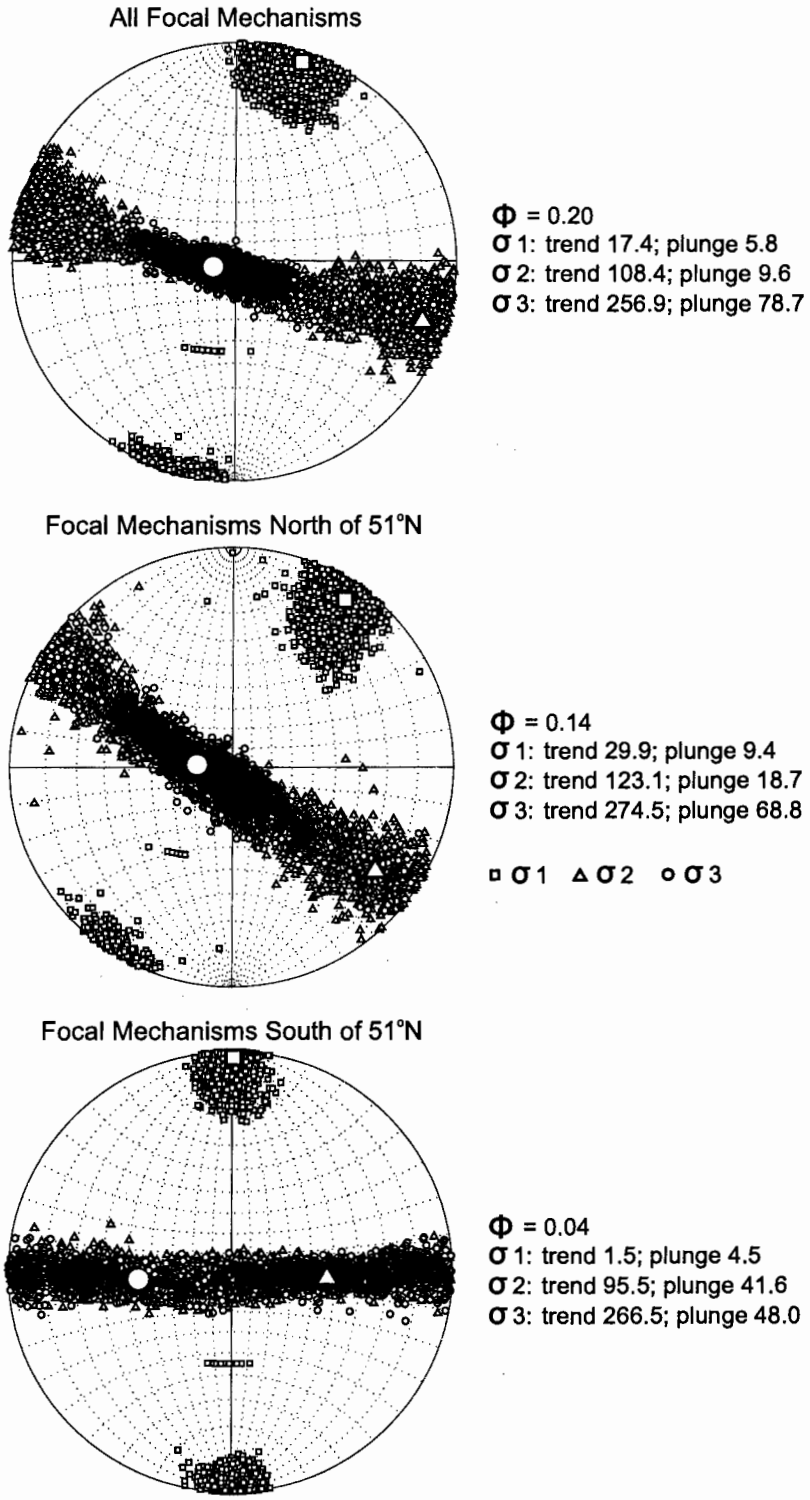

Figure 7.7 Composite stress tensors calculated for events in Figure 7.2. $\sigma 1$, $\sigma 2$, and $\sigma 3$ are the principal stresses from most compressional to least compressional. ϕ is a measure of the relative sizes of the principal stresses (see section 6.2).

Figure 7.5 there appears to be a difference in the compressive stress direction between focal mechanisms located north and south of around 50°N to 51°N. The maximum compressive stress direction appears to be NE-SW or NNE-SSW north of around 50°N to 51°N and N-S south of around 50°N to 51°N. The focal mechanisms are divided into two groups based on latitude, and stress tensors calculated to see if there is a significant difference in the direction of compressive stress (Figure 7.7 (*middle*) and (*bottom*)). The circled focal mechanism in Figure 7.2 has a mechanism more consistent with the southern group of events but geographically is closer to the northern group. For the purposes of the stress tensor analysis the circled mechanism is placed with the southern group making 51°N the dividing line between the northern and southern groups. Grouping the circled mechanism with the northern events has little effect on the results and so only one set of results will be presented here.

The maximum compressive stress direction is well defined for both the northern and southern groups (Figure 7.7 (*middle*) and (*bottom*)). $\sigma 1$ for the stress tensor calculated for the focal mechanisms north of 51°N (Figure 7.7 (*middle*)) has an azimuth of 30° compared with a $\sigma 1$ azimuth of 2° for the focal mechanisms south of 51°N (Figure 7.7 (*bottom*)). The $\sigma 1$ confidence limits do not overlap for the two groups indicating they are distinct from one another. On the basis of these results there appears to be a sharp latitudinal transition from N-S to NE-SW compression in southern British Columbia at around 50°N to 51°N. This correlates well with the northern limit of the subducted Juan de Fuca plate. Cassidy et al., (1998) defined the northern limit of the subducted Juan de Fuca plate at around 50°N beneath Vancouver Island.

As mentioned in section 7.2 the tectonic setting in western North America changes from compressional in Canada to extensional in the United States. Focal mechanisms from the southwestern United States are consistent with E-W or NE-SW extensional tectonics (e.g. Sbar et al., 1972; Zoback and Zoback, 1980; Stickney and Bartholomew, 1987; Braunmiller 1998; Stickney and Lageson, 2002) compared with N-S compression in western Canada. Sbar et al. (1972) calculated composite first motion focal mechanisms from microearthquakes from southwestern Utah to northwestern Montana and suggested that the tectonic character of this region is E-W extension. Zoback and Zoback (1980) also suggested an E-W extensional stress regime for the western Montana and western Wyoming region. Braunmiller (1998) calculated a number of regional moment tensor solutions for the western United States which show normal faulting with an E-W tension axis for the western Wyoming/southeastern Idaho region and NE-SW tension for central Idaho. Stickney and Bartholomew (1987) proposed a NE-SW tensional tectonic regime for southwest

Montana and adjacent Idaho. Stickney and Lageson (2002) presented a regional moment tensor solution calculated by John Nábělek at OSU for a $M_w = 4.8$ event in southwest Montana which was a normal faulting mechanism with a NE-SW tension axis.

The above mentioned results demonstrate that, around the Canada/United States border, the tectonic setting becomes unclear. The three regional moment tensor solutions in northwestern Montana shown in Figure 7.2 are strike-slip mechanisms with E-W tension and N-S compression. As well there are two more strike-slip mechanisms in southeastern British Columbia near the Canada/United States border with E-W tension and N-S compression. These focal mechanisms could possibly be related to the coupling effect of the Juan de Fuca plate with the North America plate causing N-S compression. However, they could also be a result of the E-W extensional tectonic regime in the western United States. E-W tension faulting on a strike-slip fault will result in a focal mechanism with N-S compression. The resulting focal mechanism could give the impression that the faulting is due to N-S compression rather than E-W tension. Therefore, the stress tensor shown in Figure 7.7 (*bottom*) may not represent the true nature of the stress regime around the Canada/United States border.

Exactly where the transition from compressional to extensional tectonics occurs is important for seismic hazard estimates in western Canada. If the compressional tectonic setting extends south to the Canada/United States border then southern British Columbia and southern Alberta, including the Calgary, Alberta area, are at risk for large thrust style earthquakes similar to the 1985 Nahanni events in the Northwest Territories. If the compressional to extensional tectonics transition occurs further north then the seismic risk from large thrust earthquakes is lower for southern British Columbia and southern Alberta. With the presently available regional moment tensor solutions it is not possible to determine where the compressional to extensional transition occurs. They do suggest that given another decade or two there may be enough solutions available to give a clearer picture of the tectonic setting.

7.4 Vancouver Island/Puget Sound Region

7.4.1 Crustal and In-Slab Stress Fields

The Vancouver Island/Puget Sound region is a tectonically complex region where the Juan de Fuca plate is subducting beneath North America. The strike of the margin changes from N-S around southern Washington to NW-SE in the vicinity of Vancouver Island. Mulder (1995) and Bolton (2003) calculated first motion focal mechanisms for events occurring

within the overlying crust and the subducting slab in the Vancouver Island/Puget Sound region. The first motion mechanisms are mainly a mixture of strike-slip and normal faulting styles with no obvious pattern in the strike of the fault planes. However, Mulder (1995) studied the stress field for crustal events in the Vancouver Island/Puget Sound region and concluded that the maximum compressive stress direction in the crust is oriented margin parallel. Bolton (2003) examined the stress field for in-slab earthquakes and concluded that the maximum tensional stress direction in the slab is oriented E-W which is consistent with down-dip tension.

38 regional moment tensor solutions are available for the Vancouver Island/Puget Sound region, calculated in this study and by OSU (Figure 7.8). Like the first motion mechanisms, the regional moment tensor solutions show no obvious pattern in faulting style, reflecting the complex tectonic setting. The regional moment tensor solutions can be divided into events occurring within the overlying crust and those occurring in the subducting slab (Figure 7.8 (*bottom*)). The two circled events have depths of 27 km and 33 km and it is uncertain whether they are located in the overlying crust or in the subducting slab. For the purposes of the stress analysis they are grouped with the crustal events. The stress tensor for the crustal events (Figure 7.9 (*left*)) has poorly constrained $\sigma 1$ and $\sigma 2$ axes. However, the best fitting $\sigma 1$ orientation is margin parallel which is consistent with the conclusions from Mulder (1995). The stress tensor for the slab events (Figure 7.9 (*right*)) is very poorly constrained. The best fitting tension axis ($\sigma 3$) is oriented E-W which is consistent with Bolton (2003) and with down-dip tension.

7.4.2 Magnitude Comparisons

Bolton (2003) compared M_w to M_L for seven in-slab events in the Vancouver Island/Puget Sound region where regional moment tensor solutions exist. For each event M_w was higher than M_L by 0.1–0.8 magnitude units. In this section, the entire data set of 38 regional moment tensor solutions is examined to investigate the relationship between M_w and M_L for the Vancouver Island/Puget Sound region. Figure 7.10 (*top*) compares M_w to M_L for all of the regional moment tensor solutions in the Vancouver Island/Puget Sound region. The dashed line represents an ideal 1:1 relationship between M_w and M_L, and the solid line is a best-fit line assuming a slope parallel to the 1:1 line (see section 4.3 for details). M_w is, on average, 0.37 ± 0.07 magnitude units larger than M_L. The events are then divided into those occurring around Vancouver Island and those occurring in the Puget Sound region (Figure 7.10 (*middle* and *bottom*)). In the Vancouver Island region, M_w is 0.32 ± 0.09 magnitude units larger than M_L (Figure 7.10 (*middle*)), and in the Puget Sound region

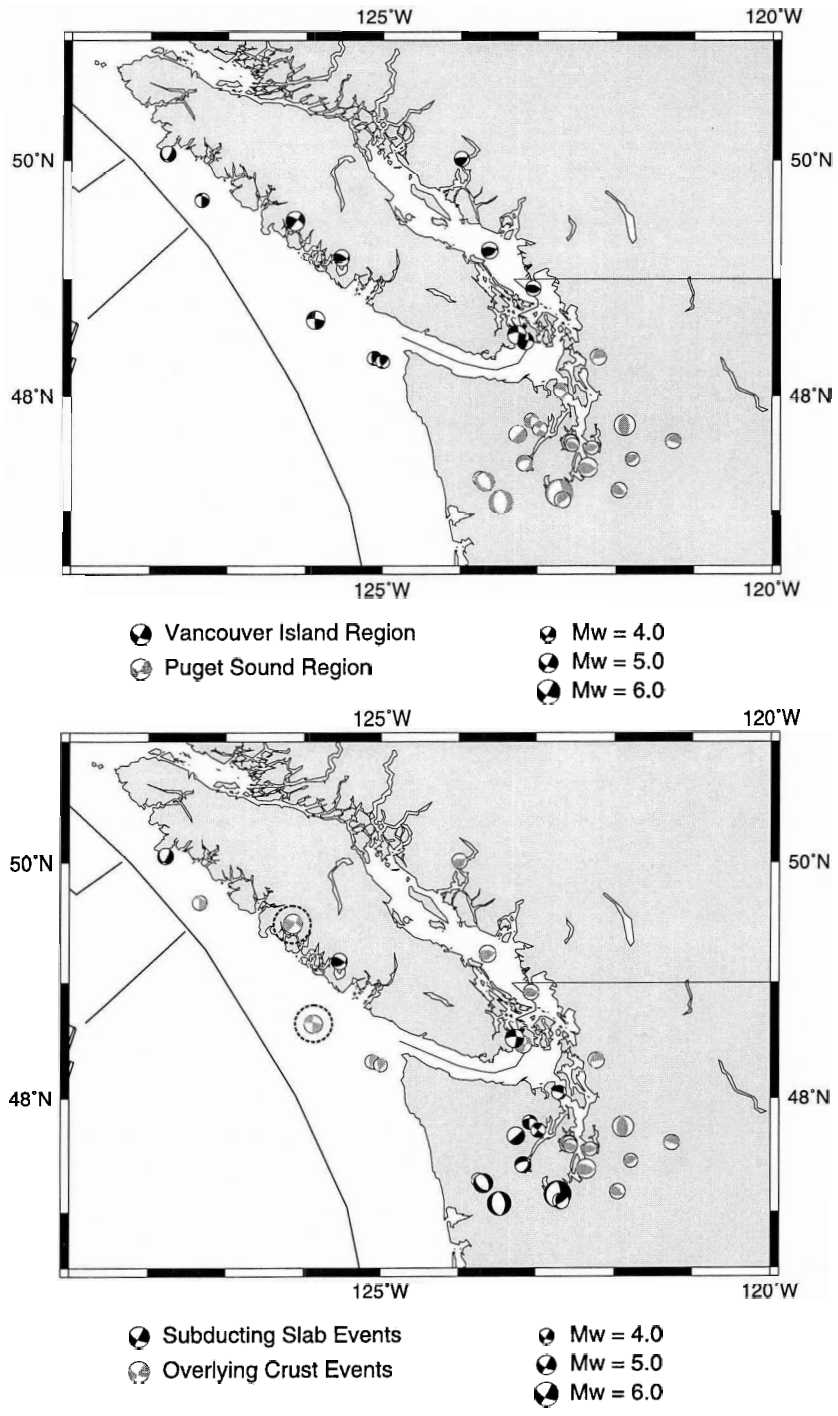

Figure 7.8 Regional moment tensor solutions for the Vancouver Island/Puget Sound region. (*Top*) Regional moment tensor solutions grouped into those located around Vancouver Island and those in the Puget Sound region. (*Bottom*) Regional moment tensor solutions grouped into events occurring in the overlying crust and events occurring in the subducting slab. The two circled mechanisms are events which may either be crustal or in-slab events.

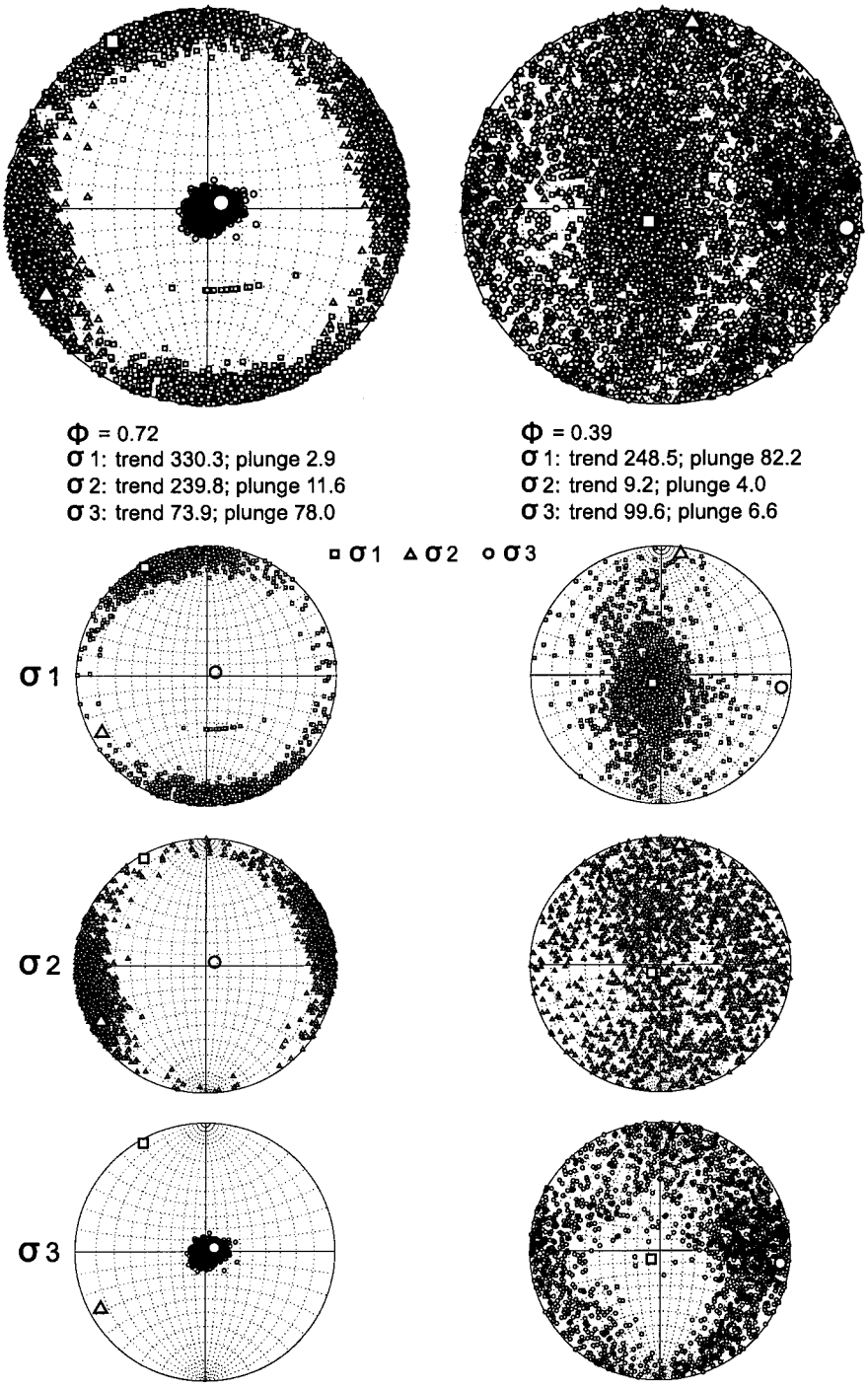

Figure 7.9 Composite stress tensors from regional moment tensor solutions in the Vancouver Island/Puget Sound region. (*Left*) Stress tensor for the crustal events with $\sigma 1$ oriented margin parallel. Also shown is separate stress tensor plots for each of the principal axes. (*Right*) Stress tensor for the slab events with $\sigma 3$ oriented in the down-dip direction. Also shown is separate stress tensor plots for each of the principal axes.

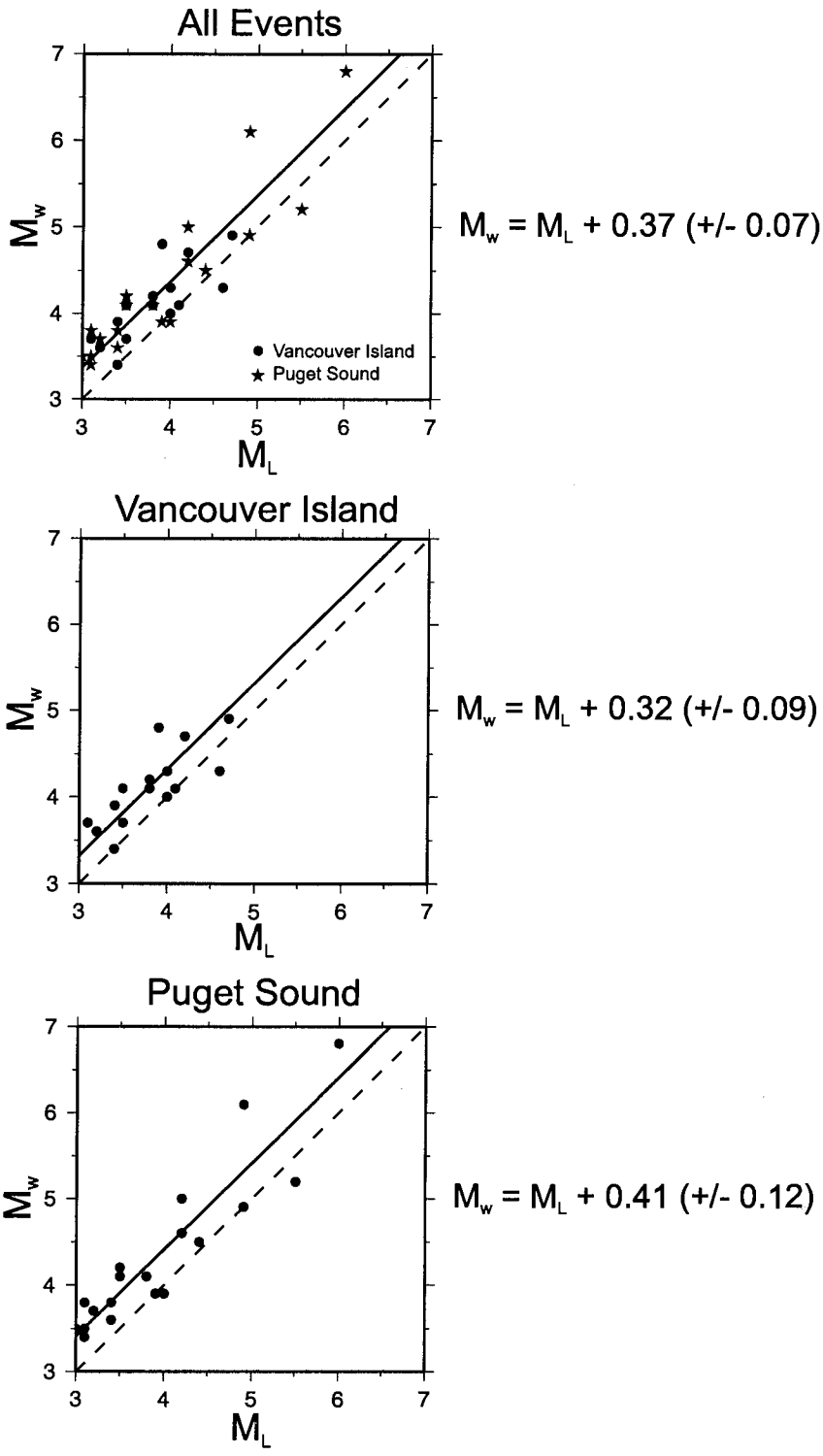

Figure 7.10 M_w-M_L comparison for events in the Vancouver Island/Puget Sound region. In each case the dashed line represents an ideal 1:1 relationship between M_w and M_L, and the solid line is a best-fit line assuming a slope parallel to the 1:1 line. The M_L correction is indicated for each zone.

M_w is 0.41 ± 0.12 magnitude units larger than M_L (Figure 7.10 (*bottom*)). The M_w/M_L discrepancies for the Vancouver Island and Puget Sound groups are within their respective error bounds. This suggests that the M_w/M_L discrepancy is consistent over the entire Vancouver Island/Puget Sound region.

Figure 7.11 compares M_w with M_L for events occurring in the overlying crust and those occurring in the subducting slab. The analysis is carried out with the circled events from Figure 7.8 (*bottom*) grouped with the crustal events and with the slab events. Figure 7.11 (*top*) compares M_w to M_L for crustal events and slab events with the uncertain mechanisms grouped with the crustal events. Figure 7.11 (*bottom*) compares M_w to M_L for crustal and slab events with the uncertain mechanisms grouped with the slab events. In both cases the M_w/M_L discrepancy is significantly higher for the slab events compared with the crustal events by about 0.35 magnitude units.

The 0.25 magnitude unit discrepancy between M_L and M_w for events in the overlying crust may or may not be significant. In a tectonically complex region such as the Vancouver Island/Puget Sound region it is difficult to accurately model the observed waveforms using only simple 1-D Earth models for calculating Green's functions, and this could result in M_o's which are less reliable. However, the 0.60 magnitude discrepancy for slab events is significant. The larger M_w/M_L discrepancy for in-slab events is probably related to the more complex source-receiver travel path for in-slab events. The magnitude relationship between crustal and slab events is a problem which could be addressed in future studies using more detailed Earth models, and carefully examining the effect of the subducting slab and overlying crust on modeled waveforms.

M_w and M_L can also be compared with coda magnitude, M_c, for events in the Vancouver Island/Puget Sound region. M_c (also called duration magnitude, M_D) is calculated based on the duration of the seismic signal. The Pacific Northwest Seismograph Network (PNSN), based at the University of Washington, calculates M_c for earthquakes in the Puget Sound region and for many events in the Vancouver Island region. Table 7.1 compares M_c with M_w for events in the Vancouver Island/Puget Sound region. Table 7.1 also compares M_c with M_L for events where M_w is available.

An examination of Table 7.1 suggests that there is a distinct difference in the relationship between M_c with M_w and M_L depending on whether the events are located in the Vancouver Island region or the Puget Sound region. In the vicinity of Vancouver Island M_w is larger than M_c, particularly for in-slab events. In the Puget Sound region M_w and

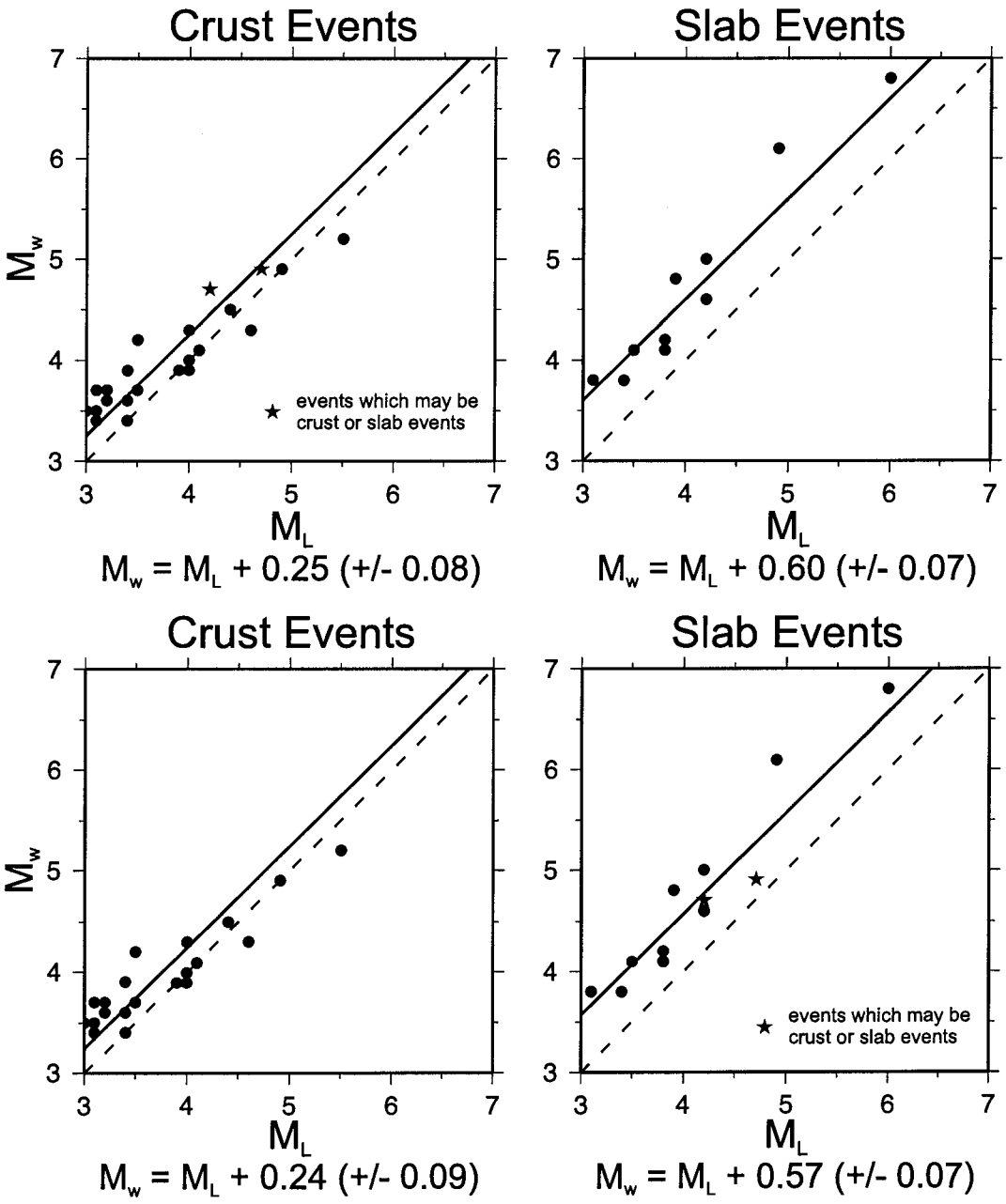

Figure 7.11 M_w-M_L comparison for events in the Vancouver Island/Puget Sound region occurring the crust and in the subducting slab. In each case the dashed line represents an ideal 1:1 relationship between M_w and M_L, and the solid line is a best-fit line assuming a slope parallel to the 1:1 line. The M_L correction is indicated for each zone. (*Top*) The two circled solutions (indicated by stars) in Figure 7.8 (*bottom*) grouped with the crustal events. (*Bottom*) The two circled solutions in Figure 7.8 (*bottom*) grouped with the slab events.

Vancouver Island/Puget Sound		
	$M_w - M_c$	$M_L - M_c$
all	0.16 ± 0.17	-0.24 ± 0.11
crust	0.03 ± 0.11	-0.25 ± 0.07
slab	0.36 ± 0.20	-0.24 ± 0.18

Vancouver Island		
	$M_w - M_c$	$M_L - M_c$
all	0.38 ± 0.03	0.03 ± 0.07
crust	0.15 ± 0.15	-0.10 ± 0.06
slab	0.83 ± 0.05	0.28 ± 0.01

Puget Sound		
	$M_w - M_c$	$M_L - M_c$
all	0.03 ± 0.10	-0.38 ± 0.07
crust	-0.05 ± 0.07	-0.32 ± 0.06
slab	0.16 ± 0.13	-0.47 ± 0.08

Table 7.1 M_w/M_c and M_L/M_c comparisons for the Vancouver Island/Puget Sound region.

M_c are comparable. M_L and M_c exhibit the opposite pattern with M_L being similar to, or larger than M_c around Vancouver Island, and M_c becoming significantly larger than M_L in the Puget Sound region. Bolton (2003) compared M_L with M_c for events in the Vancouver Island/Puget Sound region and also noted that events in the Puget Sound region have a dominant pattern of $M_c > M_L$ while events around Vancouver Island have $M_L > M_c$. Table 7.1 also shows that the M_w/M_c and M_L/M_c relationships depend on whether the events are crustal or in-slab events with the magnitude discrepancies being much larger for in-slab events. These results suggests a complex relationship between magnitude scales for the Vancouver Island/Puget Sound region which depends both on the distance from the stations used in calculating the magnitudes, and whether the events are crustal or in-slab. More regional moment tensor solutions will provide further constraints on the magnitude relationships in the Vancouver Island/Puget Sound region and provide more accurate magnitude estimates.

7.5 Summary

More than 20 regional moment tensor solutions have been calculated for the southern Canadian Cordillera where very few focal mechanisms were previously available. These regional moment tensor solutions provide valuable constraints on the tectonics and stress regime in the southern Canadian Cordillera.

M_o calculated from the regional moment tensor solutions are consistent with M_L magnitudes within 95% confidence limits. Therefore, M_L values can be directly converted to M_o and M_w for events in the southern Canadian Cordillera.

Regional moment tensor solutions provide information on crustal stresses in western Canada where no a priori stress information is available from sources such as oil well breakouts or first motion focal mechanisms. The regional stress pattern in western Canada mapped from moment tensor solutions and available first motion focal mechanisms is relatively straightforward for most of western Canada. *P* axis orientations are mainly NE-SW in the northern Canadian Cordillera from the Gulf of Alaska through to the Mackenzie Mountains. In northeast and east-central British Columbia the *P* axis direction is NE-SW and supports the idea that the whole of western Canada is being compressed in a NE-SW direction.

In southern British Columbia the compressive stress regime changes to N-S due to oblique subduction of the Juan de Fuca plate and right-lateral shear motion of the Pacific and North America plates. Stress tensor analysis shows a change in $\sigma 1$ in British Columbia at a latitude of around 50° to 51°N. South of 51°N $\sigma 1$ is almost N-S, and north of 51°N $\sigma 1$ becomes NE-SW. Regional moment tensor analysis suggests that the N-S compressive stress regime extends through to the eastern Canadian Cordillera. This may be related to the coupling effect of the Juan de Fuca plate with the North America plate. It is important to note that the N-S compressive stress results in southeastern British Columbia could also be related to the extensional tectonic regime in the western United States. E-W tension faulting will result in focal mechanisms with N-S compression. This could be erroneously interpreted as a N-S compressional stress regime instead of a E-W tensional stress regime. The regional moment tensor solutions calculated in this study cannot distinguish between a N-S compressional stress regime or a E-W tensional stress regime.

There is a transition zone from compressional tectonics in western Canada to extensional tectonics in the western United States. Regional moment tensor solutions just north and south of the Canadian/American border are strike-slip mechanisms with E-W tension which could possibly represent the compression to extension transition zone. The presently available regional moment tensor solutions cannot conclusively show where the transition zone is but they do suggest that given another decade or two there may be enough solutions available to define where the compression to extension transition occurs. This will have important implications related to the seismic risk from large thrust earthquakes in

southern British Columbia and southern Alberta.

Nearly 40 regional moment tensor solutions have been calculated for the Cascadia subduction zone in the Vancouver Island/Puget Sound region. Regional moment tensor solutions in the Vancouver Island/Puget Sound region do not show any obvious pattern in faulting style which reflects the complex tectonic environment. The stress tensor for the crustal events indicates margin-parallel compression which is consistent with results from Mulder (1995) calculated from first motion mechanisms. The stress tensor for the slab events is very poorly constrained; however, the maximum tensional orientation is oriented down-dip which is consistent with results from Bolton (2003) calculated from first motion solutions.

M_w correlates well with M_L in the Vancouver Island/Puget Sound region but with an offset in magnitude with M_w being higher than M_L by 0.37 ± 0.07 magnitude units on average. Events located in the crust have a much lower M_w/M_L discrepancy (0.25 ± 0.08 magnitude units) compared with in-slab events (0.60 ± 0.07 magnitude units). This is likely related to travel path effects with in-slab events having a more complex source-receiver travel path than crustal events. The relationship between M_w and M_c is dependent both on the latitude and whether the events are crustal or in-slab. In-slab events have a significantly larger M_w/M_c discrepancy than crustal events, and the discrepancy is much larger in the vicinity of Vancouver Island than in the Puget Sound region. The Vancouver Island/Puget Sound region is a tectonically complex region where it is difficult to calculate reliable magnitudes. There is a complex relationship between magnitude scales which depends on the both the source-receiver distance and whether the events are crustal or in-slab. Future studies using detailed Earth models to examine the effects of the subducting slab and overlying crust on seismic waveforms will be useful in examining the relationships between different magnitude scales.

Chapter 8

Queen Charlotte Islands and Glacier Bay Region

8.1 Queen Charlotte Islands Region

8.1.1 Introduction

The Queen Charlotte Islands region and north along the Alaska panhandle is a region of moderate to high seismicity dominated by several major faults (Figure 8.1). In the vicinity of the the Queen Charlotte Islands the dominant tectonic feature is the Queen Charlotte fault. The Queen Charlotte fault has been referred to as Canada's San Andreas fault since, like the San Andreas fault, it forms the boundary between the Pacific and North America plates where the Pacific plate is sliding north past the North America plate. The Queen Charlotte fault was the location of Canada's largest instrumentally recorded earthquake (22 August 1949, M = 8.1). Motion along the Queen Charlotte fault is primarily strike-slip but plate motion vectors do show a component of convergence suggesting the deeper section of the fault may be thrusting underneath the margin (e.g. Riddihough and Hyndman, 1989; Bérubé et al., 1989). A number of thrust faulting focal mechanisms in the southern Queen Charlotte Islands have been calculated in this study which suggests some convergence of the Pacific plate with the North America plate. Earthquake depths in the Queen Charlotte fault region tend to be deeper than in the offshore Explorer plate region with depths down to around 20 km (e.g. Hyndman and Ellis, 1981). Closer to the mainland the depths become shallower. Bird (1997) calculated an average depth of around 10 km for events in the Graham Island/Hecate Strait region.

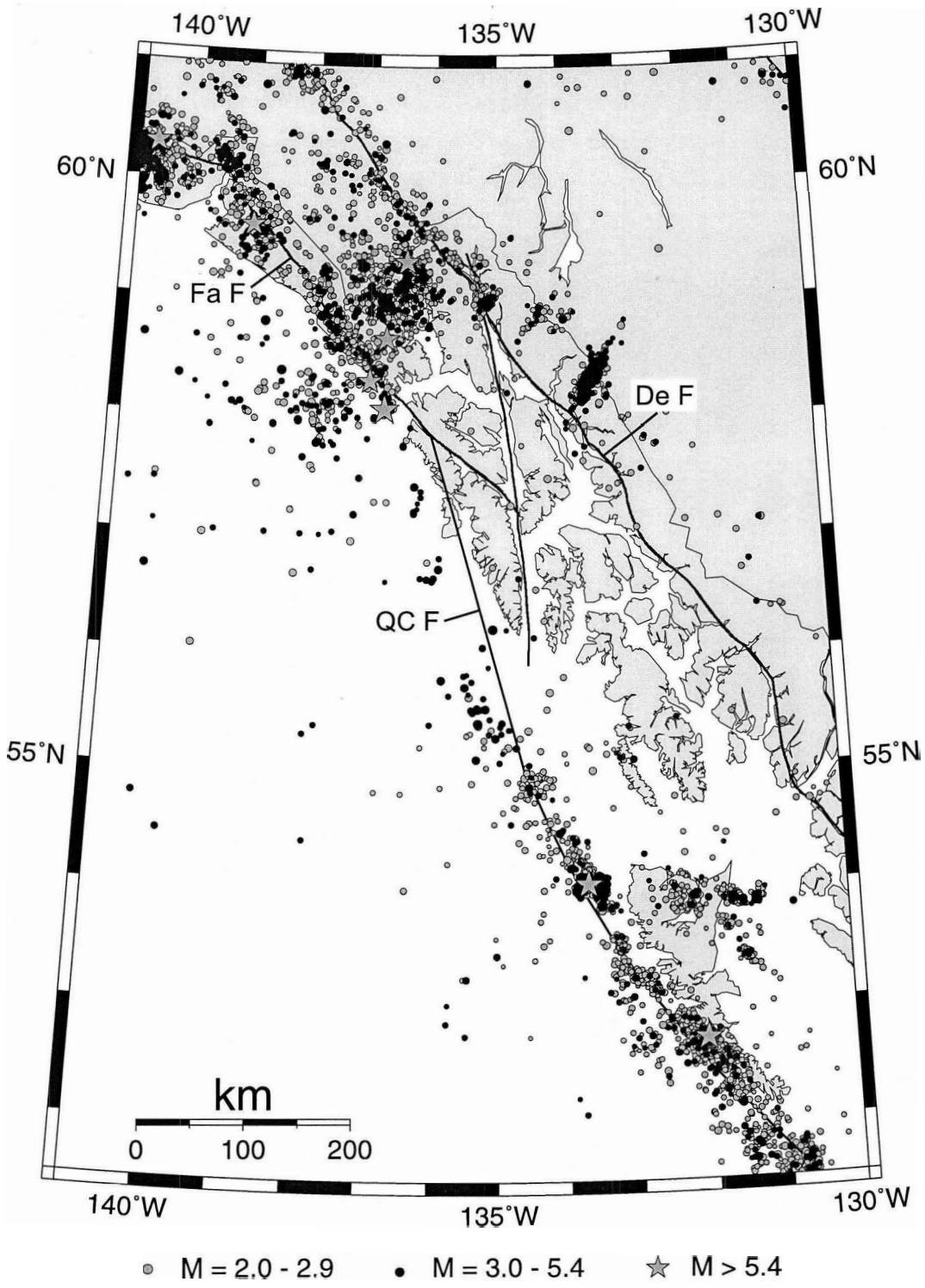

Figure 8.1 Seismicity (1982–2002) for the Queen Charlotte Islands and Alaska panhandle region. De F - Denali fault; Fa F - Fairweather fault; QC F - Queen Charlotte fault.

In addition to the 1949 earthquake two other major earthquakes have occurred in recent times in the Queen Charlotte Islands. At the southern end of the Queen Charlotte Islands a M = 7 earthquake occurred on 24 June 1970 near Cape St. James. A seismic gap on the order of 75 km exists along the Queen Charlotte fault between the locations of the 1949 and 1970 earthquakes where no major earthquake has occurred in the last century (Rogers, 1986). Rogers (1986) estimated that a M = 7.5 earthquake would be required to completely fill the gap and that the stored strain in the region is already sufficient for an earthquake of this size. A second major earthquake occurred at the northern end of the Queen Charlotte fault, near Sitka, Alaska, on 31 July 1972 (M = 7.6). Kelleher and Savino (1975) suggested the possibility of a seismic gap between the 1972 and 1949 earthquakes. Rogers (1986) concluded that the proposed northern seismic gap contains aftershocks of the great 1949 earthquake and likely ruptured during the 1949 event and is not a seismic gap.

The locations of most of the thrust faulting earthquakes in the Queen Charlotte Islands region are to the east of the Queen Charlotte fault which suggests the presence of subsidiary faults in this region (Figure 8.2). Bird (1997) calculated a number of first motion thrust faulting mechanisms around Graham Island and in Hecate Strait (Figure 8.2). GPS velocity models from sites in the Queen Charlotte Islands are consistent with a significant component of underthrusting of the Pacific plate beneath the North America plate (Mazzotti et al., 2003a). The size of thrust faulting earthquakes in the Queen Charlotte Islands region has the potential to be quite large. A M_w = 6.1 thrust faulting earthquake occurred on 12 October 2001 east of the Queen Charlotte fault and generated a small tsunami. Based on thermal modeling Smith (1999) estimated the maximum potential size for a thrust earthquake in the Queen Charlotte Islands region to be M = 8.

8.1.2 Focal Mechanisms

Approximately 20 moment tensor solutions have been calculated along the Queen Charlotte fault in this study and by Harvard (Figure 8.2). In addition to the moment tensor solutions Bird (1997) calculated 35 first motion solutions for small earthquakes in the vicinity of the Queen Charlotte fault (Figure 8.2). These first motion solutions are a mixture of single event solutions and composite focal mechanisms. Bird (1997) also calculated 28 first motion mechanisms for the Graham Island region and 29 first motion mechanisms for the Hecate Strait region. These are also a mixture of single event solutions and composite focal mechanisms.

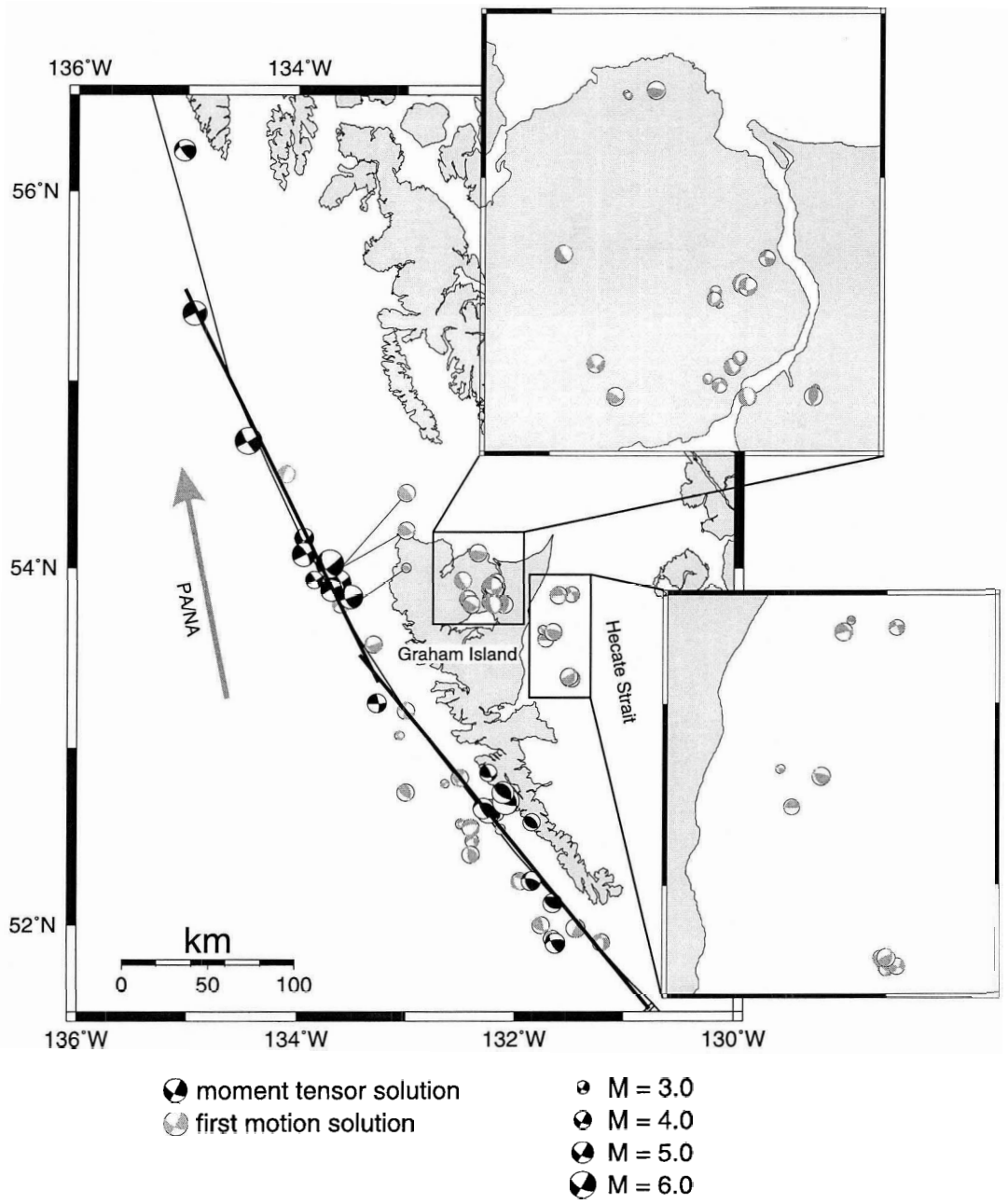

Figure 8.2 Moment tensor and first motion solutions for the Queen Charlotte Islands region. The first motion solutions are from Bird (1997). The thick black lines indicate the approximate trend of the Queen Charlotte fault in the southern and northern Queen Charlotte Islands region. The large grey arrow is the direction of Pacific/North America motion.

In the southern Queen Charlotte Islands, moment tensor solutions are consistently thrust mechanisms, some with a small strike-slip component. It has been known for some time that a component of convergence between the Pacific and North America plates exists in the Queen Charlotte Islands region (e.g. Riddihough and Hyndman, 1989; Bérubé et al., 1989), and recent GPS results from the Queen Charlotte Islands region show convergence between the Pacific and North America plates (Mazzotti et al., 2003a). However, the amount of thrust faulting present in the southern Queen Charlotte Islands, as shown by the regional moment tensor solutions calculated in this study, is unprecedented and represents a new result. In the northern Queen Charlotte Islands the moment tensor solutions are strike-slip, some with a small thrust component. The fault planes from the moment tensor solutions along the northern Queen Charlotte fault are consistent with the strike of the Queen Charlotte fault.

First motion solutions of small earthquakes in the vicinity of the Queen Charlotte fault are a mixture of thrust faulting, normal faulting, and strike-slip faulting (Bird, 1997; Bérubé et al., 1989). Some are consistent with the strike of the Queen Charlotte fault and others appear to have no relation to the Queen Charlotte fault strike. Most of the first motion solutions are for much smaller magnitude events than the moment tensor solutions and may be occurring on small subsidiary faults. In the Graham Island and Hecate Strait regions the first motion solutions for small earthquakes again show thrust, normal, and strike-slip faulting.

8.1.3 Stress Analysis

The Queen Charlotte Fault

The Queen Charlotte fault changes strike between the southern and northern Queen Charlotte Islands region. The strike changes from a NW-SE strike in the south to a NNE-SSW strike (thick black lines in Figure 8.2) and becomes even more northerly north of the Queen Charlotte Islands region. The most northerly section had almost no focal mechanisms associated with it during the period of this study and will not be discussed here. Stress tensors can be calculated for events along the Queen Charlotte fault, using the method discussed in section 6.2, to investigate the consistency of the principal stresses with the strike of the fault. For the purposes of calculating stress tensors the dividing line between the northern and southern Queen Charlotte fault will be 53°N. Moment tensor solutions north of 53°N are strike-slip mechanisms while moment tensor solutions south of 53°N have primarily thrust mechanisms.

The total shear stress (τ) on a surface is related to the maximum and minimum principal stresses ($\sigma 1$ and $\sigma 3$ respectively) by

$$\tau = \frac{\sigma 1 - \sigma 3}{2} \sin 2\theta \tag{8.1}$$

where θ is the angle between $\sigma 1$ and the fault normal (e.g. Price and Cosgrove, 1990). τ reaches a maximum, τ_{max}, when $\theta = 45°$ i.e. the maximum shear stress on a surface occurs when $\sigma 1$ is oriented 45° to the surface. In the case of brittle failure of a homogeneous material, the angle θ that a shear plane will make with $\sigma 1$ is given by

$$\theta = 45° \pm \phi/2 \tag{8.2}$$

where ϕ is the angle of internal friction for the rock (e.g. Price and Cosgrove, 1990). Mackenzie (1969) showed that on a pre-existing fault $\sigma 1$ can have an orientation anywhere within the dilatational quadrant of an earthquake focal mechanism. Therefore, the principal axes of a fault plane solution may vary significantly from the principal stress directions.

The strike of the northern Queen Charlotte fault is approximately 335° while the southern Queen Charlotte fault has a strike of approximately 320°. In the northern Queen Charlotte fault region the earthquakes are strike-slip and appear to rupture the Queen Charlotte fault. These events reflect northward motion of the Pacific plate relative to the North America plate. In the southern Queen Charlotte fault region the earthquakes are mainly thrustm mechanisms and appear to occur on faults adjacent to the Queen Charlotte fault. These events may be related to the convergence of the Pacific plate with the North America plate.

The stress tensor calculated using moment tensor solutions in the northern Queen Charlotte Islands region has a maximum compressive stress direction, $\sigma 1$, of 18° (Figure 8.3 (*top left*). This gives an angle of 43° with the northern Queen Charlotte fault which is consistent for the maximum shear stress on the fault. The stress tensor for the southern Queen Charlotte fault calculated using moment tensor solutions has $\sigma 1$ with an azimuth of 36° (Figure 8.3 (*top right*). This gives an angle of 76° with the southern Queen Charlotte fault. For pure thrust faulting the P axis orientation will be 90° to the fault plane. Along the southern Queen Charlotte fault the mechanisms are mainly thrust faulting with a small strike-slip component. Therefore, the P axis will oriented close to 90°. The orientation of $\sigma 1$ with the southern Queen Charlotte fault is consistent with the P axis orientation for fault mechanisms along the southern Queen Charlotte fault.

Strain tensors can also be calculated for the northern and southern Queen Charlotte

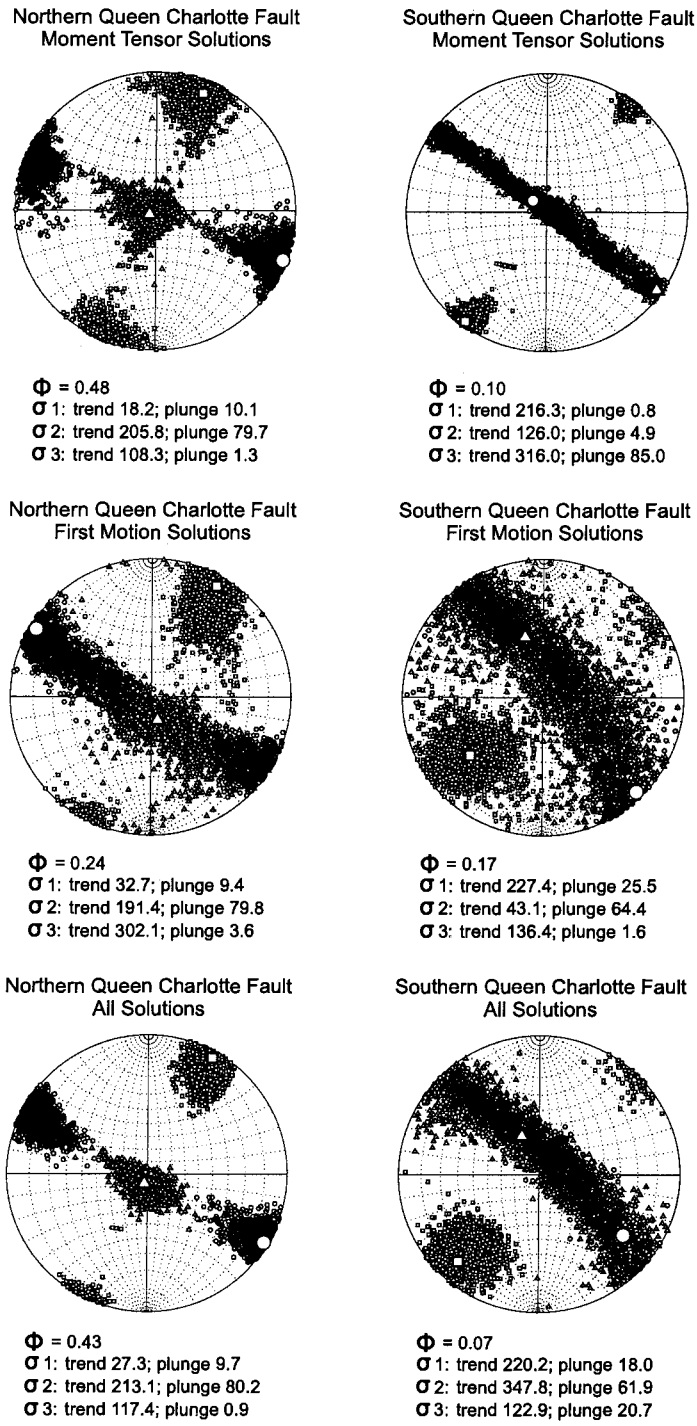

Figure 8.3 Stress tensors calculated for the northern and southern Queen Charlotte fault using moment tensor solutions (*top*), first motion solutions (*middle*) and both moment tensor and first motion solutions (*bottom*). $\sigma 1$, $\sigma 2$, and $\sigma 3$ are the principal stresses from most compressional to least compressional. ϕ is a measure of the relative sizes of the principal stresses (see section 6.2).

fault sections from the regional moment tensor solutions. The maximum compressional principal strain direction for the northern Queen Charlotte fault events has an azimuth of 11° compared with a $\sigma 1$ azimuth of 18° (Figure 8.4). In the southern Queen Charlotte fault region the maximum compressional strain direction is 212° compared with a $\sigma 1$ direction of 216° (Figure 8.4). In both regions the maximum compressional stress and strain directions are similar.

Strain tensors are dominated by the largest earthquakes while stress tensors do not depend on the magnitude of the earthquake. Focal mechanisms for small earthquakes will tend to be related to the local stress regime. Large earthquakes normally occur on pre-existing faults which may or may not be favourably oriented for failure in the local stress field. If the principal strain and stress directions are significantly different then it suggests that the faults on which the larger events occur may not be favourably oriented for failure and may be weak, i.e. less than the maximum amount of shear stress is required for slip on the fault. It is important to note that in the case of earthquakes occurring along the Queen Charlotte fault, all of the events, regardless of their magnitude, will be influenced by the orientation of the fault. Therefore, the stress tensor calculated from events occurring on, or associated with, the Queen Charlotte fault may not be representative of the true local stress field.

The first motion solutions are much more of a mixture of mechanisms and orientations than the moment tensor solutions, particularly in the southern Queen Charlotte Islands region (Figure 8.2). Bird (1997) assigned a quality factor to the first motion solutions on a scale from 0 (very good) to 3 (very poor). These are used to weight the solutions in the stress tensor calculations. The stress tensors calculated using the first motion solutions are shown in Figure 8.3 (*middle*). The confidence limits are large, particularly for the southern Queen Charlotte fault. In the southern Queen Charlotte fault region the first motion mechanisms consist of normal, thrust, and strike-slip faulting with no consistent P axis orientation. Therefore, it is not possible to calculate a well constrained stress tensor. The orientation of $\sigma 1$ is consistent with the moment tensor results for the southern Queen Charlotte fault within the 95% confidence limits. Bird (1997) calculated the average P axis direction from the first motion mechanisms for the entire Queen Charlotte fault (Table 8.1). The P axis orientation is midway between $\sigma 1$ for the northern and southern Queen Charlotte fault calculated using first motion solutions (Table 8.1). Calculating the stress tensor using all of the Queen Charlotte fault first motion solutions results in a $\sigma 1$ which is almost identical with Bird (1997) (Table 8.1).

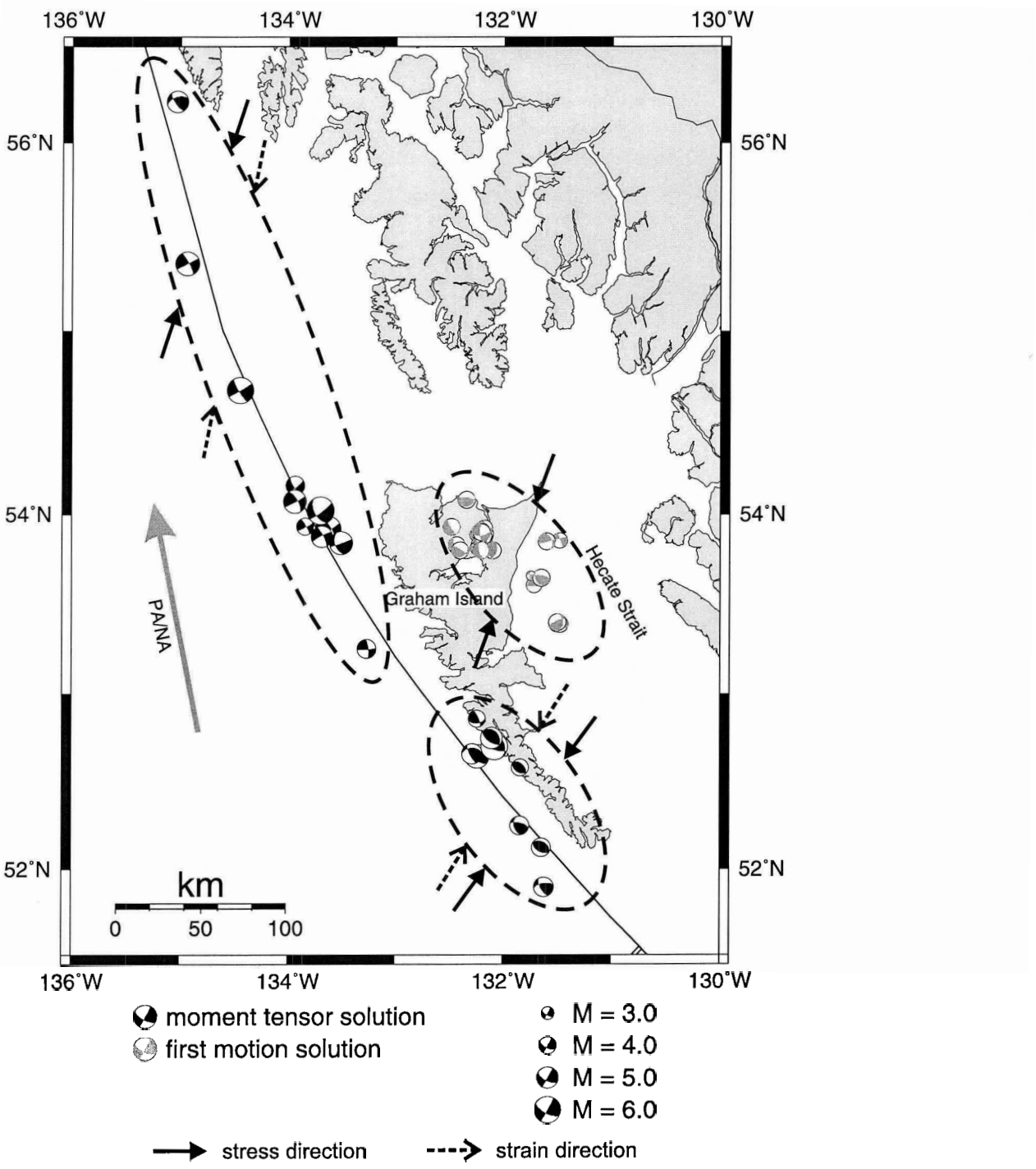

Figure 8.4 Composite stress and strain orientations for the northern and southern Queen Charlotte fault calculated from regional moment tensor solutions. Dashed lines indicate the groupings of earthquakes used to calculate the stress and strain directions, and arrows are the compressive stress and strain orientations for each group. The large grey arrow is the direction of Pacific/North America motion.

	EQCF	NQCF	SQCF
Bird (1997)	39 ± 13	–	–
This Study	41 ± 20	33 ± 15	47 ± 20

EQCF - entire Queen Charlotte fault;
NQCF - northern Queen Charlotte fault;
SQCF - southern Queen Charlotte fault.

Table 8.1 Average P axis direction (Bird, 1997) compared with $\sigma 1$ for the Queen Charlotte fault.

Combining all of the mechanisms together results in the stress tensors in Figure 8.3 (*bottom*). For the northern Queen Charlotte fault $\sigma 1$ is oriented 52° with the fault. Some of the first motion solutions for the northern Queen Charlotte fault are thrust mechanisms which change the orientation of $\sigma 1$ with the fault. The orientation is still within the 95% confidence limits of 45°. For the southern Queen Charlotte fault $\sigma 1$ is oriented 80° with respect to the fault which is very close the moment tensor results. It should be noted that these results combine data sets from events which are influenced by the Queen Charlotte fault (moment tensor solutions) with events which may not by related to the Queen Charlotte fault (first motion solutions). Therefore, it may not be reasonable to infer stress information from a combination of the data sets.

Graham Island and Hecate Strait

Almost 30 first motion solutions were calculated by Bird (1997) for each of the Graham Island and Hecate Strait regions (Figure 8.2). These events are unrelated to the Queen Charlotte fault but are still influenced by Pacific/North America motion. Like the first motion solutions along the Queen Charlotte fault these mechanisms are a mixture of thrust, normal, and strike-slip faulting. Stress tensor analysis was carried out on these mechanisms to see what information could be extracted (Figure 8.5).

The stress tensor for the events in the Graham Island region (Figure 8.5 (*top*)) has $\sigma 1$ with a more NE-SW orientation compared with events in the Hecate Strait region (Figure 8.5 (*middle*)). $\sigma 2$ and $\sigma 3$ are also similar in magnitude in the Graham Island region as indicated by the low value of ϕ. In the Hecate Strait region the magnitudes of $\sigma 2$ and $\sigma 3$ are much different. Combining the two data sets give $\sigma 1$ with an orientation midway between the $\sigma 1$ orientations for the separate data sets (Figure 8.5 (*bottom*)). The magnitude of $\sigma 2$ and $\sigma 3$ are very distinct from one another, similar to the Hecate Strait results.

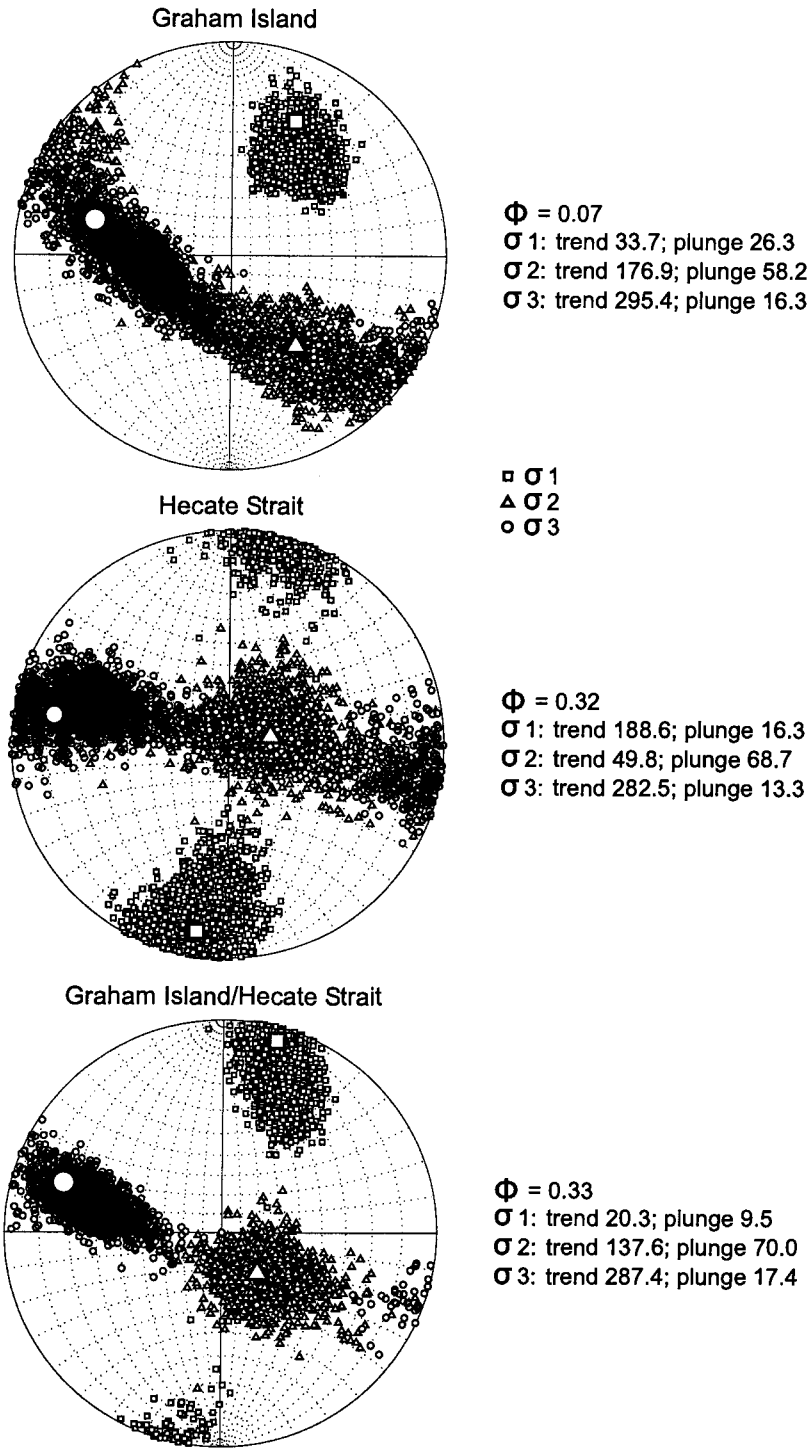

Figure 8.5 Stress tensors calculated for Graham Island (*top*), Hecate Strait (*middle*), and both Graham Island and Hecate Strait (*bottom*) from first motion solutions calculated by Bird (1997). $\sigma 1$, $\sigma 2$, and $\sigma 3$ are the principal stresses from most compressional to least compressional. ϕ is a measure of the relative sizes of the principal stresses (see section 6.2).

Bird (1997) calculated average P axis orientations for the Graham Island and Hecate Strait regions from the first motion focal mechanisms. Table 8.2 compares the average P axis orientations with the $\sigma 1$ orientations derived from the stress tensor inversions. The results agree very well within the uncertainty limits and the stress tensor results support those of Bird (1997).

The $\sigma 1$ results for the Graham Island and the Hecate Strait regions agree within the uncertainty limits. As well the P axis orientations for Graham Island and Hecate Strait obtained by Bird (1997) agree within the uncertainties. Therefore, it seems reasonable to use the stress tensor from the combined Graham Island and Hecate Strait data sets to represent the stress field for the Graham Island/Hecate Strait region (Figure 8.4).

	GI	HS	GI & HS
Bird (1997)	26 ± 7	12 ± 17	–
This Study	34 ± 20	9 ± 20	20 ± 15

GI - Graham Island; HS - Hecate Strait.

Table 8.2 Average P axis orientation (Bird, 1997) compared with $\sigma 1$ for the Graham Island and Hecate Strait regions.

The San Andreas Fault

The San Andreas fault can serve as a useful analogy for the Queen Charlotte fault. In California, the San Andreas fault forms the boundary where the Pacific plate is moving north relative to the North America plate. The San Andreas fault is one of the most intensively studied fault systems in the world and thousands of fault plane solutions have been calculated for events occurring along, or associated with, the fault (e.g. Provost and Houston, 2003).

A number of studies have examined the state of stress along the San Andreas fault (e.g. Townend and Zoback 2004; Provost and Houston, 2003; Hardebeck and Hauksson 2001; Townend and Zoback, 2001 Jones, 1988). Provost and Houston (2001) looked at the stress field along the creeping portion of the San Andreas fault in central California. They found that the maximum principal stress is oriented at high angles of up to 80° to the strike direction of the fault. Provost and Houston (2001) interpreted this as suggesting that the San Andreas fault is mechanically weak. Provost and Houston (2003) studied the stress

field of the San Andreas fault in the region of the San Francisco Bay Area and northern California. Provost and Houston (2003) found that the angle between the San Andreas fault and the maximum compressive stress is around 55° in this region, and suggested that the northern part of the fault is stronger with greater frictional strength than the southern creeping portion. Townend and Zoback (2004), Townend and Zoback (2001), Hardebeck and Hauksson (2001) and Jones (1988) also found that the maximum compressive stress is at high angles with the San Andreas fault and and interpreted this as a mechanically weak fault.

Townend and Zoback (2004) noted that the angle between the compressive stress direction and fault strike remains constant despite pronounced changes in the fault's strike. This suggests a degree of interaction between the tectonic stress field and the fault. Otherwise, with a relatively uniform stress field present, the angle between the compressive stress direction and the fault strike should vary with the strike of the fault (Townend and Zoback, 2004). High frictional strength along the San Andreas fault should result in a local heat flow anomaly along the fault but none has been found which also suggests a weak fault (e.g. Brune et al., 1969; Lachenbruch and Sass, 1992; Saffer et al., 2003).

Stress Tensor Summary

Compared with the San Andreas fault region there are relatively few focal mechanisms available for the Queen Charlotte fault and Queen Charlotte Islands region. This section will give one possible interpretation of the available focal mechanism and stress tensor data for the Queen Charlotte Islands region.

The maximum compressive stress direction of 40° for the southern Queen Charlotte fault region is $\sim 80°$ to the strike of the southern portion of the fault. This is consistent with convergence of the Pacific plate with North America in the southern Queen Charlotte fault region. Events in this region occur on small faults adjacent to the Queen Charlotte fault and the available focal mechanisms are consistent with underthrusting of the Pacific plate.

There is a distinct change in the compressive stress direction between the southern Queen Charlotte fault and the Graham Island/Hecate Strait region. Focal mechanisms from the Graham Island/Hecate Strait region are a mixture of normal, thrust, and strike-slip. $\sigma 1$ is 20° for these events which gives an orientation of $\sim 30 - 35°$ to Pacific/North America plate motion. The stress tensor for the Graham Island/Hecate Strait region may

be representative of the stress field for the Queen Charlotte Islands region. If this is the case, the maximum compressive stress is oriented approximately 45° to the strike of the northern Queen Charlotte fault segment.

As mentioned above, the southern portion of the San Andreas fault has been interpreted as being weak due to high angles ($\sim 80°$) between the strike of the fault and the compressive stress direction (e.g. Provost and Houston, 2001). The northern portion of the San Andreas fault has an angle of $\sim 55°$ between the strike of the fault and the compressive stress direction and is suggested as being stronger than the southern portion (e.g. Provost and Houston, 2003). With an angle of 45° between the fault strike and the compressive stress direction, the northern Queen Charlotte fault segment could be interpreted as being stronger than the San Andreas fault. Smith (1999) measured heat flow values across the Queen Charlotte fault and did not find evidence for a heat flow anomaly associated with the Queen Charlotte fault. This would imply a weak fault, similar to the San Andreas fault. However, large gradients in the measured heat flow values across the fault make it difficult to draw any firm conclusions about the lack of a Queen Charlotte fault heat flow anomaly. Therefore, the absence of a measured heat flow anomaly in the Queen Charlotte fault should not be taken as evidence of a weak fault.

8.2 Glacier Bay Region

8.2.1 Introduction

At about 57°N the Queen Charlotte fault turns into the Fairweather fault onshore in southern Alaska along what is known as the Alaska panhandle (Figure 8.1). In this area the Pacific/North America plate boundary begins to change from primarily strike-slip motion to oblique subduction of the Pacific plate beneath North America. This also marks the easterly edge of the Yakutat block which is colliding with the North America plate (e.g. Doser and Lomas, 2000). As a result this is a region of high seismicity where large ($M_w > 7.0$) strike-slip earthquakes occurred in 1927 and 1972 (Doser and Lomas, 2000). Moment tensor solutions in the region are a mixture of strike-slip and thrust mechanisms reflecting the complex tectonic setting (Figure 8.6).

8.2.2 Post-Glacial Rebound And Seismicity

The region around Glacier Bay, Alaska is currently undergoing high rates of post-glacial rebound (Hicks and Shofnos, 1965). Wu and Hasegawa (1996) analyzed the effect of stresses caused by glacial loading/unloading and numerically computed the mode of failure. Their

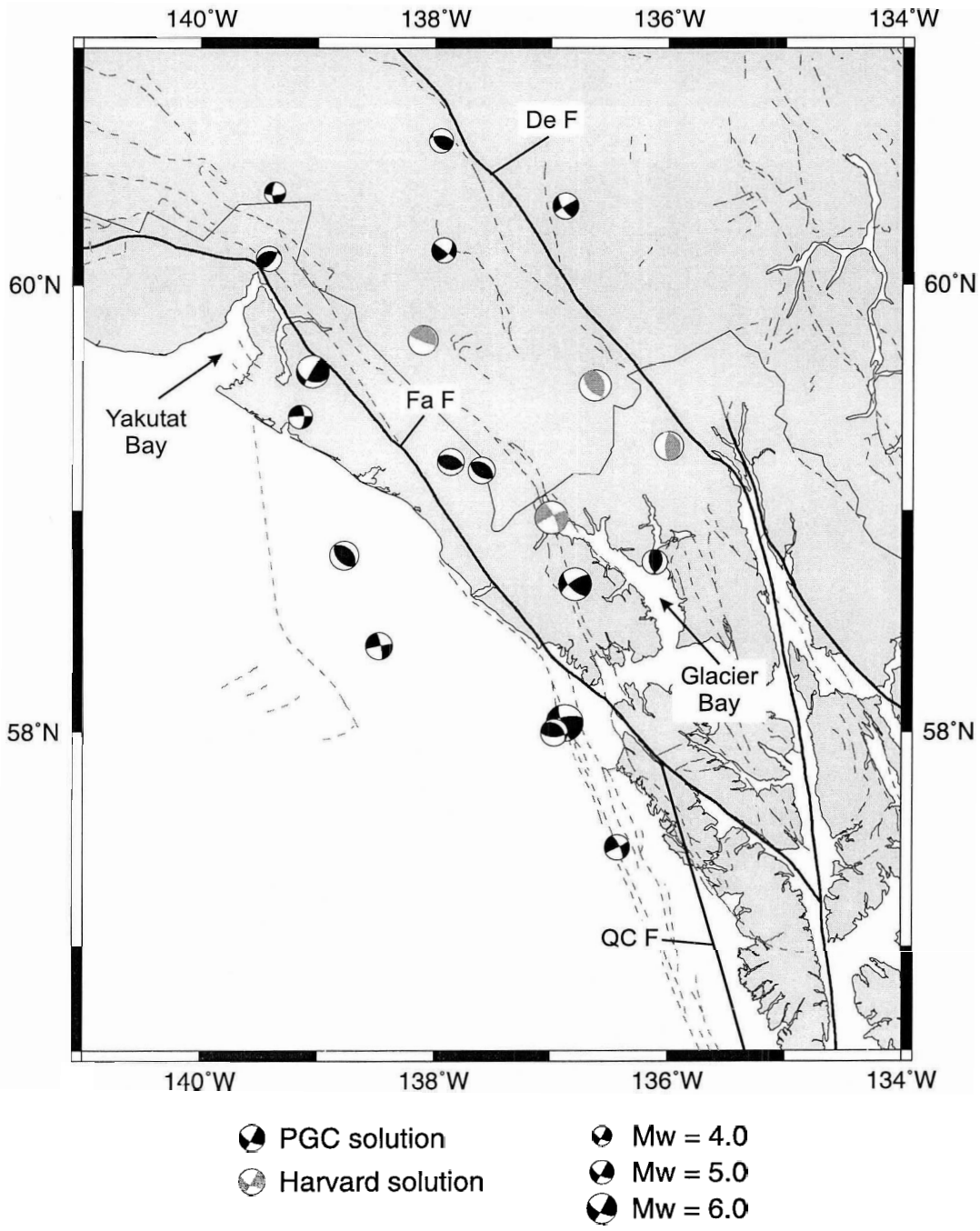

Figure 8.6 Moment tensor solutions for the Alaska panhandle region showing a mixture of strike-slip and thrust mechanisms. De F - Denali fault; Fa F - Fairweather fault.

results indicate that under all combinations of tectonic stress, crustal loading promotes fault stability directly underneath the load. Upon removal of the load, thrust faulting is predicted within the ice margin. Wu and Johnston (2000) concluded that post-glacial unloading could have triggered major paleo-earthquakes within the ice margin near Charlevoix, Quebec and Wabash Valley, Indiana.

Several moment tensor solutions with thrust faulting mechanisms are present in the region surrounding Glacier Bay (Figure 8.6). The P axis pattern around Glacier Bay is best seen by looking at the whole of western Canada and southeast Alaska (Figure 8.7). There is a distinct change in the P axis azimuths from N-S to E-W in the region surrounding Glacier Bay (circled area in Figure 8.7). This change in P axis orientation, combined with the thrust faulting mechanisms may indicate the presence of seismicity related to post-glacial rebound rather than only Pacific/North America interaction. It is difficult to separate the tectonic seismicity signal from the post-glacial rebound seismicity signal and it likely is not possible to do so with the few moment tensor solutions available. The results do suggest the possibility that the moment tensor solutions around Glacier Bay are influenced by post-glacial rebound and more moment tensor solutions in the future will help determine the true nature of the stress field in this region.

8.3 Summary

Approximately 20 moment tensor solutions have been calculated for events associated with the Queen Charlotte fault. Stress and strain tensors calculated from the moment tensor solutions show the principal stress and principal strain directions to be similar. In the Queen Charlotte fault region the stress tensor will be influenced by the orientation of the fault. Therefore, the stress tensor may not be representative of the local stress field. A number of first motion fault plane solutions have been calculated by Bird (1997) for the Queen Charlotte fault region and the Graham Island/Hecate Strait region. Stress tensor analysis of the first motion solutions gives compressive stress directions consistent with the average P axis direction calculated by Bird (1997) for the same events.

There is a change in the compressive stress direction between the Queen Charlotte fault (41°) and the Graham Island/Hecate Strait region (20°). Events in the Graham Island/Hecate Strait region are not related to the Queen Charlotte fault and may represent the stress field for the Queen Charlotte Islands region. If this is the case, the compressive stress direction is oriented $\sim 45°$ to the strike of the northern Queen Charlotte fault segment. This could indicate that the northern Queen Charlotte fault is stronger than the

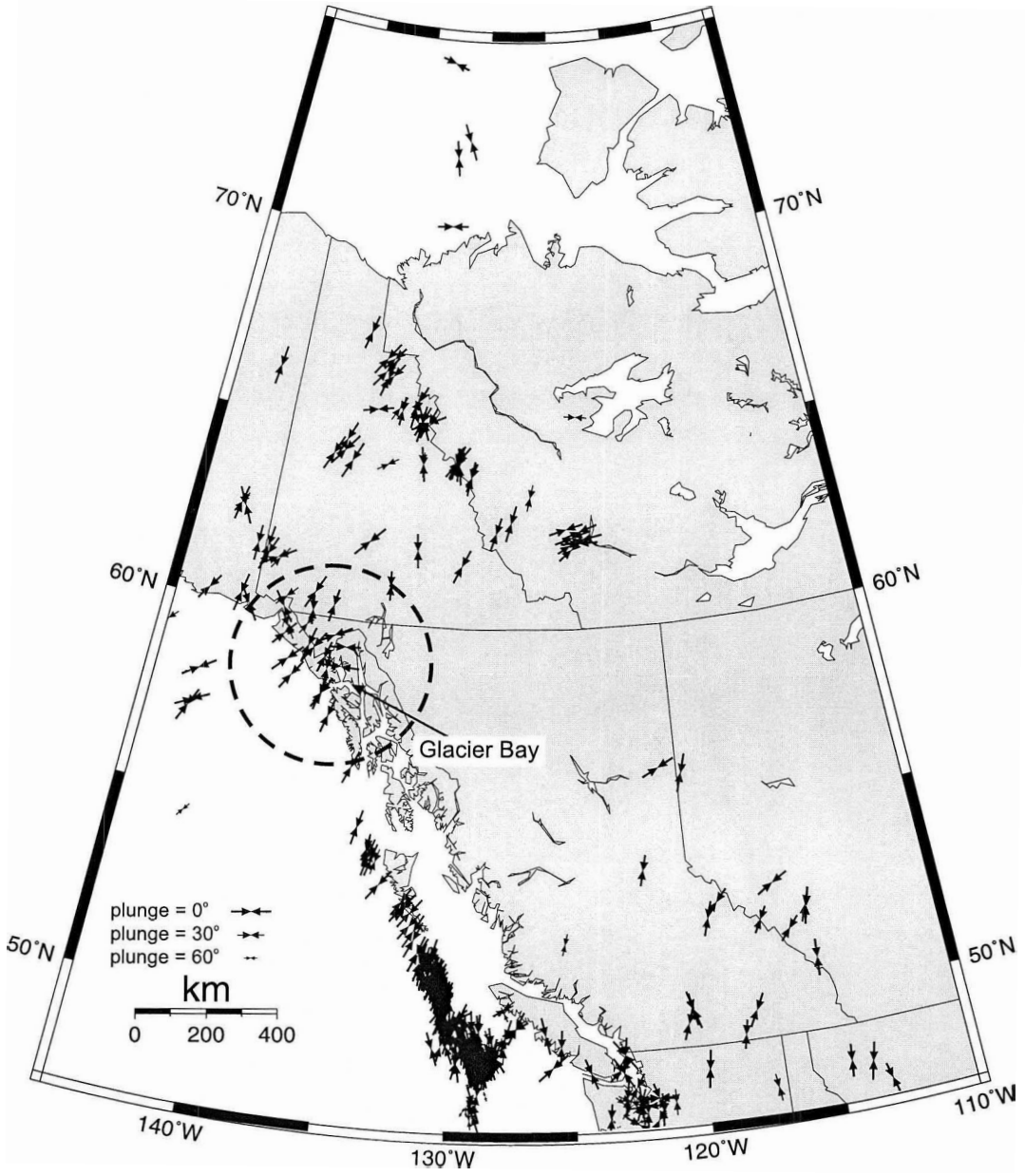

Figure 8.7 P axis azimuths from focal mechanisms in western Canada. The circled area identifies the region surrounding Glacier Bay in southeast Alaska.

San Andreas fault where the compressive stress direction is oriented at higher angles to the fault. However, the data does not prove that slip could not occur on the northern Queen Charlotte fault if the angle between the fault strike and the compressive stress direction was larger.

Moment tensor solutions around the Glacier Bay region show a mixture of strike-slip and thrust faulting. The thrust faulting is consistent with faulting associated with post-glacial rebound although separating seismicity associated with tectonic activity from post-glacial rebound activity is difficult. The moment tensor solutions do show a change in P axis orientation from N-S to E-W in the region surrounding Glacier Bay. More moment tensor solutions in the future may help determine the nature of the stress field in the Glacier Bay region.

Chapter 9

Summary

9.1 Introduction

Regional moment tensor analysis has proven itself to be a valuable technique for studying the seismotectonics of western Canada. More than 380 regional moment tensor solutions with M_w = 3.4–6.8 have been calculated for western Canada in this study for the years 1995–2004. Over the same time period, Harvard University calculated 45 centroid moment tensor solutions for the same region for earthquakes with $M_w > 5.0$. The regional moment tensor solutions provide fault plane solutions and moments for many areas of western Canada where very few, or no, focal mechanisms have previously been calculated. This chapter summarizes the results from chapters 4–8.

9.2 Moment Magnitude - Local Magnitude Calibration

For the purpose of correlating M_w with M_L in the region off Canada's west, coast three zones can be resolved with the amount of oceanic crust present in the source-receiver travel path being the main difference between them. In all three regions M_w correlates well with M_L but with an offset in magnitude, with M_L being consistently lower than M_w.

Zone 1 is clearly a distinct region from Zone 2 and Zone 3 with most of the source-receiver travel path being through continental crust. The discrepancy between M_w and M_L is also the lowest in Zone 1 (0.29 ± 0.07 magnitude units). Zone 2 and Zone 3 can be examined as one region or as separate regions. Both regions have a mixture of oceanic and continental crust in the source-receiver travel path but events in Zone 3 must travel through a greater amount of oceanic crust, and therefore the discrepancy between M_w and

M_L is larger in Zone 3 than in Zone 2 (0.69 $\pm$ 0.10 magnitude units versus 0.55 $\pm$ 0.06 magnitude units). However, treating Zone 2 and Zone 3 as one region also gives reasonable results with M_w being larger than M_L by 0.62 $\pm$ 0.08 magnitude units; the combined zone is also easier to deal with on a practical level. The different M_w-M_L discrepancies between Zone 2 and Zone 3 demonstrate that as the source moves closer to the continental margin M_L becomes closer to M_w.

Calibrating the M_L values that have been calculated for the past 27 years with M_w is important in that it allows the western Canadian earthquake database to be used more effectively for tectonic studies and seismic hazard analysis. One research area where this is important is in calculating earthquake moment release rates for faults around the Explorer plate and comparing those to predicted plate motions calculated by other methods such as GPS measurements. If the magnitudes used to calculate the moment release rates are seriously undervalued then it will not be possible to accurately compare them with plate motion results determined from other methods. Underestimating the magnitudes of offshore earthquake will also have important consequences for seismic hazard estimates. An increase in magnitude of 0.6 of an earthquake corresponds to an increase in moment release by a factor of 8. For a region such as Vancouver Island, which has the highest seismic hazard in Canada, this information is crucial. Vancouver Island is not at great risk from offshore earthquakes with M_w = 6.0–6.5 as these occur too far offshore to cause damage. However, there is the potential for major $M_w \sim 7.0$ earthquakes along the boundaries of the Explorer plate which could cause damage on Vancouver Island.

9.3 Explorer Region Tectonics

Regional moment tensor solutions provide important constraints on the motions of the Explorer plate. Moment tensor solutions are used to calculate rotation poles and rates of the Explorer plate relative to the Pacific and Juan de Fuca plates and then, through vector addition, to determine the motion of the Explorer plate relative to the North America plate. The rotation poles are calculated by leaving Pacific/Explorer motion unconstrained and by constraining Pacific/Explorer motion using moment release rates along the Pacific/Explorer plate boundary.

The locations of the Pacific/Explorer and Juan de Fuca/Explorer rotation poles are similar in both methods but the rotation rate decreases by a factor of 2 if Pacific/Explorer motion is constrained. This affects the location and rate of the North America/Explorer rotation pole. The convergence rate of the Explorer plate relative to the North America plate

is similar between the two methods but the convergence direction changes from NE-SW in the unconstrained case to almost N-S in the constrained case. The unconstrained convergence direction is consistent with GPS measurements from central and southern Vancouver Island while the constrained convergence direction is consistent with GPS measurements from northern Vancouver Island. This implies that the Explorer plate cannot be treated as a rigid plate and its motion cannot be described by a single rotation pole. The Explorer plate is likely undergoing intense internal deformation as a result of being trapped between the much larger Pacific and North America plates.

Moment tensor solutions are also used to calculate a strain tensor for the Explorer plate. The strain tensor is used to determine the principal strain axes for the Explorer plate and calculate a strain rate. The strain tensor has a compressional axis with an azimuth of N6°E, and a strain rate of 7.8×10^{-8} yr^{-1}. The moment tensor derived strain rates for the Explorer plate are consistent with GPS strain rates from central and southern Vancouver Island. GPS strain rates for northern Vancouver Island have not been calculated but would be expected to be similar to central and southern Vancouver Island. The moment tensor derived compressive strain direction is almost N-S which is consistent with GPS velocity vectors from northern Vancouver Island.

9.4 Northern Canadian Cordillera Tectonics

Nearly 100 regional moment tensor solutions have been calculated for the northern Canadian Cordillera and Yakutat collision zone which adds a great deal of information to that already available for these regions. Comparing M_o calculated from regional moment tensor solutions with M_L values demonstrates that M_L is equivalent to M_w, which is derived directly from the M_o. This is an important result for calculating moment release rates in the northern Canadian Cordillera.

Regional moment tensor solutions are used to investigate the crustal stress and strain regime for northern Canada and southeast Alaska. Focal mechanisms are divided into four groups for the analysis: the Nahanni region in the southern Mackenzie Mountains, the central and northern Mackenzie Mountains, the Richardson Mountains, and the Yakutat collision zone. $\sigma 1$ changes from nearly E-W in the Nahanni region to nearly N-S in the Mackenzie Mountains to NE-SW in the Richardson Mountains. In the Yakutat collision zone $\sigma 1$ is the same as the Mackenzie Mountains region. The principal strain directions in each of the four groups is similar to the principal stress directions except in the central and northern Mackenzie Mountains where the compressive strain direction is rotated 17°

clockwise relative to the compressive stress direction. Dividing the central and northern Mackenzie Mountains into two groups yields the same results. It is uncertain whether a 15° difference in principal compressive strain and stress directions is significant. However, the compressive strain and stress directions are within their respective uncertainties. If the difference is significant then these results suggest that the largest earthquakes in the central and northern Mackenzie Mountains occur on faults not favourably oriented for failure and may be weak. If the difference is not significant then the larger earthquakes occur on faults which are favourably aligned for failure in the prevailing stress field.

9.5 Southern Canadian Cordillera Tectonics

More than 20 regional moment tensor solutions have been calculated for the southern Canadian Cordillera where very few focal mechanisms were previously available. These regional moment tensor solutions provide valuable constraints on the tectonics and stress regime in the southern Canadian Cordillera.

Comparing M_o calculated from regional moment tensor solutions with M_L values demonstrates that M_L is equivalent to M_w, which is derived directly from the M_o. Therefore, M_L values can be directly converted to M_o and M_w for events in the southern Canadian Cordillera.

Regional moment tensor solutions provide information on crustal stresses in western Canada where no a priori stress information is available from sources such as oil well breakouts or first motion focal mechanisms. The regional stress pattern in western Canada mapped from moment tensor solutions and available first motion focal mechanisms is relatively straightforward for most of western Canada. P-axis orientations are mainly NE-SW in the northern Canadian Cordillera from the Gulf of Alaska through to the Mackenzie Mountains. In northeast and east-central British Columbia the P-axis direction is NE-SW and supports the idea that the whole of western Canada is being compressed in a NE-SW direction. In southern British Columbia the compressive stress regime changes to N-S due to oblique subduction of the Juan de Fuca plate and right-lateral shear motion of the Pacific and North America plates. The regional moment tensor solutions suggest that the N-S compressive stress regime extends through to the eastern Canadian Cordillera. This may be related to the coupling effect of the Juan de Fuca plate with the North America plate.

Stress tensor analysis also shows a change in the compressive stress direction in British

Columbia at a latitude of around 50° to 51°N. South of 51°N the compressive stress direction is almost N-S and north of 51°N the compressive stress direction becomes NE-SW. There is a transition zone from compressional tectonics in western Canada to extensional tectonics in the western United States. Regional moment tensor solutions just north and south of the Canada/United States border show E-W tension which could possibly represent the compression to extension transition zone. The presently available regional moment tensor solutions cannot conclusively show where the transition zone is but they do suggest that given another decade or two there may be enough solutions available to define where the compression to extension transition occurs. This will have important implications related to the seismic risk from large thrust earthquakes in southern British Columbia and southern Alberta.

Nearly 40 regional moment tensor solutions have been calculated for the Cascadia subduction zone in the Vancouver Island/Puget Sound region. Regional moment tensor solutions in the Vancouver Island/Puget Sound region do not show any obvious pattern in faulting style which reflects the complex tectonic environment. The stress tensor for the crustal events indicates margin-parallel compression which is consistent with results from Mulder (1995) calculated from first motion mechanisms. The stress tensor for the slab events is very poorly constrained; however, the maximum tensional orientation is oriented down-dip which is consistent with results from Bolton (2003) calculated from first motion solutions.

M_w correlates well with M_L in the Vancouver Island/Puget Sound region but with an offset in magnitude with M_w being higher than M_L by 0.37 ± 0.07 magnitude units on average. Events located in the crust have a much lower M_w/M_L discrepancy (0.25 ± 0.08 magnitude units) compared with in-slab events (0.60 ± 0.07 magnitude units). This is likely related to travel path effects with in-slab events having a more complex source-receiver travel path than crustal events. The relationship between M_w and M_c is dependent both on the latitude and whether the events are crustal or in-slab. In-slab events have a significantly larger M_w/M_c discrepancy than crustal events, and the discrepancy is much larger in the vicinity of Vancouver Island than in the Puget Sound region. The Vancouver Island/Puget Sound region is a tectonically complex region where it is difficult to calculate reliable magnitudes. There is a complex relationship between magnitude scales which depends on the both the source-receiver distance and whether the events are crustal or in-slab. Future studies using detailed Earth models to examine the effects of the subducting slab and overlying crust on seismic waveforms will be useful in examining the relationships between different magnitude scales.

9.6 Queen Charlotte Islands and Glacier Bay Region

Approximately 20 moment tensor solutions have been calculated for events associated with the Queen Charlotte fault. Stress and strain tensors calculated from the moment tensor solutions show the principal stress and principal strain directions to be similar. In the Queen Charlotte fault region the stress tensor will be influenced by the orientation of the fault. Therefore, the stress tensor may not be representative of the local stress field. A number of first motion fault plane solutions have been calculated by Bird (1997) for the Queen Charlotte fault region and the Graham Island/Hecate Strait region. Stress tensor analysis of the first motion solutions gives compressive stress directions consistent with the average P axis direction calculated by Bird (1997) for the same events.

There is a change in the compressive stress direction between the Queen Charlotte fault (41°) and the Graham Island/Hecate Strait region (20°). Events in the Graham Island/Hecate Strait region are not related to the Queen Charlotte fault and may represent the stress field for the Queen Charlotte Islands region. If this is the case, the compressive stress direction is oriented $\sim 45°$ to the strike of the northern Queen Charlotte fault segment. This could indicate that the northern Queen Charlotte fault is stronger than the San Andreas fault where the compressive stress direction is oriented at higher angles to the fault.

Moment tensor solutions around the Glacier Bay region show a mixture of strike-slip and thrust faulting. The thrust faulting is consistent with faulting associated with post-glacial rebound although separating seismicity associated with tectonic activity from post-glacial rebound activity is difficult. The moment tensor solutions do show a change in P axis orientation from N-S to E-W in the region surrounding Glacier Bay. More moment tensor solutions in the future may help determine the nature of the stress field in the Glacier Bay region.

References

Adams, J., (1987), Canadian crustal stress database: A compilation to 1987: Geological Survey of Canada Open File 1622, 130 p.

Adams, J., (1990), Paleoseismicity of the Cascadia subduction zone: evidence from turbidites off the Oregon-Washington margin, *Tectonics*, **9**, 569-583.

Adams, J., and Bell, J.S., (1991), Crustal stresses in Canada, *in*, Slemmons, D.B., Engdahl, E.R., Zoback, M.D., and Blackwell, D.D., eds., Neotectonics of North America: Boulder, Colorado, Geological Society of America, Decade Map Volume 1.

Aki, K., and Richards, P.G., (1980), Quantitative Seismology: Theory and Methods, W.H. Freeman and Co., New York, 932 p.

Ammon, C.J., (2001), Moment-tensor inversion overview, <URL: http://www.essc.psu.edu/~ammon/HTML/MTinvDocs/mtinv01.html>, last modified July 31, 2001.

Anderson, J.G., and Luco, J.E., (1983), Consequences of slip rate constraints on earthquake recurrence relations, *Bull. Seism. Soc. Amer.*, **73**, 471–496.

Angelier, J., (1979), Determination of the mean principal directions of stresses for a given fault population, *Tectonophysics*, **56**, T17–T26.

Angelier, J., (1984), Tectonic analysis of fault slip data sets, *J. Geophys. Res.*, **89**, 5835–5848.

Atwater, B.F., (1987), Evidence for great Holocene earthquakes along the outer coast of Washington State, *Science*, **236**, 942–944.

Atwater, T., (1989), Plate tectonic history if the Northeast Pacific and western North America, *in* Winterer, E.L., Hussong, D.M., and Decker, R.W., eds., The Eastern Pacific Ocean and Hawaii: Boulder, Colorado, Geological Society of America, The Geology of North America, v. N, 21–72.

Bérubé, J., Rogers, G.C., Ellis, R.M., and Hasselgren, E.O., (1989), A microseismicity study of the Queen Charlotte Islands region, *Can. J. Earth Sci.*, **26**, 2556–2566.

Bird, A.L., (1997), Earthquakes in the Queen Charlotte Islands Region: 1982–1996, M.Sc. Thesis, University of Victoria, 123 p.

Bolton, M.K., (2003), Juan de Fuca plate seismicity at the northern end of the Cascadia subduction zone, M.Sc. Thesis, University of Victoria, 238 p.

Botros, M., and Johnson, H.P., (1988), Tectonic evolution of the Explorer - northern Juan de Fuca region from 8 Ma to the present, *J. Geophys. Res.*, **93**, 10421–10437.

Braunmiller, J., (1998), Seismotectonics of the Explorer region and Blanco transform fault zone, Ph.D. Dissertation, Oregon State University, 158 p.

Braunmiller, J., and Nábělek, J., (2002), Seismotectonics of the Explorer region, *J. Geophys. Res.*, **107**, 2208, doi:10.1029/2001JB000220.

Braunmiller, J., Nábělek, J., and Leitner, B., (1995), The 1993 Klamath Falls, Oregon earthquake sequence: source mechanisms from regional data, *Geophys. Res. Lett.*, **22**, 105–108.

Brune, J.N., Henyey, T.L., and Roy, R.F., (1969), Heat flow, stress, and rate of slip along the San Andreas fault, California, *J. Geophys. Res.*, **74**, 3821–3827.

Carbotte, S.M., Dixon, J.M., Farrar, E., Davis, E.E., and Riddihough, R.P., (1989), Geological and geophysical characteristics of the Tuzo Wilson Seamounts: implications for plate geometry in the vicinity of the Pacific-North America-Explorer triple junction, *Can. J. Earth Sci.*, **26**, 2365–2384.

Cassidy, J.F., and Bent, A.L., (1993), Source parameters of the 29 May and 5 June 1940 Richardson Mountains earthquakes, *Bull. Seism. Soc. Amer.*, **83**, 636–659.

Cassidy, J.F., and Bent, A.L., (2003), The 1953–1957 Mackenzie Mountains earthquake sequence, *Bull. Seism. Soc. Amer.*, submitted.

Cassidy, J.F., Ellis, R.M., Karavas, C., and Rogers, G.C., (1998), The northern limit of the subducted Juan de Fuca plate system, *J. Geophys. Res.*, **103**, 26949–26961.

Davis, E.E. and Currie, R.G., (1993), Geophysical observations of the northern Juan de Fuca ridge system: lessons in sea-floor spreading, *Can. J. Earth Sci.*, **30**, 278–300.

Davis, E.E. and Riddihough, R.P., (1982), The Winona Basin: structure and tectonics, *Can. J. Earth Sci.*, **16**, 767–788.

Delouis, B., and Legrand, D., (1999), Focal mechanism determination and identification of the fault plane of earthquakes using only one or two near-source seismic recordings, *Bull. Seism. Soc. Amer.*, **89**, 1558–1574.

DeMets, C., and Dixon, T.H., (1999), New kinematic models for Pacific-North America motion from 3 Ma to present, I: Evidence for steady state motion and biases in the NUVEL-1A model, *Geophys. Res. Lett.*, **13**, 1921–1924.

DeMets, C., Gordon, R.G., Argus, D.F., and Stein, S., (1990), Current plate motions, *Geopys. J. Int.*, **101**, 425–478.

Doser, D.I., and Lomas, R., (2000), The transition from strike-slip to oblique subduction in southeastern Alaska from seismological studies, *Tectonophysics*, **316**, 45–65.

Dragert, H., Hyndman, R.D., Rogers, G.C., and Wang, K., (1994), Current deformation and the width of the seismogenic zone of the northern Cascadia subduction thrust, *J. Geophys. Res.*, **99**, 653–668.

Dreger, D.S., and Helmberger, D.V., (1993), Determination of source parameters at regional distances with three-component sparse network data, *J. Geophys. Res.*, **98**, 8107–8125.

Dziewonski, A.M., Chou, T.-A., and Woodhouse, J.H., (1981), Determination of earthquake source parameters from waveform data for studies of global and regional seismicity, *J. Geophys. Res.*, **86**, 2825–2852.

Ekström, G., and England, P., (1989), Seismic strain rates in regions of distributed continental deformation, *J. Geophys. Res.*, **94**, 10231–10257.

Ellis, R.M., and Rogers, G.C., (1986), Preliminary investigation of earthquakes west of Vancouver Island, *Geol. Surv. Can. Open File Rept.*, **1400**.

Estabrook, C.H., Nábělek, J.L., and Lerner-Lam, A.L., (1992), Tectonic model of the Pacific-North American plate boundary in the Gulf of Alaska from broadband analysis of the 1979 St. Elias, Alaska, earthquake and its aftershocks, *J. Geophys. Res.*, **97**, 6587–6612.

Fletcher, H.J., and Freymueller, J.T., (1999), New GPS constraints on the motion of the Yakutat Block, *Geophys. Res. Lett.*, **26**, 3029–3032.

Frohlich, C., and Apperson, K.D., (1992), Earthquake focal mechanisms, moment tensors, and the consistency of seismic activity near plate boundaries, *Tectonics*, **11**, 279–296.

Frohlich, C., and Davis, S.D., (1999), How well constrained are well-constrained T, B, and P axes in moment tensor catalogs?, *J. Geophys. Res.*, **104**, 4901–4910.

Gephart, J.W., and Forsyth, D.W., (1984), An improved method for determining the regional stress tensor using earthquake focal mechanism data: application to the San Fernando earthquake sequence, *J. Geophys. Res.*, **89**, 9305–9320.

Goldstein, P., (2000), SAC Home Page, <URL: http://www.llnl.gov/sac/>, last modified April 19, 2000.

Gutenberg, B., and Richter, C.F., (1954), Seismicity of the Earth and associated phenomena, 2nd ed., Princeton University Press.

Hanks, T.C., and Kanamori, H., (1979), A moment magnitude scale, *J. Geophys. Res.*, **84**, 2348–2350.

Hardebeck, J.L., and Hauksson, E., (2001), Crustal stress field in southern California and its implications for fault mechanics, *J. Geophys. Res.*, **106**, 21859–21882.

Hasegawa, H.S., Chou, C.W., and Basham, P.W., (1979), Seismotectonics of the Beaufort Sea, *Can. J. Earth Sci.*, **16**, 816–830.

Henton, J.A., Dragert, H., McCaffrey, R., Wang, K., and Hyndman, R.D., (2000), GPS monitoring of deformation at the northern Cascadia subduction zone, *EOS Trans. AGU*, **81**: Fall Meet. Suppl., Abstract F328.

Herrmann, R.B., and Wang, C.Y., (1985), A comparison of synthetic seismograms, *Bull. Seism. Soc. Amer.*, **75**, 41–56.

Hicks, S.D., and Shofnos, W., (1965), The determination of land emergence from sea level observations in southeast Alaska, *J. Geophys. Res.*, **70**, 3315–3320.

Hildebrand, R.S., Hoffman, P.F., and Bowring, S.A., (1987), Tectonic magmatic evolution of the 1.9-Ga Great Bear Magmatic Zone, Wopmay orogen, NW Canada, *J. Volc. Geotherm. Res.*, **32**, 99–118.

Hoffman, P.F., and Bowring, S.A., (1984), Short-lived 1.9 Ga continental margin and its destruction, Wopmay orogen, *Geology*, **12**, 68–72.

Horner, R.B., Barclay, J.E., and MacRae, J.M., (1994), Earthquakes and hydrocarbon production in the Fort St. John area of northeastern British Columbia, *Can. J. Expl. Geophys.*, **30**, 39–50.

Hutton, L.K., and Boore, D.M., (1987), The *ML* scale in southern California, *Bull. Seism. Soc. Amer.*, **77**, 2074–2094.

Hyndman, R.D., (1995), Giant earthquakes of the Pacific Northwest, *Sci. Amer.*, **273**, 50–57.

Hyndman, R.D., and Ellis, R.M., (1981), Queen Charlotte fault zone: microearthquakes from a temporary array of land stations and ocean bottom seismographs, *Can. J. Earth Sci.*, **18**, 776–788.

Hyndman, R.D., and Wang, K., (1995), The rupture zone of Cascadia great earthquakes from current deformation and the thermal regime, *J. Geophys. Res.*, **100**, 22133–22154.

Hyndman, R.D., and Weichert, D.H., (1983), Seismicity and rates of relative motion on the plate boundaries of western North America, *Geophys. J. R. Astron. Soc.*, **72**, 59–82.

Hyndman, R.D., Riddihough, R.P., and Herzer, R., (1979), The Nootka fault zone — a new plate boundary off western Canada, *Geophys. J. R. Astron. Soc.*, **72**, 667–683.

Isachsen, C.E., and Bowring, S.A., (1994), Evolution of the Slave craton, *Geology*, **22**, 917–920.

Jones, L.M., (1988), Focal mechanisms and the state of stress on the San Andreas fault in southern California, *J. Geophys. Res.*, **93**, 8869–8891.

Jost, M.L., and Herrmann, R.B., (1989), A student's guide to and review of moment tensors, *Seism. Res. Lett.*, **60**, 37–57.

Kanamori, H., (1977), The energy release in great earthquakes, *J. Geophys. Res.*, **82**, 2981–2987.

Kanamori, H., and Anderson, D.L., (1975), Theoretical basis of some empirical relations in seismology, *Bull. Seism. Soc. Amer.*, **65**, 1073–1095.

Keen, C.E., and Hyndman, R.D., (1979), Geophysical review of the continental margins of eastern and western Canada, *Can. J. Earth Sci.*, **19**, 1657–1669.

Kelleher, J., and Savino, J., (1975), Distribution of seismicity before large strike-slip and thrust-type earthquakes, *J. Geophys. Res.*, **50**, 260–271.

Kostrov, V.V., (1974), Seismic moment and energy of earthquakes, and seismic flow of rock, *Izv. Acad. Sci. USSR Phys. Solid Earth*, Engl. Transl., **1**, 23–44.

Lachenbruch, A.H., and Sass, J.H., (1992), Heat flow from Cajon Pass, fault strength, and tectonic implications, *J. Geophys. Res.*, **97**, 4995–5015.

Lahr, J.C., Plafker, G., Stephens, C.O., Fogleman, K.A., and Blackford, M.E., (1979), Interm report on the St. Elias earthquake of 28 February 1979, US Geol. Survey Open File Rep., 79-670, 23 p.

Lane, L.S., (2002), Tectonic evolution of the Canadian Beaufort Sea - Mackenzie Delta region: a brief review, *Can. Soc. Explor. Geophys. Recorder*, **February Issue**, 49–56.

Langston, C.A., (1981), Source inversion of seismic waveforms: The Koyna, India, earthquakes of 13 September, 1967, *Bull. Seism. Soc. Amer.*, **71**, 1–24.

Lay, T., and Wallace, T.C., (1995), Modern global seismology, Academic Press, Inc., San Diego, 521 p.

Leonard, L.J., Hyndman, R.D., Mazzotti, S., (2004), Coseismic subsidence in the 1700 great Cascadia earthquake: coastal estimates versus elastic dislocation models, *Geol. Soc. Amer. Bull.*, in press.

Mazzotti, S., and Hyndman, R.D., (2002), Yakutat collision and strain transfer across the northern Canadian Cordillera, *Geology*, **30**, 495–498.

Mazzotti, S., Dragert, H., Hyndman, R.D., Miller, M.M., and Henton, J.A., (2002), GPS deformation in a region of high crustal seismicity: N. Cascadia forearc, *Earth Planet. Sci. Lett.*, **198**, 41–48.

Mazzotti, S., Hyndman, R.D., Flück, P., Smith, A.J., and Schmidt, M., (2003a), Distribution of the Pacific/North America motion in the Queen Charlotte Islands-S. Alaska plate boundary zone, *Geophys. Res. Lett.*, **30**, 1762, doi:10.1029/2003GL017586.

Mazzotti, S., Dragert, H., Henton, J., Schmidt, M., Hyndman, R., James, T., Lu, Y, and Craymer, M., (2003b), Current tectonics of northern Cascadia from a decade of GPS measurements, *J. Geophys. Res.* in press.

McKenzie, D.P., (1969), The relation between fault plane solutions for earthquakes and the directions of the principal stresses, *Bull. Seism. Soc. Amer.*, **59**, 591–601.

Menard, H., (1978), Fragmentation of the Farallon plate by pivoting subduction, *J. of Geology*, **86**, 99–110.

Michael, A.J., (1984), Determination of stress from slip data: faults and folds, *J. Geophys. Res.*, **89**, 11517–11526.

Michael, A.J., (1987), Use of focal mechanisms to determine stress: a control study, *J. Geophys. Res.*, **92**, 357–368.

Milne, W.G., Rogers, G.C., Riddihough, R.P., McMechan, G.A., and Hyndman, R.D., (1978), Seismicity of western Canada, *Can. J. Earth Sci.*, **15**, 1170–1193.

Minster, J.B., and Jordan, T.H., (1978), Present day plate motions, *J. Geophys. Res.*, **83**, 5331–5354.

Molnar, P., (1979), Earthquake recurrence intervals and plate tectonics, *Bull. Seism. Soc. Amer.*, **69**, 115–133.

Molnar, P., and Atwater, T., (1978), Interarc spreading and Cordilleran tectonics as alternates related to the age of subducted oceanic lithosphere, *Earth Planet. Sci. Lett.*, **41**, 330–340.

Mulder, T.L., (1995), Small earthquakes in southwest British Columbia (1975–1991), M.Sc. Thesis, University of Victoria, 117 p.

Oldenburg, D.W., (1975), A physical model for the creation of the lithosphere, *Geophys. J. R. Astron. Soc.*, **43**, 425–451.

Plafker, G., Moore, J.C., and Winkler, G.R., (1994), Geology of the southern Alaska margin, *in* Plafker, G., and Berg, H.C., eds., The Geology of Alaska: Boulder, Geological Society of America, Geology of North America, v. G1, 389–449.

Press, F., and Ewing, M., (1952), Two slow surface waves across North America, *Bull. Seism. Soc. Amer.*, **42**, 219–228.

Price, N.J., and Cosgrove, J.W., (1990), Analysis of geological structures, Cambridge University Press, Cambridge, 502 p.

Provost, A.-S., and Houston, H., (2001), Orientation of the stress field surrounding the creeping section of the San Andreas fault: evidence for a narrow mechanically weak fault zone, *J. Geophys. Res.*, **106**, 11373–11386.

Provost, A.-S., and Houston, H., (2003), Stress orientations in northern and central California: evidence for the evolution of frictional strength along the San Andreas plate boundary system, *J. Geophys. Res.*, **108**, 2175, doi:10.1029/2001JB001123.

Randall, G.E., Ammon, C.J., and Owens, T.J., (1995), Moment tensor inversion estimation using regional seismograms from a Tibetan Plateau portable network deployment, *Geophys. Res. Lett.*, **22**, 1665–1668.

Ratchkovski, N.A., (2001), Seismological constraints on tectonics of southern and central Alaska: earthquakes locations and source mechanisms, Ph.D. Dissertation, University of Alaska Fairbanks, 149 p.

Ratchkovski, N.A., Hansen, R.A., Stachnik, J.C., Cox, T., Fox, O., Rao, L., Clark, E., Lafevers, M., Estes, S., MacCormack, J.B., and Williams, T., (2003), Aftershock sequence of the M_w 7.9 Denali fault, Alaska, earthquake of 3 November 2002 from regional seismic network data, *Seism. Res. Lett.*, **74**, 743–752.

Richter, C.F., (1935), An instrumental earthquake magnitude scale, *Bull. Seism. Soc. Amer.*, **25**, 1–32.

Riddihough, R.P., (1977), A model for recent plate interactions off Canada's west coast, *Can. J. Earth Sci.*, **14**, 384–396.

Riddihough, R.P., (1984), Recent movements of the Juan de Fuca plate system, *J. Geophys. Res.*, **89**, 6980–6994.

Riddihough, R.P., Currie, R.G., and Hyndman, R.D., (1980), The Dellwood Knolls and their role in triple junction tectonics off northern Vancouver Island, *Can. J. Earth Sci.*, **17**, 577–593.

Riddihough, R.P., and Hyndman, R.D., (1989), Queen Charlotte Islands margin, *in* Winterer, E.L., Hussong, D.M., and Decker, R.W., eds., The Eastern Pacific Ocean and Hawaii: Boulder, Colorado, Geological Society of America, The Geology of North America, v. N, 403–411.

Rogers, G.C., (1986), Seismic gaps along the Queen Charlotte fault, *Earthq. Predict. Res.*, **4**, 1–11.

Rogers, G.C., and Ellis, R.M., (1979), The eastern British Columbia earthquake of February 4, 1918, *Can. J. Earth Sci.*, **16**, 1484–1493.

Rogers, G.C., and Muraro, J., (1981), Magnitudes from signal duration compiled at the Pacific Geoscience Centre, Internal Report of the Earth Physics Branch, Pacific Geoscience Centre, **No. 81-2**.

Rogers, G.C., Ellis, R.M., and Hasegawa, H.S., (1980), The McNaughton Lake earthquake of May 14, 1978, *Bull. Seism. Soc. Amer.*, **70**, 1771–1788.

Rogers, G.C., Cassidy, J.F., and Ellis, R.M., (1990), The Prince George, British Columbia, earthquake of 21 March 1986, *Bull. Seism. Soc. Amer.*, **80**, 1144–1161.

Saffer, D.M., Bekins, B.A., and Hickman, S., (2003), Topographically driven groundwater flow and the San Andreas heat flow paradox revisited, *J. Geophys. Res.*, **108**, 2274, doi:10.1029/2002JB001849.

Satake, K., Shimazaki, K., Yoshinobu, T., and Ueda, K., (1996), Time and size of a giant earthquake in Cascadia inferred from Japanese tsunami records of January 1700, *Nature*, **379**, 246–249.

Savage, J.C., and Simpson, R.W., (1997), Surface strain accumulation and the seismic moment tensor, *Bull. Seism. Soc. Amer.*, **87**, 1345–1353.

Sbar, M.L., Barazangi, M., Dorman, J., Scholz, C.H., and Smith, R.B., (1972), Tectonics of the Intermountain Seismic Belt, western United States: microearthquake seismicity and composite fault plane solutions, *Geol. Soc. Amer. Bull.*, **83**, 13–28.

Sipkin, S.A., (1986), Estimation of earthquake source parameters by the inversion of waveform data: global seismicity, 1981–1983, *Bull. Seism. Soc. Amer.*, **76**, 1515–1541.

Sipkin, S.A., (2000), The use of waveform shapes to automatically determine earthquake focal depth, *Bull. Seism. Soc. Amer.*, **90**, 248–254.

Smith, R.A.J., (1999), Structure, deformation and thermal regime of the Queen Charlotte transform margin, M.Sc. Thesis, University of Victoria, 179 p.

Stickney, M.C., and Bartholomew, M.J., (1987), Seismicity and late Quaternary faulting of the northern Basin and Range Province, Montana and Idaho, *Bull. Seism. Soc. Amer.*, **77**, 1602–1625.

Stickney, M.C., and Lageson, D.R., (2002), Seismotectonics of the 20 August 1999 Red Rock Valley, Montana, earthquake, *Bull. Seism. Soc. Amer.*, **92**, 2449–2464.

Townend, J., and Zoback, M.D., (2001), Implications of earthquake focal mechanisms for the frictional strength of the San Andreas fault system, *in* Holdsworth, R.E., Strachan, R.A., Magloughlin, J.F., and Knipe, R.J., eds., The nature and tectonic significance of fault zone weakening, Geological Society, London, Special Publications, **186**, 13–21.

Townend, J., and Zoback, M.D., (2004), Regional tectonic stress near the San Andreas fault in central and southern California, *Geophys. Res. Lett.*, in press.

Wang, C.Y., and Herrmann, R.B., (1980), A numerical study of *P*-, *SV*-, and *SH*-wave generation in a plane layered medium, *Bull. Seism. Soc. Amer.*, **70**, 1015–1036.

Wang, K., He, J., and Davis, E.E., (1997), Transform push, oblique subduction resistance, and intraplate stress of the Juan de Fuca plate, *J. Geophys. Res.*, **102**, 661–674.

Weichert, D.H., (1980), Estimation of the earthquake recurrence parameters for unequal observation periods for different magnitudes, *Bull. Seism. Soc. Amer.*, **70**, 1337–1346.

Weichert, D.H., and Horner, R.B., (1985), A calibration of local-body-duration magnitudes for the Canadian Juan de Fuca-Explorer seismic zone, Internal Report of the Earth Physics Branch, Pacific Geoscience Centre, **No. 85-2**.

Wells, D.L., and Coppersmith, K.J., (1994), New empirical relationships among magnitude, rupture length, rupture width, rupture area and surface displacement, *Bull. Seism. Soc. Amer.*, **84**, 974–1002.

Wessel, P., and Smith, W.H.F., (1991), Free software helps map and display data, *EOS*, **72**, 441.

Wetmiller, R.J., (1986), Earthquakes near Rocky Mountain House, Alberta, and their relationship to gas production facilities, *Can. J. Earth Sci.*, **23**, 172–181.

Wetmiller, R.J., Drysdale, J.A., Horner, R.B., and Lamontagne, M., (1989), Canadian earthquakes — 1985–1986, Geological Survey of Canada Paper **88–14**.

Wetmiller, R.J., Horner, R.B., Hasegawa, H.S., North, R.G., Lamontagne, M., Weichert, D.H., and Evans, S.G., (1988), An analysis of the 1985 Nahanni earthquakes, *Bull. Seism. Soc. Amer.*, **78**, 590–616.

Wiemer, S., (2001), A software package to analyze seismicity: ZMAP, *Seism. Res. Lett.*, **72**, 373–382.

Wilson, D.S., (1988), Tectonic history of the Juan de Fuca Ridge over the last 40 million years, *J. Geophys. Res.*, **93**, 11863–11876.

Wilson, D.S., (1993), Confidence intervals for motion and deformation of the Juan de Fuca plate, *J. Geophys. Res.*, **98**, 16053–16071.

Wilson, D.S., Hey, R.N., and Nishimura, C., (1984), Propagation as a mechanism of ridge reorientation: a model for the tectonic evolution of the Juan de Fuca ridge, *J. Geophys. Res.*, **89**, 9215–9225.

Wu, P., and Hasegawa, H.S., (1996), Induced stresses and fault potential in eastern Canada due to a realistic load: a preliminary analysis, *Geophys. J. Int.*, **127**, 215–229.

Wu, P., and Johnston, P., (2000), Can deglaciation trigger earthquakes in N. America?, *Geophys. Res. Lett.*, **27**, 1323–1326.

Wyss, M., Liang, B., Tanigawa, W.R., and Wu, X., (1992), Comparison of orientations of stress and strain tensors based on fault plane solutions in Kaoiki, Hawaii, *J. Geophys. Res.*, **97**, 4769–4790.

Zhang, T.-R., and Lay, T., (1995), Why the L_g phase does not traverse oceanic crust, *Bull. Seism. Soc. Amer.*, **85**, 1665–1678.

Zhu, L., (2004), Downloads, <URL: http://mnw.eas.slu.edu/People/LZhu/downloads>, last modified January 20, 2004.

Zoback, M.L., and Zoback, M., (1980), State of stress in the Conterminous United States, *J. Geophys. Res.*, **85**, 6113–6156.

Appendix A

Moment Tensor Solutions

Date yyyymmddhhmm	Lat	Long	S/D/R	M_w	Mo (Nm)	CD (km)	SD	SR	Q
199501090650	51.012	-130.790	154/64/-160	4.8	1.9E16	6	145	2	B
199503081629	50.485	-130.246	137/83/169	4.9	2.4E16	12	138	2	B
199504230929	50.453	-130.196	129/86/163	4.4	5.1E15	9	130	2	C
199505310338	50.954	-130.676	144/81/176	5.3	9.6E16	12	145	2	B
199506121723	60.952	-138.404	296/38/101	4.8	1.5E16	9	12	11	B
199509122244	51.209	-131.225	142/81/166	5.3	8.5E16	15	144	2	B
199509130759	51.107	-131.135	141/79/166	5.4	1.4E17	12	144	2	B
199509131119	51.104	-131.082	138/86/178	4.8	1.7E16	9	138	2	B
199510150129	48.849	-128.571	108/71/175	4.4	3.9E15	9	110	6	C
199511121304	48.838	-129.180	124/73/168	4.6	1.1E16	9	128	6	C
199512010329	50.353	-129.973	133/88/167	4.5	6.1E15	9	133	2	B
199603102112	50.573	-130.436	140/80/164	4.7	1.4E16	12	143	2	B
199603162318	50.471	-130.331	140/88/160	5.1	5.9E16	12	141	2	B
199603180801	49.689	-127.306	251/75/2	5.0	4.4E16	24	251	7	B
199603290910	48.770	-128.630	228/59/18	4.5	5.4E15	9	218	7	C
199604231516	48.983	-128.223	222/63/16	4.4	4.4E15	9	215	7	B
199605122137	48.790	-128.980	299/81/-180	4.3	2.8E15	9	299	6	C
199605251251	48.630	-128.540	68/79/23	4.2	2.4E15	9	63	7	B

Date: year, month, day, hour, minute. Lat, Long: latitude, longitude. S/D/R: strike, dip, rake. M_w: moment magnitude. Mo: seismic moment. CD: centroid depth. SD: slip direction. SR: source region; 1: Queen Charlotte Islands; 2: Revere-Dellwood-Wilson Fault; 3: Explorer Ridge; 4: Interior of Explorer Plate; 5: Western Sovanco Fracture Zone; 6: Eastern Sovanco Fracture Zone; 7: Nootka Fault Zone; 8: Juan de Fuca Ridge; 9: Vancouver Island Region; 10: Gulf of Alaska; 11: Yukon & Northwest Territories; 12: Central Cordillera (B.C., Alberta, Montana). Q: quality factor; A: excellent; B: very good; C: fair; D: poor

Table A.1 Regional moment tensor solutions calculated in this study. A total of 387 solutions are listed in this table.

Date yyyymmddhhmm	Lat	Long	S/D/R	M_w	Mo (Nm)	CD (km)	SD	SR	Q
199607212038	64.371	-137.577	303/48/82	4.9	2.5E16	9	225	11	B
199608160341	51.062	-130.748	150/63/178	5.2	6.7E16	9	151	2	B
199608160954	51.138	-130.671	157/57/180	4.8	1.9E16	9	157	2	B
199608202241	50.508	-130.274	319/85/-161	4.1	1.5E15	9	317	2	B
199608230533	70.332	-132.275	141/32/41	4.5	6.7E15	18	105	11	D
199608230913	47.506	-129.348	148/63/-106	4.7	1.2E16	6	90	8	B
199609030518	61.340	-140.210	323/42/81	4.2	2.3E15	12	245	10	C
199609092228	49.011	-128.833	126/70/166	4.2	1.9E15	9	131	4	C
199610062013	48.804	-128.408	42/81/-15	6.3	2.7E18	6	44	7	A
199610062029	48.848	-128.167	234/73/12	4.8	2.0E16	12	230	7	C
199610062043	48.792	-128.250	230/81/25	4.9	2.2E16	9	226	7	C
199610070204	48.815	-128.157	63/86/-9	4.6	1.0E16	9	64	7	B
199610070737	48.831	-128.324	208/87/-2	4.5	6.9E15	9	208	7	C
199610071018	48.944	-128.259	242/76/13	4.5	6.2E15	6	239	7	B
199610071836	48.920	-128.113	12/84/-15	4.9	2.9E16	9	14	7	B
199610090712	49.492	-129.962	148/76/166	5.8	4.9E17	9	151	5	A
199610090952	49.546	-129.920	145/78/-139	4.2	2.5E15	6	135	5	C
199610131133	48.899	-128.163	24/76/-45	4.5	5.6E15	6	38	7	B
199610142303	48.841	-128.203	25/87/-39	4.6	8.7E15	6	27	7	C
199610160433	64.129	-137.053	320/51/125	4.7	1.1E16	3	2	11	C
199610262005	63.945	-130.011	264/26/56	4.7	1.2E16	3	211	11	C
199611041738	49.510	-129.800	118/69/159	4.9	2.4E16	12	126	4	B
199611060655	50.454	-130.213	315/88/-167	4.5	6.5E15	12	315	2	C
199611210124	49.586	-128.795	129/71/146	4.4	5.2E15	9	141	4	C
199611210130	49.588	-128.816	308/89/-161	4.2	2.0E15	9	308	4	B
199612022154	49.660	-129.970	149/89/167	4.6	9.9E15	12	149	4	C
199612241240	51.895	-131.620	152/64/145	4.6	8.7E15	15	169	2	B
199701300528	59.180	-144.950	192/50/-161	5.0	3.3E16	21	180	10	C
199702051927	51.549	-131.439	156/74/167	5.1	5.7E16	9	160	2	C
199702051929	51.529	-131.377	163/79/163	5.4	1.4E17	9	166	2	A
199702240104	58.770	-136.110	19/40/115	4.3	3.7E15	9	78	10	B
199703091433	66.511	-135.782	337/48/133	4.6	8.8E15	15	13	11	C
199703290545	50.475	-130.226	136/87/169	4.5	6.1E15	9	137	2	B
199703300650	50.485	-130.221	130/82/157	4.5	6.7E15	9	133	2	C
199704132025	51.348	-131.200	145/76/172	4.9	2.5E16	12	147	2	B
199705050710	66.220	-142.380	141/88/176	4.3	2.9E15	3	141	11	C
199707100649	49.231	-127.881	19/39/-31	4.4	5.2E15	6	44	7	C
199708160623	48.848	-129.196	124/64/-174	4.4	4.4E15	6	121	6	C
199709200439	50.761	-130.588	166/83/145	5.3	8.5E16	12	171	2	B
199709200709	50.779	-130.571	170/79/153	5.3	1.2E17	12	176	2	B
199710041515	47.932	-128.477	139/48/-132	4.4	5.0E15	9	102	8	C
199710210810	50.411	-130.169	131/78/162	4.6	9.5E15	6	135	2	B
199711252103	64.209	-132.882	315/74/-154	4.4	3.9E15	6	307	11	C
199711252228	64.221	-132.924	307/85/-168	4.7	1.4E16	6	306	11	C
199712200422	50.447	-130.342	133/76/164	4.7	1.2E16	12	137	2	C
199801282201	58.881	-137.599	261/21/16	4.3	3.0E15	3	246	10	C
199802051833	58.390	-138.470	349/79/-178	4.7	1.4E16	15	349	10	B

Table A.1 Regional moment tensor solutions calculated in this study (continued).

Date yyyymmddhhmm	Lat	Long	S/D/R	M_w	Mo (Nm)	CD (km)	SD	SR	Q
199802081911	50.499	-130.287	327/74/-139	4.5	6.6E15	9	314	2	B
199802140545	50.845	-130.505	154/51/-177	4.5	6.3E15	9	152	2	C
199802140619	50.855	-130.511	155/72/162	4.6	8.0E15	9	161	2	C
199802181846	49.543	-129.858	132/84/154	4.6	7.7E15	9	135	4	B
199803030419	49.168	-118.351	56/82/-26	3.6	2.7E14	6	60	12	D
199804070511	64.650	-137.530	159/87/-176	4.6	8.5E15	9	159	11	C
199804270428	61.017	-134.076	47/87/-32	4.0	9.8E14	6	49	11	D
199804301122	48.690	-129.020	310/73/173	4.2	2.2E15	9	312	6	C
199804301135	48.710	-129.020	319/73/175	4.2	2.0E15	9	320	6	C
199805311102	48.710	-128.650	185/78/-76	4.1	1.4E15	3	225	8	C
199806122024	48.892	-129.032	120/54/173	4.4	4.1E15	12	124	6	C
199806252251	49.994	-130.236	145/75/175	5.3	1.0E17	12	146	3	A
199807100305	50.548	-130.328	319/89/-162	4.1	1.4E15	9	319	2	C
199807140105	48.728	-129.144	132/77/178	4.7	1.3E16	9	132	6	B
199807140149	48.773	-129.009	304/81/177	4.3	2.8E15	9	304	6	B
199807140227	48.773	-129.015	120/44/174	4.5	7.3E15	9	124	6	B
199807150030	47.519	-129.195	27/54/-62	4.7	1.3E16	6	75	8	B
199807281138	59.220	-137.860	290/52/97	4.6	1.0E16	15	9	10	B
199807310740	51.362	-130.782	160/52/179	4.7	1.3E16	9	161	2	B
199807310818	51.341	-130.798	150/63/178	4.3	2.9E15	12	151	2	C
199808060243	52.126	-131.644	121/49/91	4.4	5.1E15	12	209	1	B
199808061811	48.879	-129.223	112/41/166	4.6	9.2E15	9	123	6	B
199808061817	48.884	-129.349	116/56/173	4.8	2.1E16	9	120	6	B
199808131138	51.708	-116.047	104/25/56	3.5	2.2E14	6	51	12	D
199808161925	50.009	-130.245	151/73/161	4.3	2.8E15	12	157	3	B
199808190439	50.386	-130.338	135/83/165	4.9	2.8E16	12	137	2	A
199808301133	50.905	-130.663	162/76/-171	6.2	2.3E18	9	160	2	B
199809010743	50.901	-130.710	137/69/172	4.3	3.1E15	9	140	2	B
199809010919	49.143	-127.775	49/78/-30	4.5	6.0E15	9	56	7	B
199809011812	50.732	-130.583	151/60/168	4.8	2.1E16	12	157	2	B
199809091448	54.158	-133.937	148/75/-162	4.4	3.9E15	9	143	1	B
199809191425	49.957	-130.253	153/55/-177	5.0	3.5E16	9	151	3	B
199809260513	63.436	-126.639	155/63/-164	4.3	3.2E15	9	148	11	C
199809301115	48.899	-129.132	132/53/-178	4.0	1.2E15	3	131	6	C
199811100132	59.420	-139.150	360/65/-175	4.1	1.9E15	9	358	11	B
199901011101	48.484	-128.752	50/82/19	4.3	3.6E15	9	47	7	C
199904171133	50.490	-130.261	141/81/174	4.7	1.3E16	12	142	2	B
199904171221	50.504	-130.283	318/89/-171	4.5	5.6E15	12	318	2	B
199905120334	61.635	-130.337	255/78/23	4.4	4.4E15	6	250	11	B
199905240522	60.110	-139.420	261/39/126	4.4	4.9E15	12	308	10	B
199905270808	58.671	-136.789	136/63/159	5.7	3.7E17	18	146	10	B
199906082014	47.888	-128.915	234/34/-73	4.6	9.4E15	12	304	8	C
199906090049	47.753	-129.044	203/52/-80	4.7	1.5E16	9	277	8	C
199906091908	47.938	-128.801	321/88/-161	4.6	2.8E16	9	320	8	C
199906190929	47.721	-128.954	297/85/180	4.6	7.5E15	9	297	8	D
199906210726	47.417	-128.944	31/80/27	4.4	5.2E15	9	26	8	C
199906281021	48.834	-129.288	107/38/-178	4.9	2.3E16	6	105	6	B

Table A.1 Regional moment tensor solutions calculated in this study (continued).

Date yyyymmddhhmm	Lat	Long	S/D/R	M_w	Mo (Nm)	CD (km)	SD	SR	Q
199907021145	49.230	-129.433	127/65/148	5.8	5.5E17	9	142	4	B
199907030143	47.074	-123.464	175/38/-89	6.1	1.8E18	45	264	9	C
199907050334	49.427	-129.410	127/64/167	4.1	1.4E15	6	133	4	D
199907060530	47.290	-129.055	170/20/-162	4.3	3.5E15	6	153	8	D
199907172007	47.654	-129.013	218/74/-40	4.8	1.6E16	6	231	8	B
199907221207	50.711	-130.556	133/88/174	4.2	2.0E15	9	133	2	C
199908141716	48.226	-129.118	355/58/-94	4.0	1.2E15	3	273	8	D
199910071203	50.535	-130.367	321/88/-163	4.2	2.5E15	9	320	2	C
199910100252	48.777	-129.650	330/63/170	4.6	9.2E15	9	335	6	B
199910101336	48.739	-129.632	307/88/-171	4.6	8.9E15	9	307	6	C
199910140829	50.467	-130.214	135/89/155	4.4	4.1E15	9	135	2	C
199910190549	57.998	-136.964	91/62/69	4.6	9.0E15	6	40	10	C
199910260136	49.026	-129.770	142/50/-159	4.6	9.1E15	3	128	6	C
199911291003	62.172	-124.485	178/19/123	4.1	1.7E15	3	234	11	C
199912111253	48.521	-123.272	269/75/-17	4.8	1.5E16	54	274	9	C
199912121637	51.343	-131.061	150/70/-173	4.8	1.6E16	9	148	2	C
199912250649	48.647	-125.872	274/76/7	4.7	1.3E16	27	272	9	B
200001031226	50.476	-130.327	314/89/-166	4.3	3.5E15	12	314	2	C
200001061042	58.042	-136.872	160/78/154	6.4	4.0E18	15	166	10	A
200001180656	50.551	-130.367	143/85/164	4.5	5.4E15	12	144	2	C
200001230553	52.249	-131.844	164/42/142	4.3	2.9E15	15	194	1	C
200002082327	47.511	-128.856	164/43/-132	4.6	7.8E15	3	125	8	C
200002181054	48.913	-128.592	299/17/41	4.4	4.7E15	9	259	7	D
200002212235	49.188	-130.055	295/85/-176	4.8	1.9E16	3	295	5	C
200003172107	48.826	-129.131	128/87/177	4.8	1.9E16	9	128	6	D
200003251629	49.433	-127.729	62/89/4	4.5	6.0E15	15	62	7	B
200003271521	48.790	-128.800	203/88/-12	4.4	4.6E15	12	203	7	D
200004010228	50.553	-130.358	138/89/156	4.2	1.9E15	9	138	2	B
200004061528	49.186	-130.285	333/60/-179	4.3	3.2E15	6	332	5	C
200004300158	50.846	-130.615	160/77/162	4.3	3.2E15	6	164	2	C
200004300549	50.783	-130.648	156/70/146	4.6	9.7E15	6	169	2	B
200004300829	50.831	-130.649	163/72/-176	5.4	1.3E17	6	162	2	A
200004301013	50.980	-130.610	166/54/-160	5.7	4.4E17	9	154	2	C
200004301054	50.960	-130.780	164/71/-175	5.1	5.2E16	12	162	2	B
200005011110	50.620	-130.528	146/73/-174	4.7	1.3E16	9	144	2	B
200005022359	59.620	-139.046	111/39/168	5.6	2.4E17	6	120	10	B
200005082309	52.583	-131.841	122/39/80	3.9	8.2E14	15	45	1	D
200005142001	49.947	-130.180	319/89/-155	4.9	2.3E16	12	319	3	A
200005150512	49.997	-130.213	162/58/-171	4.7	1.3E16	9	157	3	B
200005150558	49.989	-130.141	126/80/168	5.3	1.1E17	12	128	3	A
200005150706	50.051	-130.171	337/84/-151	4.4	4.5E15	9	334	3	B
200005150711	49.938	-130.325	156/77/175	5.6	2.6E17	9	157	3	A
200005150749	50.032	-130.214	151/70/-160	4.4	4.9E15	9	144	3	B
200006092125	50.070	-130.432	133/73/-177	4.6	8.1E15	15	132	3	B
200006101504	50.527	-130.419	144/82/166	5.0	3.8E16	12	146	2	A
200006221415	49.427	-128.427	307/60/-137	3.6	3.1E14	3	282	4	C
200007180853	65.264	-133.436	202/47/5	3.9	1.3E15	12	199	11	C

Table A.1 Regional moment tensor solutions calculated in this study (continued).

Date yyyymmddhhmm	Lat	Long	S/D/R	M_w	Mo (Nm)	CD (km)	SD	SR	Q
200008012133	49.493	-126.133	301/73/171	4.9	2.8E16	33	304	9	B
200008031312	60.334	-136.875	147/67/177	4.5	7.1E15	12	148	10	B
200009031455	60.391	-139.372	87/71/-22	3.6	2.6E14	3	94	10	C
200009190549	49.668	-127.335	183/81/130	3.7	3.9E14	3	194	9	D
200009270345	50.499	-130.492	144/78/179	4.9	3.0E16	12	144	2	A
200009301905	57.273	-142.870	195/82/160	5.3	9.8E16	18	198	10	C
200010190929	50.428	-130.182	139/88/170	4.8	1.7E16	9	139	2	A
200010220953	51.336	-130.973	335/62/168	4.0	1.2E15	9	341	2	D
200010230506	60.259	-141.711	272/46/76	4.5	7.3E15	12	202	10	C
200011041749	58.799	-138.770	314/42/88	5.0	3.4E16	15	227	10	B
200011192038	50.772	-130.471	152/69/173	4.8	2.0E16	12	155	2	A
200011192214	50.752	-130.488	155/83/168	4.9	2.8E16	12	156	2	A
200011200515	50.823	-130.416	151/57/-162	4.0	1.2E15	12	141	2	D
200011201404	50.564	-130.365	329/85/-158	4.0	1.3E15	9	327	2	D
200011251640	51.057	-130.708	332/86/-140	4.3	3.0E15	6	329	2	D
200011271146	51.071	-130.663	159/68/171	4.8	1.6E16	9	162	2	B
200011271421	51.034	-130.739	141/70/174	4.2	2.4E15	6	143	2	C
200012041949	50.659	-130.562	138/71/176	4.1	1.5E15	9	139	2	C
200012051613	48.700	-128.590	218/89/-11	4.2	2.2E15	9	218	7	D
200012080317	49.400	-127.791	60/79/-44	4.0	1.3E15	3	70	7	C
200012160115	57.104	-143.041	10/85/-172	4.9	2.5E16	12	9	10	C
200101110004	48.899	-129.305	121/72/165	6.0	1.3E18	9	126	6	A
200101110014	48.912	-129.264	113/85/154	4.2	2.6E15	9	115	4	B
200101131102	48.999	-129.253	331/70/-149	4.9	2.1E16	3	319	4	B
200101200014	50.494	-130.362	163/56/159	5.5	2.3E17	9	175	2	B
200101230939	49.334	-128.787	107/61/154	5.7	3.5E17	15	120	4	A
200101231443	49.174	-129.099	119/81/166	5.5	1.7E17	9	121	4	A
200101231454	49.420	-128.880	192/83/173	4.5	6.1E15	15	193	4	B
200101231515	49.101	-129.285	316/59/-180	4.5	5.4E15	6	316	4	C
200101231703	49.215	-129.042	136/86/-165	4.1	1.5E15	9	135	4	D
200101301415	66.342	-135.617	291/50/94	3.9	7.3E14	18	15	11	D
200101310805	58.117	-142.904	191/87/-173	3.7	4.7E14	15	191	10	D
200102050349	64.327	-130.910	305/37/108	5.3	1.0E17	6	13	11	A
200102060121	50.550	-130.387	320/84/-159	3.9	8.1E14	12	318	2	C
200102122240	50.524	-130.280	321/89/-169	4.5	6.2E15	12	321	2	B
200102170921	64.330	-130.874	271/63/33	3.4	1.3E14	6	255	11	D
200102172011	54.020	-133.700	151/53/-167	6.3	2.8E18	12	143	1	A
200102172039	53.876	-133.688	334/77/-172	5.0	3.3E16	15	332	1	C
200102172119	53.840	-133.510	161/48/-179	5.3	1.1E17	12	160	1	B
200102242106	65.284	-133.124	251/38/90	4.2	1.9E15	6	161	11	C
200102250818	72.477	-131.326	207/86/11	4.5	7.0E15	15	206	11	D
200102262117	52.250	-119.324	240/78/-3	3.7	4.1E14	9	241	12	D
200102281854	47.155	-122.713	356/73/-97	6.8	2.0E19	48	289	9	A
200103090710	64.225	-130.919	311/27/110	5.2	8.1E16	6	19	11	A
200103091902	64.269	-130.952	333/34/147	4.3	3.3E15	3	1	11	B
200103210751	50.402	-130.213	133/88/165	4.4	4.3E15	12	134	2	B
200103291820	64.310	-130.931	319/37/134	4.5	6.5E15	6	359	11	A

Table A.1 Regional moment tensor solutions calculated in this study (continued).

Date yyyymmddhhmm	Lat	Long	S/D/R	M_w	Mo (Nm)	CD (km)	SD	SR	Q
200103292026	64.300	-130.984	334/55/176	3.8	5.1E14	6	336	11	C
200104010639	53.932	-133.844	331/78/172	4.0	1.1E15	15	333	1	C
200104021854	64.283	-130.995	324/36/136	4.6	7.5E15	6	2	11	A
200104100936	50.475	-130.404	139/74/167	5.3	8.9E16	12	143	2	A
200104121846	64.220	-130.773	297/51/141	3.9	7.6E14	3	324	11	D
200104140220	56.081	-119.807	117/48/107	5.4	1.4E17	15	182	12	A
200104190142	50.541	-130.355	139/79/166	4.4	4.2E15	9	142	2	A
200105012313	49.911	-130.145	134/70/163	4.5	6.3E15	9	140	3	B
200105020153	49.974	-130.109	136/80/151	4.6	8.2E15	9	141	3	A
200105020205	49.914	-130.152	134/63/167	5.4	1.4E17	12	140	3	A
200105020548	49.940	-130.108	134/78/153	4.7	1.5E16	9	140	3	B
200105091705	48.864	-128.356	36/76/-34	4.5	6.4E15	9	45	7	B
200105131409	49.450	-129.499	124/45/172	4.3	2.8E15	9	129	4	D
200105140722	54.429	-142.127	181/60/-133	5.2	7.3E16	12	153	10	B
200105160421	50.417	-130.227	136/72/155	4.8	2.0E16	9	144	2	A
200105201004	50.477	-130.239	138/70/173	4.6	1.0E16	12	140	2	A
200105201010	50.481	-130.240	127/79/155	4.1	1.7E15	9	132	2	B
200105201130	50.464	-130.236	135/87/163	4.1	1.8E15	9	136	2	B
200105201301	50.465	-130.221	134/63/168	4.3	3.7E15	6	140	2	B
200105230215	49.861	-129.616	154/70/155	4.0	1.2E15	6	163	4	C
200106040330	64.253	-138.189	267/59/48	3.8	5.7E14	12	237	11	D
200106071215	48.472	-124.392	296/68/-178	4.9	2.5E16	33	295	9	D
200106101319	47.254	-123.671	133/45/110	5.0	3.8E16	39	70	9	B
200106121009	56.278	-120.814	348/57/113	4.2	2.4E15	9	40	12	C
200106261405	61.337	-140.073	339/20/135	5.9	6.7E17	6	22	11	A
200106270645	50.498	-130.237	319/86/-154	3.9	9.2E14	9	317	2	B
200107021532	52.932	-116.468	166/37/115	4.0	9.4E14	6	226	12	D
200107090326	50.586	-130.357	146/83/172	4.9	2.3E16	12	147	2	A
200107090926	56.214	-135.036	252/53/26	4.9	2.2E16	9	236	10	A
200107221513	47.094	-122.675	57/73/121	4.1	1.7E15	54	83	9	C
200108011619	49.274	-128.274	125/88/162	4.6	8.0E15	9	126	4	C
200108041113	47.487	-128.998	127/49/-148	4.2	2.3E15	3	105	8	C
200108051111	50.009	-130.247	126/80/158	4.7	1.3E16	12	130	3	B
200108101541	64.282	-130.977	286/27/95	4.3	3.3E15	3	10	11	B
200108112122	62.498	-128.537	62/80/-11	4.4	4.7E15	6	64	11	B
200108212221	60.221	-143.356	318/28/111	4.4	4.2E15	12	25	10	D
200109072059	48.826	-128.523	28/89/-84	4.7	1.1E16	3	37	8	C
200109072256	48.763	-128.675	344/77/-85	5.1	5.5E16	3	53	8	B
200109080643	48.738	-128.749	128/33/-154	5.1	5.3E16	3	106	8	B
200109080808	48.828	-128.667	195/48/-48	4.6	1.1E16	6	232	8	C
200109081424	48.788	-128.631	220/67/-30	4.5	6.9E15	6	233	8	C
200109081704	48.779	-128.659	202/77/-3	4.4	4.9E15	6	203	8	C
200109081719	48.749	-128.702	174/45/-113	4.8	1.9E16	6	115	8	B
200109100631	48.815	-128.560	29/80/-68	4.8	1.8E16	3	52	8	B
200109121248	48.778	-128.653	177/19/-83	5.2	8.1E16	3	260	8	B
200109121318	48.805	-128.642	193/35/-54	4.5	6.8E15	3	241	8	C
200109121351	48.758	-128.636	186/40/-61	4.8	1.7E16	3	240	8	B

Table A.1 Regional moment tensor solutions calculated in this study (continued).

Date yyyymmddhhmm	Lat	Long	S/D/R	M_w	Mo (Nm)	CD (km)	SD	SR	Q
200109121404	48.840	-128.601	21/81/-61	4.7	1.3E16	3	37	8	C
200109122224	48.732	-128.639	144/47/-125	5.2	7.6E16	3	100	8	B
200109122230	48.718	-128.669	164/59/-90	5.2	6.8E16	6	254	8	B
200109130447	48.681	-128.652	26/80/-84	4.7	1.3E16	3	85	8	C
200109130543	48.753	-128.551	165/34/-104	4.4	5.0E15	6	92	8	C
200109130956	48.790	-128.624	194/60/-74	5.3	9.2E16	6	254	8	B
200109140445	48.691	-128.712	61/84/-21	6.0	1.2E18	6	63	8	A
200109140538	48.763	-128.430	27/80/-49	5.1	4.4E16	6	38	8	B
200109141236	48.847	-128.509	210/81/11	4.7	1.3E16	9	208	8	B
200109141539	48.727	-128.645	80/76/-30	4.8	1.6E16	6	88	8	B
200109142046	48.783	-128.694	180/36/-83	4.8	2.0E16	9	261	8	B
200109151050	48.563	-128.559	227/89/-109	5.5	1.8E17	3	224	8	C
200109162248	48.469	-128.662	226/83/-44	4.8	1.8E16	6	233	8	B
200109162256	48.546	-128.540	50/83/23	4.5	6.7E15	9	47	8	C
200109162320	48.536	-128.597	229/75/0	5.7	3.6E17	6	229	8	A
200109171505	48.528	-128.628	66/78/25	4.3	3.0E15	9	60	8	C
200109180030	48.493	-128.761	239/84/-20	4.9	2.3E16	9	241	8	B
200109241944	48.570	-128.566	41/81/31	4.4	3.9E15	9	36	8	C
200110110848	50.000	-130.130	144/89/147	4.4	3.9E15	12	145	3	D
200110120502	52.703	-132.078	330/24/127	6.1	1.7E18	6	20	1	A
200110120527	52.660	-132.283	153/71/126	4.7	1.2E16	9	177	1	C
200110200018	50.057	-127.774	149/31/-145	4.1	1.4E15	36	118	9	C
200110260441	65.252	-133.223	236/83/-2	4.0	9.6E14	9	236	11	C
200111051041	48.859	-129.147	123/75/171	4.3	2.8E15	9	125	6	C
200111101831	48.920	-123.060	78/46/128	3.9	7.4E14	15	120	9	D
200111102020	48.868	-129.098	128/74/165	4.7	1.4E16	9	133	6	B
200111111600	47.688	-117.400	261/18/88	3.7	4.3E14	12	173	12	D
200111180209	60.145	-137.919	306/89/146	4.3	3.6E15	6	307	11	B
200111280418	64.490	-113.540	280/39/-91	4.5	5.7E15	15	191	11	D
200112090121	49.575	-129.352	136/68/170	4.4	5.3E15	9	140	4	C
200112261621	49.754	-117.824	251/84/-8	4.5	6.5E15	12	252	12	D
200112310752	49.497	-129.554	332/68/-177	4.3	2.8E15	9	331	4	C
200201041351	48.940	-129.040	122/79/175	4.1	1.8E15	9	123	4	D
200201050204	48.567	-128.432	75/77/57	4.0	1.1E15	9	56	8	C
200201051813	50.506	-130.337	319/85/-158	4.3	3.1E15	9	317	2	C
200201232114	50.739	-130.516	138/74/167	4.3	2.7E15	12	142	2	B
200201281141	50.278	-130.243	350/80/-136	4.7	1.1E16	12	340	3	B
200202140433	64.252	-130.844	287/31/111	4.6	8.1E15	6	353	11	B
200202200317	51.134	-131.102	142/75/165	5.1	5.4E16	9	148	2	A
200203072115	52.047	-117.180	339/88/139	3.7	3.7E14	6	341	12	D
200203212318	51.051	-130.950	140/79/151	4.2	2.6E15	9	146	2	B
200203242106	59.178	-145.549	89/33/-70	4.9	2.5E16	6	156	10	C
200204040429	50.528	-130.415	146/80/171	4.8	1.8E16	9	148	2	A
200204180051	49.513	-129.505	148/53/-157	4.0	9.7E14	3	134	4	C
200204180119	49.629	-129.058	131/84/172	4.6	7.5E15	15	132	4	B
200205130332	50.465	-130.257	320/86/-170	4.9	2.4E16	12	319	2	A
200206061537	50.081	-130.286	134/64/166	4.7	1.3E16	15	140	3	B

Table A.1 Regional moment tensor solutions calculated in this study (continued).

Date yyyymmddhhmm	Lat	Long	S/D/R	M_w	Mo (Nm)	CD (km)	SD	SR	Q
200206101300	51.018	-130.616	162/62/167	4.1	1.8E15	9	168	2	B
200206290640	52.860	-132.240	336/73/133	4.0	1.3E15	21	353	1	C
200207031434	50.520	-130.370	136/87/162	4.2	2.1E15	12	137	2	B
200207101019	49.006	-128.918	128/85/-180	4.3	3.1E15	9	128	4	B
200207102131	49.030	-128.821	308/81/-157	4.8	2.0E16	6	304	4	B
200207110052	49.062	-128.775	123/64/176	4.6	8.1E15	9	125	4	B
200207130722	49.241	-129.503	113/84/137	4.3	3.5E15	9	119	4	B
200207140019	48.976	-128.840	121/65/171	4.7	1.2E16	9	125	4	B
200207150531	48.941	-128.897	317/70/-167	4.4	4.0E15	6	312	4	B
200207191958	47.430	-113.140	123/75/-166	4.2	2.4E15	21	119	12	D
200207281649	50.852	-115.137	91/37/89	3.7	3.5E14	6	2	12	D
200208171606	49.951	-120.265	251/43/89	4.5	6.9E15	9	162	12	B
200208231640	63.922	-130.064	76/64/54	3.8	6.3E14	3	45	11	C
200209051129	54.069	-133.941	330/68/175	5.2	7.5E16	6	332	1	B
200209210055	48.469	-123.159	12/65/12	4.1	3.1E15	27	7	9	B
200210030015	48.540	-128.770	227/86/-19	4.1	1.5E15	24	228	7	D
200210031028	48.530	-128.730	70/77/36	4.2	2.7E15	9	61	7	C
200210080849	49.120	-130.618	298/69/175	4.4	5.0E15	15	300	5	C
200210110109	48.491	-128.840	72/77/-2	5.2	7.3E16	9	72	7	B
200210150556	48.571	-128.704	73/88/-7	4.5	6.8E15	15	73	7	C
200210161657	49.770	-129.830	107/75/-18	4.5	6.4E15	15	112	4	C
200210162212	49.890	-129.770	184/45/158	4.6	1.0E16	6	200	4	B
200210162232	49.864	-129.803	295/73/28	4.7	1.3E16	3	286	4	C
200210212041	61.596	-140.862	261/46/65	4.3	3.6E15	9	205	11	C
200210300232	52.750	-132.104	322/31/104	5.0	3.3E16	12	36	1	B
200211030149	51.306	-131.119	165/84/162	5.8	4.9E17	6	167	2	A
200211030630	51.499	-130.805	148/65/165	4.6	8.7E15	9	154	2	B
200211060655	61.972	-132.809	125/83/154	4.0	1.2E15	12	128	11	C
200211180822	60.613	-137.946	276/56/61	4.1	1.6E15	9	231	11	C
200211200457	48.809	-129.176	306/85/-168	4.1	1.7E15	9	305	6	C
200211232210	50.696	-130.559	144/85/177	4.8	1.9E16	12	144	2	A
200211291152	48.920	-123.060	286/54/102	3.9	6.7E14	18	356	9	C
200212131551	50.168	-130.296	166/75/150	5.5	2.3E17	6	174	3	B
200212141951	62.098	-135.469	290/50/54	4.4	3.8E15	9	249	11	B
200212170851	50.368	-130.221	155/76/143	4.3	3.0E15	9	165	2	C
200212170857	50.417	-130.167	144/65/138	4.2	2.6E15	6	165	2	C
200212181914	51.060	-130.597	155/58/170	4.4	4.1E15	9	160	2	B
200212220415	50.445	-130.155	147/70/-173	4.6	1.0E16	12	145	2	B
200301051839	48.884	-129.181	126/65/173	4.3	3.5E15	9	129	6	C
200301071300	50.542	-130.303	321/79/-164	4.5	6.6E15	12	318	2	B
200302040145	47.496	-129.010	221/43/-77	4.1	1.6E15	9	293	8	D
200302040948	48.867	-128.232	17/63/-31	4.1	1.4E15	9	32	7	D
200302132126	65.597	-134.669	83/88/-40	4.2	7.0E14	6	85	11	D
200302141356	65.540	-134.470	281/69/94	4.2	2.6E15	9	360	11	C
200303031536	49.900	-130.191	139/68/153	4.8	1.5E16	9	150	3	B
200303111359	50.420	-130.190	134/80/161	4.5	5.7E15	9	137	2	B
200303190823	62.190	-124.480	195/36/161	4.0	1.1E15	9	211	11	B

Table A.1 Regional moment tensor solutions calculated in this study (continued).

Date yyyymmddhhmm	Lat	Long	S/D/R	M_w	Mo (Nm)	CD (km)	SD	SR	Q
200303300744	48.650	-129.050	123/84/164	4.4	3.8E15	9	125	6	C
200303301003	47.610	-129.100	156/63/-82	4.3	3.6E15	6	229	8	C
200304141148	62.540	-142.750	332/85/-129	4.1	1.6E15	12	326	11	C
200304251002	47.670	-123.250	47/88/-95	4.6	8.3E15	45	25	9	B
200305052131	51.310	-131.300	151/85/-178	3.9	7.4E14	9	151	2	D
200305211006	62.530	-142.750	239/87/19	4.5	5.7E15	15	238	10	B
200305220408	59.180	-137.590	306/41/93	4.6	9.8E15	12	32	10	B
200305290528	48.480	-128.810	134/29/-166	4.9	2.5E16	3	122	8	B
200306091534	61.610	-141.400	137/70/174	4.0	9.8E14	6	139	11	B
200306301220	62.480	-142.520	109/85/-180	4.3	2.8E15	6	109	11	B
200307011549	50.510	-130.270	144/83/170	5.0	3.6E16	12	145	2	A
200307122301	54.680	-134.450	150/80/-177	6.0	1.0E18	12	149	1	A
200307220352	57.470	-136.420	334/73/178	4.3	2.7E15	9	335	11	B
200307221853	50.100	-130.230	164/31/-151	4.3	3.7E15	9	139	3	C
200308200833	49.960	-120.290	217/45/27	3.7	4.2E14	15	197	12	D
200309221052	53.252	-133.267	354/76/174	4.4	4.2E15	12	355	1	B
200310202216	67.469	-137.036	330/89/160	3.9	8.9E14	9	330	11	C
200310230816	50.508	-130.311	143/87/176	4.9	2.9E16	12	143	2	A
200311040100	65.497	-123.871	308/49/-18	4.2	2.1E15	9	320	11	B
200311071316	48.816	-129.183	130/44/-170	4.8	1.9E16	9	123	6	B
200311071421	48.823	-129.089	126/36/-174	5.0	3.5E16	9	121	6	B
200311172320	60.020	-141.202	242/41/94	4.2	2.5E15	6	327	10	C
200311282319	51.833	-125.299	40/41/-13	3.9	9.0E14	15	50	12	C
200312061628	64.141	-134.977	284/13/35	4.0	1.3E15	6	250	11	C
200312190532	48.853	-129.193	140/42/148	5.4	1.5E17	12	129	6	B
200401070242	50.531	-130.211	139/75/-179	4.2	1.9E15	12	139	2	C
200401070353	50.487	-130.271	320/89/-177	4.6	8.0E15	12	320	2	A
200401121531	61.087	-138.069	349/58/157	4.1	1.5E15	3	2	11	C
200401150445	49.150	-127.933	55/81/5	4.7	1.3E16	12	54	7	B
200401251512	49.096	-128.063	49/75/-23	5.4	1.3E17	9	55	7	B
200401251535	49.181	-127.956	218/68/0	4.7	1.3E16	6	218	7	B
200401261813	49.166	-127.952	56/84/5	4.1	1.6E15	9	55	7	C
200402051923	54.221	-133.980	148/84/-167	4.2	2.4E15	9	147	1	C
200402280157	50.945	-130.644	146/41/178	4.8	1.8E16	12	148	2	C
200402280200	50.933	-130.630	154/32/-174	4.9	2.7E16	12	149	2	B
200402280205	50.959	-130.650	148/42/-179	5.1	4.5E16	12	147	2	B
200402280254	51.002	-130.527	140/43/159	4.1	1.4E15	6	156	2	D
200403040003	48.662	-128.910	115/85/179	4.2	2.6E15	9	115	6	C
200403171134	48.332	-122.225	84/80/125	4.2	2.0E15	3	98	9	B
200404190142	50.576	-130.477	141/89/173	4.3	2.7E15	9	141	2	B

Table A.1 Regional moment tensor solutions calculated in this study (continued).

Date yyyymmddhhmm	Lat	Long	S/D/R	M_w	Mo (Nm)	CD (km)	SD	SR
199401030126*	49.583	-127.042	254/40/332	5.6	2.8E17	20	95	7
199402120704*	49.102	-129.350	131/82/157	5.7	4.0E17	6	315	6
199404122114*	50.302	-130.190	324/84/211	4.6	9.4E15	10	320	3
199404270030*	48.677	-129.145	134/63/168	4.8	1.5E16	8	320	6
199406150822	47.417	-123.158	256/61/-56	4.1	1.8E15	45	292	9
199406180701	47.610	-121.260	109/80/113	3.9	7.7E14	9	131	9
199407150502*	50.472	-130.065	136/86/165	4.8	1.5E16	10	317	2
199408211305*	50.398	-130.430	140/86/166	5.1	4.8E16	12	321	2
199409100743	47.180	-121.950	317/61/116	3.9	7.6E14	21	2	9
199411021352*	50.515	-130.286	141/84/166	4.3	2.9E15	12	323	2
199411200122	49.180	-125.535	301/65/130	4.2	1.9E15	60	328	9
199501090650	51.045	-130.737	335/63/187	4.7	1.2E16	4	332	2
199501160701*	49.971	-130.096	142/85/157	4.4	3.9E15	15	324	3
199501170813*	50.026	-130.120	148/62/168	4.5	6.8E15	6	334	3
199501171442*	50.004	-130.188	151/58/174	5.1	4.9E16	6	334	3
199501290311	47.380	-122.350	291/59/116	4.9	2.1E16	18	338	9
199503081630	50.503	-129.965	139/84/167	4.8	1.5E16	12	320	2
199504230929	50.457	-130.219	132/87/169	4.4	4.5E15	12	313	2
199505021931	48.070	-114.530	234/80/35	3.7	4.1E14	9	227	12
199505310338	50.931	-130.683	146/79/168	5.2	5.9E16	12	328	2
199506212024*	50.919	-130.747	158/61/193	5.4	1.5E17	6	332	2
199509122244	51.143	-131.200	333/86/216	5.2	7.9E16	9	330	2
199509130759	51.312	-130.900	148/90/155	5.3	1.1E17	9	328	2
199509131119	51.092	-131.034	148/87/151	4.8	1.5E16	9	330	2
199510150129	48.850	-128.601	310/79/214	4.4	4.8E15	9	303	6
199510311940*	50.617	-130.456	146/83/165	4.4	5.0E15	12	328	2
199511121305	48.838	-129.179	130/67/166	4.8	1.5E16	9	316	6
199512010329	50.363	-130.038	135/77/156	4.4	4.1E15	9	321	2
199601031312*	49.473	-130.242	134/84/169	5.2	7.9E16	6	315	5
199601211606	47.450	-121.780	276/30/125	3.5	1.9E14	24	327	9
199601281130*	48.945	-129.276	135/80/161	4.6	7.7E15	6	318	6
199603102112	50.573	-130.436	143/85/169	4.7	1.2E16	12	324	2
199603162318	50.690	-129.880	324/86/194	5.2	6.9E16	12	323	2
199603180801	49.791	-127.103	246/61/343	5.0	4.1E16	15	74	7
199604231516	48.983	-128.233	215/62/0	4.4	3.9E15	9	35	7
199605030404	47.754	-121.881	350/52/78	5.2	7.6E16	10	279	9
199605032314	47.750	-121.880	351/39/72	3.4	1.3E14	9	284	9
199605041438	47.750	-121.880	357/17/54	3.4	1.2E14	6	347	9

Date: year, month, day, hour, minute. Lat, Long: latitude, longitude. S/D/R: strike, dip, rake. M_w: moment magnitude. Mo: seismic moment. CD: centroid depth. SD: slip direction. SR: source region; 1: Queen Charlotte Islands; 2: Revere-Dellwood-Wilson Fault; 3: Explorer Ridge; 4: Interior of Explorer Plate; 5: Western Sovanco Fracture Zone; 6: Eastern Sovanco Fracture Zone; 7: Nootka Fault Zone; 8: Juan de Fuca Ridge; 9: Vancouver Island Region; 10: Gulf of Alaska; 11: Yukon & Northwest Territories; 12: Central Cordillera (B.C., Alberta, Montana); *: indicates regional moment tensor solution that was not re-calculated in this study

Table A.2 Regional moment tensor solutions calculated by Oregon State University from 1994–1998.

Date yyyymmddhhmm	Lat	Long	S/D/R	M_w	Mo (Nm)	CD (km)	SD	SR
199605190544	52.240	-115.260	298/63/88	3.9	6.6E14	4	212	12
199608160341	51.097	-130.645	155/88/170	5.1	4.9E16	4	335	2
199608160954	51.150	-130.670	158/83/176	4.7	1.4E16	4	338	2
199608202241	50.512	-130.277	323/73/192	4.0	1.1E15	9	319	2
199608230913	47.727	-129.261	10/62/270	4.8	1.7E16	9	100	8
199609092228	49.011	-128.833	115/75/188	4.2	1.9E15	6	293	6
199609241245	47.719	-122.967	217/89/-179	3.8	4.7E14	51	217	9
199609292307	48.050	-122.700	286/86/-51	3.8	6.3E14	60	291	9
199610062013	48.965	-128.208	41/86/335	6.2	2.4E18	4	43	7
199610062029	48.863	-128.144	42/88/337	4.8	2.0E16	4	43	7
199610062043	48.792	-128.250	227/80/12	4.8	1.8E16	4	45	7
199610070204	48.815	-128.157	246/80/25	4.5	6.6E15	4	61	7
199610070737	48.831	-128.324	23/88/341	4.5	5.9E15	4	24	7
199610071018	48.944	-128.259	57/90/347	4.4	4.4E15	4	57	7
199610071836	48.920	-128.113	189/68/349	4.8	2.1E16	6	19	7
199610090712	49.581	-129.977	147/75/153	5.8	5.8E17	6	335	5
199610090952	49.546	-129.920	128/73/168	4.3	3.4E15	9	312	5
199610131133	48.899	-128.164	29/86/342	4.3	2.7E15	6	30	7
199610142304	48.841	-128.203	31/83/332	4.5	5.8E15	4	35	7
199610190744	52.214	-115.215	302/51/67	4.0	1.0E15	4	246	12
199611060655	50.454	-130.213	323/69/199	4.4	4.4E15	9	316	2
199611210124	49.579	-128.786	316/88/203	4.4	5.2E15	6	315	4
199611210130	49.583	-128.813	304/79/204	4.1	1.8E15	6	299	4
199612241240	51.867	-131.715	157/79/159	4.5	5.8E15	15	341	2
199701120601	49.601	-120.514	270/64/67	3.8	5.6E14	6	224	12
199702051927	51.615	-131.432	159/87/184	5.0	3.4E16	6	339	2
199702051929	51.543	-131.474	159/87/182	5.3	8.7E16	6	339	2
199702100426	47.554	-122.301	284/46/116	3.5	2.3E14	9	339	9
199703290545	50.475	-130.226	324/77/189	4.4	3.9E15	9	322	2
199703300650	50.485	-130.221	322/84/189	4.3	3.6E15	6	319	2
199704132025	51.388	-131.224	330/82/197	4.7	1.5E16	9	328	2
199706231913	47.599	-122.574	275/65/89	4.5	7.0E15	4	187	9
199706241423	48.377	-119.885	286/49/103	4.1	1.4E15	12	357	9
199706271047	47.608	-122.568	282/58/93	3.6	3.2E14	4	6	9
199707100649	49.231	-127.881	20/75/334	4.3	3.5E15	6	27	7
199707110128	47.580	-122.550	292/57/96	3.5	1.8E14	4	11	9
199708011255	47.280	-123.730	260/41/58	3.7	4.5E14	9	210	9
199708160623	48.848	-129.196	114/65/177	4.6	7.7E15	12	295	6
199709200439	50.892	-130.298	56/76/282	5.3	8.8E16	4	325	2
199709200709	50.754	-130.523	61/79/284	5.4	1.4E17	4	331	2
199710041515	48.057	-129.022	120/87/232	4.5	5.5E15	4	115	8
199710210810	50.412	-130.169	320/82/203	4.6	8.4E15	9	317	2
199711260005	47.789	-123.074	274/46/-175	3.8	5.5E14	42	271	9
199712200422	50.447	-130.342	141/89/164	4.6	9.5E15	9	321	2
199802081911	50.499	-130.287	323/79/197	4.4	4.8E15	9	320	2
199802140545	50.845	-130.505	156/66/199	4.4	4.5E15	4	328	2

Table A.2 Regional moment tensor solutions calculated by Oregon State University from 1994–1998 (continued).

Date yyyymmddhhmm	Lat	Long	S/D/R	M_w	Mo (Nm)	CD (km)	SD	SR
199802140619	50.855	-130.511	154/51/179	4.4	5.0E15	4	335	2
199802181846	49.543	-129.858	131/80/160	4.6	1.0E16	12	315	5
199803030419	49.168	-118.351	140/89/175	3.4	1.3E14	4	140	12
199804150228	47.960	-113.740	326/80/165	3.4	1.6E14	9	329	12
199806122024	48.892	-129.032	122/83/170	4.5	5.7E15	9	304	6
199806252251	50.085	-130.269	144/81/160	5.4	1.2E17	9	328	3
199806271020	49.630	-127.160	250/66/337	4.0	9.8E14	24	80	7
199807100305	50.548	-130.328	146/83/199	4.0	1.1E15	9	324	2
199807140105	48.728	-129.144	127/74/175	4.7	1.1E16	6	308	6
199807140149	48.773	-129.009	128/59/179	4.0	1.0E15	6	309	6
199807140227	48.773	-129.015	127/75/169	4.4	4.8E15	6	310	6
199807150030	47.821	-129.285	5/57/261	4.7	1.2E16	6	103	8
199807310740	51.362	-130.782	158/71/177	4.6	7.7E15	6	339	2
199807310818	51.341	-130.798	153/79/178	4.0	1.3E15	6	333	2
199808060243	52.126	-131.664	312/37/110	4.4	5.0E15	15	18	1
199808061811	48.789	-129.223	116/70/172	4.6	8.0E15	12	299	6
199808061817	48.885	-129.349	119/68/173	4.8	1.9E16	9	302	6
199808131138	51.710	-116.050	151/68/98	3.6	3.2E14	6	220	12
199808161925	50.009	-130.245	144/61/170	4.2	2.1E15	9	329	3
199808190439	50.386	-130.338	321/79/191	4.9	2.4E16	9	319	2
199808301133	50.969	-130.658	160/50/181	6.2	1.9E18	4	339	2
199809010743	50.901	-130.710	327/84/180	4.2	2.3E15	9	327	2
199809010919	49.143	-127.775	49/78/323	4.4	3.9E15	6	58	7
199809011812	50.732	-130.584	156/63/189	4.6	1.0E16	6	332	2
199809091448	54.160	-133.940	329/51/179	4.4	4.6E15	9	330	1

Table A.2 Regional moment tensor solutions calculated by Oregon State University from 1994–1998 (continued).

Date yyyymmddhhmm	Lat	Long	S/D/R	M_w	Mo (Nm)	CD (km)	SD	SR
197602231514	51.452	-130.656	355/80/-169	6.0	1.1E18	23	353	1
197612202033	48.766	-129.405	127/89/-179	6.7	1.2E19	15	307	6
197806111455	49.156	-129.691	315/89/179	6.3	3.4E18	11	315	5
197807110255	52.647	-132.236	296/28/79	5.4	1.3E17	15	26	1
197902282127	60.500	-141.390	271/13/96	7.5	1.9E20	19	354	10
197903020934	60.370	-140.700	353/44/-36	5.1	5.4E16	15	20	10
197903130951	49.770	-130.177	330/89/179	5.4	1.6E17	10	330	3
197903131200	49.802	-130.027	315/89/179	5.7	3.9E17	10	315	5
197904201249	60.630	-141.200	276/15/121	5.4	1.5E17	15	334	10
197906211703	51.107	-130.973	323/88/171	5.5	2.2E17	15	323	1
197907111228	55.360	-134.940	332/80/178	5.5	2.0E17	15	332	10
197907111407	62.770	-127.720	255/47/44	5.1	4.9E16	15	221	11
198005162234	49.593	-128.191	300/89/179	5.4	1.2E17	15	300	4
198010020342	50.115	-130.394	345/89/179	5.5	2.2E17	15	345	2
198012171622	49.417	-129.888	326/89/179	6.7	1.4E19	10	326	5
198205021536	60.120	-141.180	311/15/121	5.4	1.5E17	15	9	10
198205151848	50.178	-130.438	331/89/179	5.8	5.8E17	10	331	2
198303301806	61.390	-140.750	305/39/109	5.4	1.7E17	13	11	11
198306280325	60.210	-141.440	260/15/85	5.8	7.4E17	17	175	10
198406242133	50.916	-130.914	160/80/-172	5.8	6.1E17	10	339	1
198408120024	50.086	-130.258	142/76/-179	5.3	1.1E17	10	321	3
198408301228	53.920	-133.630	328/71/169	5.9	8.3E17	10	331	1
198510051524	62.530	-123.930	334/38/81	6.6	8.4E18	10	255	11
198512230516	62.330	-123.790	354/45/98	6.7	1.5E19	15	72	11
198512231937	62.240	-123.950	17/39/115	5.1	6.1E16	10	76	11
198601010437	62.600	-124.650	358/34/109	4.9	3.2E16	15	65	11
198603212356	53.640	-121.860	246/35/38	5.5	2.2E17	15	213	12
198703300313	74.400	-133.120	235/24/134	5.2	9.1E16	15	278	11
198711141548	59.290	-135.990	335/25/64	5.0	3.8E16	15	273	10
198711170847	58.870	-143.620	356/85/-147	7.1	6.6E19	15	352	10
198711180618	59.110	-143.740	346/81/-146	5.3	1.3E17	15	340	10
198711180713	58.980	-143.230	184/78/-172	5.0	3.9E16	15	182	10
198711181301	58.850	-143.500	354/87/-178	5.8	5.5E17	15	354	10
198711230718	61.560	-141.090	268/49/72	5.5	2.1E17	15	204	10
198711301923	58.170	-142.040	355/70/-172	7.8	7.3E20	15	352	10
198712011204	58.050	-142.560	356/82/-172	5.8	5.3E17	15	355	10
198712020153	58.820	-143.660	11/82/-177	5.3	1.2E17	15	10	10
198712030920	58.650	-142.770	207/90/180	5.4	1.6E17	15	207	10
198712151511	59.330	-142.360	174/90/180	5.4	1.8E17	15	174	10

Date: year, month, day, hour, minute. Lat, Long: latitude, longitude. S/D/R: strike, dip, rake. M_w: moment magnitude. Mo: seismic moment. CD: centroid depth. SD: slip direction. SR: source region; 1: Queen Charlotte Islands; 2: Revere-Dellwood-Wilson Fault; 3: Explorer Ridge; 4: Interior of Explorer Plate; 5: Western Sovanco Fracture Zone; 6: Eastern Sovanco Fracture Zone; 7: Nootka Fault Zone; 8: Juan de Fuca Ridge; 9: Vancouver Island Region; 10: Gulf of Alaska; 11: Yukon & Northwest Territories; 12: Central Cordillera (B.C., Alberta, Montana) *: indicates regional moment tensor solution also calculated.

Table A.3 Centroid moment tensor solutions calculated by Harvard from 1976–2003.

Date yyyymmddhhmm	Lat	Long	S/D/R	M_w	Mo (Nm)	CD (km)	SD	SR
198803062235	57.370	-143.530	182/75/-168	7.7	4.9E20	15	178	10
198803100416	59.220	-144.920	223/11/51	5.4	1.3E17	15	172	10
198803152356	57.080	-143.410	182/63/175	5.0	4.5E16	15	184	10
198803251936	62.390	-124.290	170/39/101	6.2	2.5E18	16	246	11
198804260147	57.900	-143.200	351/83/-164	5.8	6.5E17	15	349	10
198805221918	62.070	-124.410	165/32/127	5.0	3.4E16	15	213	11
198805261901	48.886	-128.765	116/88/178	5.2	7.6E16	15	296	6
198806061501	59.760	-138.100	344/15/141	5.2	9.2E16	15	22	10
198807191054	50.391	-130.234	167/87/175	5.6	3.0E17	15	347	2
198811270036	50.614	-130.470	319/41/178	5.6	3.2E17	15	321	2
198904080122	57.270	-144.010	177/90/180	5.1	5.3E16	15	177	10
198908061317	60.180	-140.820	228/25/44	5.3	1.2E17	15	186	10
199002030954	50.834	-130.542	338/89/179	5.5	2.0E17	15	338	1
199002161328	49.033	-127.972	208/85/12	5.4	1.4E17	15	27	4
199007111514	59.560	-136.620	349/43/115	5.5	2.5E17	15	46	10
199106240459	58.970	-136.990	335/77/-172	5.6	3.0E17	15	333	10
199107170712	50.692	-130.636	329/80/176	5.5	2.2E17	15	330	2
199201021640	48.602	-129.610	315/89/174	6.0	1.3E18	23	315	6
199201130608	49.060	-129.212	306/75/-157	5.4	1.3E17	15	300	5
199204061354	50.860	-130.520	331/73/-169	6.7	1.2E19	15	328	2
199204061516	50.580	-130.790	166/76/-179	6.0	1.0E18	15	346	2
199204070042	50.663	-131.116	354/89/179	5.2	8.2E16	15	354	1
199204230540	51.341	-131.108	327/52/179	5.6	3.1E17	15	327	1
199208071819	57.590	-142.920	173/86/158	6.8	1.8E19	15	174	10
199307271144	59.560	-144.500	257/58/-72	5.1	4.8E16	15	315	10
199308030720	50.880	-130.680	355/60/-166	6.0	1.2E18	15	347	2
199401030126*	49.410	-126.910	251/41/-26	5.6	2.9E17	21	171	3
199501290311*	47.350	-121.530	147/32/100	5.0	4.5E16	17	241	11
199506212024*	51.070	-130.880	161/90/175	5.4	1.5E17	15	338	11
199610062013*	48.940	-128.030	46/86/8	6.2	2.2E18	15	299	11
199610090712*	49.570	-130.150	240/86/-18	5.7	5.2E17	15	345	2
199610222215	63.560	-144.960	238/46/49	5.7	4.8E17	15	157	1
199702051929*	51.460	-131.170	350/75/-160	5.2	7.4E16	15	395	1
199709200709*	50.700	-130.750	167/63/-171	5.2	7.6E16	15	49	8
199806252251*	50.030	-130.340	335/67/-161	5.3	1.2E17	15	57	8
199808301133*	50.980	-130.580	348/81/-168	6.1	1.6E18	15	239	7
199905270809*	58.490	-137.370	310/54/146	5.6	3.2E17	15	276	8
199907021145*	49.130	-129.380	315/81/176	5.9	7.4E17	15	61	8
199907030143*	47.100	-123.430	199/34/-61	5.8	6.3E17	45	374	11
200001061042*	58.270	-136.800	343/65/-166	6.1	1.6E18	15	98	10
200004300829*	50.960	-130.780	345/80/-162	5.2	8.4E16	15	142	3
200004301013*	50.980	-130.610	347/77/-172	5.5	2.2E17	15	204	12
200005022359*	59.700	-139.480	351/51/138	5.3	1.2E17	15	345	11
200005150558*	49.850	-130.260	312/65/-175	5.2	8.3E16	15	85	9
200005150711*	50.110	-130.280	337/75/-173	5.4	1.8E17	15	331	1
200009301905*	58.220	-139.340	173/19/164	5.2	7.9E16	15	127	11
200101110004*	48.880	-129.300	306/88/-177	6.0	1.3E18	24	302	4

Table A.3 Centroid moment tensor solutions calculated by Harvard from 1976–2003 (continued).

Date yyyymmddhhmm	Lat	Long	S/D/R	M_w	Mo (Nm)	CD (km)	SD	SR
200101200014*	50.570	-130.650	347/85/-149	5.4	1.4E17	15	113	4
200101230939*	49.410	-129.070	113/85/180	5.6	2.7E17	15	344	2
200101231443*	49.240	-128.900	302/85/-179	5.4	1.5E17	15	306	6
200102050349*	64.430	-131.150	117/64/159	5.3	1.2E17	15	188	10
200102172011*	54.020	-133.660	334/56/-175	6.2	2.2E18	15	335	3
200102281854*	47.140	-122.530	2/73/-88	6.8	1.8E19	47	310	3
200103090710*	64.470	-131.490	329/46/158	5.0	4.7E16	15	381	10
200104140220*	56.380	-119.360	272/44/74	5.2	9.1E16	15	345	2
200105020205*	49.970	-130.520	144/85/-156	5.3	1.0E16	15	342	2
200105140722*	54.590	-142.740	90/73/-27	5.2	7.2E16	15	337	10
200106261405*	61.470	-140.310	323/45/120	5.6	3.7E17	15	255	9
200109122224*	49.650	-128.210	141/44/-97	5.2	8.6E16	15	316	4
200109130957*	48.830	-128.460	351/30/-103	5.1	5.9E16	15	332	10
200109140445*	48.820	-128.590	239/86/-6	5.9	9.7E17	15	346	2
200109151050*	48.620	-128.260	61/82/28	5.5	2.2E17	15	327	3
200109162320*	48.490	-128.540	49/89/2	5.6	3.1E17	15	163	2
200110120502*	52.640	-132.180	309/26/94	6.0	1.4E18	15	345	1
200209051129*	54.260	-134.160	157/90/-180	5.1	5.5E16	15	199	10
200211030149*	51.630	-130.890	356/66/-154	5.5	2.5E17	15	241	7
200211032213	63.230	-144.890	296/71/171	7.9	7.5E20	15	45	7
200211080404	62.220	-141.820	294/64/116	5.0	4.1E16	15	161	1
200211082029	62.990	-143.490	242/88/27	5.1	6.4E16	15	225	9
200212131551*	50.300	-130.330	171/88/-180	5.4	1.4E17	15	271	9

Table A.3 Centroid moment tensor solutions calculated by Harvard from 1976–2003 (continued).

Appendix B

Waveform Fits

This appendix shows examples of waveform fits for several regional moment tensor solutions of varying magnitude and location. There are four events from the region off Canada's west coast, three from the Yukon/Northwest Territories, and one from the Puget Sound area. In each case waveform fits for all of the components used are shown, an misfit versus depth plot, and the final mechanism with the distribution of stations plotted.

B.1 10 April 2001, 09:36 UT, Revere-Dellwood-Wilson Fault

This event from along the Revere-Dellwood-Wilson fault is an example of a good quality regional moment tensor solution. This was a $M_L = 4.9$, $M_w = 5.3$ earthquake which is likely just under the magnitude threshold for calculating a teleseismic moment tensor solution. This event was filtered in the 0.02–0.05 s passband and used 26 components from 11 stations to obtains the regional moment tensor solution. There is a very good match between the observed and synthetic waveforms and the moment and focal mechanism stay stable which suggests they are well resolved. At the best-fit depth the moment was 8.94×10^{16} Nm ($M_w = 5.3$) and 66% double-couple.

B.2 20 May 2001, 10:04 UT, Revere-Dellwood-Wilson Fault

This event from the Revere-Dellwood-Wilson fault is the type of earthquake that regional moment tensor solutions are ideally suited for. This was a $M_L = 4.2$, $M_w = 4.6$ event that is too small for teleseismic methods but still generates sufficient low frequency energy to calculate a good quality regional moment tensor solution. This event was filtered in the 0.02–0.05 s passband and used 19 components from eight stations to obtain the regional

Figure B.1 Waveform fits for the 10 April 2001 earthquake. In Figures B.1–B.11 the observed and synthetic waveform fits are shown for each station. Beneath each station code is the azimuth and distance to each station from the epicentre. At the bottom right is a plot of the rms error versus depth and the best-fit focal mechanism with the azimuthal distribution of the stations plotted on the edge. The minimum and maximum peak-to-peak amplitude is indicated for each example. Note that most of the examples have more than one time scale for the waveforms.

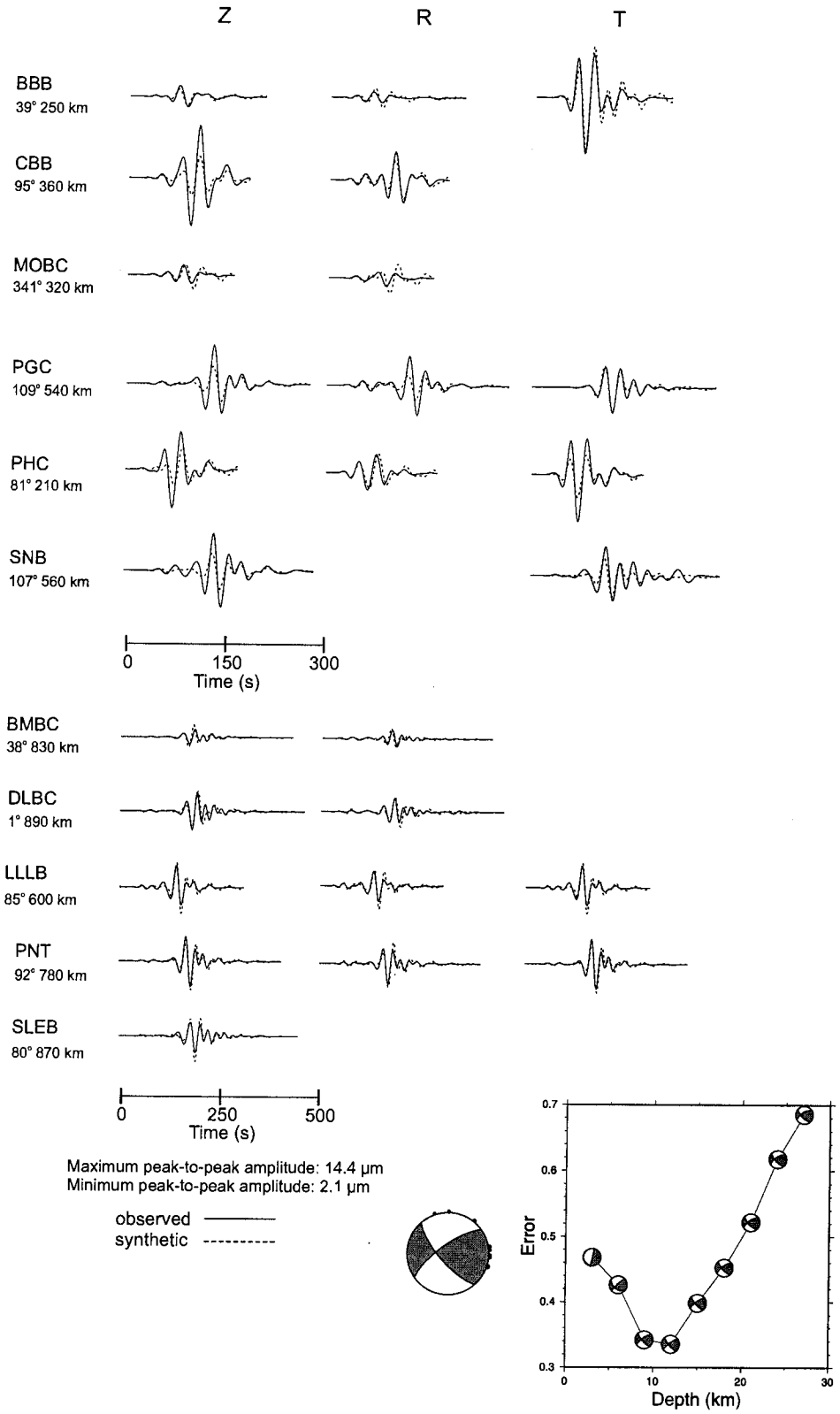
Z
R
T
BBB
39° 250 km
CBB
95° 360 km
MOBC
341° 320 km
PGC
109° 540 km
PHC
81° 210 km
SNB
107° 560 km
0
150
300
Time (s)
BMBC
38° 830 km
DLBC
1° 890 km
LLLB
85° 600 km
PNT
92° 780 km
SLEB
80° 870 km
0
250
500
Time (s)
Maximum peak-to-peak amplitude: 14.4 μm
Minimum peak-to-peak amplitude: 2.1 μm
observed
synthetic
Error
Depth (km)

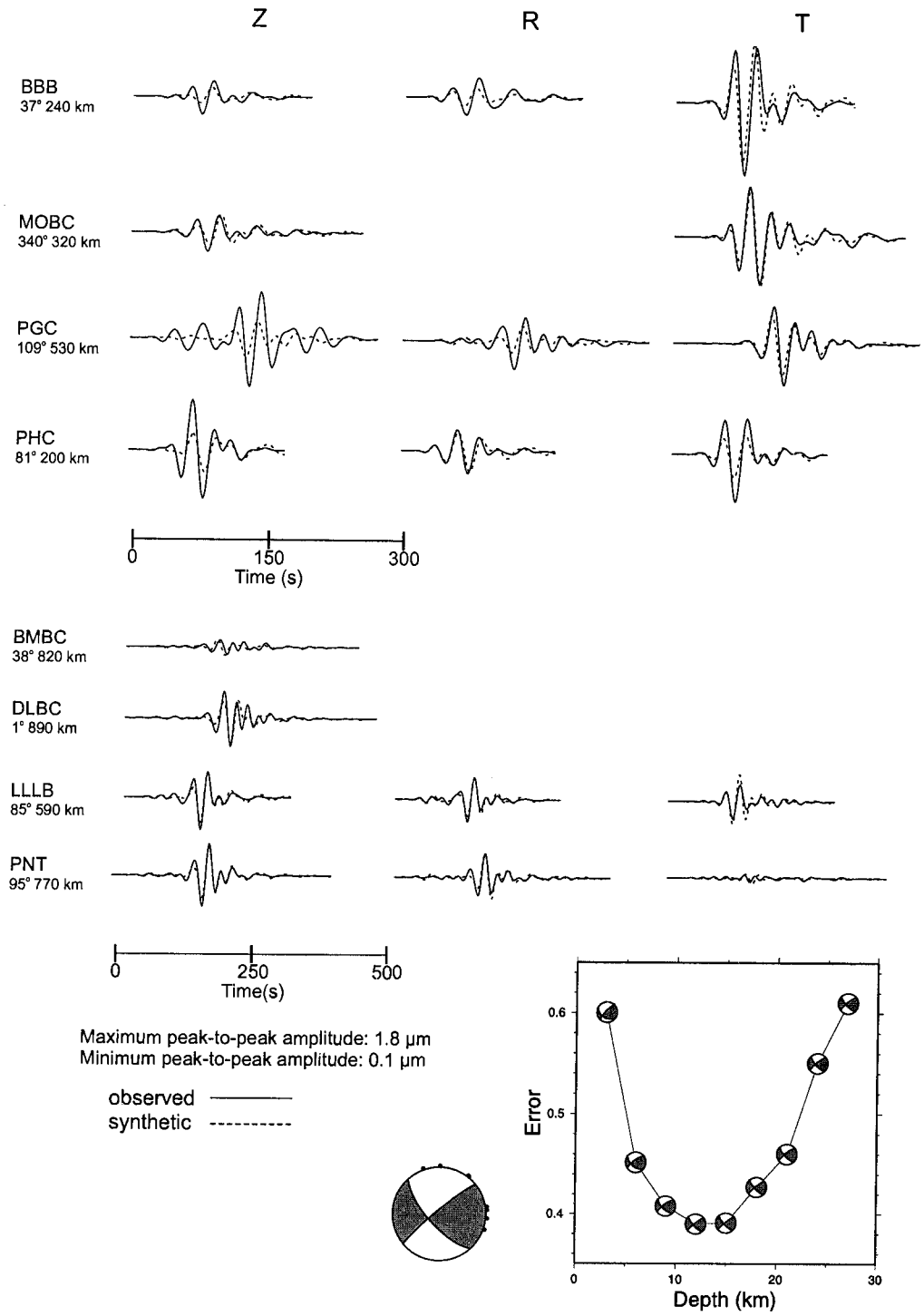

Figure B.2 Waveform fits for the 20 May 2001 earthquake.

moment tensor solution. The match between the observed and synthetic waveforms is still quite good and the moment and focal mechanism are fairly stable over the depth range. At the best-fit depth the moment was 9.97×10^{15} Nm ($M_w = 4.6$) and 98% double-couple.

B.3 14 July 1998, 01:49 UT, Sovanco Fracture Zone

This $M_L = 3.7$,$M_w = 4.3$ event from the Sovanco Fracture Zone is an example of about the lower limit for calculating a regional moment tensor solution. This event was filtered with a 0.03–0.075 s passband and used 12 components from six stations to calculate the regional moment tensor solution. The match between the observed and synthetic waveforms is not great and the focal mechanism varies substantially over the depth range. However, the best-fit depth is at 9 km which is around the expected depth for earthquakes in this region, and the focal mechanism at this depth is consistent with the tectonic setting and with other focal mechanisms from the same region. At the best-fit depth the moment was 2.83×10^{15} Nm ($M_w = 4.3$) and 90% double-couple.

B.4 14 September 2001, 04:45 UT, Nootka Fault Zone

This event from along the Nootka Fault Zone was large enough to have moment tensor solutions calculated by Harvard and the USGS (see Figure C.10 for comparison). This was the largest event ($M_L = 5.0$, $M_w = 6.0$) from a large swarm along the Juan de Fuca Ridge/Nootka Fault Zone during September, 2001. This event was filtered with a 0.01–0.05 s passband and used 30 components from 13 stations to calculate the solution. The match between the observed and synthetic waveforms is very good and the moment and focal mechanism remain stable over the depth range. At the best-fit depth the moment was 1.23×10^{18} Nm ($M_w = 6.0$) and 80% double-couple. The moment and focal mechanism was consistent with the Harvard and USGS solutions (Figure B.11).

B.5 9 March 2001, 07:10 UT, Mackenzie Mountains, NWT

This event was one of the largest earthquakes to occur in the Mackenzie Mountains in several years ($M_L = 5.2$, $M_w = 5.2$) and was large enough for Harvard to calculate a moment tensor solution (see Figure C.10 for comparison). It is a example of a regional moment tensor solution calculated in a continental crust environment instead of a oceanic crust environment. This event was filtered with a 0.02–0.05 s passband and used 19 components from seven stations to obtain the solution. The seven stations used for this event are typical and are the only stations within $\sim$ 1000 km for earthquakes in the Yukon and

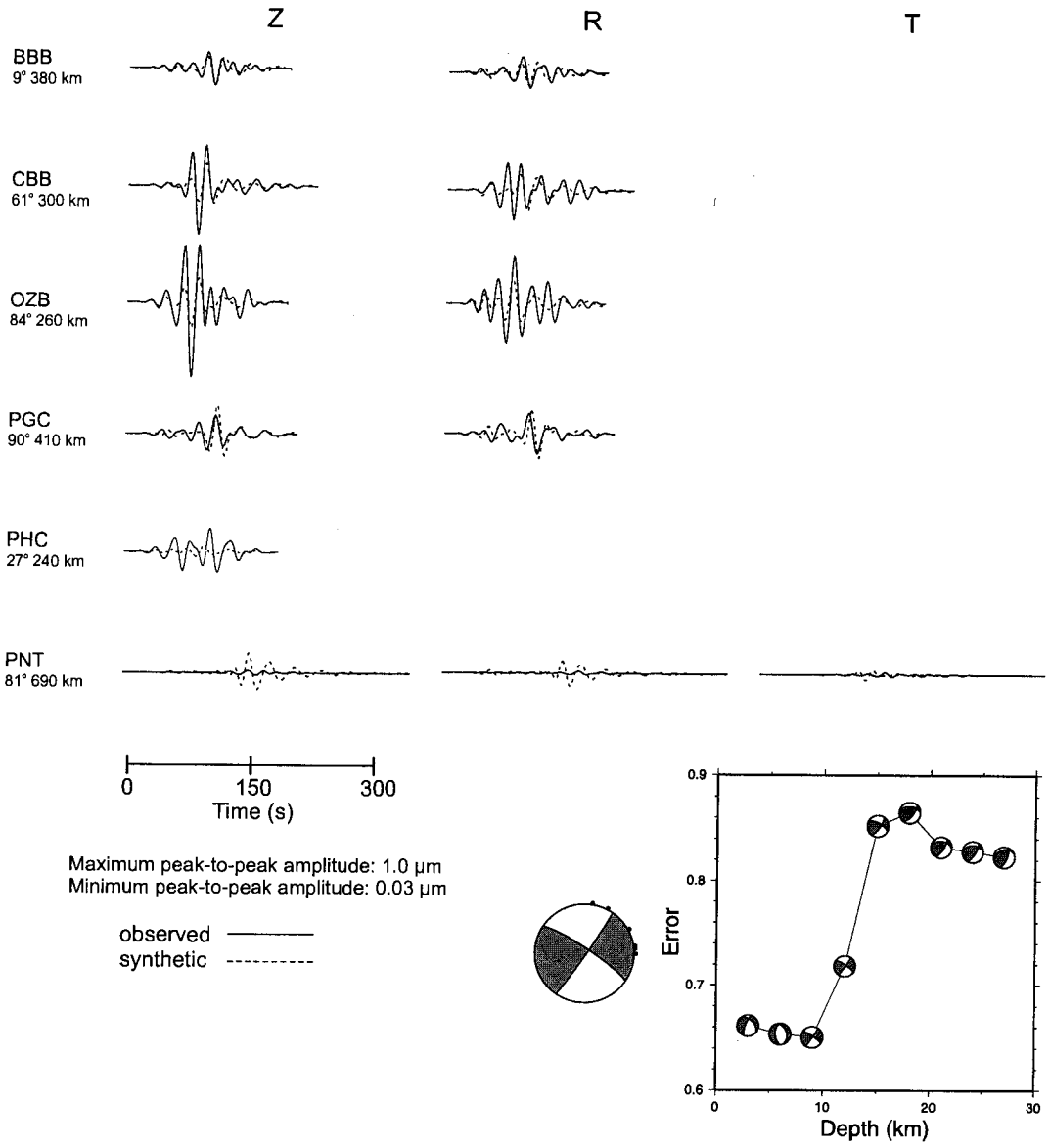

Figure B.3 Waveform fits for the 14 July 1998 earthquake.

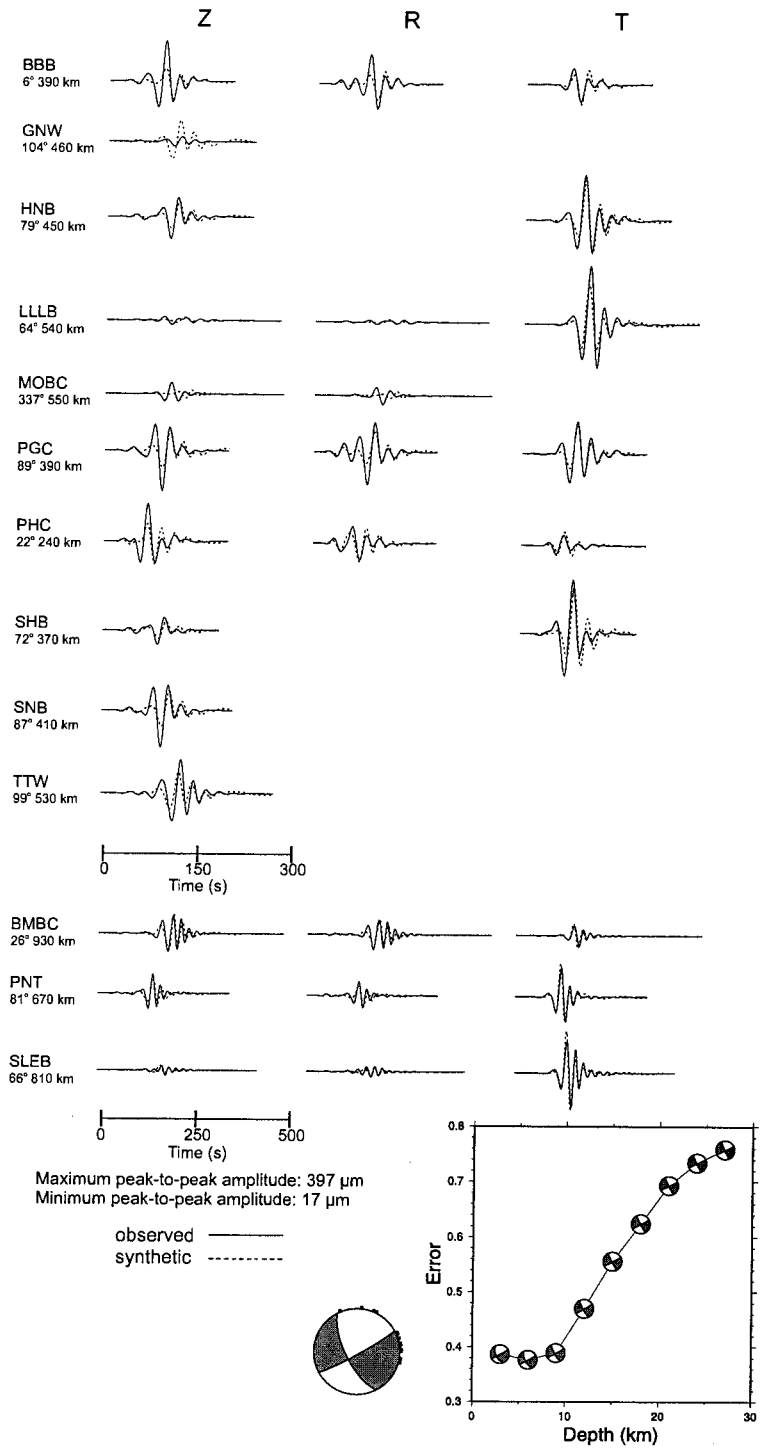

Figure B.4 Waveform fits for the 14 September 2001 earthquake.

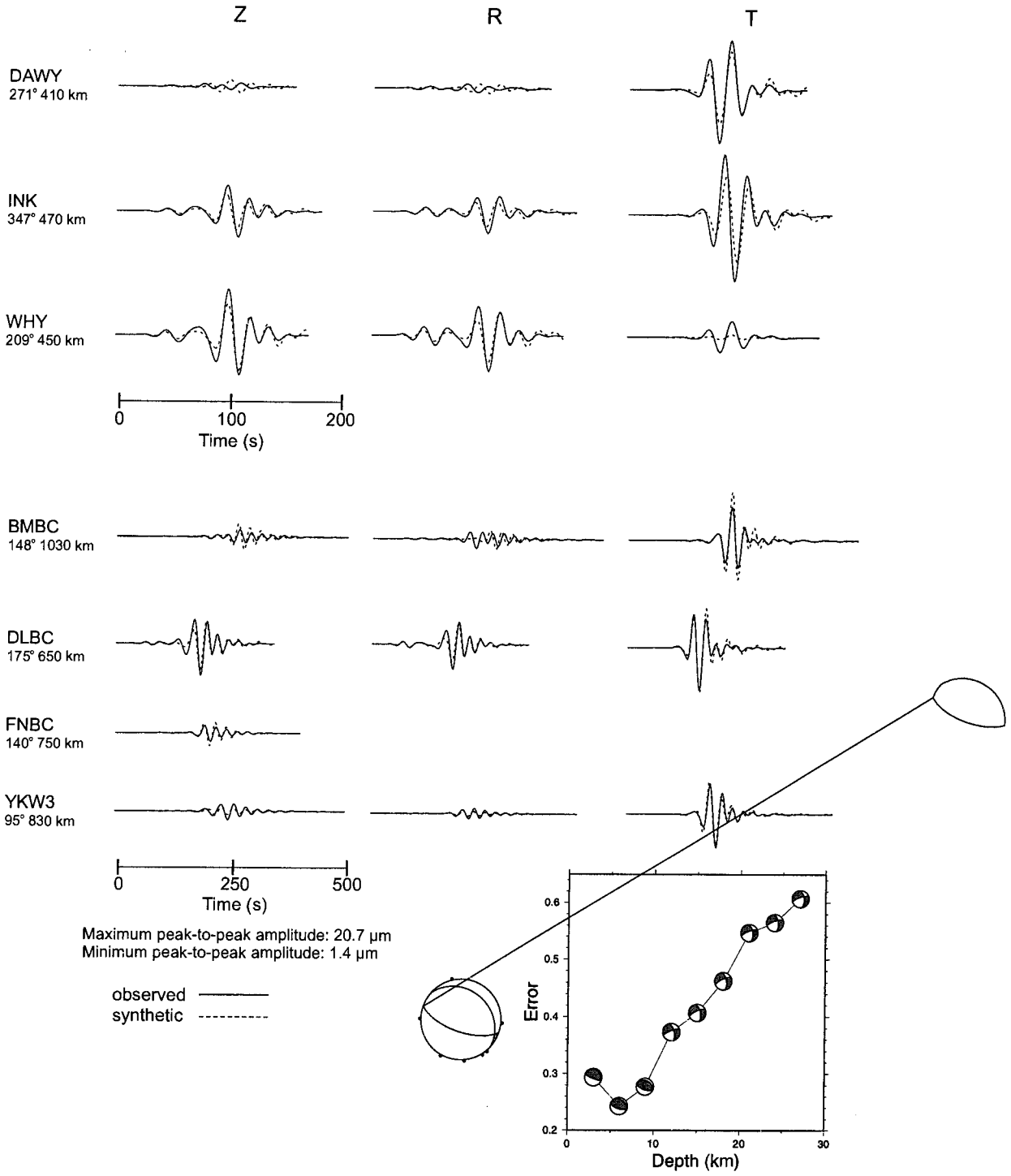

Figure B.5 Waveform fits for the 9 March 2001 earthquake at 07:10 UT.

Northwest Territories. The match between the observed and synthetic waveforms is very good and the focal mechanism stays fairly consistent over the depth range. The best-fit depth was shallow (6 km) which is typical for earthquakes in this region. At the best-fit depth the moment was 8.11×10^{16} ($M_w = 5.2$) and 57% double-couple. The moment and focal mechanism are consistent with the Harvard solution (Figure C.10).

B.6 9 March 2001, 19:02 UT, Mackenzie Mountains, NWT

This event ($M_L = 4.6$, $M_w = 4.3$) was an aftershock to the $M_w = 5.2$ event at 07:10 UT. The waveforms were filtered with a 0.02–0.05 s passband and used 16 components from seven stations. The match between the observed and synthetic waveforms is still quite good but the focal mechanism changes substantially at depths greater than 9 km. The best-fit depth was still shallow (3 km) and the moment was 3.30×10^{15} Nm and 92% double-couple.

B.7 29 March 2001, 20:26 UT, Mackenzie Mountains, NWT

This is an example of about the lower threshold ($M_L = 4.1$, $M_w = 3.8$) for calculating regional moment tensor solutions in the Yukon/Northwest Territories region. The waveforms were filtered with a 0.03–0.075 s passband and used 12 components from six stations. The waveforms were quite noisy, however the best-fit depth is at 6 km which is around the expected depth, and the focal mechanism is very similar to other mechanisms from that region. The moment was 5.08×10^{14} and the solution was 92% double-couple.

B.8 10 June 2001, 13:19 UT, Puget Sound, Washington

This is an example of an event within the subducting Juan de Fuca plate beneath the Olympic Peninsula, Washington. This event was a $M_L = 4.2$, $M_w = 5.0$ with a similar location and mechanism to the February 28, 2001 Nisqually earthquake. The waveforms were filtered with a 0.02–0.05 s passband and used 23 components from 10 stations to calculate the solution. The waveform fits were quite good and the focal mechanism remained stable over a range of depths. At depths around the best-fitting depth of 39 km the error was fairly constant which suggests that the depth is not well constrained. At the best-fit depth the moment was 3.77×10^{16} ($M_w = 5.0$) and 78% double-couple.

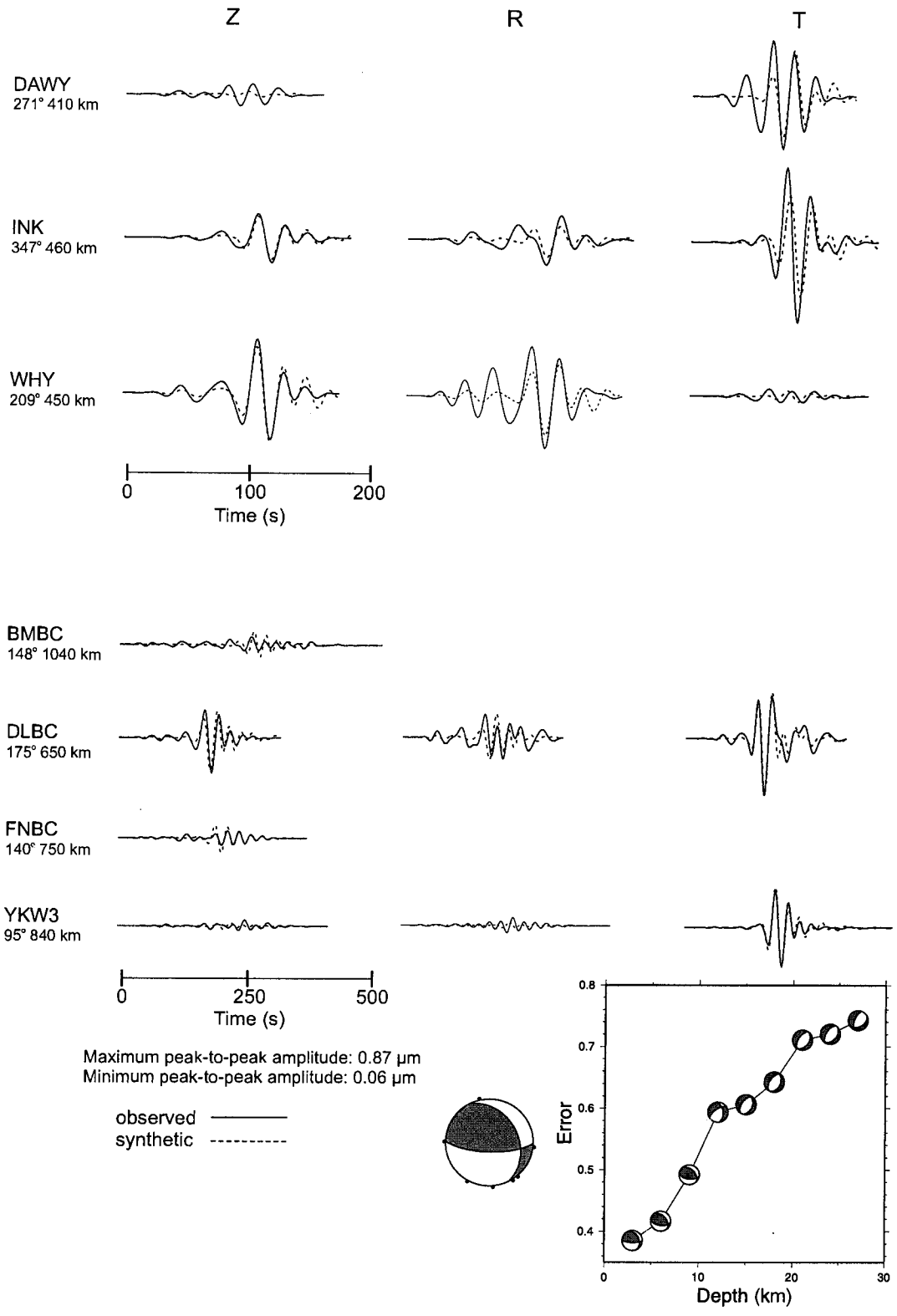

Figure B.6 Waveform fits for the 9 March 2001 earthquake at 19:02 UT.

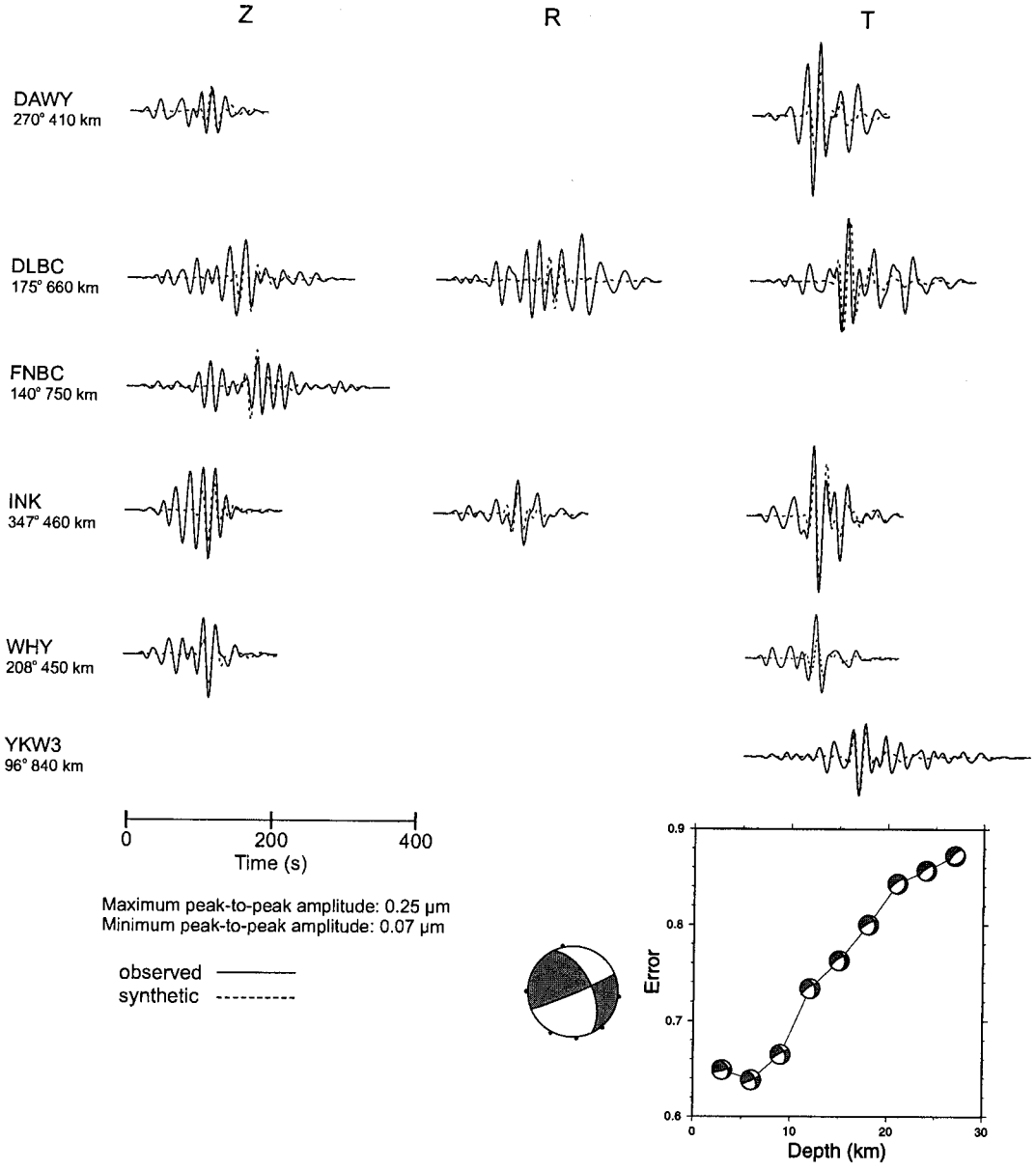

Figure B.7 Waveform fits for the 29 March 2001 earthquake.

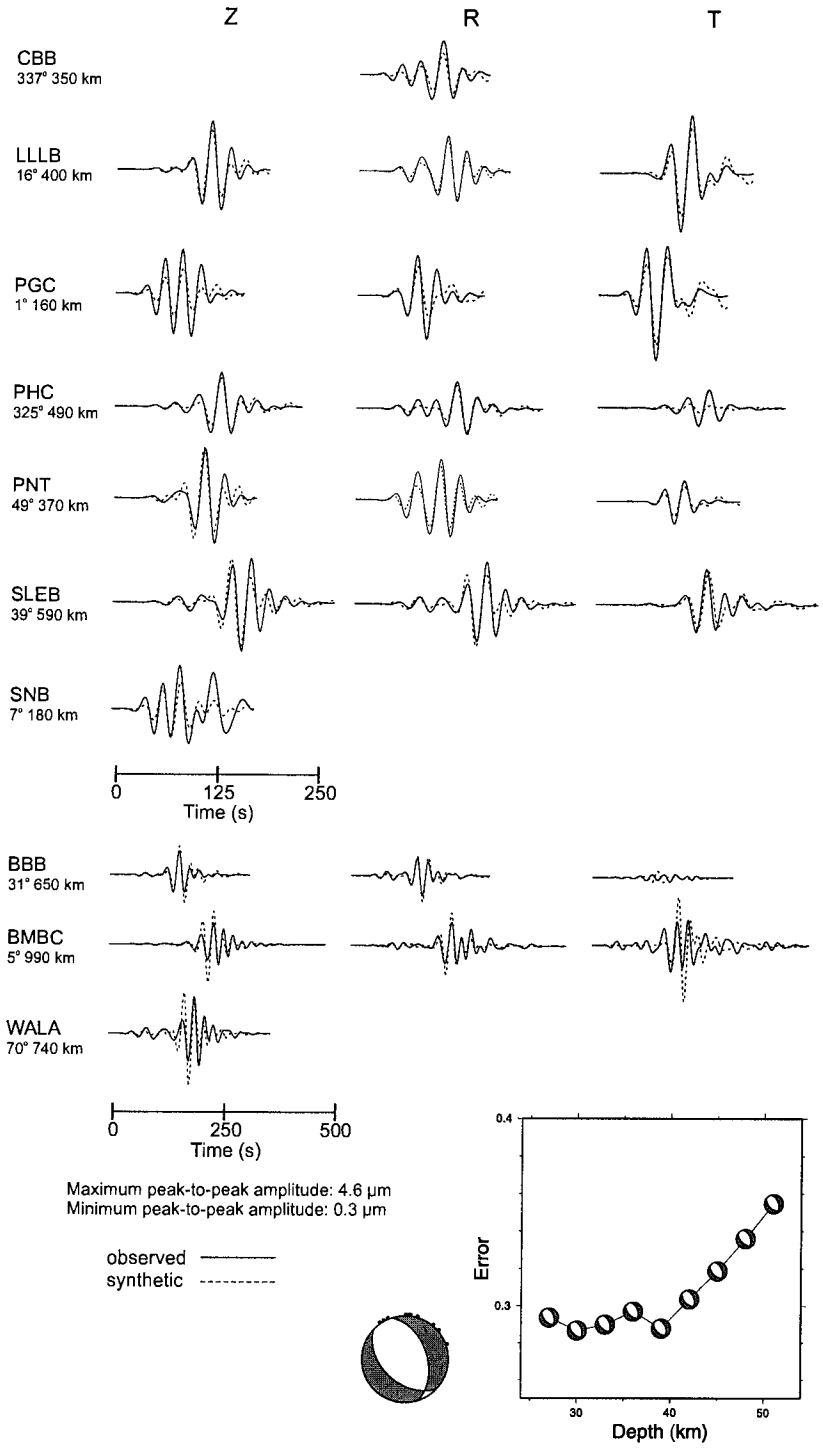

Figure B.8 Waveform fits for the 10 June 2001 earthquake.

Appendix C

Moment Tensor Solution Comparisons

Section C.1 compares regional moment tensor solutions calculated using Green's functions calculated at 10 km intervals and Green's functions calculated to the nearest kilometre. Section C.2 investigates the ability of the moment tensor method to calculate a solution using only one or two stations. Section C.3 looks at the potential of using the moment tensor method to calculate solutions of older events before digital broadband seismic stations were available. Section C.4 examines the accuracy of the regional moment tensor derived depths using synthetic seismograms calculated from source mechanisms at known depths. Section C.5 is a comparison between regional moment tensor solutions and USGS and Harvard moment tensor solutions for three large events, and regional moment tensor solutions calculated in this research and by OSU.

C.1 Green's Function Comparison

The Green's functions used to calculate the regional moment tensor solutions presented in this research are calculated at 10 km intervals as described in section 3.4. As mentioned in section 3.4 this means that the Green's functions used can be off by up to $\pm$ 5 km from the correct Green's function which is roughly equal to the error in earthquake locations in western Canada. Here the regional moment tensor solution for the 20 May 2001 earthquake from section B.2 is calculated using Green's functions calculated to the nearest kilometre (Figure C.1) and compared with the result from section B.2 (Table C.1). The regional moment tensor solution calculated using Green's functions calculated every 10 km will be

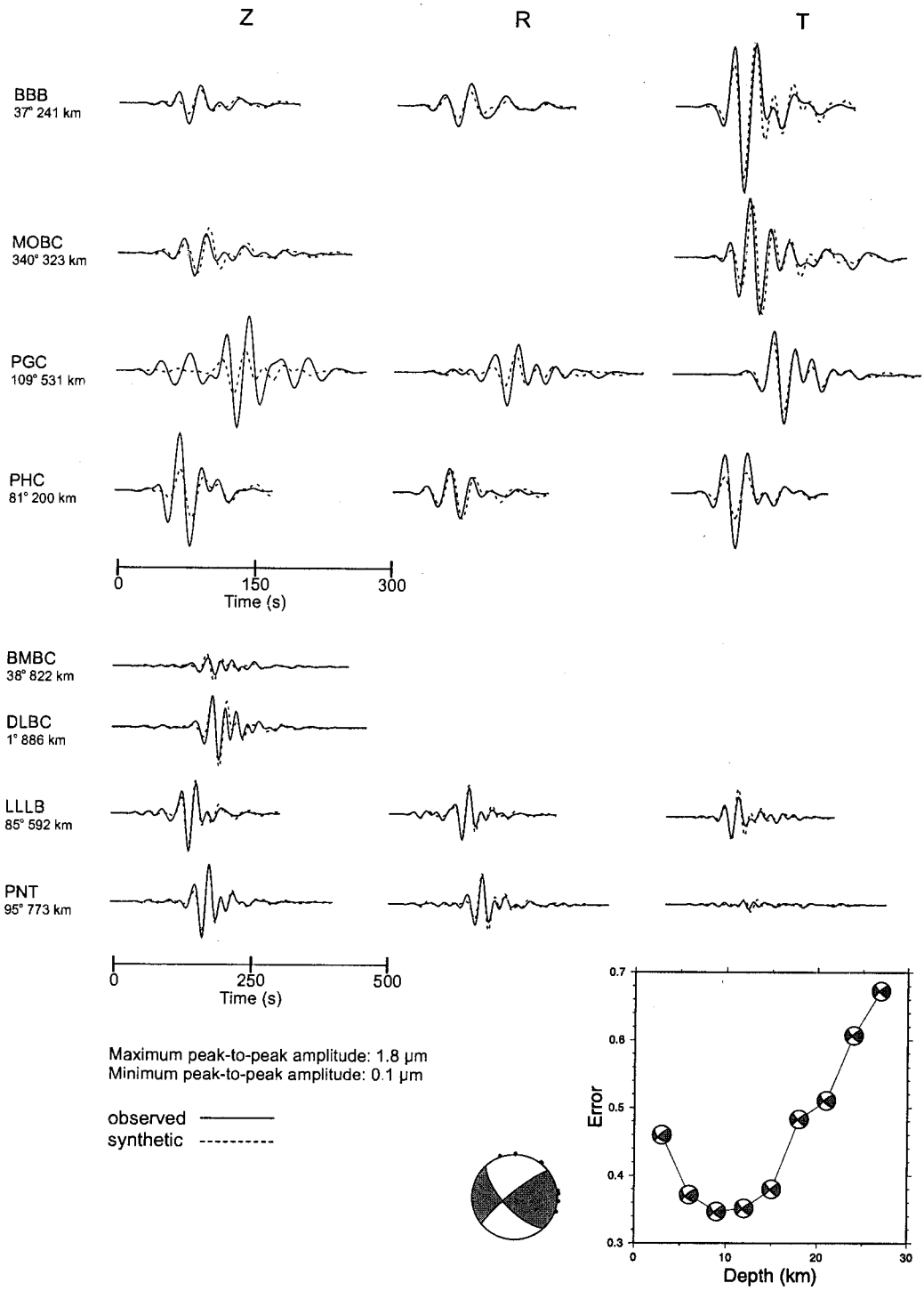

Figure C.1 Regional moment tensor solution for the 20 May 2001 earthquake calculated using Green's functions calculated to the nearest kilometre.

referred to as method 1, and the solution calculated using Green's functions calculated to the nearest kilometre will be referred to as method 2.

Method	M_w	M_o ($\times 10^{15}$ Nm	S/D/R	Depth (km)	%DC
1	4.6	10.0	138/70/173	12	98
2	4.6	9.6	137/68/170	9	88

Method 1 - Green's functions calculated every 10 km; Method 2 - Green's functions calculated to the nearest kilometre.

Table C.1 Regional moment tensor solutions from Green's functions calculated every 10 km and to the nearest kilometre.

The regional moment tensor solutions have almost identical focal mechanisms (strike, dip, rake) and moments. The depth for the solution calculated using method 1 is deeper, 12 km versus 9 km, but the misfit at a depth of 9 km for method 1 is almost the same as for a 12 km depth. The regional moment tensor solution calculated using method 1 is almost pure double-couple (98%) compared with 88% for the method 2 regional moment tensor solution. In this example using Green's functions calculated every 10 km is adequate for calculating a regional moment tensor solution.

C.2 Moment Tensor Solutions Using One Or Two Stations

The displacement field from a given double-couple is unique. Therefore, if the entire displacement field at a given point can be modeled, it should be possible to determine the source mechanism. In other words, three-component data from a single station should be sufficient to determine the source parameters of an earthquake. However, in practice errors in the Green's functions due to limitations in the Earth models used to calculate them, simplification of the source-time function, bandwidth limitations in the seismometers, and overall noise make it difficult to accurately model the entire waveform. Previous studies have had success in recovering source parameters using as few as one station for the inversion (e.g. Delouis and Legrand, 1999; Dreger and Helmberger, 1993). Here the 20 May 2001 M_w = 4.6 earthquake (section B.2) is used as an example of calculating a regional moment tensor using only one or two stations.

In Figure C.2 the regional moment tensor solution is calculated using stations BBB and LLLB. The observed and synthetic waveform fits are very good and the minimum

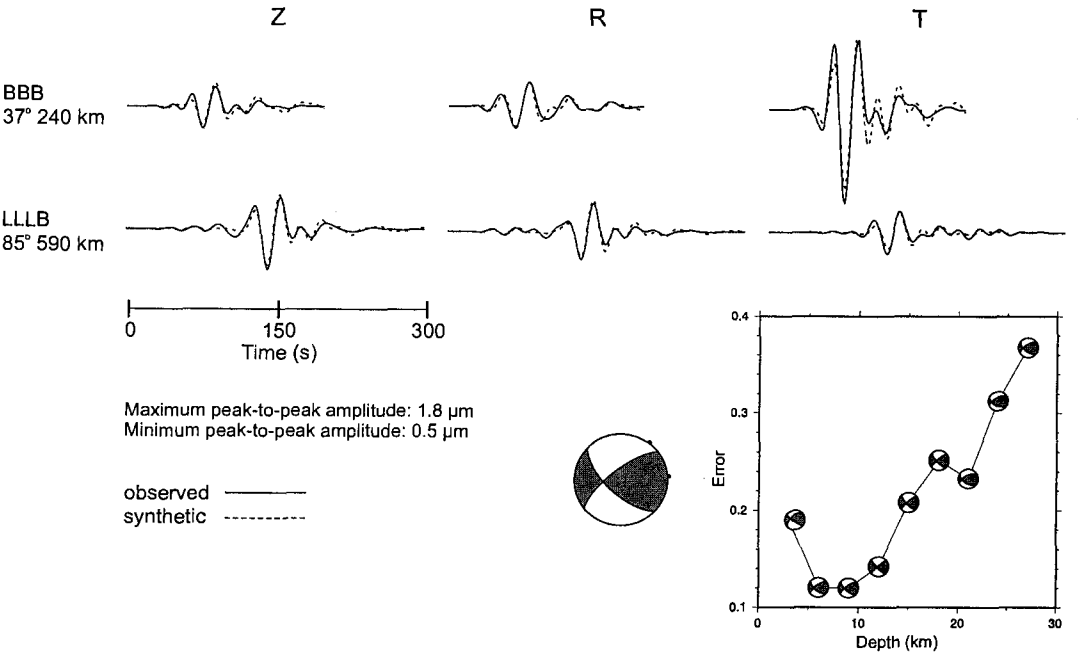

# Stations	M_o (x 10^{15} Nm)	M_w	% DC	Depth	S/D/R
8	9.97	4.6	98	12	138/70/174
2	10.6	4.7	53	9	133/65/160

Figure C.2 Regional moment tensor solution calculated using two stations. (*Top*) observed and synthetic waveform fits; (*centre*) error vs. depth plot and the best-fit focal mechanism with the station distribution; (*bottom*) comparison of key source parameters between the regional moment tensor solutions calculated using eight stations and two stations.

error is at a depth of around 6–9 km. The best-fitting focal mechanism is shown with the station distribution. A comparison of key parameters between the regional moment tensor solutions calculated using eight stations and two stations (Figure C.2 *bottom*) shows very good agreement between the moment and the focal mechanism for the two solutions. In this case two stations are sufficient to recover the source parameters.

In Figure C.3 the regional moment tensor solution is calculated using only station BBB (*top*) and only station LLLB (*bottom*). In both cases the depth minimum is at more than 20 km which is unrealistic for an earthquake along the Revere-Dellwood-Wilson fault, and in the case of the solution calculated using only LLLB the focal mechanism at those depths is not what would be expected. The difference in the minimum and maximum RMS error is quite small which suggests that the depth is not well resolved. Using the same depth as in the two station case (9 km) as a realistic depth gives the two chosen focal mechanisms

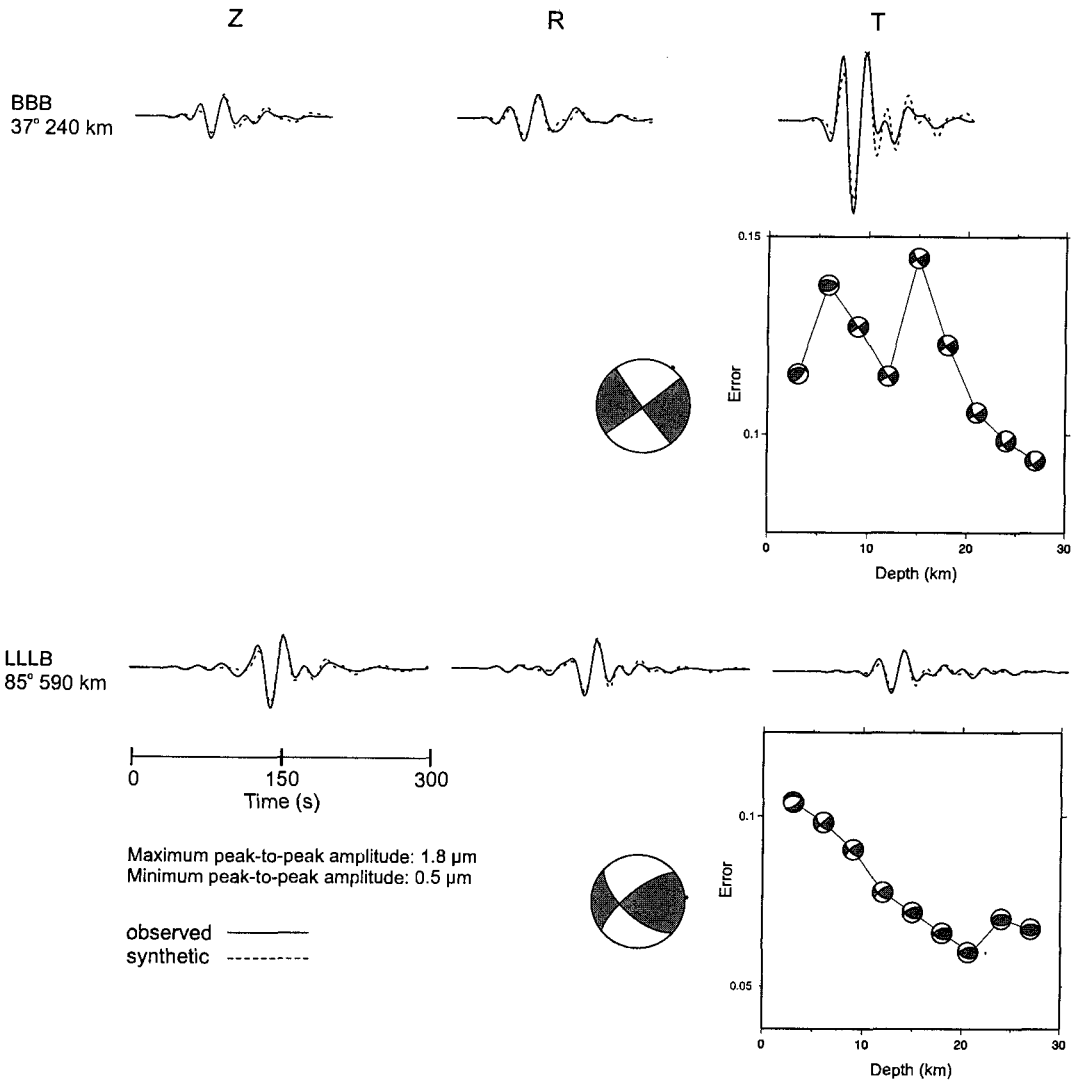

# Stations	M_o (x 10^{15} Nm)	M_w	% DC	Depth	S/D/R
8	9.97	4.6	98	12	138/70/174
1 - BBB	10.4	4.6	91	9	143/87/-178
1 - LLLB	10.8	4.7	65	9	132/63/160

Figure C.3 Regional moment tensor solution calculated using one station. (*Top*) observed and synthetic waveform fits, error vs. depth plot, and focal mechanism at 9 km depth for BBB. (*Centre*) observed and synthetic waveform fits, error vs. depth plot, and focal mechanism at 9 km depth for LLLB. (*Bottom*) comparison of key source parameters between the regional moment tensor solutions calculated using eight stations and one station.

to the left of the error vs. depth plots. At the very bottom of Figure C.3 is a comparison of key parameters for each of the single station examples and the regional moment tensor solutions calculated using eight stations. The moments and focal mechanisms compare very well at a depth of 9 km. In this case a single station is not able to resolve the centroid depth but at a realistic depth of 9 km the source parameters agree very well with the regional moment tensor solution calculated using eight stations.

C.3 Moment Tensor Solutions For Older Events

Prior to the early 1990's there were relatively few three-component long period seismometers in western Canada and no three-component broadband seismometers. Figure C.4 shows the three-component long period stations that were operational prior to the early 1990's and the years when they were installed. Station SES (Suffield) was replaced by WALA (Waterton Park) in the early 1990's and so the records from WALA were used in the following examples. YKC (Yellowknife) was replaced by the current Yellowknife array in the early 1990's but the station location is almost identical. MBC (Mould Bay) ceased operation in 1997 and was not replaced. FSJ (Fort St. John) had its long period seismometer removed in 1979 and has been only a short period station since.

This section investigates the feasibility of calculating regional moment tensor solutions for older events where the records could be digitized from the existing paper records from long period seismographs. Several regional moment tensor solutions from different regions in western Canada were selected and the solutions re-calculated using only data from the stations shown in Figure C.4. The earthquakes needed to be large enough that good signals could be recorded more than 1000 km away but not so large that the waveforms would be off scale on paper records. Earthquakes with M_w = 4.5–5.5 fit this criteria and are also the types of earthquakes that work well for regional moment tensor solutions. Wherever possible earthquakes with magnitudes close to M_w = 4.5 were chosen as this would be about the lowest threshold for calculating solutions for older events.

C.3.1 10 November 2001, 20:20 UT, Sovanco Fracture Zone

This event is from the Sovanco Fracture Zone and the original regional moment tensor solution was calculated using eight stations while this solution used five (Figure C.5). The furthest stations were EDM and WALA which were 1100–1200 km away. Even at that distance the waveform fits are still quite good. It should be noted that since EDM is normally not used for calculating solutions for offshore events there has never been a source-receiver Earth model determined for it. Here, and in all subsequent solutions where

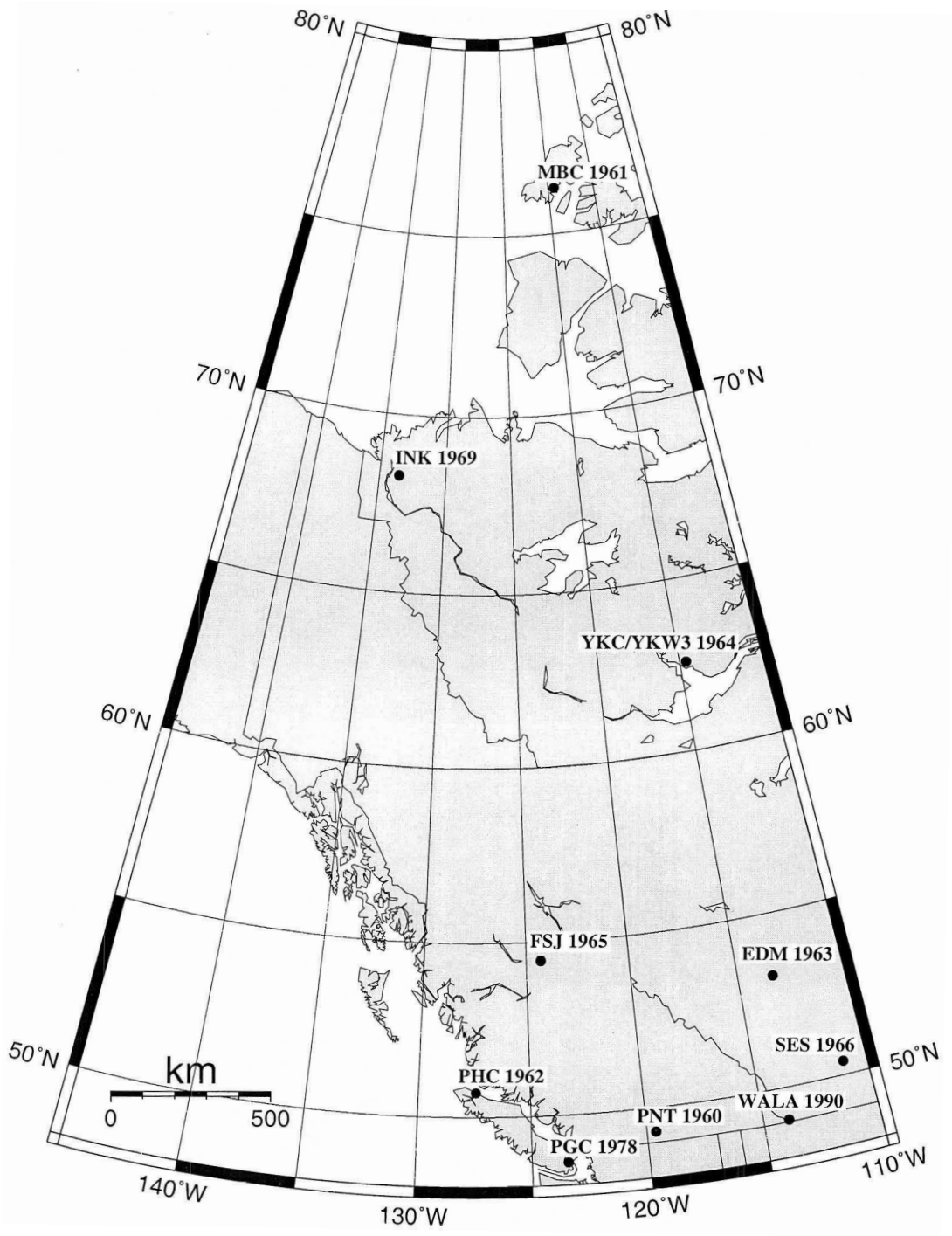

Figure C.4 Three-component long period seismometers in the Canadian seismograph network prior to the early 1990's. Years are when the stations became operational. WALA is a broadband station but is used in place of SES in the examples.

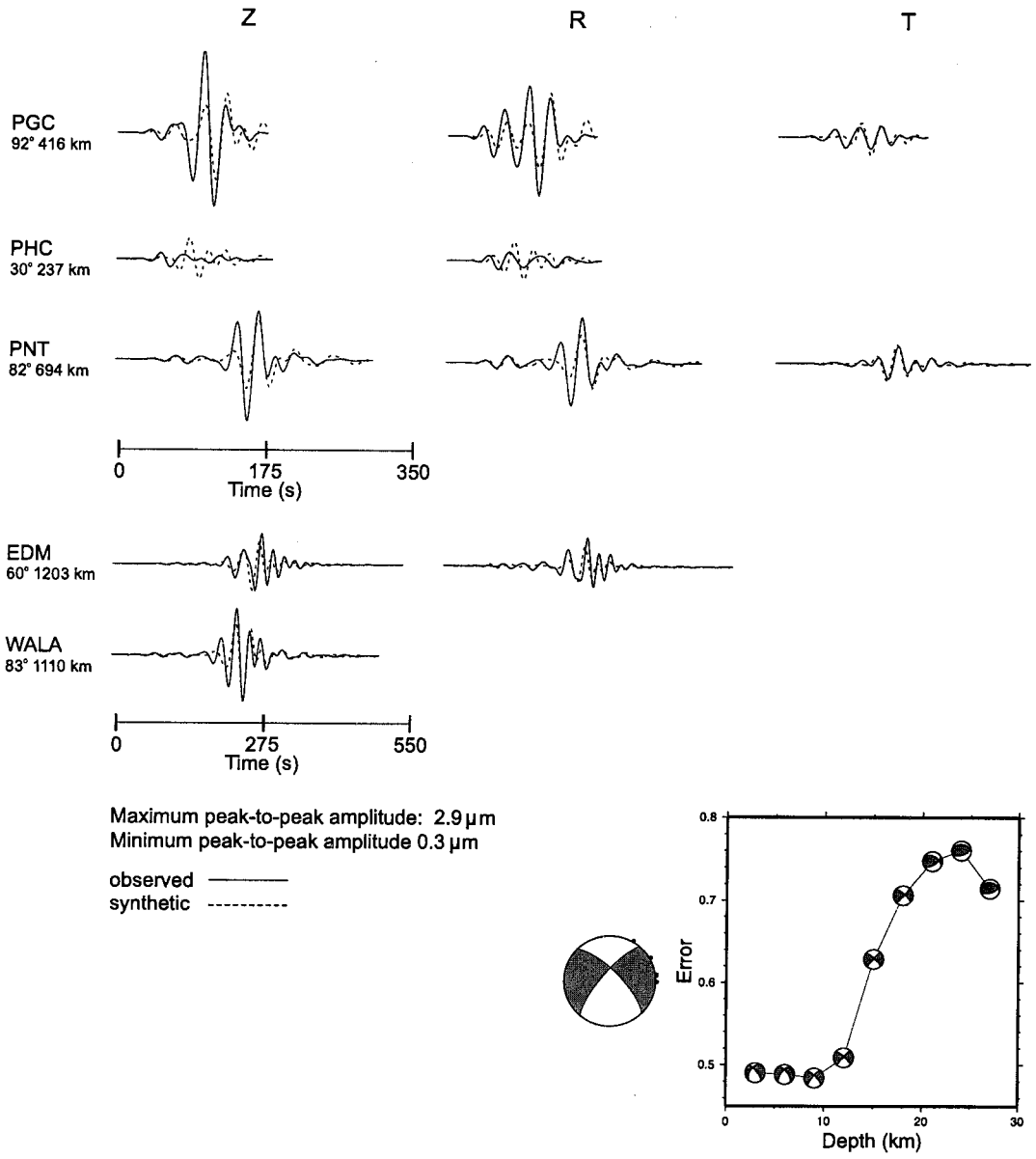

# Stations	M_o (x 10^{15} Nm)	M_w	% DC	Depth	S/D/R
8	13.8	4.7	68	9	128/74/165
5	15.0	4.7	90	9	315/72/-164

Figure C.5 Regional moment tensor solution for the 10 November 2001 event calculated using only stations available prior to the early 1990's. (*Top*) observed and synthetic waveform fits; (*centre*) error vs. depth plot and the best-fit focal mechanism with the station distribution; (*bottom*) comparison of key source parameters between the regional moment tensor solutions calculated using eight stations and five stations.

EDM is used, the Green's functions used are the same as those for PNT and WALA. This may lead to some synthetic/observed waveform misfit problems if the EDM source-receiver travel path is significantly different than the WALA or PNT source-receiver travel path. The depth is not well constrained except to say that it is less than 12 km. At the best-fit depth of 9 km the two solutions are very similar in M_o, depth, and focal mechanism.

C.3.2 4 April 2002, 04:29 UT, Revere-Dellwood-Wilson Fault

This event is from the Revere-Dellwood-Wilson fault and the original regional moment tensor solution used eight stations while this solution used five (Figure C.6). The furthest stations were EDM and WALA which were both $\sim$ 1200 km away. The waveform fits are quite good even for the distant stations. The depth is not well constrained but appears to be about 12 km which is similar to the solution calculated using eight stations. At the best-fit depth the M_o and focal mechanism for the two solutions are consistent with one another.

C.3.3 5 September 2002, 11:29 UT, Queen Charlotte Islands

This event is from the Queen Charlotte Islands and the original regional moment tensor solution used 11 stations while this solution used five (Figure C.7). The furthest stations were EDM and WALA which were 1300–1500 km away. The depth is not well constrained but except to say that it is less than 15 km. The depth, M_o, and focal mechanism are all consistent between the two solutions.

C.3.4 14 February 2002, 04:33 UT, Mackenzie Mountains, NWT

This event is from the Mackenzie Mountains region and the original regional moment tensor solution used seven stations while this solution used three (Figure C.8). The furthest station was EDM which was over 1500 km away. The depth is actually well constrained in this solution at 3 km which is similar to the seven station regional moment tensor solution. The M_o and focal mechanism between the two solutions are also consistent with one another.

C.3.5 17 August 2002, 16:06 UT, Southern British Columbia

This event is from the Kelowna area in southern British Columbia. The original regional moment tensor used seven while this solution used five (Figure C.9). Since a number of the older broadband seismometers were located around southern British Columbia the two solutions should be similar. At the best-fit depth of 6 km the two solutions are consistent in M_o and mechanism and the best-fit depths are almost the same.

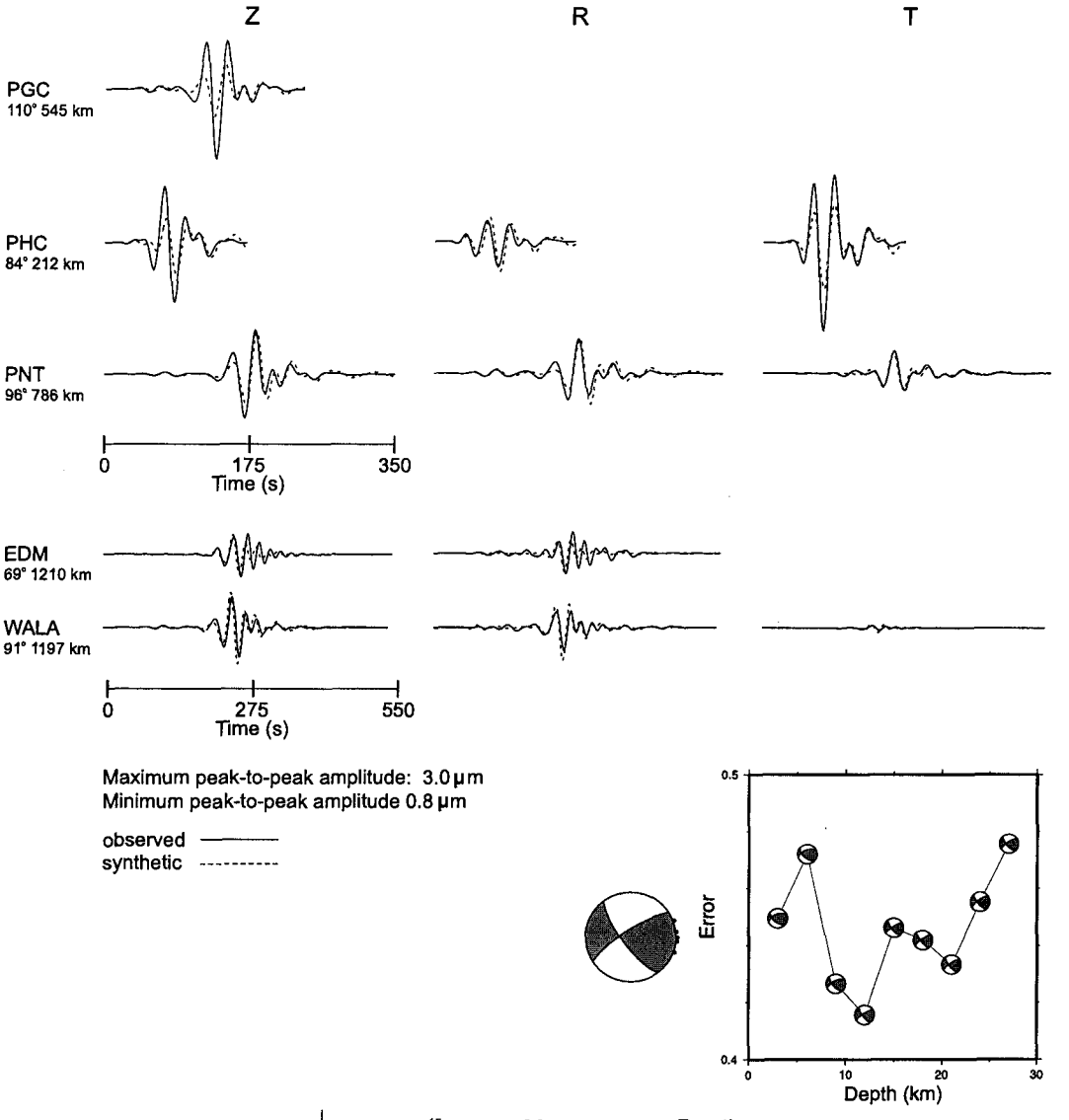

# Stations	M_o (x 10^{15} Nm)	M_w	% DC	Depth	S/D/R
8	17.9	4.8	42	9	147/81/171
5	23.0	4.9	64	12	143/75/166

Figure C.6 Regional moment tensor solution for the 4 April 2002 calculated using only stations available prior to the early 1990's. (*Top*) observed and synthetic waveform fits; (*centre*) error vs. depth plot and the best-fit focal mechanism with the station distribution; (*bottom*) comparison of key source parameters between the regional moment tensor solutions calculated using eight stations and five stations.

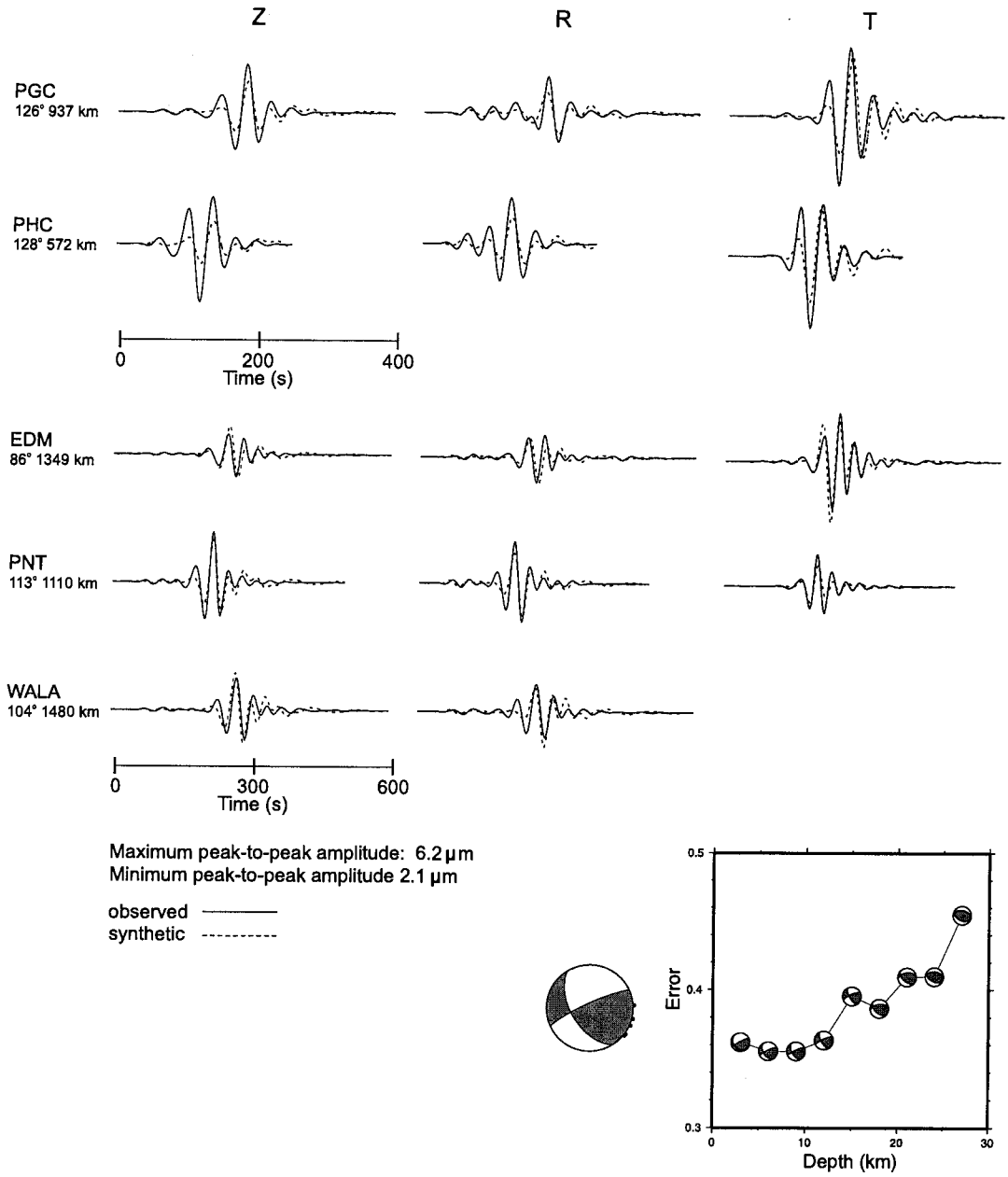

# Stations	M_o (x 10^{15} Nm)	M_w	% DC	Depth	S/D/R
11	80.5	5.2	65	6	330/58/180
5	72.0	5.2	100	9	149/55/169

Figure C.7 Regional moment tensor solution for the 5 September 2002 calculated using only stations available prior to the early 1990's. (*Top*) observed and synthetic waveform fits; (*centre*) error vs. depth plot and the best-fit focal mechanism with the station distribution; (*bottom*) comparison of key source parameters between the regional moment tensor solutions calculated using eight stations and five stations.

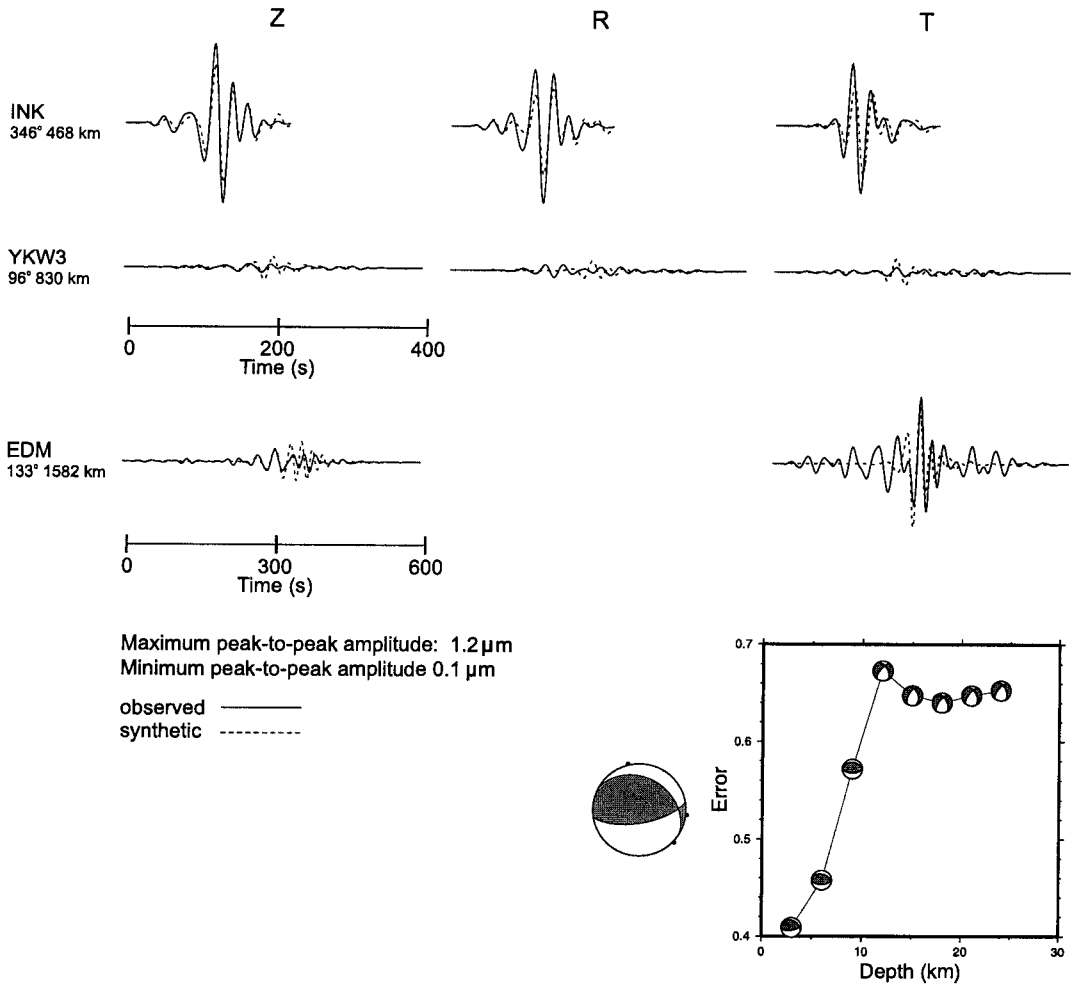

# Stations	M_o (x 10^{15} Nm)	M_w	% DC	Depth	S/D/R
7	8.06	4.6	92	6	83/61/78
3	6.20	4.5	92	3	80/66/71

Figure C.8 Regional moment tensor solution for the 14 February 2002 calculated using only stations available prior to the early 1990's. (*Top*) observed and synthetic waveform fits; (*centre*) error vs. depth plot and the best-fit focal mechanism with the station distribution; (*bottom*) comparison of key source parameters between the regional moment tensor solutions calculated using eight stations and five stations.

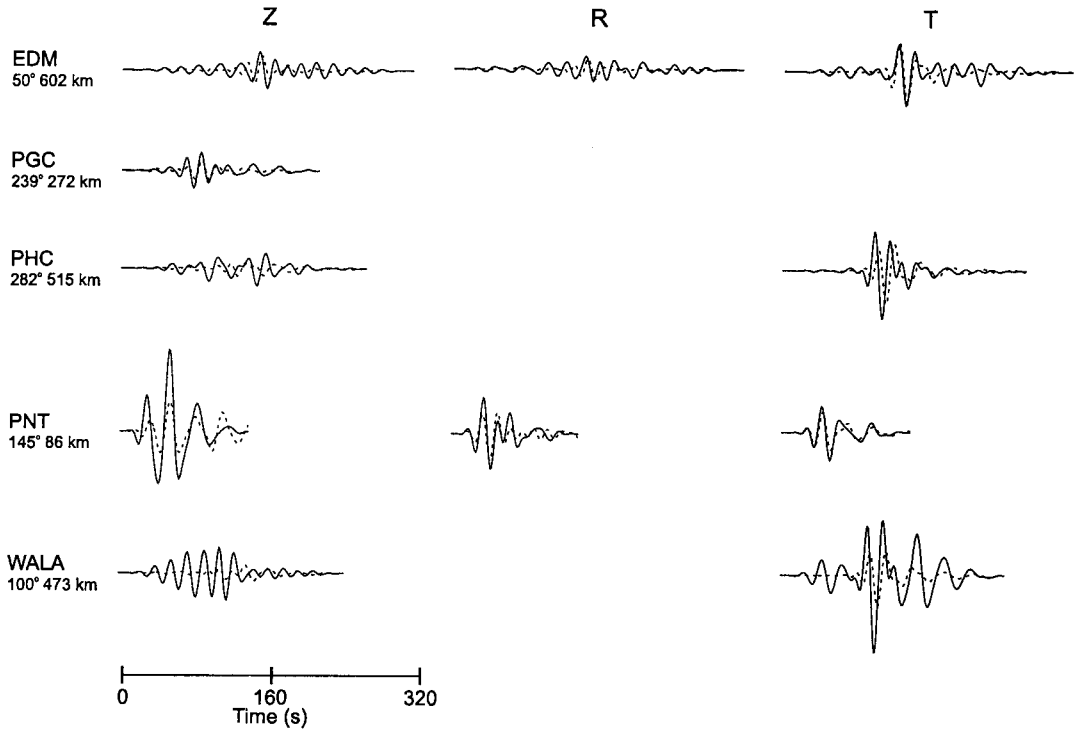

# Stations	M_o (x 10^{15} Nm)	M_w	% DC	Depth	S/D/R
7	6.80	4.5	95	9	251/44/89
5	7.10	4.5	78	6	251/38/84

Figure C.9 Regional moment tensor solution for the 17 August 2002 calculated using only stations available prior to the early 1990's. (*Top*) observed and synthetic waveform fits; (*centre*) error vs. depth plot and the best-fit focal mechanism with the station distribution; (*bottom*) comparison of key source parameters between the regional moment tensor solutions calculated using eight stations and five stations.

C.3.6 Summary

All of the regional moment tensor solutions calculated using only stations that were operational prior to the early 1990's produced solutions that are consistent with the solutions calculated using all of the currently available stations. This is not unexpected as the previous section showed that very few stations are required to calculate a reliable moment tensor solution. Even stations as far away as 1500 km provided usable data. In most of the examples it was difficult to constrain the depth other then to say that it was below a certain depth but all of the other important parameters (e.g. M_o, focal mechanism) could be determined. These examples demonstrate that it should be possible to calculate regional moment tensor for older earthquakes in western Canada with M_w = 4.5–5.5 where paper records exist and can be digitized.

C.4 Accuracy of Moment Tensor Calculated Depths

An important feature of the moment tensor method is the ability to determine the depth of an event. However, without having a priori knowledge of the depth of an earthquake it is not possible to know how accurate the depth calculation is. To test the ability of the regional moment tensor method used in this study to determine the depth of an event, synthetic seismograms are generated at various source depths with continental and oceanic crustal models using code available from L. Zhu (2004). This code calculates Green's functions for a double-couple source at a given source-receiver distance and source depth using an input Earth model. Synthetic seismograms are calculated from the Green's functions where the source mechanism (strike, dip, slip, magnitude) and source-receiver azimuth are given.

The first test uses a simple two layer Earth model with a 35 km thick crust over the mantle to represent a continental environment. Source depths of 3 km and 10 km are tested (Figure C.10 (*top left* and *top right*)). 10 stations are used with source-receiver distances ranging from 300–750 km. The station azimuths are uniformly distributed around the source (focal mechanism at the bottom of Figure C.10). For both the 3 km and 10 km depths there is minimum in the error at depths slightly lower than the true depth. However, the difference between the rms error at the true depth and the calculated depth is less than 5% in both cases. The second test uses a two layer Earth model with a 10 km thick crust over the mantle to represent a oceanic environment. Source depths of 3 km and 6 km are tested (Figure C.10 (*bottom left* and *bottom right*)). The same number of stations, source-receiver distances, and station azimuthal distribution are used as for the continental crust test. In both cases there is a minimum in the error at the same depth as

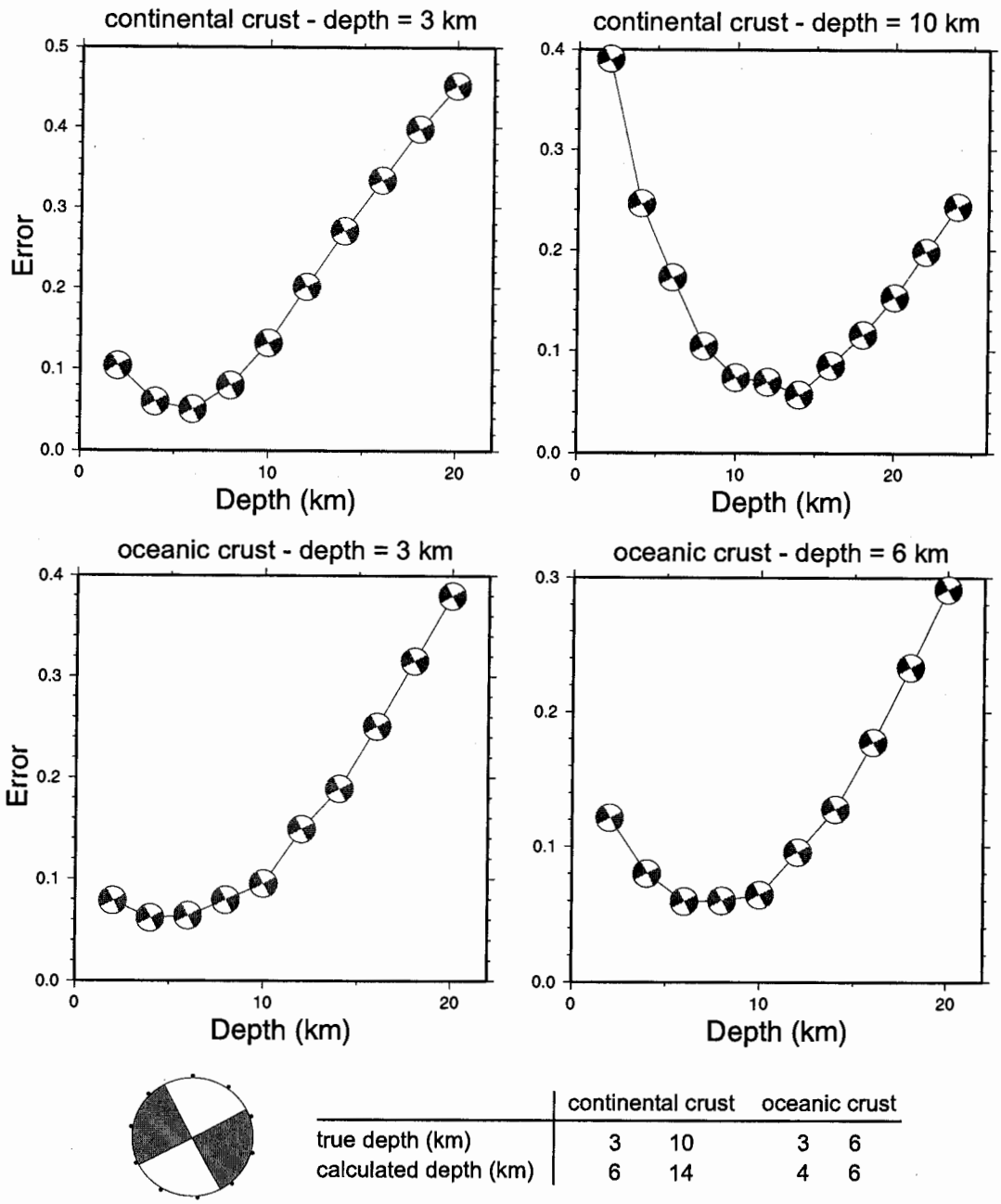

	continental crust		oceanic crust	
true depth (km)	3	10	3	6
calculated depth (km)	6	14	4	6

Figure C.10 Depth calculations from synthetic seismograms generated using continental and oceanic crust Earth models and various source depths. (*Top left*) continental crust with a 3 km source depth; (*Top right*) continental crust with a 10 km source depth; (*Bottom left*) oceanic crust with a 3 km source depth; (*Bottom right*) oceanic crust with a 6 km source depth. The very bottom shows the station azimuthal distribution and a comparison between the true source depths and the calculated source depths.

the true depths. These results demonstrate that the regional moment tensor method can calculate the depth of events with an accuracy of $\sim \pm$ 3 km.

To confirm that depths can be determined using a minimal number of stations, the case using a oceanic crust with the source at a depth of 6 km is calculated using only three stations (Figure C.11 (*left*)) and compared with the 10 station solution (Figure C.11 (*right*)). The three station case determined a source depth of 6 km, the same as the 10 station case, and the error-versus-depth plots are very similar.

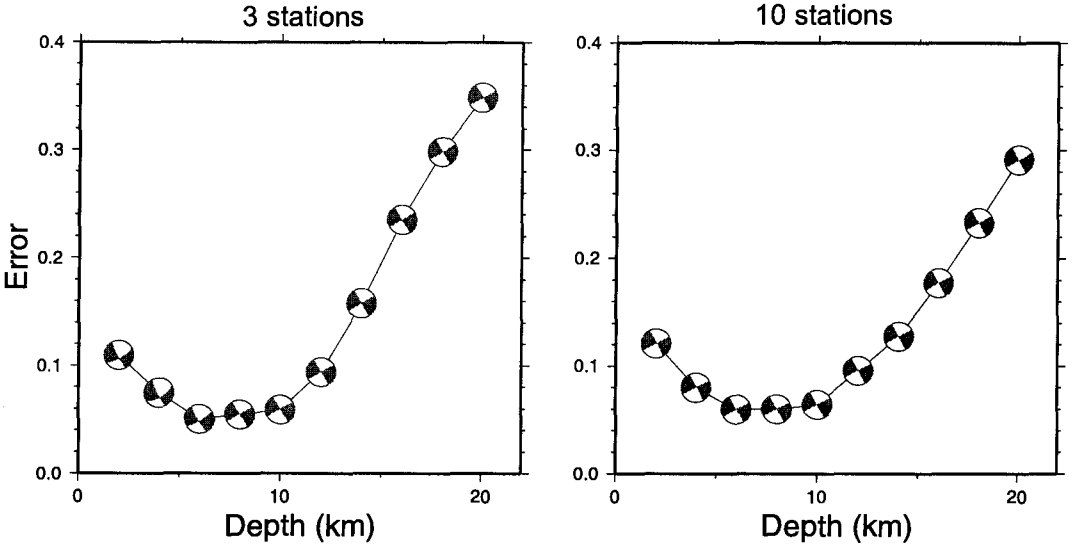

Figure C.11 Depth calculations for a source located at 6 km depth in oceanic crust using three stations (*left*) and 10 stations (*right*). The three station solution determined the same depth (6 km) as the 10 stations solution.

C.5 Moment Tensor Solution Comparison

A comparison was done for three events from different regions which were large enough for Harvard and the USGS to calculate moment tensor solutions (Figure C.12). For the events along the Nootka Fault Zone and in the Queen Charlotte Islands all three solutions agree very well in both the focal mechanism and the moment, however the regional moment tensor solution has a significantly shallower depth. The Harvard solutions are fixed at 15 km while the USGS moment tensor method tends to give greater depths for shallow events and have a depth resolution of about 5 to 10 km (Sipkin, 1986; Sipkin, 2000). Also teleseismic moment tensor solutions have low depth resolution due to the use of long period signals

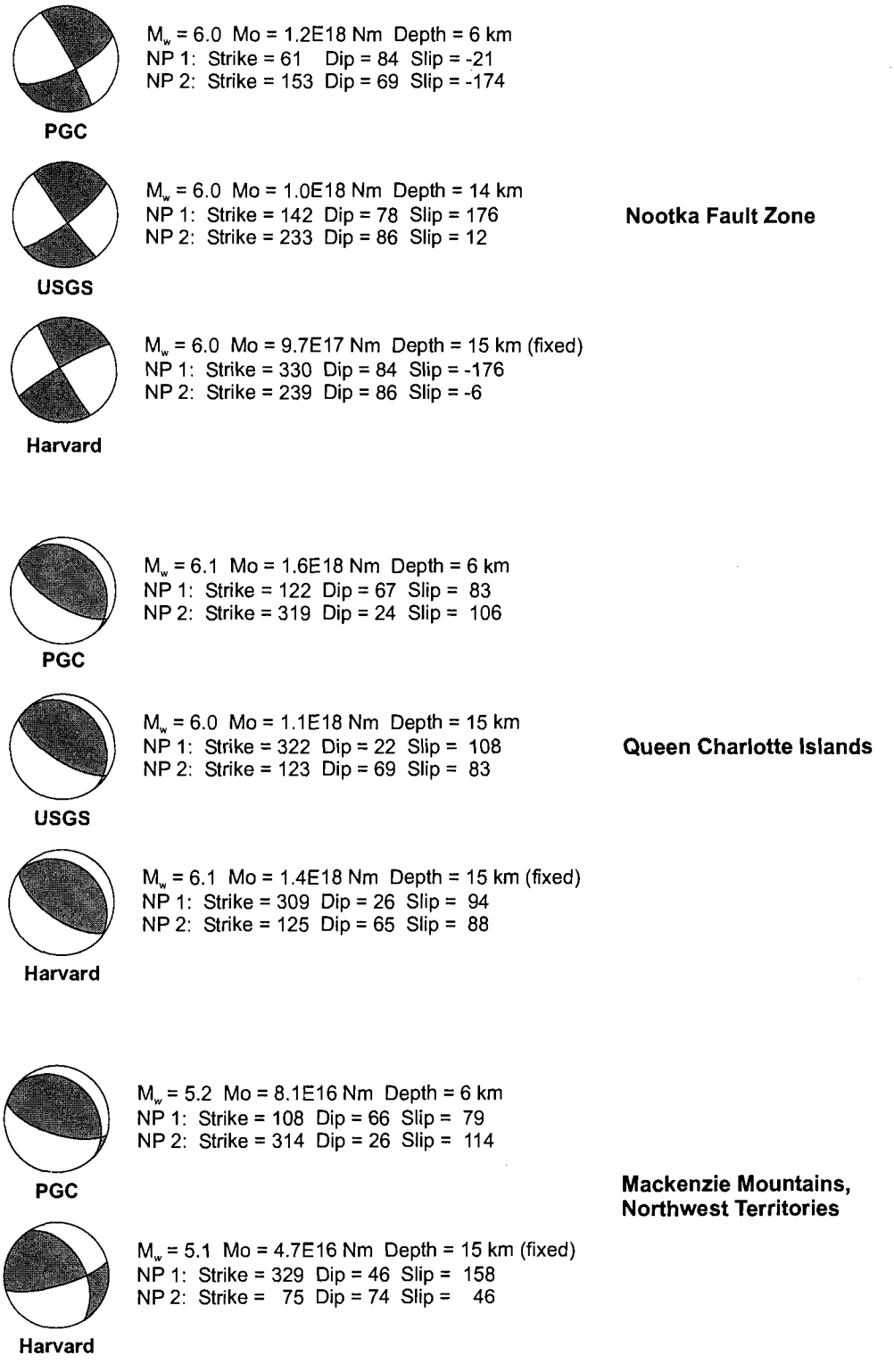

Figure C.12 Comparison of moment tensor solutions from PGC, USGS and Harvard.

(Ekström and England, 1989). The third event is from the Mackenzie Mountains region in the Northwest Territories which the USGS did not calculate a solution for. The regional moment tensor and Harvard centroid moment tensor solutions have somewhat different mechanisms with the regional moment tensor mechanism being almost pure thrust which the Harvard solution has a significant strike-slip component. The moment for the regional moment tensor solution is also almost twice that of the Harvard solution. This event is at about the lower limit for Harvard centroid moment tensor solutions and may be a lower quality centroid moment tensor.

All of the OSU regional moment tensor solutions were re-calculated for this research in order to have a consistent data set. The exceptions are those indicated in Table A.2 where the original waveform data was not available Figure C.13 compares PGC and OSU regional moment tensor solutions for several events with M_w ranging from 4.1–6.2 (the PGC solution is the top one and the OSU solution is the bottom one in each case). The PGC and OSU solutions are consistent in mechanism, moment, and depth. M_w and moment for all of the re-calculated events are compared in Figure C.14. In each plot the dashed line represents an ideal 1:1 relationship between the PGC and OSU results. M_w and moment cluster very tightly around the 1:1 line which demonstrates that the PGC and OSU moments and M_w's agree very well.

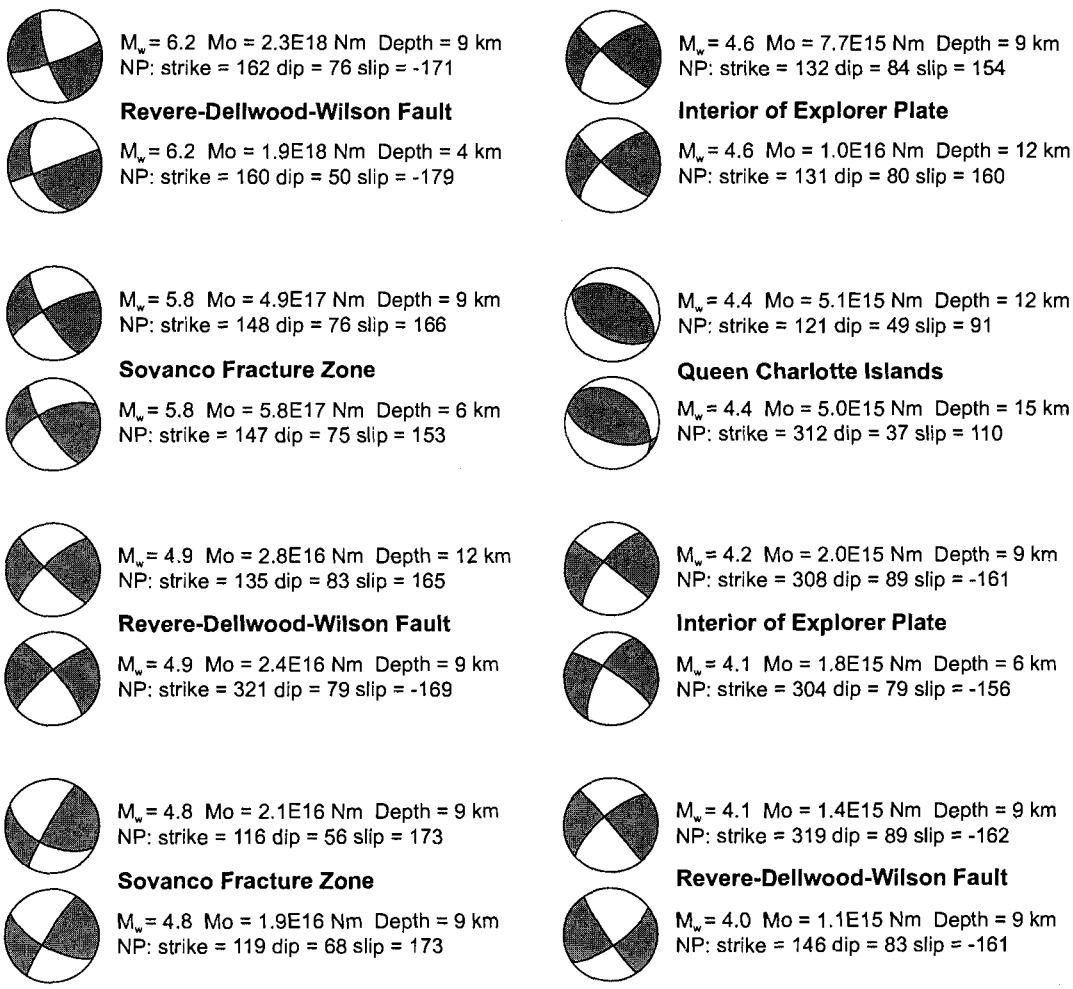

Figure C.13 Comparison of moment tensor solutions from PGC and OSU. In each case the PGC solution is the top one and the OSU solution is the bottom one.

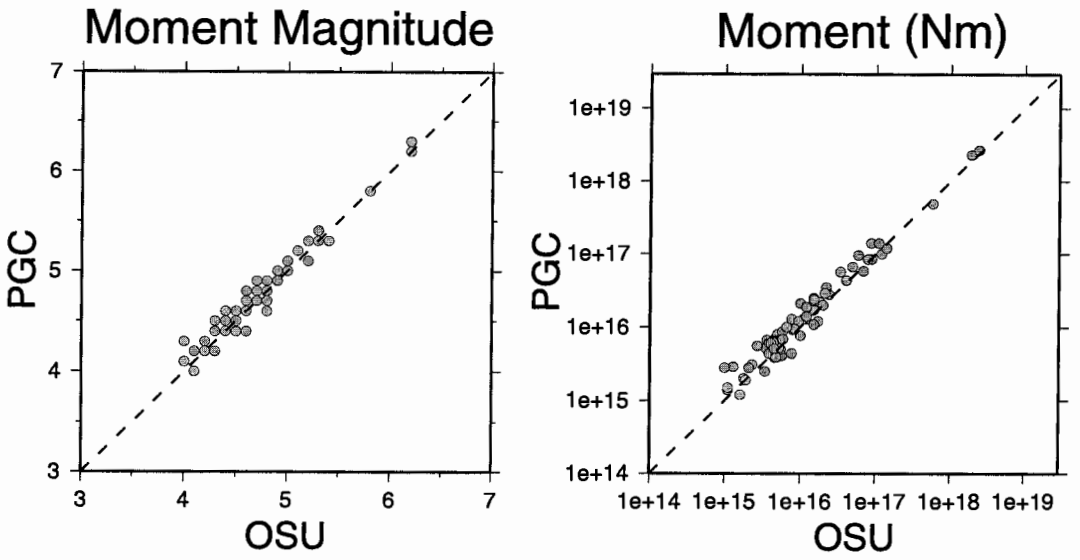

Figure C.14 (*Left*) Comparison of M_w calculated in this research and by OSU for the same events. (*Right*) Comparison of moment calculated in this research and by by OSU for the same events. In both plots the dashed line represents an ideal 1:1 relationship between the PGC and OSU results.

Appendix D

Coordinate Systems

D.1 PGC, OSU and Harvard Coordinate Systems

The regional moment tensor solutions calculated in this research and by OSU, and the centroid moment tensor solutions calculated by Harvard use different coordinate systems. In order to combine moment tensor elements from the PGC, OSU and Harvard catalogues the moment tensor elements must be adjusted to be in the same coordinate system. The regional moment tensor solutions calculated in this research and by OSU both use a cartesian coordinate system where the moment tensor elements are defined as M_{xx}, M_{yz}, etc., and the x-axis is defined as positive north, the y-axis as positive east, and the z-axis as positive down (Figure D.1 (*left*)). The moment tensor code used in this research has motion towards the source (compressional) defined as positive and motion away from the source (tensional) defined as negative. This will make the largest positive eigenvalue the P axis and the largest negative eigenvalue the T axis which is the opposite of the standard convention. The moment tensor elements calculated in this research need to be multiplied by -1 to put them in the standard convention. The OSU regional moment tensor follow the standard convention and do not need to be changed.

The Harvard centroid moment tensor convention is a spherical coordinate system based on (r, t, p) where r is the source-to-epicentre distance, t is the co-latitude (0 at the north pole), and p is the epicentral longitude (Figure D.1 (*right*)). Aki and Richards (1980) provide a relation between spherical and cartesian coordinate systems which is given as

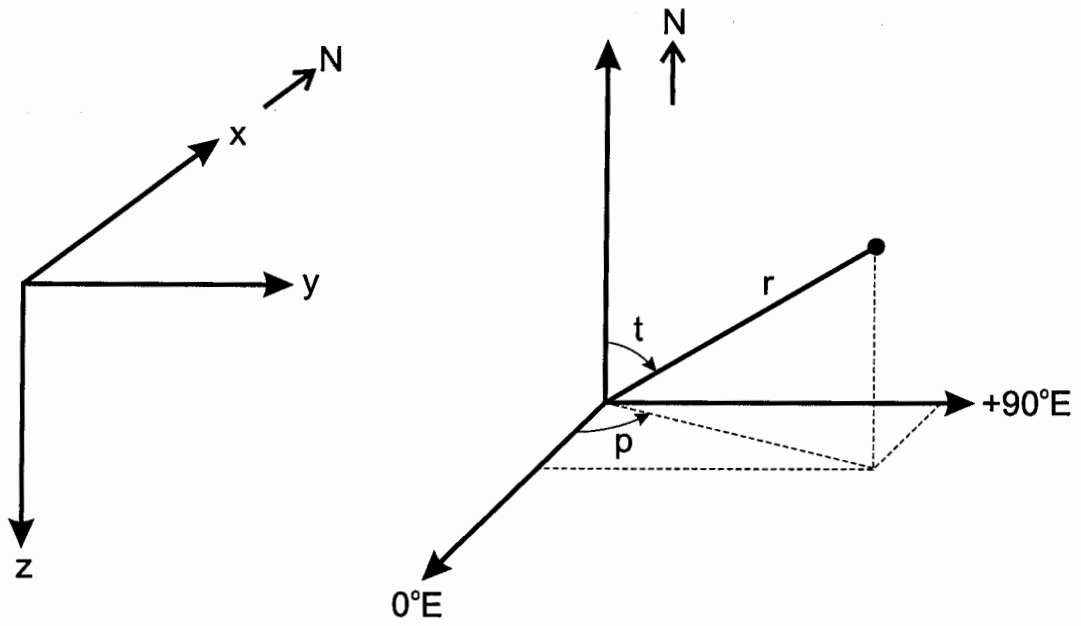

Figure D.1 (*Left*) Coordinate system used for the regional moment tensor solutions calculated in this research and by OSU. (*Right*) Coordinate system used for Harvard centroid moment tensor solutions which follows the convention of Aki and Richards (1980).

$$\begin{aligned} M_{rr} &= M_{zz} \quad M_{rt} = M_{xz} \\ M_{tt} &= M_{xx} \quad M_{rp} = -M_{yz} \\ M_{pp} &= M_{yy} \quad M_{tp} = -M_{xy}, \end{aligned} \tag{D.1}$$

or in matrix form as

$$\begin{bmatrix} M_{rr} & M_{rt} & M_{rp} \\ M_{tr} & M_{tt} & M_{tp} \\ M_{pr} & M_{pt} & M_{pp} \end{bmatrix} = \begin{bmatrix} M_{zz} & M_{zx} & -M_{zy} \\ M_{xz} & M_{xx} & -M_{xy} \\ -M_{yz} & -M_{yx} & M_{yy} \end{bmatrix}. \tag{D.2}$$

D.2 First Motion Solutions and Moment Tensors

First motion fault plane solutions and moment tensors are related by

$$M_{ij} = M_o(u_i\nu_j + u_j\nu_i), \tag{D.3}$$

where M_o is the seismic moment, ν_i is a unit vector normal to the fault plane, and u_j is a unit vector in the slip direction. This method requires two assumptions to made. The

first is that it is possible to convert the calculated magnitude of the earthquake to seismic moment. If a well known relationship between seismic moment and other magnitude scales exists for the region of interest then this is straightforward. The second assumption is that the first motion solution is a pure double-couple mechanism. If a solution has a large non-double-couple component it can have a significant effect on the values of the moment tensor elements. Smaller earthquakes generally have a simple fault mechanism and can be adequately modeled by a pure double-couple mechanism.

Appendix E

Earth Models

The format for the Earth models used to calculate the Green's functions is as follows.

first line	number of layers					
subsequent lines	thickness (km)	v_p (km/s)	v_s (km/s)	density	Q_p	Q_s

The last four columns are for absorption band information which is commented out in the code but is still required as input. For some of the Earth models the final layer is listed twice. This is because the moment tensor code does not allow the source to be in the model half-space. However some of the Earth models, in particular the oceanic models, are not very thick (< 20 km) above the half-space and therefore it is necessary for the source to be in the half-space in order to calculate deeper solutions. Inserting a thick layer above the half-space with the same model parameters as the half-space does not affect the calculation of the Green's functions but essentially allows the source to be in the half-space.

Earth models to use for events along the Revere-Dellwood-Wilson fault.

For stations BBB, MOBC, and RUBB:

```
5
01  4.00  2.11  2.10  225.  100.  1.e4  0.0001  1.e4  0.0001
04  5.00  3.13  2.40  225.  100.  1.e4  0.0001  1.e4  0.0001
15  6.00  3.68  2.70  225.  100.  1.e4  0.0001  1.e4  0.0001
50  7.81  4.68  3.00  225.  100.  1.e4  0.0001  1.e4  0.0001
00  7.81  4.68  3.00  225.  100.  1.e4  0.0001  1.e4  0.0001
```

For stations CBB, HNB, OZB, PHC, and SHB:

6

1.5	4.50	2.60	2.21	225.	100.	1.e4	0.0001	1.e4	0.0001
02	5.50	3.44	2.53	225.	100.	1.e4	0.0001	1.e4	0.0001
09	6.00	3.68	2.69	225.	100.	1.e4	0.0001	1.e4	0.0001
21.5	6.80	4.12	2.95	225.	100.	1.e4	0.0001	1.e4	0.0001
04	7.30	4.22	3.11	225.	100.	1.e4	0.0001	1.e4	0.0001
00	7.70	4.45	3.22	225.	100.	1.e4	0.0001	1.e4	0.0001

For stations BMBC, DLBC, FNBC, LLLB, PNT, SLEB, and WALA:

9

0.5	4.50	2.60	2.10	225.	100.	1.e4	0.0001	1.e4	0.0001
01	5.30	3.06	2.30	225.	100.	1.e4	0.0001	1.e4	0.0001
02	5.50	3.18	2.35	225.	100.	1.e4	0.0001	1.e4	0.0001
04	5.76	3.33	2.40	225.	100.	1.e4	0.0001	1.e4	0.0001
01	6.00	3.47	2.45	225.	100.	1.e4	0.0001	1.e4	0.0001
05	6.28	3.63	2.50	225.	100.	1.e4	0.0001	1.e4	0.0001
25	6.71	3.88	2.65	225.	100.	1.e4	0.0001	1.e4	0.0001
50	7.60	4.39	2.80	225.	100.	1.e4	0.0001	1.e4	0.0001
00	7.60	4.39	2.90	225.	100.	1.e4	0.0001	1.e4	0.0001

For stations PGC and SNB:

5

01	5.00	2.89	2.40	225.	100.	1.e4	0.0001	1.e4	0.0001
05	6.00	3.47	2.50	225.	100.	1.e4	0.0001	1.e4	0.0001
18	6.70	3.87	2.70	225.	100.	1.e4	0.0001	1.e4	0.0001
13	7.10	4.10	2.85	225.	100.	1.e4	0.0001	1.e4	0.0001
00	8.10	4.68	3.10	225.	100.	1.e4	0.0001	1.e4	0.0001

Earth models to use for events along the Sovanco Fracture Zone and Nootka Fault Zone.

For stations BBB, MOBC, and RUBB:

7

01	4.00	2.09	2.00	500.	250.	1.e4	0.0001	1.e4	0.0001
01	4.60	2.65	2.30	500.	250.	1.e4	0.0001	1.e4	0.0001
01	5.20	3.06	2.40	500.	250.	1.e4	0.0001	1.e4	0.0001
08	5.80	3.50	2.50	500.	250.	1.e4	0.0001	1.e4	0.0001
11	6.00	3.60	2.60	500.	250.	1.e4	0.0001	1.e4	0.0001
60	7.81	4.43	3.10	500.	250.	1.e4	0.0001	1.e4	0.0001
00	8.20	5.20	3.40	500.	250.	1.e4	0.0001	1.e4	0.0001

For stations BMBC and DLBC:

2

40	6.00	3.68	2.50	500.	250.	1.e4	0.0001	1.e4	0.0001
00	7.81	4.43	3.00	500.	250.	1.e4	0.0001	1.e4	0.0001

For stations CBB, OZB, and PHC:

6

01	4.00	2.09	2.00	500.	250.	1.e4	0.0001	1.e4	0.0001
05	5.20	2.89	2.20	500.	250.	1.e4	0.0001	1.e4	0.0001
20	5.90	3.45	2.50	500.	250.	1.e4	0.0001	1.e4	0.0001
05	6.50	3.80	2.80	500.	250.	1.e4	0.0001	1.e4	0.0001
25	7.81	4.43	3.00	500.	250.	1.e4	0.0001	1.e4	0.0001
00	8.40	4.86	3.22	500.	250.	1.e4	0.0001	1.e4	0.0001

For stations LLLB, PNT, SLEB, WALA, and NEW:

6

04	5.00	3.05	1.30	500.	250.	1.e4	0.0001	1.e4	0.0001
06	5.50	3.20	1.40	500.	250.	1.e4	0.0001	1.e4	0.0001
30	6.00	3.65	2.35	500.	250.	1.e4	0.0001	1.e4	0.0001
32	7.81	4.43	2.90	500.	250.	1.e4	0.0001	1.e4	0.0001
10	8.20	4.90	3.00	500.	250.	1.e4	0.0001	1.e4	0.0001
00	8.50	5.05	3.10	500.	250.	1.e4	0.0001	1.e4	0.0001

For stations PGC and SNB:

5

01	4.00	2.09	2.00	225.	100.	1.e4	0.0001	1.e4	0.0001
04	5.00	3.03	2.30	225.	100.	1.e4	0.0001	1.e4	0.0001
04	5.50	3.31	2.50	225.	100.	1.e4	0.0001	1.e4	0.0001
21	6.00	3.68	2.70	225.	100.	1.e4	0.0001	1.e4	0.0001
00	7.81	4.43	3.10	225.	100.	1.e4	0.0001	1.e4	0.0001

For stations GNW, LON, RWW, and TTW:

3

01	4.00	2.09	2.00	500.	250.	1.e4	0.0001	1.e4	0.0001
30	6.00	3.68	2.50	500.	250.	1.e4	0.0001	1.e4	0.0001
00	7.81	4.43	3.00	500.	250.	1.e4	0.0001	1.e4	0.0001

Earth models for events in the Queen Charlotte Islands region.

for stations BBB, MOBC, and RUBB:

5

01	4.40	2.44	1.60	500.	250.	1.e4	0.0001	1.e4	0.0001
03	5.20	2.97	1.60	500.	250.	1.e4	0.0001	1.e4	0.0001
17	6.20	3.54	2.00	500.	250.	1.e4	0.0001	1.e4	0.0001
03	6.50	3.71	2.00	500.	250.	1.e4	0.0001	1.e4	0.0001
00	8.20	4.69	3.10	500.	250.	1.e4	0.0001	1.e4	0.0001

For stations CBB, OZB, and PHC:

5

01	3.50	1.94	1.70	500.	250.	1.e4	0.0001	1.e4	0.0001
04	4.40	2.51	2.00	500.	250.	1.e4	0.0001	1.e4	0.0001
01	5.00	2.86	2.50	500.	250.	1.e4	0.0001	1.e4	0.0001
13	6.20	3.54	2.50	500.	250.	1.e4	0.0001	1.e4	0.0001
00	8.20	4.69	3.00	500.	250.	1.e4	0.0001	1.e4	0.0001

For stations BMBC, DLBC, LLLB, PNT, and SLEB:

8

0.5	4.00	2.22	2.10	225.	100.	1.e4	0.0001	1.e4	0.0001
01	5.00	2.86	2.30	225.	100.	1.e4	0.0001	1.e4	0.0001
02	5.50	3.14	2.35	225.	100.	1.e4	0.0001	1.e4	0.0001
04	5.76	3.29	2.40	225.	100.	1.e4	0.0001	1.e4	0.0001
01	6.00	3.43	2.45	225.	100.	1.e4	0.0001	1.e4	0.0001
05	6.28	3.59	2.50	225.	100.	1.e4	0.0001	1.e4	0.0001
25	6.71	3.83	2.65	225.	100.	1.e4	0.0001	1.e4	0.0001
00	7.50	4.29	3.00	225.	100.	1.e4	0.0001	1.e4	0.0001

For stations PGC and SNB:

2

27	6.20	3.54	2.50	500.	250.	1.e4	0.0001	1.e4	0.0001
00	8.20	4.69	3.00	500.	250.	1.e4	0.0001	1.e4	0.0001

Earth models for events in the Yukon and Northwest Territories.

For stations BMBC, DAWY, DLBC, FNBC, INK, and WHY:

5

08	5.50	3.35	2.65	500.	250.	1.e4	0.0001	1.e4	0.0001
09	6.20	3.58	2.70	500.	250.	1.e4	0.0001	1.e4	0.0001
10	6.40	3.70	2.90	500.	250.	1.e4	0.0001	1.e4	0.0001
12	6.60	3.82	3.00	500.	250.	1.e4	0.0001	1.e4	0.0001
00	7.90	4.57	3.20	500.	250.	1.e4	0.0001	1.e4	0.0001

For station YKW3:

5

04	5.80	3.25	2.60	500.	250.	1.e4	0.0001	1.e4	0.0001
09	6.20	3.58	2.70	500.	250.	1.e4	0.0001	1.e4	0.0001
13	6.40	3.70	2.90	500.	250.	1.e4	0.0001	1.e4	0.0001
13	6.70	3.88	3.00	500.	250.	1.e4	0.0001	1.e4	0.0001
00	7.85	4.54	3.20	500.	250.	1.e4	0.0001	1.e4	0.0001

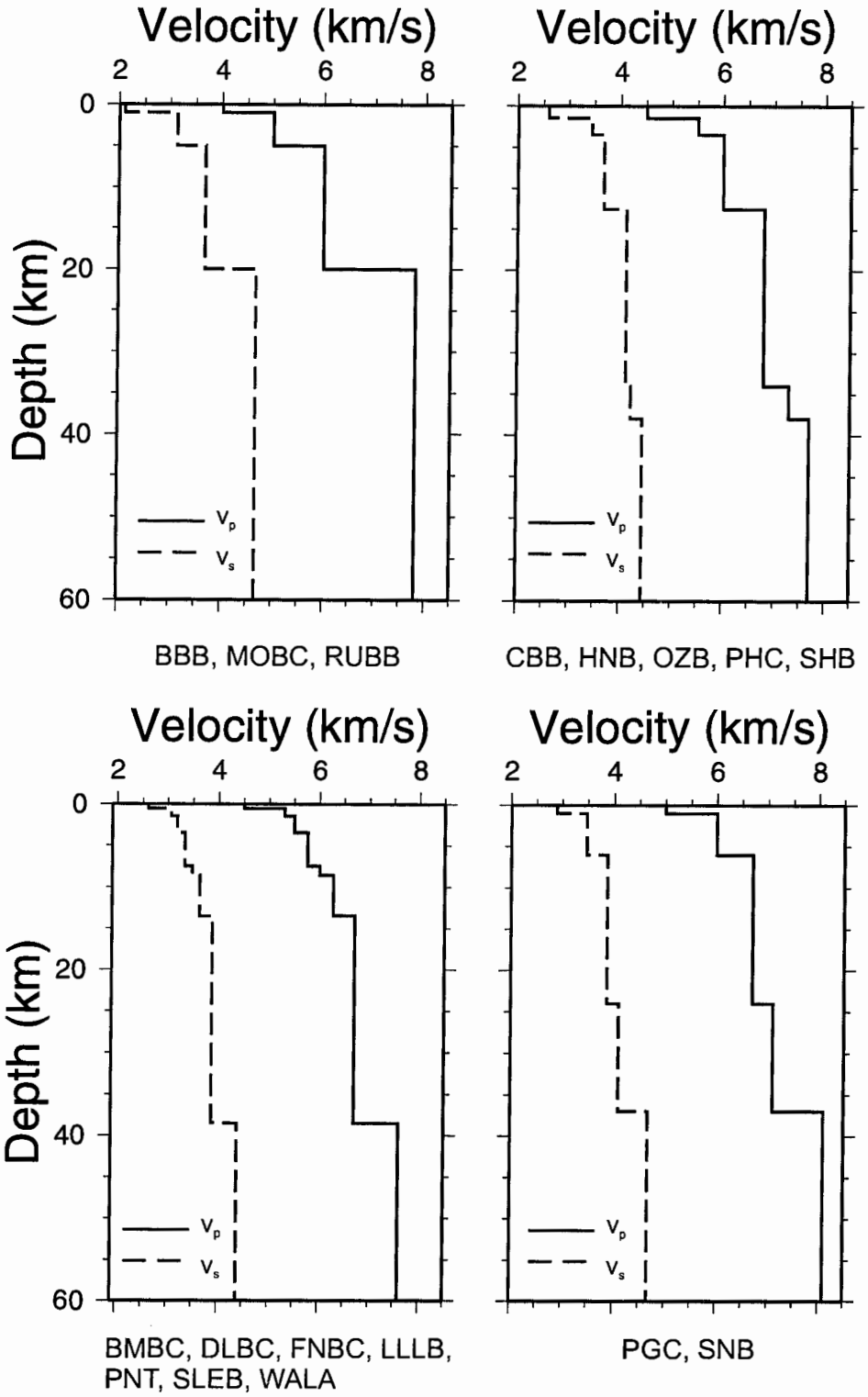

Figure E.1 Earth models used for events in the Revere-Dellwood-Wilson fault region.

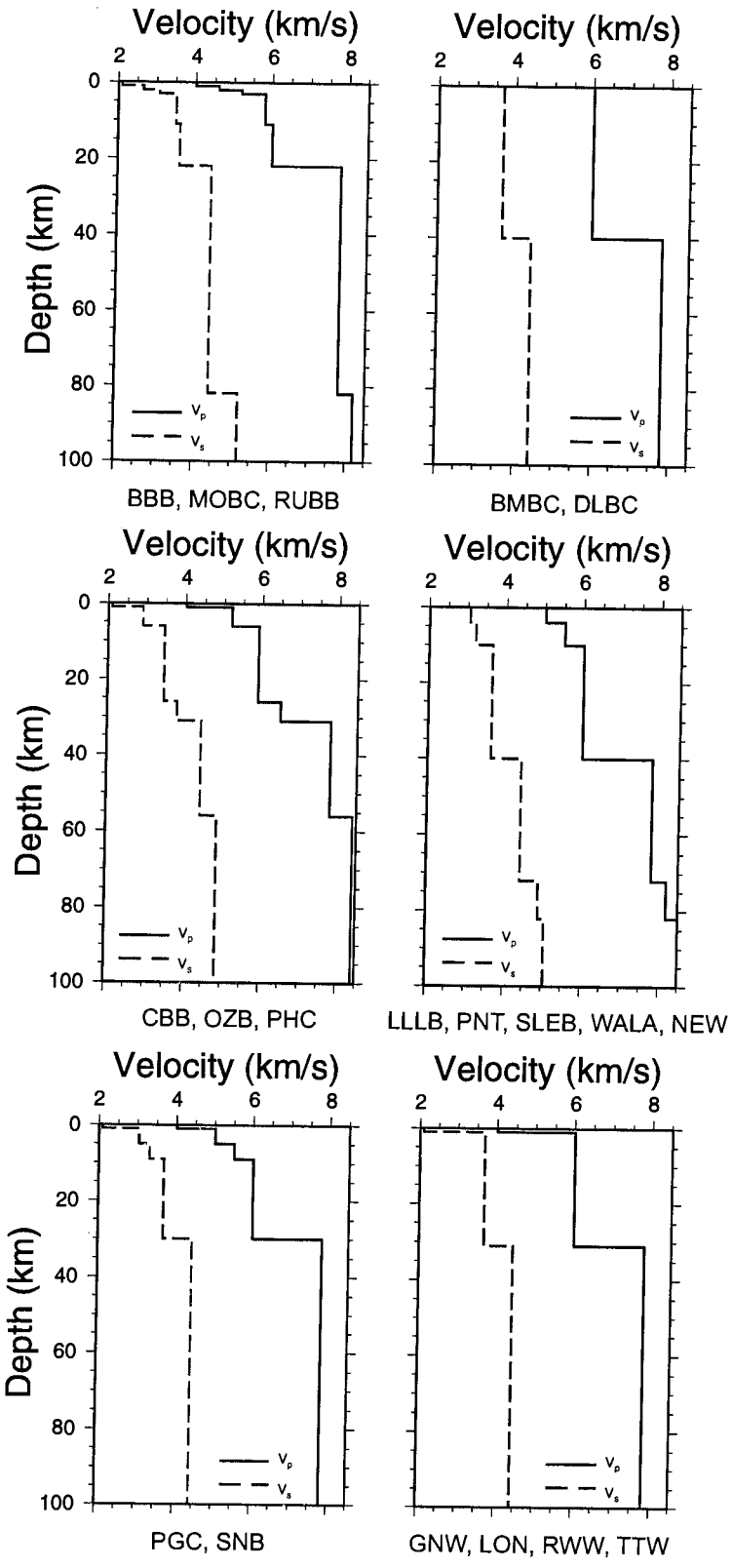

Figure E.2 Earth models used for events in the Sovanco Fracture Zone region.

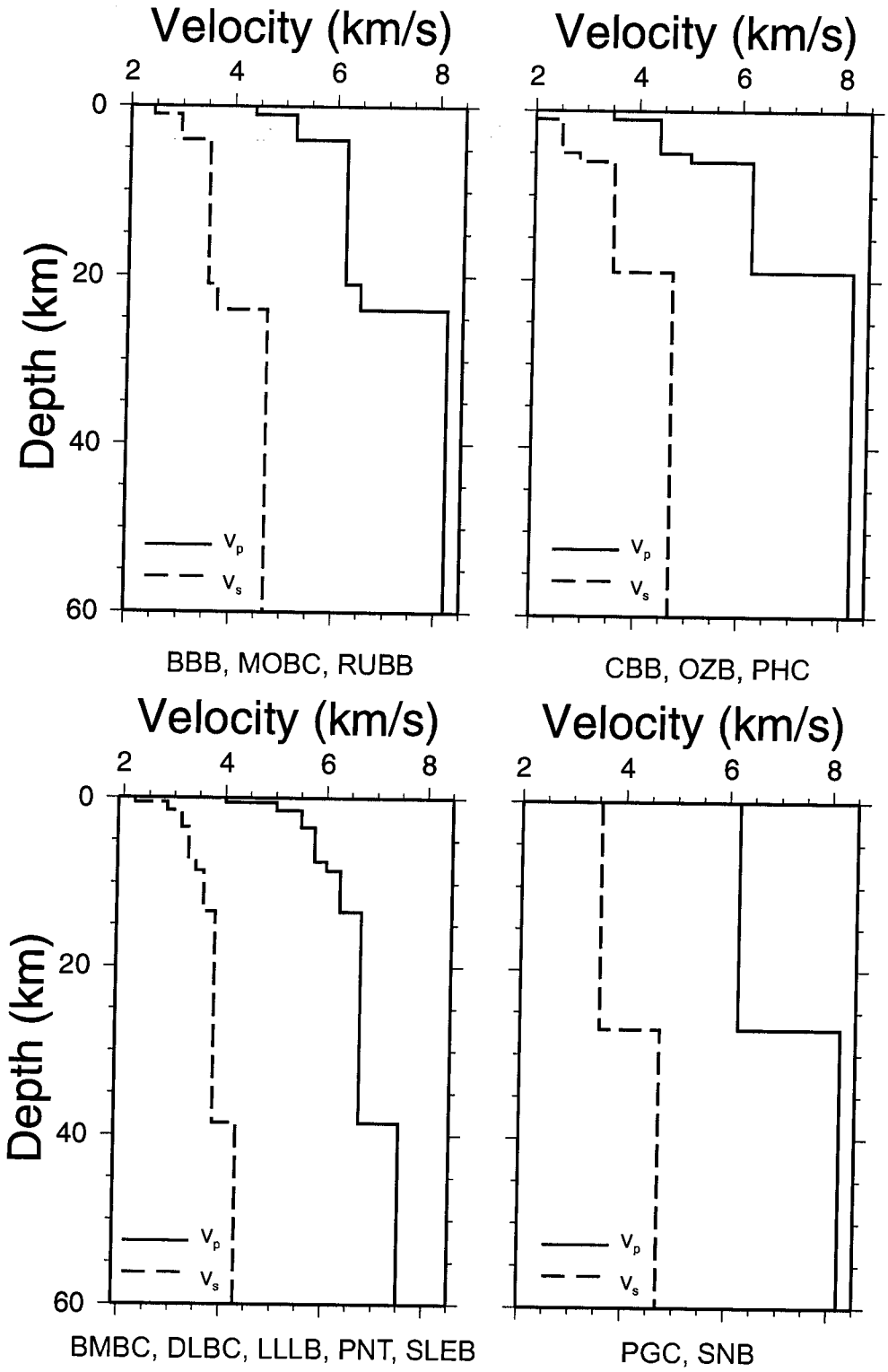

Figure E.3 Earth models used for events in the Queen Charlotte Islands region.

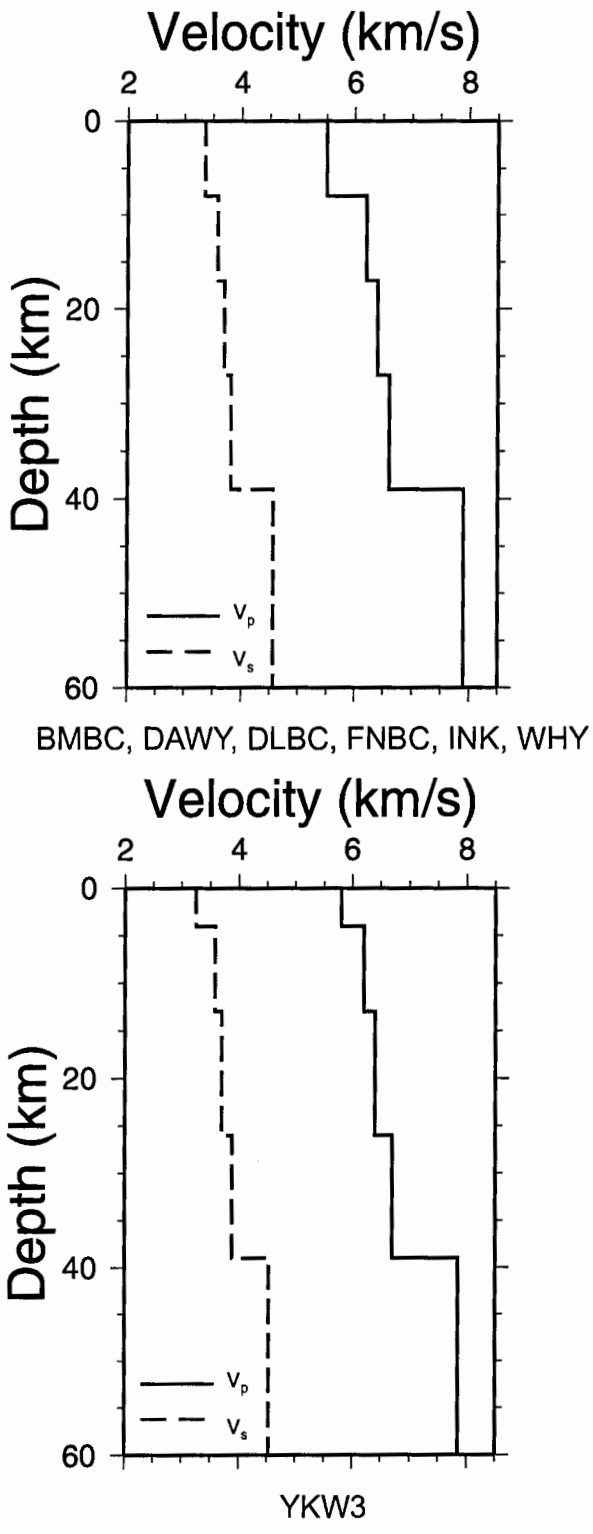

Figure E.4 Earth models used for events in the Yukon and Northwest Territories.